Progress in Materials Science 155 (2026) 101519

Contents lists available at ScienceDirect

Progress in Materials Science

journal homepage: www.elsevier.com/locate/pmatsci

Mechanical behavior of microstructurally stable nanocrystalline alloys: Processing, properties, performance, and prospects

K.A. Darling [a], Y. Mishin [b], N.N. Thadhani [c,*], Q. Wei [d], K. Solanki [e,*]

[a] Army Research Directorate, DEVCOM Army Research Laboratory, APG, MD 21005, USA
[b] Department of Physics and Astronomy, George Mason University, MSN 3F3, Fairfax, VA 22030, USA
[c] School of Materials Science and Engineering, Georgia Institute of Technology, 771 Ferst Dr. NW, Atlanta, GA 30332, USA
[d] Department of Mechanical Engineering and Engineering Science, University of North Carolina at Charlotte, Charlotte, NC 28223, USA
[e] School for the Engineering of Matter, Transport, and Energy, Arizona State University, Tempe, AZ 85287, USA

A B S T R A C T

This review presents a comprehensive overview of the scientific revolution enabled by recent emergence of structurally stabilized NC materials. It captures major breakthroughs in achieving nanoscale stability through thermodynamic and kinetic pathways, and critically examines the fundamental mechanisms underpinning the stabilization, including GB segregation, solute drag, Zener pinning, and nanocluster formation. It describes how stabilization of NC materials can enable unprecedented access to their intrinsic mechanical and physical behaviors, revealing phenomena previously inaccessible due to the microstructural evolution during testing. Examples include superlative strength-ductility synergy, infinite fatigue endurance limits, creep resistance rivaling single crystals, radiation damage tolerance, and evidence of defect-mediated self-healing. The review also explores how stabilized NC materials challenge long-held assumptions about the mechanisms of deformation, recrystallization, and phase transformations. It further examines how stabilized NC alloys have revolutionized our theoretical understanding of these mechanisms and created new avenues for their fabrication as well as industrial applications. While significant challenges remain with scalable fabrication processes and standardization, we outline new design principles, manufacturing pathways, and strategic directions for future exploration and application frontiers that are poised to overcome long-standing limitations making structurally stabilized NC materials as a transformative class of structural materials for extreme environments and advanced technologies.

Abbreviations: APT, Atom probe tomography; ARB, Accumulative roll bonding; BCC, Body-centered cubic; cBN, Cubic boron nitride; CDX, Continuous dynamic recrystallization; CSL, Coincidence site lattice; CVD, Chemical vapor deposition; DC, Diamond cubic; DDRX, Discontinuous dynamic recrystallization; DFT, Density-functional theory; DOS, Density of states; dpa, Displacement per atom; ECAE, Equal channel angular extrusion; FCC, Face-centered cubic; FIB, Focused ion beam; FOA, Funding Opportunity Announcement; GB, Grain boundary; GP, Guiner-Preston; GRDX, Geometric dynamic recrystallization; HAADF, High-angle annular dark-field; HCP, Hexagonal close-packed; HEA, High-entropy alloys; HEL, Hugoniot elastic limit; HIP, Hot isostatic pressing; HPT, High-pressure torsion; HRTEM, High-resolution transmission electron microscopy; IGC, Inert gas condensation; KMC, Kinetic Monte Carlo; LDF, Laser-driven flyer; MC, Microcrystalline; MD, Molecular dynamics; MDBT, Miniaturized disk bend test; MEMS, Micro-electromechanical system; MIM, Metal injection molding; MMC, Metal matrix composite; NC, Nanocrystalline; ND, Normal direction; NSS, Nano-sized superlattice cluster; ODS, Oxide dispersion strengthened; OFHC, Oxygen-free high thermal conductivity; PDV, Photon Doppler velocimetry; PKA, Primary knock-on atom; PM, Powder metallurgy; PSB, Persistent slip band; PVD, Physical vapor deposition; RD, Rolling direction; SAED, Selected area electron diffraction; SME, Shape memory effect; SOC, Self-organized criticality; SPD, Severe plastic deformation; SPT, Shear punch testing; SRS, Strain rate sensitivity; STEM, Scanning transmission electron microscopy; TBC, Thermal barrier coating; TD, Transverse direction; TDI, Transverse displacement interferometer; TEM, Transmission electron microscopy; TJ, Triple junction; TKD, Transmission Kikuchi diffraction; UFG, Ultrafine-grained; XRD, X-ray diffraction.

* Corresponding authors.
E-mail addresses: naresh.thadhani@mse.gatech.edu (N.N. Thadhani), kiran.solanki@asu.edu (K. Solanki).

https://doi.org/10.1016/j.pmatsci.2025.101519
Received 12 February 2023; Received in revised form 29 April 2025; Accepted 21 May 2025
Available online 25 May 2025

1. Introduction

The mechanical behavior of nanocrystalline (NC) metals and alloys has been investigated intensely for over four decades [1–85]. However, much remains to be understood with respect to their deformation and failure mechanisms. All previous review articles have discussed the behavior of NC materials that did not necessarily have stable microstructures during the tests.

Extensive grain growth in NC materials, driven by moderate temperatures and applied stresses, can obscure the true mechanical response by coarsening the microstructure [17,33,86]. This issue becomes especially significant under extreme conditions, where the already unstable microstructure can completely reorganize due to strong driving forces, such as high temperature or high stress. Grain boundary (GB) instability plays a crucial role, as the energy stored in GBs can lead to grain growth, GB migration, or even phase transformations, further complicating the mechanical behavior of the material. The instability of GBs may also result in phenomena such as GB sliding or the formation of defects, which destabilize the microstructure and promote alternate forms of deformation. Decoupling the effects of microstructure instability from the nanoscale mechanical behavior remains a highly challenging task. This inability to separate the two processes has led to a pessimistic view of the performance of NC materials, particularly for structural load-bearing applications. While NC materials are known for their enhanced strength due to the fine-grained structure, the instability of GBs and the rapid coarsening of grains under stress or elevated temperatures can significantly degrade their mechanical properties, including strength, ductility, and fracture toughness.

The ability to stabilize nanostructures has only emerged in recent years. This critical achievement has opened new frontiers in fundamental research and new opportunities for overcoming the barriers to realizing the extraordinary mechanical and physical properties of NC materials. The ability to stabilize nanostructures has been incredibly impactful for understanding and designing new materials operating under extreme and far-from-equilibrium conditions.

The breakthrough in stabilizing nanostructures came after the publication of the seminal review paper by Meyers et al. [33]. At that time, significant stabilization of nanostructures did not seem achievable. Since then, great advances have been made in developing experimental and computational capabilities to understand the new class of stabilized NC materials. Many existing challenges in the processing and consolidation of such materials have been overcome, opening the door for synthesizing significantly stabilized NC metals and alloys in bulk forms. Investigations of the physical and mechanical properties of such materials have changed our understanding of the deformation and fracture mechanisms at the nanoscale. New mechanisms have been uncovered, some of which were predicted theoretically or by simulations but never observed in experiments. These developments have reinvigorated the field [87,88] and opened new horizons for designing NC materials with previously unimagined properties. The time is ripe for a critical review of the recent progress in this field and outlining promising directions for future research.

This paper aims to review the emergence, the current status, and an outlook for the future of the new class of thermo-mechanically stable NC materials. We will present recent results related to the synthesis and processing of NC materials, grain size evolution and stability, and GB processes, as well as their effects on physical and mechanical behaviors. A broad range of properties of stable NC materials will be discussed, including plastic deformation, fracture, creep resistance, fatigue, and shock compression, and their response to intense irradiation. It will be shown that NC materials exhibit multi-physics behaviors, often combining seemingly mutually exclusive properties. The impact of the microstructure stabilization on overcoming the perceived limitations of the traditional NC materials will be reviewed in detail. Examples of the drastically improved properties will include *nano-grain stability near the melting point*, *exceptional steady-state creep resistance*, *ability to evade the strength-ductility trade-off*, *infinite fatigue endurance limit*, *single-crystal-like strength properties*, and the *capability to absorb defects* generated by various thermal, nuclear, and mechanical energy fluxes. We will examine the capacity of stabilized NC materials to undergo recrystallization and microstructure rejuvenation under intense stimuli and novel mechanisms of their mechanical and physical behavior under extreme conditions. In many cases, overlaps between seemingly unrelated research areas are discovered, such as the response to intense irradiation, creep, fatigue, and shock compression.

The recent work on computer modeling and simulations will be reviewed, especially the efforts to understand the fundamentals of nano-grain stabilization and re-examine the dominant deformation mechanisms. While the previous review [33] was focused on mechanical properties, the present review broadens the scope by including a spectrum of physical properties and many aspects surrounding the problem of stabilization of NC materials. Much attention is devoted to discussing the nature and physical mechanisms of the microstructural stability at the nanoscale. While earlier research often focused on retaining the nanoscale grain size, recent work has demonstrated that structures associated with the grain-boundary region also play an essential role in stabilizing the material and leading to extraordinary mechanical and physical behaviors [67]. Hence, the present review extends the discussion into inter-granular microstructures, and to a lesser extent, intra-granular features.

This paper primarily focuses on metallic NC materials, although the concepts reviewed here are equally relevant to the nanoscale stabilization and mechanical behavior of ceramics. The term “nano” refers to the grain size, not the sample dimensions. The review does not consider low-dimensional systems such as epitaxial thin films, 2D materials, nanowires, and single-crystalline nanoparticles. Although we occasionally use terms such as “nanomaterials” and “nanostructures,” our focus is on the crystalline matter.

To better understand and appreciate the recent developments and provide an outlook for the future, we examine the historical context leading to the present state of the field. Hence, this paper reviews the timeline of the development of the basic concepts, models, and simulation approaches related to microstructure stabilization in general, as well as the experimental efforts to create stable nanomaterials and the investigation of their mechanical responses. References [1–85] highlight some of the earlier review articles and original publications that were critical for the progress in synthesizing stable NC materials and understanding their properties. Although we do not claim that this list of citations included is exhaustive, it represents a set of milestones, putting the previous work in a historical perspective. Many of these publications will be discussed in more detail below.

2. Stabilization of nanocrystalline materials: From past to present

2.1. Importance of microstructure stabilization

When the average grain size in materials falls well below ~ 100 nm, the volume fraction of defect cores becomes comparable to that of the crystal lattice. The NC material thus obtained can exhibit properties significantly different from those of coarse-grained materials, opening a new field of fundamental discoveries and the design of new materials with unprecedented properties. This vision was first put forward by Gleiter in 1981 and became a reality when the first NC metals were produced by inert gas condensation (IGC) [1,89].

The IGC method operates in a vacuum chamber backfilled with low-pressure inert gas [89,90]. The chosen material is evaporated using one of several methods, such as thermal evaporation, laser evaporation, sputtering, electric arc discharge, or plasma heating. After evaporation, the gas is rapidly condensed on a cold finger. The condensate is scraped off the finger, and the recovered powder is compacted under ultra-high vacuum to maintain surface cleanliness. Due to the non-equilibrium nature of this synthesis, it produces a narrow size distribution of equiaxed crystallites measuring a few nanometers in size. The mean and width of the grain size distribution can be influenced by factors such as the inert gas pressure and temperature, evaporation rate, and gas composition. Despite the ability to produce very small grain sizes, the method has its drawbacks, including slow processing rates, incompatibility with certain source precursors, and uneven evaporation rates for alloys. These drawbacks, coupled with the limited availability of the required equipment, have hindered the widespread adoption of this method. In the late 1980's and early 1990's, more readily available alternative techniques gained popularity, including physical vapor deposition (PVD) and chemical synthesis via colloidal, sol–gel, and precipitation techniques, alongside chemical vapor deposition (CVD) and chemical vapor condensation methods [4]. Ultimately, these techniques faced similar challenges as IGC, including slow deposition rates, the need for expensive equipment, problems with maintaining chemical purity, varying evaporation rates, and difficulties in synthesizing complex compounds.

Mechanical ball-milling methods, including high-energy mechanical alloying, were also employed [10,16]. Mechanical attrition achieves a nanoscale grain size not by cluster assembly but through structural decomposition of the solutions produced by severe plastic deformation (SPD). Unlike deposition techniques, mechanical alloying is a robust and versatile synthesis method utilizing affordable and commercially accessible equipment. Its roots can be traced back to the mid-1960's and 1970's when efforts were made to overcome the limitations of melt processing [7,16], to effectively fabricate alloys with extended solubility limits, and incorporate highly reactive elements such as Zr, Ti, and Al. Mechanical alloying was also instrumental in commercially developing Ni-based oxide dispersion-strengthened (ODS) alloys. In the 1980 s, mechanical alloying found utility in producing the first amorphous (glassy) metallic materials and blended elemental powder mixtures, ordered compounds, and quasi-crystalline phases [9]. Mechanical milling was thus applied to refine grain sizes in elemental materials and synthesize NC solid solutions, nano-structured composites, and amorphous and ordered/disordered phases. The increased availability of the diverse types of NC materials enabled by these techniques led to the proliferation of experimental studies and a rapid upturn in the number of publications on nanomaterials [7].

Another synthesis technique, electro-deposition, emerged in the early to mid-2000 s [91] and offered significant advantages over the powder processing approaches, including the production of fully consolidated materials in an adequate volume and within a reasonable timeframe [92]. The availability of electro-deposited materials facilitated hardness and other micro-mechanical property measurements. This process, along with later techniques such as high-pressure torsion (HPT), equal-channel angular pressing (ECAP), and accumulative roll bonding (ARB), became prominent in producing bulk NC materials with significantly reduced grain sizes [25,34,44,93,94]. Collectively, the availability of bulk NC samples enabled more comprehensive microstructural analysis, revealing intricate structures and sub-features formed during synthesis and providing insights into their correlations with mechanical properties.

This emergence of NC metals sparked fundamental scientific inquiry to determine whether their properties entail novel physics or merely follow the anticipated extrapolation of the grain-size dependence to significantly smaller dimensions [11]. Despite the increased availability of NC samples, answering this question was challenging because most synthesis techniques did not yield bulk materials of adequate quality. For example, NC powders synthesized by mechanical alloying require an additional step to fully densify the material and produce well-bonded volumes of high-quality NC materials suitable for precise testing and measurements [95]. The inherent instability of nano-grained structures prevented successful consolidation efforts and, thus, detailed studies of the microstructures and their mechanical properties. The experimental techniques were limited to characterization by basic TEM and X-ray diffraction (XRD), and hardness measurements. The unsuccessful attempts to densify the NC powders/particulates by high-temperature powder metallurgy methods only confirmed the severity of the thermal instability problem in nanostructures.

The collective data suggests that the onset of grain growth in NC metals scales with their melting point. Lower melting point metals such as Sn, Pb, Al, Zn, and Mg exhibit extensive grain growth already at room temperature [3,89,96]. Higher melting point metals, such as Cu, Ag, and Pd, are characterized by slower grain growth. However, the latter can still occur even at room temperature, depending on the chemical purity [96]. In some transition metals, such as Ni, Fe, and Co, the grain growth starts between 350 and 450 °C [92,97–99]. In refractory elements, such as W, Mo, and Ta, the grain growth starts closer to 1000 °C [7]. Generally, most nominally pure NC metals exhibit extensive grain growth, pushing the average grain size past 100 nm at temperatures less than or close to 0.5 times the melting temperature [45,60]. This severe structural instability hindered the progress in fundamental understanding of the nanoscale effects and the prospects of technological applications [66,100]. The need to overcome the grain instability curse became a critically important scientific and practical problem [61].

2.2. Why are nanocrystalline materials unstable?

The grain size instability in NC materials is a fundamental phenomenon. Grain boundaries (GBs) carry excess free energy relative to the single-crystalline state. Grain growth in a polycrystalline material is driven by capillary forces acting to reduce the total GB free energy. The specific GB area (per unit volume) in an NC material is very large, as is the associated excess free energy. As a result, the capillary forces driving the grain growth are exceedingly high, often up to several hundred MPa. In a chemically pure metal, these forces easily overcome the friction experienced by moving GBs, making grain coarsening virtually unstoppable.

In the linear-response approximation, the local GB velocity v behaves as [101]

$$v = M\gamma\kappa, \tag{1}$$

where M is the GB mobility coefficient, γ is the GB free energy (per unit area), and κ is the mean GB curvature. GB curvature is roughly inversely proportional to the mean GB size D, i.e., $\kappa \propto 1/D$. As a result, the small grain size causes fast GB migration and, thus, rapid grain growth. Equation (1) predicts that, as long as $\gamma > 0$, GBs always move, even though their motion at low temperatures can be relatively slow. Any polycrystalline metal is, thus, *thermodynamically unstable*. All applications of thermodynamics to polycrystalline materials implicitly rely on the assumption of constrained equilibrium.

Several approaches have been proposed for suppressing, or at least reducing, grain growth. The most effective strategy is to alloy metals with suitably chosen solutes. Equation (1) suggests two ways to slow down the GB motion: by lowering the GB free energy (γ) or decreasing GB mobility (M). These two strategies are called the *thermodynamic* and *kinetic* stabilization mechanisms, respectively. Different research groups have pursued one of the two directions. Due to the fundamental importance of this subject, the *thermodynamic* and *kinetic* approaches are discussed below in more detail.

2.3. Thermodynamic stabilization

The thermodynamic stabilization approach aims to suppress the grain growth by alloying with a solute or several solutes, that segregate to the GBs and reduce the GB free energy (γ) and, thus, the capillary driving force. The inverse relation between solute segregation and the interface free energy γ was predicted by Gibbs in the 19th century [102]. According to Gibbs' interface adsorption equation, the increase in the amount of solute segregated at the interface is proportional to the resulting decrease in the interface free energy. Thermodynamically, it is this reduction in the interface free energy that drives solute segregation. Gibbs' work focused on interfaces between fluid phases; the existence of solid solutions was unknown at that time. Later, Gibbs' interface thermodynamics was extended to solid–solid interfaces, including the effects of applied mechanical stresses on γ [103–107]. It was realized that a solid–solid interface possesses two properties characterizing its tension: the interface free energy γ and interface stress τ, which are different quantities both conceptually and numerically [103–107]. (This distinction was already recognized by Gibbs [102].) Different interfacial processes in materials are controlled by either γ or τ, although some depend on both. According to Equation (1), the GB velocity is controlled by γ (not τ). It is worth noting that γ should not be confused with the GB cohesive energy, which is defined as the work of interface separation under given external conditions (fixed chemical composition or fixed chemical potentials of the components) [108–110].

Tremendous progress in interface thermodynamics has been achieved in the post-Gibbsian era. However, the main conclusion remains unchanged, i.e., solute segregation lowers the interface free energy and increases the interface stability. Accordingly, much research has been devoted to analyzing the physical mechanisms of GB segregation and searching for solutes exhibiting the strongest GB segregation. Several factors controlling the GB segregation have been investigated, including the solute–solvent atomic size mismatch, the chemical bond difference between the components, and the electronic and vibrational contributions. Extensive experimental measurements of GB segregation in many materials have been conducted [111–113] and practically useful correlations were discovered that could guide the search for stabilizing solutes.

For example, the segregation factor (the ratio of GB and lattice concentrations of the solute) is found to be inversely proportional to the solubility limit of the solute on the system's phase diagram [111,113]. The term "segregation engineering" was coined to describe the design approach in which the desired material's properties are achieved through GB segregation control [58]. A series of influential papers has been published examining the trends in GB segregation energy and harmonic vibrational entropy across many binary systems modeled with classical interatomic potentials [114–119]. It has been shown that the segregation energy exhibits significant site-to-site variations within the GB region and between crystallographically different GBs. These findings challenge the traditional characterization of GB segregation in polycrystals by a single "effective" segregation energy. Instead, a spectrum of segregation energies must be considered for a more reliable prediction of the segregation propensity and a more accurate calculation of the solute concentrations in GBs. Calculations of GB segregation spectra in polycrystalline alloys are computationally expensive but can be accelerated by machine learning methods [120].

On the theory side, Weissmuller published a thermodynamic treatment of GB segregation in NC materials with varying grain sizes [5,6]. A remarkable result of his work was the prediction of the existence of a finite grain size minimizing the total free energy of the NC material. At this grain size, the driving force for grain coarsening vanishes, and the material becomes stable against grain growth. The analysis in [5,6] was based on several approximations, including the assumptions of a dilute solution in the grains, solute saturation in GBs, and complete relaxation of the mixing energy in GBs. Later, Kirchheim [121–123], Krill et al. [124], and Shvindlerman and Gottstein [125] investigated the thermodynamics of grain stabilization in greater detail and arrived at similar conclusions. Their analysis also relied on many assumptions and approximations. Nevertheless, the theoretical possibility of fully stabilizing a NC

material by alloying was confirmed both in their work and many subsequent calculations based on more accurate models [40,45,47,53,63,84,126,127,127–133]; see examples in Fig. 1. In particular, the dilute solution approximation was replaced with the regular solution model and the segregation energy included both the chemical bonding effect and atomic size mismatch [131,134,135].

To facilitate alloy design based on thermodynamic stabilization, grain stability maps were constructed using the regular solution model for binary systems [47,53,126–129]. Such maps are typically presented with the GB segregation enthalpy plotted along the ordinate versus the mixing enthalpy in the bulk solid solution along the abscissa (Fig. 2). Different domains on the map represent alloys predicted to be stable or unstable with respect to grain coarsening or bulk phase separation (precipitation). The construction of the map usually assumes that the mixing enthalpy is positive, corresponding to alloys with a miscibility gap on the bulk phase diagram. Other critical factors, such as the chemical composition and temperature, are not reflected on the map.

Several modeling and simulation methods were developed to study GB segregation and its impact on NC stability. They included formal thermodynamic analysis [121–125,130], phase-field simulations [137–141], discrete atomistic simulations using the Monte Carlo method [47,128,142,143], molecular statics and dynamics [144–152], and first-principles density-functional theory (DFT) calculations [153–156]. In recent years, DFT calculations have been boosted by machine-learning methods. Some of the modeling approaches are in Refs. [61,83,84,134,157].

Perhaps the most direct demonstration of grain size stabilization comes from Monte Carlo simulations [47,128,143]. This method represents the atomic interactions by nearest-neighbor bonds on a rigid lattice [158,159]. No local structural relaxations or atomic vibrations are considered. However, all configurational effects are captured exactly without assuming a dilute, perfect, regular, or any other solution model. The average solute concentration in the alloy and the temperature can be varied as control parameters. No thermodynamic model is used: the Monte Carlo process automatically drives the polycrystal toward thermodynamic equilibrium under imposed boundary conditions/constraints. An example is shown in Fig. 3 [128]. In the elemental system, the grain size expectedly increases during the Monte Carlo simulation process (Fig. 3(a)-(c)). In the presence of solute atoms and under certain choices of the pair interaction energies, the system arrives at equilibrium with a *finite* grain size (Fig. 3(d)-(f)). It should be emphasized, however, that this prediction still relies on the approximation of pairwise atomic interactions and several other simplifying assumptions. The NC stabilization with a finite grain size was only observed for certain combinations of the interaction parameters. Whether such combinations can be realized in practice remains an open question.

There are at least three challenges in the computational search for stabilizing solutes. First, GB segregation thermodynamically competes with bulk phase transformations. Instead of forming a strong GB segregation that could potentially stabilize the single-phase NC state, the solute may prefer to precipitate as a second phase. Some of the grain stability diagrams mentioned above [47,53,126–129] attempt to include the second phase formation simplistically. A practically useful stability diagram should be based on an accurate thermodynamic description of the bulk phases appearing on the system's phase diagram, as well as possible metastable phases. The accurate bulk phase thermodynamics must be computed within the same statistical and atomic-interaction model as the GB segregation, which is a daunting task.

The second challenge is that the segregation models assume that the solute forms a uniform GB layer. To ensure strong segregation, preference is given to solutes that form a wide miscibility gap on the phase diagram. However, such solutes tend to form a strong short-

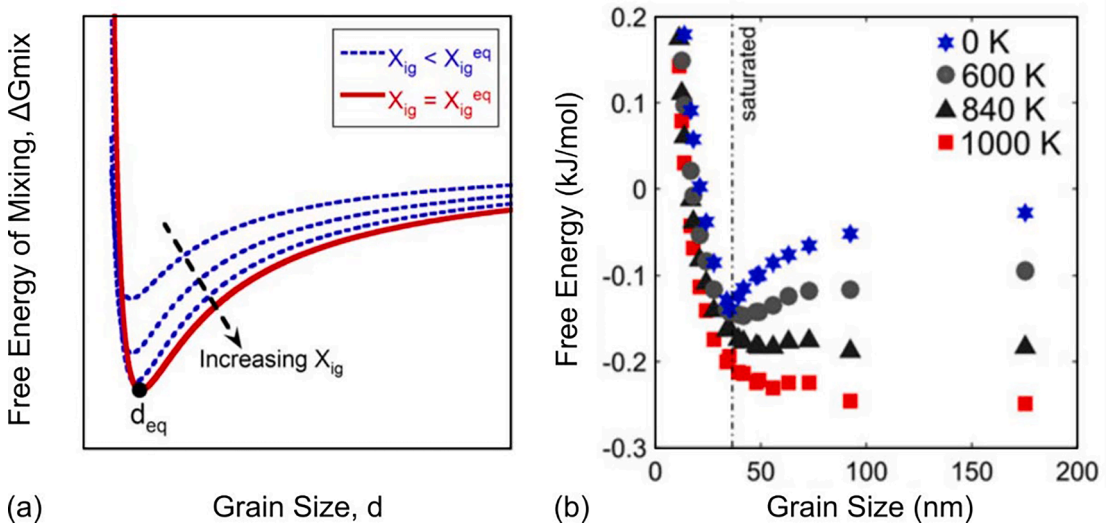

Fig. 1. Computational prediction of thermodynamically stabilized NC alloys. The plots show the free energy as a function of grain size obtained by (a) numerical calculation within the regular solution model [47], and (b) Monte Carlo simulations of 1 at.% solute alloy [136]. The minimum on the curves corresponds to the equilibrium grain size. In (a), the dotted lines show non-equilibrium curves converging to the equilibrium state (red curve) as solute concentration in GBs increases. In (b), the free energy curves calculated at several temperatures demonstrate that the NC alloy becomes stable below 800 K. (For interpretation of the references to color in this Fig. legend, the reader is referred to the web version of this article.)

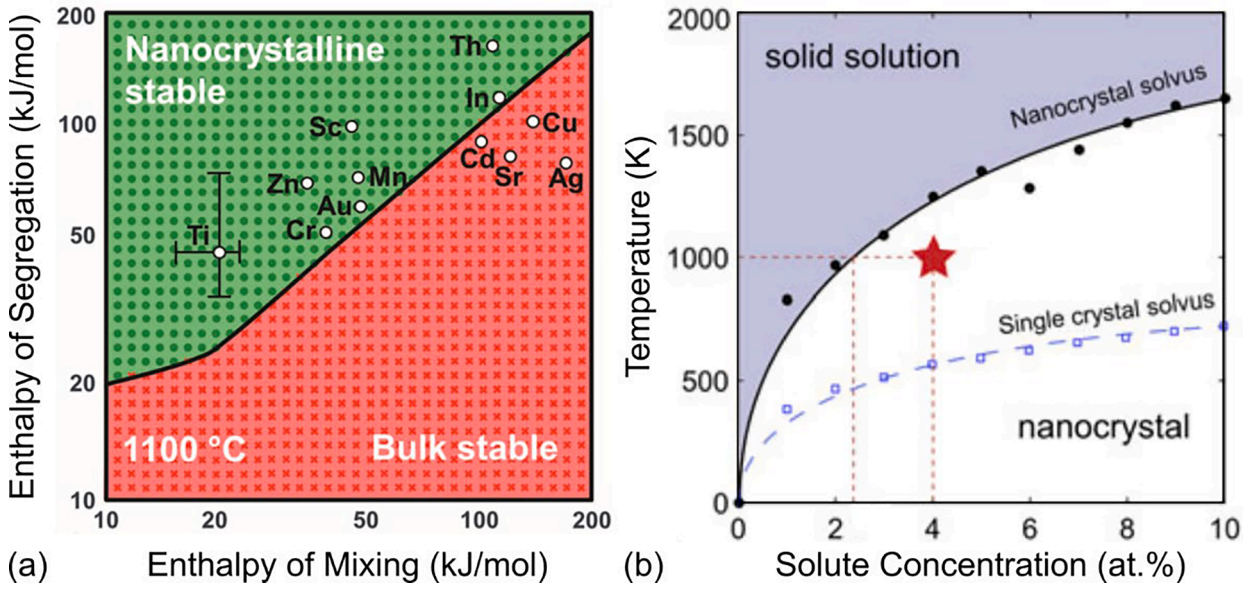

Fig. 2. Examples of NC stability maps. (a) Stability map for several tungsten-based alloys at 1100 °C calculated within the regular solution approximation. The red and green regions represent alloys in which the NC state is less stable and more stable than the single-crystalline solid solution [53]. (b) Phase diagram of a stable NC alloy obtained by Monte Carlo simulations [132]. The solid black and dashed blue lines represent the stable NC and single-crystalline solvus curves, respectively. The NC state with solute segregation is stable below the NC solvus line and unstable above it. The single-crystalline solvus appears on the traditional phase diagram assuming single-crystalline phases. The star symbol marks a 4 at.% solute alloy in which the grains of the stable NC alloy contain about 2.4 at.% of the solute. (For interpretation of the references to color in this Fig. legend, the reader is referred to the web version of this article.)

range order, leading to a highly non-uniform distribution in GBs. Instead of a uniform layer, the solute atoms often form islands or clusters decorating the GBs. For example, this behavior was observed in the recent atomistic simulations of Pb in Al GBs [148–150]. The clustering is especially pronounced in GBs with strongly inhomogeneous and/or anisotropic structures, as illustrated by the example of Mg segregation at low-angle Al GBs [152] (Fig. 4). Alternatively, when solute segregation is close to saturation, the segregated layer can have significant holes/gaps (Fig. 4(c,d)) [160]. Compositional fluctuations and solute patterning in GBs have been observed by atom probe tomography [161–163]. The existing segregation models do not capture such heterogeneous forms of GB segregation. In addition to reducing the GB free energy, the clusters and other heterogeneous features can pin the GBs and stabilize the grain size through the kinetic mechanism discussed next. Moreover, GB segregation is sensitive to GB crystallography and GB structure. As such, it can vary widely in a polycrystal, from one GB to the next [160] (Fig. 4(a)).

The third issue is related to the *global* character of all previous calculations/simulations of the NC stability. In the numerical calculations [5,6,47], the total free energy of the system is expressed as a function of the GB site fraction f (assumed to be proportional to the average grain size D) within the regular solution model for the lattice and GB sites. The total free energy is then minimized with respect to f under the constraints of GB/lattice equilibrium and a fixed total amount of the solute (closed system). If a minimum occurs at a finite f, then it is said to represent a stable NC state. This reasoning tacitly assumes that a slight variation in size of one grain causes immediate redistribution of the solute atoms across the entire system to create a new GB/lattice equilibrium with slightly different GB and grain concentrations. The Monte Carlo simulations [47,128] are similarly global: the solute and solvent atoms are randomly exchanged across the entire system, ensuring fast global re-equilibration after each fluctuation in the number of GB sites. This “spooky action at a distance” (Einstein’s “spukhafte Fernwirkung”) is incompatible with the finite rate of solute diffusion.

Every polycrystal has a grain size distribution. By Equation (1), every GB is driven by a different capillary force in a different direction, depending on the local curvature and constraints from adjacent boundaries. The GB displacements are accompanied by local changes in the GB area and thus absorption or rejection of some amount of the solute segregated at the GBs. This, in turn, causes a *diffusion-controlled* redistribution of the solute atoms. The GB displacements and the solute diffusion are *local* processes that do not have to follow the global closed-system constraint. It remains unclear whether the predicted total free energy minimum with respect to the *average* grain size represents a structure stable against perturbations in the grain size distribution. Answering this question would be a good topic for further research.

Due to the abovementioned complexities, the grain stability maps based on the thermodynamic criteria can only be considered a useful general guide and should not be taken literally.

2.4. Kinetic stabilization

We next discuss the kinetic mechanism of nanostructure stabilization. In this case, the grain growth is suppressed by reducing the

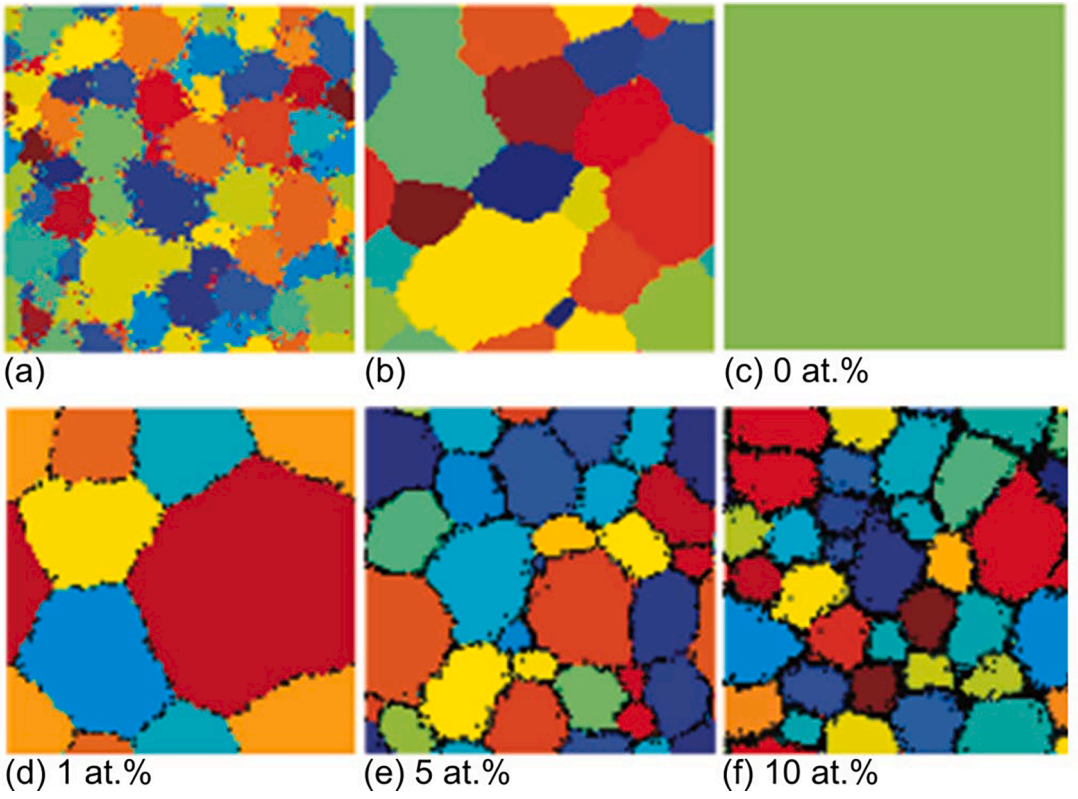

Fig. 3. Evolution of a NC grain size material in Monte Carlo simulations at 500 °C (adapted from [128]). Upper row: evolution of a solute-free system. The initial grain size (a) coarsens (b), and the material eventually transforms into a single crystal (c). Lower row: final states of simulations with the solute concentrations of (d) 1 at.%, (e) 5 at.%, and (f) 10 at.%. The equilibrium grain size decreases with increasing solute content in the alloy.

GB mobility, which can be achieved due to the solute drag effects [137,141,164–176] or by Zener pinning of GBs by small second-phase particles [137,177–185]. Both approaches have deep roots in classical metallurgy and have been extensively studied for decades as fundamental phenomena and alloy design strategies for applications requiring stable microstructures. Nevertheless, some aspects remain the subject of current research.

Solute drag arises due to GB segregation, which is also required for the previously discussed thermodynamic mechanism of nanostructure stabilization. A moving GB must drag the segregation atmosphere with it, which is a diffusion-controlled (and thus slow) process. A larger driving force is required to move a segregated GB than the same GB in a pure metal or in a uniform solution. Analytical models of the solute drag process developed by Cahn [164] and Lücke et al. [186] predict a highly nonlinear relation between the GB velocity v and the drag force F. At a critical velocity v^*, the drag force reaches a maximum separating two kinetic regimes. At low velocities ($v < v^*$), the GB drags the segregation atmosphere. In the high-velocity regime ($v > v^*$), the GB breaks away from the initial atmosphere and forms a lighter atmosphere that poses less resistance to its motion. The maximum in F sets the upper limit F^* of the drag force opposing the capillary force. Once the capillary force overcomes the maximum drag force F^*, GB motion continues with less resistance, resulting in rapid grain growth. In most cases, the maximum drag force diminishes with increasing temperature. The maximum of the function $F(v)$ predicted by classical models [164,186] has been confirmed by several theoretical and simulation methods, as shown in Fig. 5.

Existing analytical and numerical models of solute drag [141,164–166,168–171,173–176,186] have limitations similar to those of the thermodynamic stabilization models. Most solute drag models consider a single planar GB with a uniform segregation atmosphere. As mentioned above, GB segregation can be highly non-uniform. In a polycrystalline sample, the segregation can vary widely from one GB to the next according to crystallographic parameters and curvature. Some GBs can break away from the atmosphere while others remain pinned. The impact of the significant dispersion of the capillary and solute drag forces on grain size distribution and grain growth has not been studied sufficiently.

Some of the limitations of the analytical solute drag models [164,186] have been overcome in computer simulations using phase-field [137,141,165,187,189,190] and phase-field crystal [188] methods, kinetic Monte Carlo simulations [175,176,191–193], and MD simulations [167,170,172,191,194,195]. Most simulations consider a single planar GB, but many are for polycrystalline samples or at least curved GB segments. Some simulations capture the inhomogeneous solute distributions in GBs. Recent two-dimensional phase-field simulations suggest that solute drag reduces the time exponent of grain growth relative to the parabolic growth [189] and can

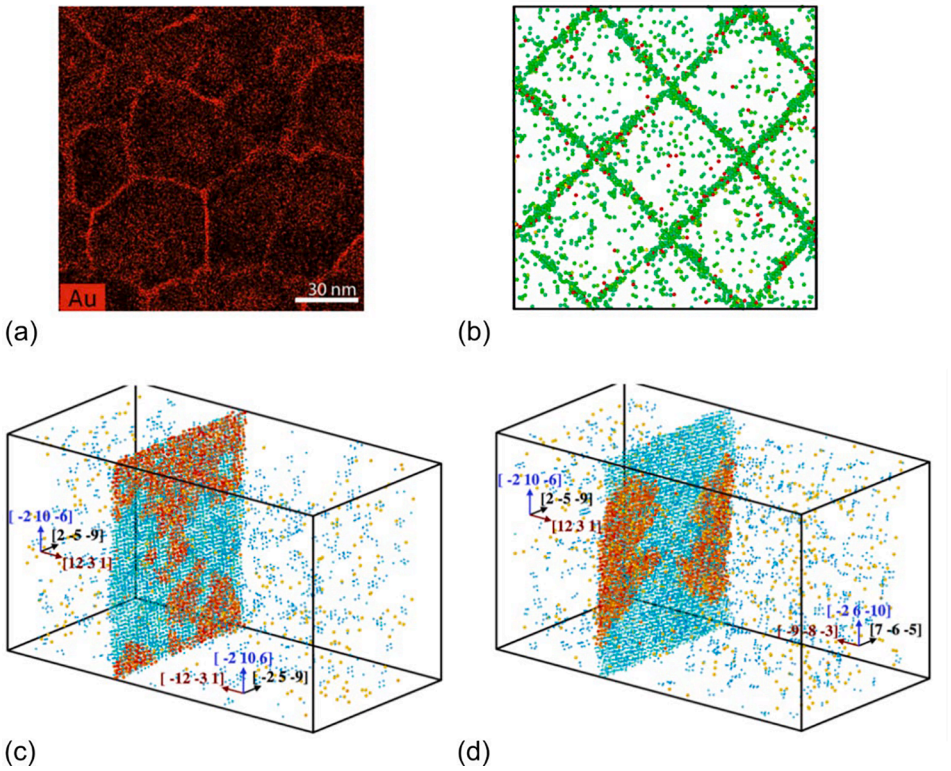

Fig. 4. (a) STEM-EDS image of a Pt-10at%Au film after a 30 min anneal at 775 K [160]. Note the nonuniform destitution of Au (bright color) in the GBs. (b) Distribution of Mg atoms in a low-angle twist GB in Al obtained by off-lattice Monte Carlo simulations at 700 K [161]. The red and green colors represent Mg atoms and distorted Al atoms, respectively. The Mg distribution is highly nonuniform due to the preferential Mg segregation to GB dislocations. (c,d) Examples of Au segregation in typical high-angle GBs in Pt obtained by off-lattice Monte Carlo simulations at 775 K [160]. The Au and Pt atoms are shown in orange and blue, respectively. Note the holes in the segregated layer (c) and the formation of segregation islands/clusters (d). In (b)-(d), the atoms in nearly perfect FCC environments are invisible for a clearer presentation of GB segregation. (For interpretation of the references to color in this Fig. legend, the reader is referred to the web version of this article.)

even trigger abnormal grain growth [170] as shown in Fig. 6.

MD is the most powerful approach as it provides access to all details of solute distribution and GB motion. MD simulations do not rely on any approximations other than those built into the interatomic potential. Unfortunately, the MD timescale is too short for reliable modeling of solid-state diffusion by the vacancy mechanism. Thus, solute diffusion inside the grains cannot be adequately captured. GB diffusion is much faster than lattice diffusion and can be readily observed and accurately quantified by MD [152,167,172,196–198]. Recent MD simulations [167,172] have shown that GBs drastically accelerate solute diffusion in lattice regions swept by the GB motion. This provides sufficient diffusion mobility to observe solute drag on the MD timescale. Furthermore, fast GB diffusion creates a highly non-uniform redistribution of the solute atoms inside and behind the moving boundary. In some cases, these compositional fluctuations are akin to solute clusters, which amplify the solute drag by a mechanism similar to the Zener pinning. These findings reveal the critical role of in-plane GB diffusion in the solute drag process. Note that in-plane GB diffusion is not included in the classical models [164,186], which treat the GB as compositionally uniform, thus not requiring in-plane diffusion.

Zener pinning is another kinetics-based mechanism of reducing GB mobility [137,177–185]. In this case, small particles scattered over the material act as pinning obstacles imposing a significant resistance to GB migration, which can effectively immobilize the GBs. The particles can be introduced externally or by precipitation from a solid solution by a phase transformation. In the latter case, the process typically involves mechanical attrition of the base metal with much harder insoluble components, followed by a thermal treatment during which nanometer-scale clusters precipitate in the lattice and at GBs [7,42,68].

Assuming that the pinning particles are spherical with a radius r, the driving force required for unpinning the GB is [178]

$$p_{max} = \pi r \gamma n, \tag{2}$$

where n is the number of particles per unit GB area. This equation assumes a 45° contact angle θ between the GB and the particle, which maximizes the force (Fig. 7). Once the driving force exceeds the critical value ($p > p_{max}$), the GB breaks away from the set of pinning particles, only to be stopped by a new set. The larger the number of particles n, the greater the resistance to GB motion. Smaller particles are more effective stabilizers at the same volume fraction of the second phase. In recent atomistic simulations of the Zener pinning of Cu GBs by Ta nanoclusters [178], the GB free energy back-calculated from Eq.(2) was found to be independent of the cluster

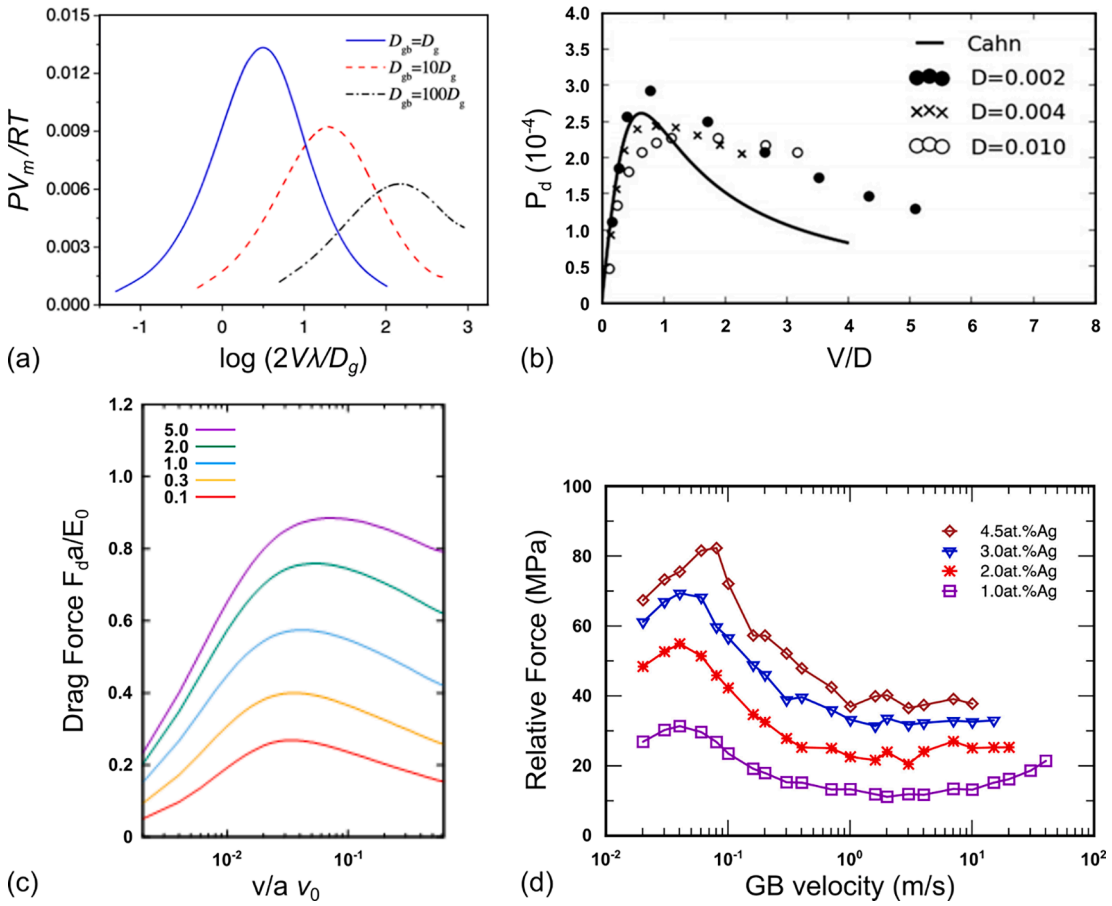

Fig. 5. Solute drag force as a function of GB velocity predicted by several simulation methods. (a) Phase-field simulation with three different ratios of GB diffusivity D_{gb} to grain diffusivity of solute D_g [187]. (b) Phase-field crystal simulation for different values of GB diffusivity [188]. The results are compared with Cahn's analytical model [164]. (c) Kinetic Monte Carlo simulation for several values of GB diffusivity of the solute relative to lattice diffusivity [175]. (d) MD simulations for Cu-Ag alloys at 1000 K with four different chemical compositions [167]. In all cases shown, the drag curve exhibits a maximum at a critical velocity.

size and in good agreement with independent calculations, validating the Zener model.

As with other stabilization methods, the Zener mechanism has its limitations. The uniformity of the spatial distribution of the particles is difficult to control. The inevitable particle coarsening reduces their pinning efficiency. The participles tend to dissolve at high temperatures, setting the upper bound of high-temperature stabilization by this mechanism.

Research on kinetically pinned microstructures has focused on manipulating the nano-scale particles composed of oxides/carbides/nitrides, intermetallic compounds, metal solutes clusters or larger phases, or a combination of several types, including GB segregated solutes [60,61,67,200–223]. The solute clusters, typically with diameters no greater than 5 nm, exhibit a coherent or semi-coherent relationship with the parent lattice. The number density of the clusters typically surpasses 10^{23} particles per cubic meter. The combination of the small size and high number density enables the particles (or clusters) to preserve nano-grain sizes, typically less than 100 nm, up to high temperatures. This, in turn, permits the successful consolidation of powders into bulk NC materials [67,88,130,178,184,185,224–244].

In the domain of Fe-based ODS alloys, the emphasis of research has been on utilizing high-energy mechanical alloying, aiming to achieve a high number density of oxide particles based on yttrium or Y-Ti [200,245–251]. In most cases, Ti was employed as an oxide-refining agent [246–248], although a few studies explored other transition metals, or even Al, for this purpose [250,252]. The controlled incorporation of such additions, whether in oxide or metallic form and the degree of their dissolution in the Fe matrix during mechanical alloying remain active areas of ongoing research [253]. Heat treatment after mechanical alloying leads to the formation of complex nanoscale oxides exceeding 5 nm in size or coherent oxide clusters with diameters ranging from 2 to 5 nm. While extensive research has been conducted on Y-based oxides, investigations of oxides based on group IV elements such as Zr and Hf are relatively new [200,245]. Exploring alternative oxides based on group IV elements presents an intriguing opportunity for tailoring the properties of ODS alloys. Overall, the work on ODS alloys has allowed some of the first bulk NC metals to be produced and evaluated for mechanical and physical properties.

Trimodal aluminum (Al) alloys with a nano-scale microstructure typically consist of three distinct phases or microconstituents: a

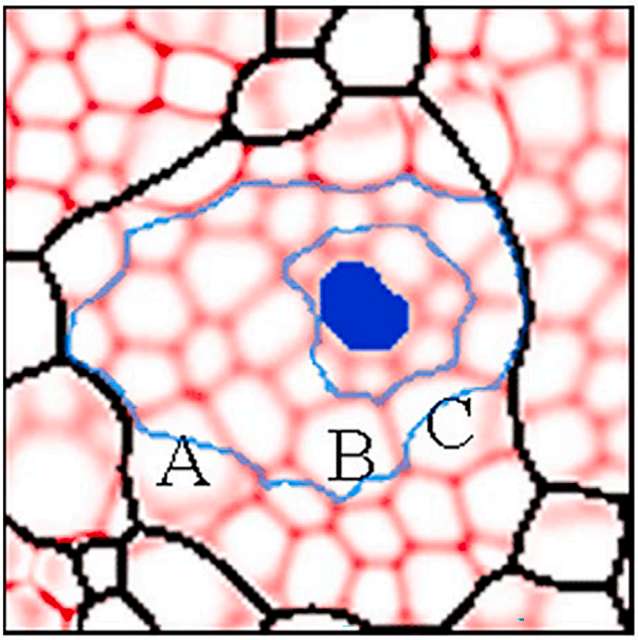

Fig. 6. Phase-field simulation of abnormal grain growth triggered by solute drag [170]. The red color indicates solute-enriched regions replicating the initial structure with GB segregation. Black lines correspond to the current GB positions. The blue-colored grain, which is about the same initial size as grains A, B, and C, grows abnormally to a large size surrounded by much smaller neighbors. The physical size of the image is approximately 10x10 micrometers. (For interpretation of the references to color in this Fig. legend, the reader is referred to the web version of this article.)

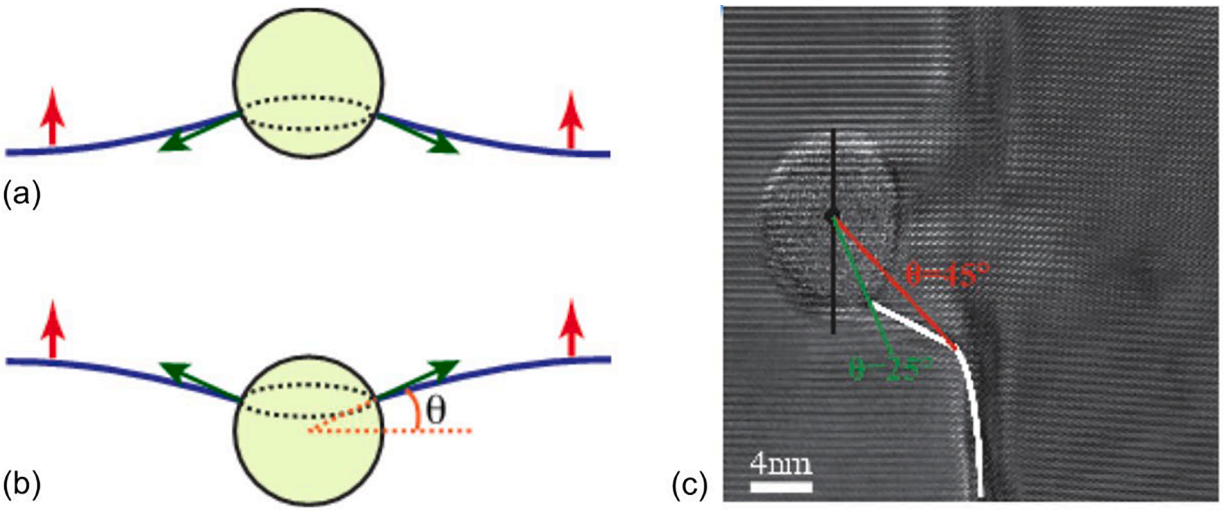

Fig. 7. Interaction of a moving GB with a spherical obstacle in the Zener model of GB pinning [178]. (a) The GB moving up (red arrows) encounters an obstacle. GB tension (green arrows) pulls the GB towards the obstacle, creating an attractive force. (b) The GB tries to break away from the obstacle, but the capillary force pulls it back, creating the pinning effect. (c) high-resolution TEM (HRTEM) image of a Ta nanoparticle pinning a GB in a Cu-Ta-Zr alloy [199]. The red and green lines show two possible choices of the particle-GB contact angle used for comparison with the Zener model. (For interpretation of the references to color in this Fig. legend, the reader is referred to the web version of this article.)

coarse-grained phase, a NC or UFG phase, and a hard-phase particulate reinforcement [254–260]. The coarse-grained phase typically consists of around 1 μm size grains, and contributes to the alloy's overall ductility. The NC or UFG phase, with grain sizes ranging from sub-100 to 500 nm, significantly enhance the material's strength through grain refinement and dispersion strengthening mechanisms. The third phase, such as the hard particulate reinforcement (e.g., B4C), though other ceramic phases have also been tried (e.g., SiC, or TiB2), further strengthens the material by hindering dislocation motion and preventing grain growth, thereby improving the overall hardness and wear resistance [254–258,261]. The interfaces between the microconstituents play a critical role in the performance of

trimodal alloys by acting as "bridges" that efficiently transfer stress between the coarse-grained phase, the UFG phase, and the hard-phase reinforcement. This efficient load transfer across the interfaces helps to enhance the overall mechanical properties of the alloy, particularly its strength and toughness.

A similar stabilization approach has also been utilized in the development of NC Cu-based alloys, where Zener pinning mechanisms—through the use of ceramic, intermetallic compounds or other metal phases—help to strengthen and stabilize interfaces [60]. These alloys can exhibit a wide immiscibility gap [60,130,239,303]. Like the ODS alloys, they are primarily synthesized via high-energy mechanical alloying or other SPD methods, such as HPT, or PVD. Cu binary base systems with a positive immiscibility gap can be partitioned into two groups based on their equimolar enthalpy of mixing ΔH_m between the elements: systems with a lower enthalpy of mixing, $\Delta H_m < 10 kJ/mol$ (such as Cu–Ag, and Cu–Co), and those with a higher ΔH_m, such as Cu–Mo, Cu–W, Cu–Ta, and Cu–Nb [218,220,239,899]. Alloys of the first group exhibit larger solubility limits. In contrast, alloys of the second group only allow a limited degree of alloying and exhibit a strong tendency to separate into two phases [218,220,239,899]. During the synthesis process or upon annealing, coherent/semi-coherent nanoclusters with approximately spherical morphologies precipitate from the oversaturated solid solution. These clusters are scattered stochastically throughout the microstructure, largely suppressing its coarsening and improving the alloy performance.

In recent years, the kinetically stabilized Cu-Ta system has been extensively researched to understand the formation, structure, morphology, chemical composition, coherency relationship, and spatial optimization of Ta-based nanoclusters (Fig. 8) together with other dopant elements. Research on Cu-Ta and other phase-separated Cu-based alloys has demonstrated that kinetic stabilization by nanoclusters can be more potent than thermodynamic stabilization. Recent research has also shown the possibility of retaining

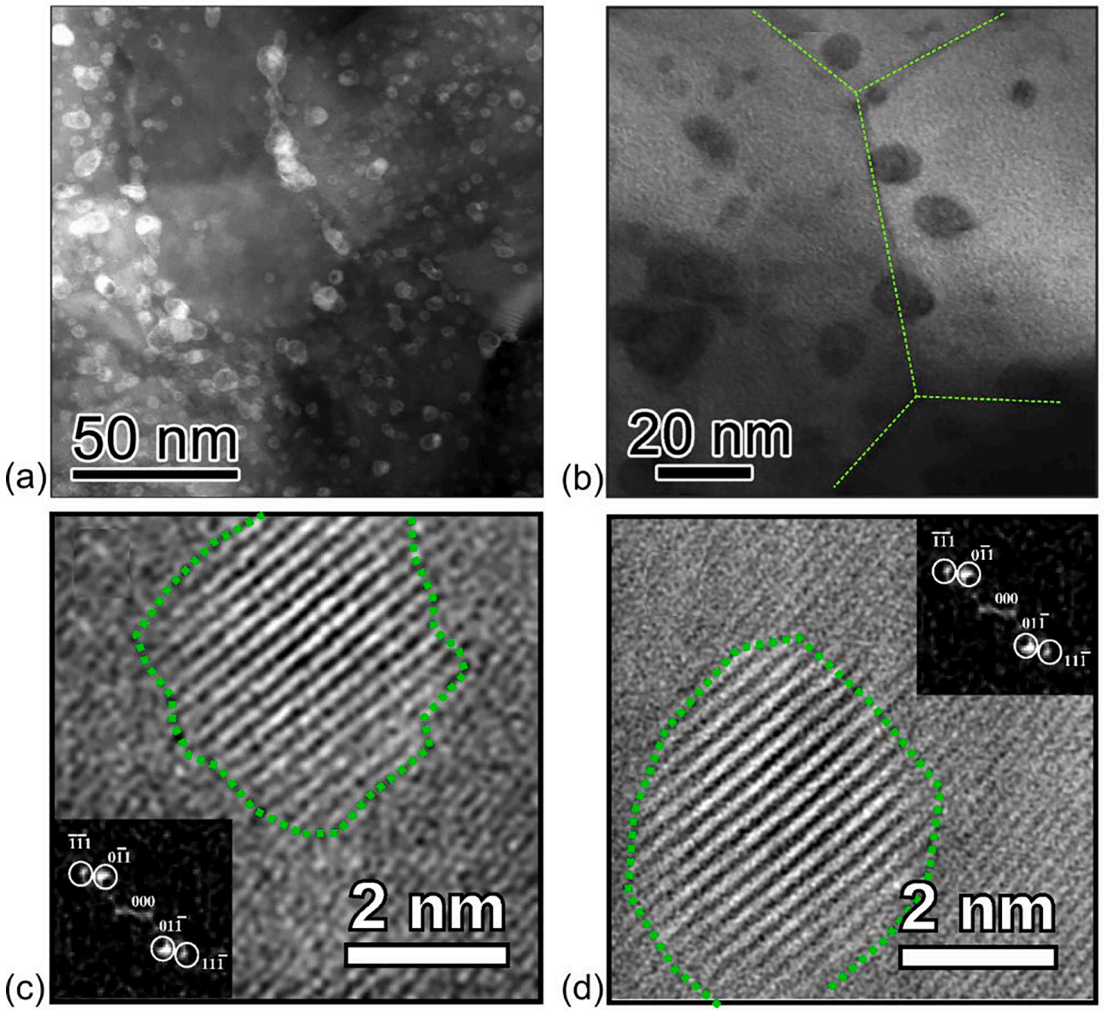

Fig. 8. Representative microstructure of immiscible NC Cu-Ta alloys produced by mechanical alloying. (a,b) High-resolution high-angle annular dark-field (HAADF) scanning transmission electron microscopy (STEM) image of Cu-3at.%Ta alloy consolidated by ECAE [184]. (a) Typical grain decorated with Ta clusters. (b) Zoom-in image showing Ta clusters residing at and near GBs. Dashed lines outline the approximate GB positions. (c,d) HRTEM images of (c) coherent (size = 3.47 nm) and (d) semi-coherent (size = 4.11 nm) Ta nanoclusters in NC Cu-10 at.% Ta alloy [224]. The cluster/matrix interface is outlined. Inset: Indexed selected area electron diffraction (SAED) patterns confirming nanocrystallinity.

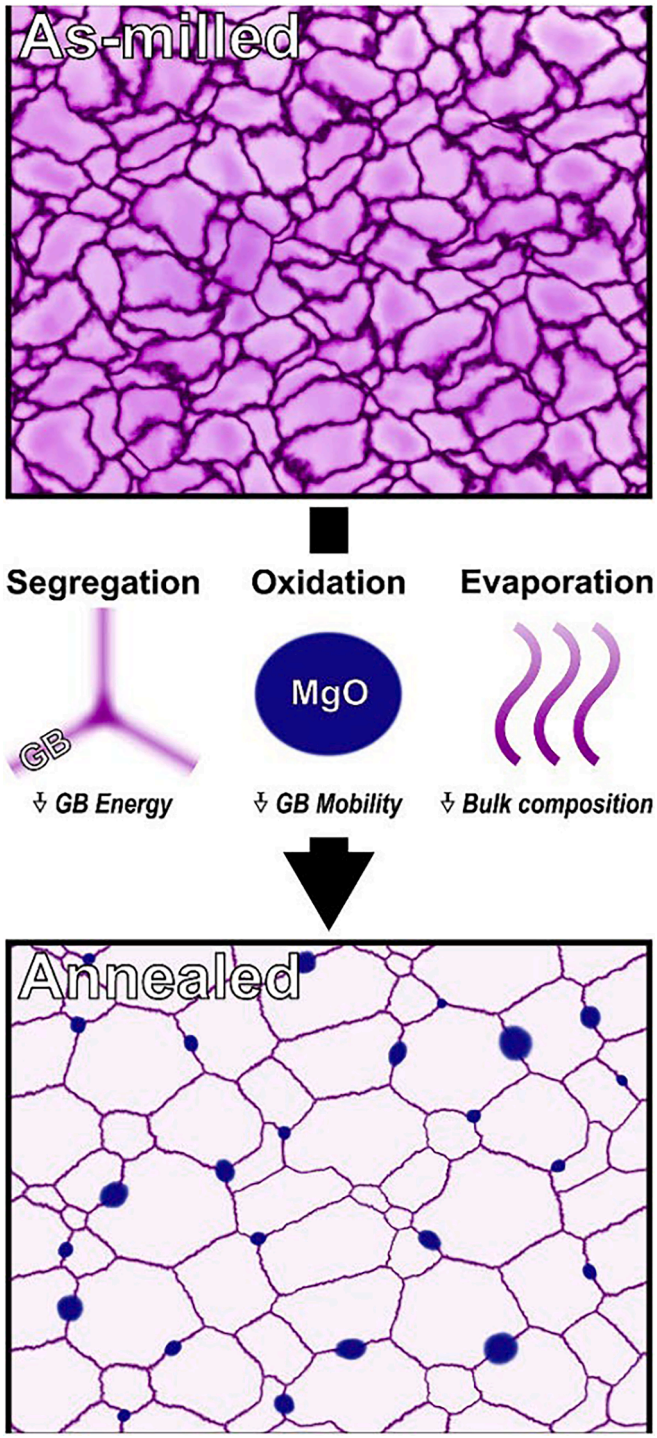

Fig. 9. Schematic illustration of microstructure development in ball-milled NC Fe-Mg alloy [262]. Upon annealing, Mg segregates to Fe GBs, reducing their free energy and causing solute drag. At the same time, Mg oxidation creates an array of MgO particles pinning the GBs by the Zener mechanism. The nanostructure obtained is stabilized by a combination of the thermodynamic and kinetic mechanisms. The darker shade of purple corresponds to a higher Mg concentration. (For interpretation of the references to color in this Fig. legend, the reader is referred to the web version of this article.)

nanograins at homologous temperatures exceeding 0.7 for durations surpassing 10,000 h of exposure [233]. The extreme stability of the microstructure has allowed the milled Cu-Ta powder mixture to be fully consolidated utilizing equal channel angular extrusion (ECAE) on a reasonably large scale. Powder processing can be scaled up in size like for ODS alloys, enabling the production of larger-scale billets through the more traditional processes of HIPing, forging, and extrusion, while retaining the nanostructure. Due to the strong stabilization provided by the Ta clusters, Cu-Ta alloys exhibit extreme responses under quasi-static loading, dynamic (shock) loading, and intense irradiation. More details related to the synthesis, processing, and properties of Cu-Ta and other immiscible alloys are discussed in subsequent sections of this review.

2.5. Thermodynamics or kinetics?

Grain growth retardation by alloying has been demonstrated in numerous alloy systems, including Fe-Based: Fe-Ni [211,212], Fe-Ag [213], Fe-Cu [210], Fe-Cr [214], Fe–Zr [215,245], Fe–Ti [216], Fe-Mg [262], and Fe-Al [203,204]; Ni-Based: Ni-Co [92,223], Ni-Fe [263–265], Ni–P [266], Ni–W [40], Ni-Cu [267], and Ni-Mn [268,269]; Al-Based: Al-Pb [270,271], Al-Mg [272,273], Al-W [274], and Al-Cu [275]; Pd-Based: Pd-Fe [276,277], Pd-Y [278], and Pd–Zr [124]; Cu-Based [201,202,205–207,209,210,218–220,222,279,280]: Cu-Nb, Cu-Zr, Cu-Fe, Cu-Ag, Cu-Bi, Cu-Sb, Cu-Pb, Cu-Ta, Cu-W, Cu-Mo, Cu-Y and Cu-Cr. Various arbitrary systems including: Ru–Al–Fe [281], Ti–Cu [282], Y–Fe [283], TiO_2–Ca [284], Mo-Au [285], Co-P [286,287], Co-W [288], Ag-Cu [289], Au-Ni [290], Cr-Ni [291], Zn-Ni [292,293], Nb-Cu [294], Pt-Au [295], and W-Cu [296]. Many of these studies were enabled by recent advances in characterization methods. Using the focused ion beams (FIBs) became more prevalent [297], significantly improving the capability to precisely extract and image microstructures in specific locations by techniques such as TEM/STEM and atom probe tomography (APT) [297,298] and providing accurate quantification of the excess solute at GBs and small-phase chemistry.

Despite the abundant evidence of grain growth inhibition by alloying, the exact mechanism responsible for the effect remains the subject of debate and ongoing research [61,71,172,262,299–302]. To our knowledge, there is no convincing evidence that the fully thermodynamically stabilized NC state (minimizing the total free energy) predicted by theory [5,6,121–123,125] and simulations [40,45,47,53,63,84,123,124,124–130,141] has been realized in practice in any system.

Clean separation of the thermodynamic and kinetic mechanisms is a challenging task. The only case in which the distinction is clear is the Zener pinning of nano-grains in highly immiscible alloys such as Cu-Ta. In this case, almost all solutes exist in the form of nanoclusters (Fig. 8). The Ta concentration in the lattice and at GBs is small. The lack of any significant GB segregation rules out the GB free energy reduction and solute drag as stabilization mechanisms. In fact, the impingement of moving GBs on the clusters is likely to damage the GB structure and *increase* the GB energy. The stabilization mechanism is purely kinetic.

Separation of thermodynamic stabilization from the solute drag effect is much more difficult. Solute atoms segregating to GBs and reducing their free energy also reduces the GB mobility due to the solute drag. Arguably, the latter effect is stronger than the former. Indeed, the GB-free energy depends on the solute concentration and temperature as a relatively slow (roughly logarithmic or linear) function, while the GB mobility increases exponentially. Thus, kinetic stabilization of nanomaterials can be more effective than thermodynamic stabilization. Recent MD simulations back this argument [172], but convincing experimental validation is still lacking. Carefully crafted experiments are required to further clarify the roles of the thermodynamic and kinetic factors.

In the meantime, it is assumed that the thermodynamic and kinetic mechanisms can coexist and interact. This view is embodied in the so-called thermokinetic model [71,299,300], which considers a concurrent operation of the solute drag and the GB-free energy reduction. Furthermore, there is experimental evidence that some NC materials can be stabilized by a combination of solute segregation and Zener pinning. Amram and Schuh [262] studied the thermal stability of ball-milled Fe-Mg alloys in a wide range of compositions and temperatures. Mg was found to segregate at GBs and oxidize, forming nm-scale MgO precipitates (Fig. 9). The nonmonotonic composition dependence of the annealed grain size was explained by a superposition of the thermodynamic mechanism and kinetic stabilization due to solute drag and Zener pinning by the MgO precipitates. Similarly, Cunningham et al. [285] have demonstrated a gradual shift from segregation-induced stabilization towards Zener pinning by Au nanoclusters in the Mo-Au system.

One of the factors complicating the investigations of stabilization mechanisms is the effect of impurities. Precise characterization of solute concentration has improved our understanding of the significant role played by contaminations in the stability of NC materials [303–305]. In particular, interstitial carbon, nitrogen, oxygen, and sulfur are commonly observed in fabrication processes such as mechanical alloying and electro-deposition [303]. Even in vapor deposition methods, which are more carefully controlled, trace contamination persists. Although low contamination levels may not seem particularly important, even ppm-level contamination can influence GB mobility and contribute to embrittlement by reducing GB cohesion [306–309]. Small clusters that emerge due to contamination are usually coherent with the matrix and have diameters of only a few nanometers [67,200]. Typically, such clusters exhibit considerable partitioning of interstitial elements, reducing the average atomic number and posing challenges to detecting nanoclusters using traditional X-ray diffraction and TEM. The short-circuit GB and dislocation pipe diffusion of impurities [310] at elevated temperatures can cause a transition from the GB-segregated state to a GB-precipitated state or vice versa [184]. Recent research has shown that contamination plays a role in amorphous intergranular films, which can stabilize microstructures against grain growth [305,311].

To conclude this section, the past decade has seen significant progress in the fundamental understanding of stabilizing nanostructures in many alloys at moderately high temperatures. Some cutting-edge systems push boundaries further by demonstrating the ability to preserve their nanostructure at temperatures surpassing 80 % of the melting point for extended durations. Although this is a significant advance, many engineering materials are exposed to even higher homologous temperatures for hundreds, if not tens of thousands of hours throughout their lifespan in practical applications. Designing NC alloys exhibiting such extreme thermal stability is one of the greatest challenges in modern materials science and engineering. Achieving this goal hinges upon further progress in

understanding the nanoscale stabilization mechanisms and the physical properties of stabilized nanomaterials. The next section discusses our vision of future research in this direction.

3. Stabilization of nanocrystalline materials: Outlook for future research

In this section, we discuss several unresolved problems, including unexplored or poorly explored research directions, and discovery opportunities in the field of nanostructure stabilization.

3.1. How do we quantify stability?

Several issues complicate investigations of stability in NC materials. One of them is the lack of a well-defined metric, or Fig. of merit, of structural stability. For example, the temperature–time domain in which the stability of nanomaterials is assessed varies from one material to another, from one intended application of the material to another, and even among different research groups. If a chosen characterization method detects significant grain coarsening after 10 h of exposure at 1000 °C in one material and after 100 h at 700 °C in another material, which material is considered more stable? It should also be mentioned that, in most tests, the material is only exposed to high temperatures for a few hours or, at most, a few hundred hours [40,53,312–315]. These times are one to two orders of magnitude shorter than required for many real applications. It is questionable whether the conclusions about alloy stability derived from such short-term thermal excursions are relevant to commercial alloys that are required to withstand high temperatures for thousands of hours. It is desirable and, in fact, necessary to adopt technologically relevant standards of stability tests for nanomaterials. This is especially important for materials designed for service in extreme environments.

Another issue concerns the choice of structural parameters characterizing materials' stability. Most stabilization efforts focus on retaining the nanometer-scale grain size. However, grain size alone does not adequately represent the structural characteristics that must be retained for the material's performance. Other structural elements that should be considered include the crystallographic texture, nano-twin density, grain size distribution, and the presence or retention of different phases in nanocomposites. Completely suppressing grain growth is not always necessary for achieving the desired properties. Some mechanical and physical properties are controlled by the microstructure of the *trans*-granular regions, which should also be stabilized.

3.2. Is grain growth driven by grain boundary curvature?

Average grain size alone does not accurately represent the thermodynamic driving force for grain coarsening. The common justification for using the average grain size is that it correlates with the average GB curvature, which is assumed to be proportional to the driving force of GB migration according to Eq. (1). While the velocity-curvature relation predicted by this equation has been verified by bicrystal experiments [316] and computer simulations [172,184,317–319], recent experimental observations in real polycrystalline materials have revealed significant deviations from this relationship [320]. For example, recent studies of grain growth in polycrystalline Ni [321] and $SrTiO_3$ [322] found no correlation between the GB curvature and the GB velocity (Fig. 10a). In fact, 37 % of GBs were observed to migrate in the direction *opposite* to their curvature [322]. A recent MD study [323]confirmed the absence of a correlation between the GB velocity and curvature during grain growth in model nanocrystals. The discovery that GB migration in polycrystals does not follow Eq.(1) suggests that the total energy reduction driving grain growth can be accomplished by mechanisms different from the curvature-driven GB migration. For example, it was found that the reduction in total GB energy during grain

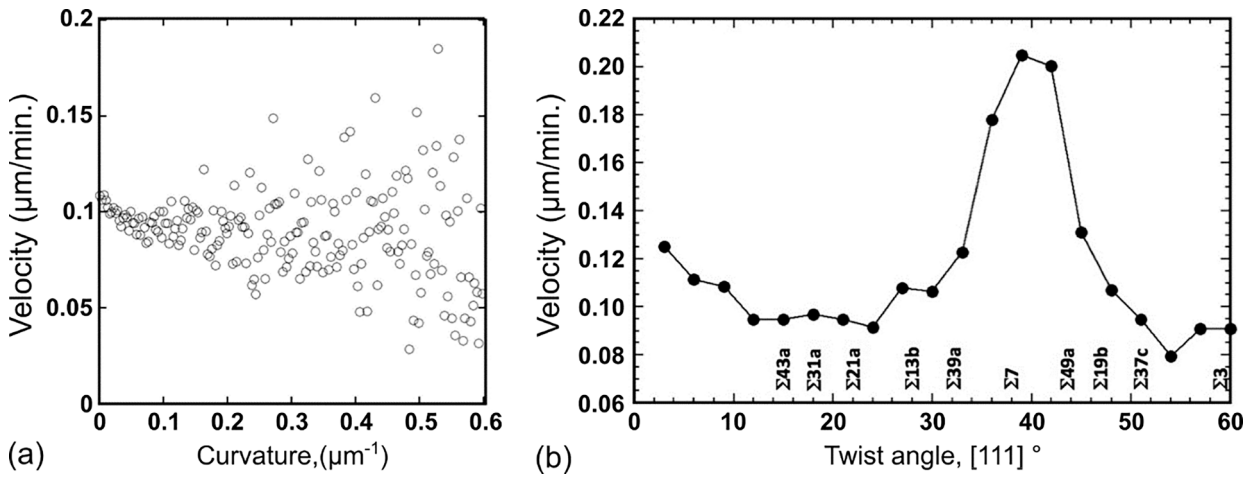

Fig. 10. Grain growth in polycrystalline Ni [321]. (a) GB velocity as a function of GB curvature. Note the absence of correlation beyond the statistical scatter of the data points (standard deviation is of the same order as the mean velocity). (b) GB velocity as a function of misorientation angle for [111] twist GBs. Several coincidence site lattice (CSL) GBs are labeled by the reciprocal CSL density Σ.

coarsening in Ni occurs by eliminating higher-angle GBs in favor of lower-angle GBs [324].

The curvature-driven model also contradicts the commonly observed phenomenon of grain growth stagnation in many polycrystalline materials [325–327]. The grain growth virtually stops, preventing the material from transforming into a single crystal as thermodynamics prescribes. Furthermore, some controversy remains regarding the role of GB crystallography. The latter has been found to strongly influence GB migration in experiments on Ni [321] (Fig. 10b). On the other hand, in polycrystalline α-Fe, GB mobility does not correlate with GB crystallography [328]. While the mobility of individual GBs is known to be misorientation-dependent [101,316,321,329,330], the impact of GB crystallography on GB mobility in polycrystals deserves more detailed future investigations.

We emphasize that the experimental results mentioned above do not invalidate Eq.(1), which is grounded in irreversible thermodynamics and can be safely used in fundamental studies of *individual* GBs not subject to constraints. The equation may serve as a general, qualitative guide in the pursuit of nano-grain stabilization, suggesting that the latter could be achieved by reducing the GB mobility or lowering the GB free energy. However, grain coarsening in real polycrystals does not follow this simple relation. In the future, more accurate models of GB migration must be developed to enable more reliable stability predictions required for designing new NC materials.

There can be several reasons why polycrystals do not follow the curvature-driven kinetics. One is the significant dispersion of GB mobilities, which can span several orders of magnitude. In addition to the impurity effect on GB dynamics, several other intrinsic factors can cause the mobility variations. As mentioned above, the mobility of individual GBs depends on GB crystallography. GBs can undergo a roughening transition [176,331,332], which changes the GB migration mechanism and can result in a dramatic change in GB mobility. Smooth GBs existing below the roughening transition are characterized by much lower mobility than rough GBs above the transition. Computer simulations [326] have shown that even a small fraction of smooth GBs can effectively pin the polycrystalline structure and cause grain growth stagnation.

GB faceting is another transition [333] influencing GB mobility. Adjacent flat facets can have different mobilities, and their coordinated motion can be kinetically controlled by the mobility of the inter-facet junction line. In addition, there is always a significant dispersion of GB-free energies caused by crystallography, impurity effects, and GB phase transitions such as roughening and faceting. Perhaps the most impactful factor is the network constraint. The GBs in polycrystalline alloys form a connected network in which each GB is subject to constraints imposed by adjacent GBs. The motion of a given GB is accompanied by an extension or shrinkage of the adjacent boundaries. As a result, the migration velocity (including direction) of each GB depends on the energies, mobilities, and geometric arrangements of the adjacent boundaries. The GB velocity may also depend on the mobility of the triple junctions (TJs) separating the GB from its neighbors. The internal stresses arising in polycrystals due to the shear-coupling effect could be a contributing factor [327,334].

3.3. Role of triple junctions on nanocrystalline stability

The role of TJs can be significant in NC materials, in which the fraction of atoms located in the TJ cores relative to the GB atoms cannot be neglected [308,335–350]. The impact of TJs on nano-stability can be significant and is often underappreciated. TJs can affect the kinetics of grain growth [335,351–353]. During grain growth, the migration of each TJ is driven by the imbalance among the tensions of the three GBs terminated at the TJ. As the GBs move, the TJ must also move to maintain the GB tension balance. Consequently, GB migration is constrained by the motion of the TJs bounding the GB area. The result is a coupled motion of the GBs and TJs with competing rates. Experiments [316,343,351,353] and simulations [335,335,352] have shown that TJs often have a lower mobility than GBs, especially at relatively low temperatures. The slow TJ kinetics give rise to the TJ drag effect on the moving GBs. In NC materials, TJ drag can result in TJ-controlled grain growth [354,355]. In this kinetic regime, the average grain size increases as a linear function of time ($D \propto t$), in contrast to the GB-controlled growth in which grain size increase is parabolic ($D \propto \sqrt{t}$) [316,351]. TJ drag can also cause deviations from the curvature-driven GB migration and violation of the topological rules such as the 2D von Neumann–Mullins $(n-6)$ rule and its 3D generalization [356].

In addition to grain growth, TJs are involved in many other processes occurring in NC materials. They are typical sites for heterogeneous nucleation of new phases during phase transformations and locations of damage initiation during plastic deformation and fracture. They can act as sinks for non-equilibrium point defects during recovery from intense irradiation in nuclear materials. As such, the role of TJs must be considered in the search for radiation-tolerant NC materials. Furthermore, similar to GBs, TJs are fast diffusion pathways [308,336,337,342,345,347] and can contribute to the rate of high-temperature creep deformation. A percolating TJ network can mediate the redistribution of solute components during the synthesis and processing of nanomaterials, especially during the sintering of powders.

TJs are not part of the thermodynamic stabilization models discussed in the previous section. It is critical to include them in future research. TJs contribute to the excess free energy of NC materials and are responsible for at least part of the thermodynamic driving force for grain coarsening. Although lines at which three phases meet were discussed already by Gibbs [102], calculations and even a rigorous thermodynamic definition of their excess free energy (line tension) remain challenging [308,349,357]. Such challenges are especially significant for solid phases.

Although thermodynamic treatments of TJs have been proposed [340,358], their role has not been analyzed thoroughly from the perspective of NC stability. Meanwhile, TJs provide additional segregation sites relative to GBs. Their excess free energy can be reduced by solute segregation in a manner similar to the thermodynamic stabilization of GBs.

There is a need for experimental investigations and generalized models targeting the combined TJ-GB system in NC alloys. Models of solute drag should also be generalized to include the coupled motion of TJs and GBs together with their segregation atmospheres. In

the future, the goal of stabilizing GBs should be replaced by the goal of stabilizing GBs *and* TJs as a unified system. Progress should be made in understanding the mechanisms of TJ migration. For elemental materials at relatively low temperatures below the GB roughening transition, the disconnection model [72] successfully describes the coupled GB-TJ dynamics [352]. More general models are required to describe situations in which some or all GBs are rough and do not support disconnections. In fact, the roughening transition at TJs is another appealing topic for future research.

Even if a stationary GB is smooth (and contains disconnections), it can develop significant roughness during migration, altering the migration mechanism. The phenomenon is called dynamic roughening [176] and its existence makes the modeling of moving GBs extremely challenging. The effect of solute segregation on the GB-TJ dynamics and mechanisms is another open question that should be addressed in the future. Finally, the role of quadruple junctions [359,360] (meeting points of four TJs) in NC stability remains a virtually unexplored topic relevant to nano-grain stabilization by solute segregation.

3.4. Phase transformations at grain boundaries and triple junctions

NC stability can also be impacted by GB phase transformations [333,358,361–364] (sometimes referred to as "complexion transitions" [365]). The GB phase transformations can cause abrupt changes in the GB free energy, GB mobility, and other thermodynamic, kinetic (e.g., diffusivity [366]), and physical properties of GBs. They further broaden the distributions of GB properties in an NC material and add more complexity to the already complex stability analyses. Nonetheless, GB phase transformations can play a significant role in stabilizing GBs and must be part of future efforts to design structurally stable nanomaterials.

GB phase transformations in metallic systems have been observed experimentally, including *direct* observations of the atomic structures of different GB phases by HRTEM [199,367,368]. GB phases and phase transformations have been extensively studied by MD, Monte Carlo, and other atomistic methods [364,366–374], often demonstrating good agreement with the experiments [199,367]. In alloys, GB phase transformations can be caused by solute segregation. The segregation atmosphere can have its own miscibility gap and, below a critical point, can decompose into two or more GB phases. Segregation-induced GB transformations have also been studied by atomistic simulations [370] and confirmed experimentally [199,295,375]. Such transformations can be presented on GB phase diagrams [133,376] generalizing the conventional bulk phase diagrams. In addition to the congruent GB transformations [333] preserving the GB plane and crystallographic misorientation, non-congruent transformations have been observed experimentally and studied by simulations, including the GB faceting transformation [332,377–380].

Efforts have been made to understand the potential impact of GB phase transformations on NC stability and apply this knowledge to control grain growth. Of particular interest are the recent computational studies of NC materials stabilized by amorphous GB layers (called "complexions") in multicomponent alloys [381,382]. Furthermore, a recent study of Fe-Mn alloys combining phase-field modeling and APT observations indicates that a GB segregation atmosphere can undergo a spinodal decomposition and form chemically heterogeneous GB structures [383]. The chemical fluctuations in the spinodal structure can cause a pinning effect similar to the Zener pinning. The impact of these and other GB transformations on the nano-grain stability needs to be further investigated in the future.

An especially relevant type of GB transformation is GB premelting. Most GBs become increasingly disordered at high temperatures, especially when the temperature approaches the bulk melting point T_m [101,157]. Near T_m, many GBs develop liquid-like characteristics and often transform into a liquid film, a phenomenon referred to as premelting. Premelting can drastically change the thermodynamic, kinetic, and mechanical properties of GBs. Mechanical properties usually deteriorate. For example, GBs weaken or even lose their resistance to applied shear stresses [384,385]. Premelting has been studied experimentally [375,384,386–390] and by several computational approaches, including MD [196,385,391–395] and Monte Carlo [396–398] simulations. In alloys, the impact of premelting is stronger than in pure metals. This is especially true for alloys with a low-temperature eutectic or another low-temperature phase. In such systems, GBs premelt at significantly lower temperatures than the respective elements, often forming a GB phase reminiscent of one of the low-temperature bulk phases. In eutectic systems, when the bulk composition and temperature are slightly below the solidus line, GBs can become liquid layers with a chemical composition close to the liquidus line on the bulk phase diagram [398–400] (Fig. 11).

Given the large GB area in NC materials, their properties can be susceptible to the effects of GB premelting. Avoiding GB premelting is one of the challenges in stabilizing NC materials. Solutes exhibiting strong GB segregation commonly have a lower melting temperature than the host metal and often form eutectics at even lower temperatures. Such solutes weaken the interatomic bonds and suppress the local melting temperature in the GB regions.

The latter trend underscores the advantages of kinetic stabilization by atomic clusters in immiscible alloys composed of lower-melting species, where a refractory element is involved. In these alloys, the solute is a refractory metal with a significantly higher melting temperature than the host metal. The solute is present at GBs primarily in the form of nanoclusters. The concentration of randomly distributed solute atoms in the GBs is relatively small. The solute atoms strengthen the chemical bonds at the GB without increasing the structural disorder or causing GB phase transformations. They raise the "local melting temperature" at the GBs and improve their thermal stability. This can explain why the GBs in NC Cu-Ta alloys do not premelt up to temperatures as high as $0.9T_m$.

In light of the preceding discussion of the TJ drag (section 3.3), it is also essential to investigate the possibility of segregation-induced phase transitions at TJ lines, including TJ premelting. Some prerequisites are available. 1D thermodynamics applicable to TJs has been developed [340,358], "wetting" transitions at TJs in alloys have been observed experimentally [401], and 1D phases (referred to as "linear complexions") forming on dislocation cores have been studied computationally [402,403]. Further work is required to incorporate the TJ phase transformations into the NC stabilization analysis.

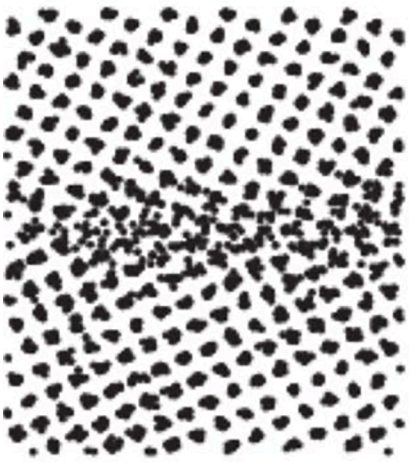

T = 1100 K

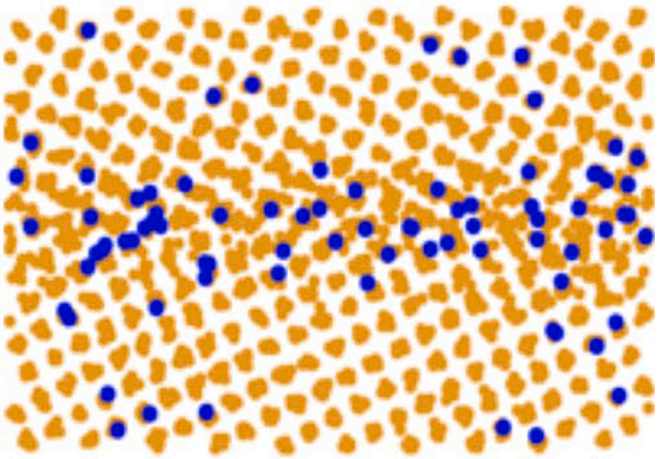

Δc = -2.7%

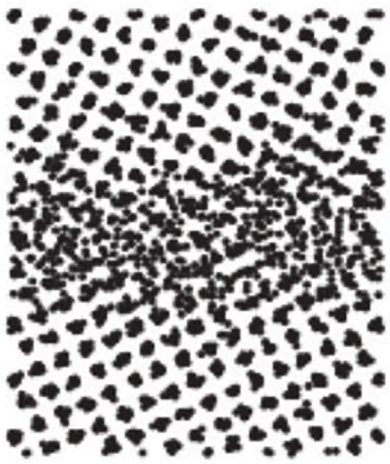

T = 1300 K

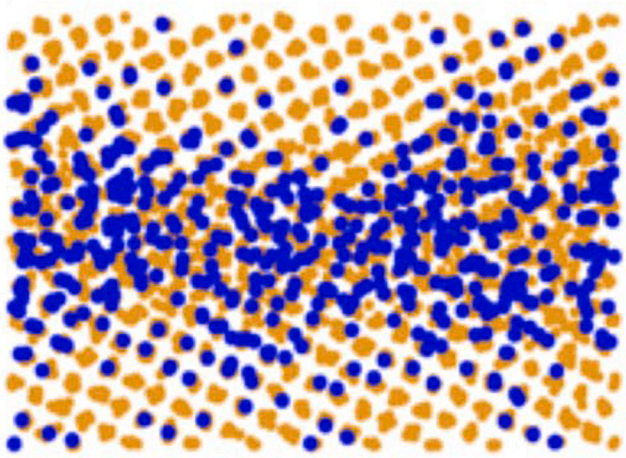

Δc = -0.26%

T = 1324 K

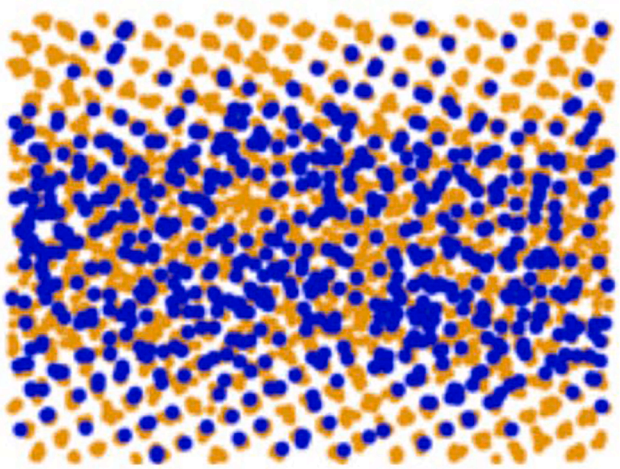

Δc = -0.11%

(caption on next page)

Fig. 11. Premelting of symmetrical tilt Σ5 (210) GB in Cu [400] predicted by atomistic simulations. The atomic positions are projected along the [001] tilt axis normal to the page. Left column: pure Cu GB at temperatures indicated under the images. The melting temperature of Cu with the interatomic potential used in the simulations is 1327 K. Right column: same GB in the Cu-Ag solution at 1100 K for different compositional deviations Δc (at.%Ag) from the solidus line. Note the increasing segregation and formation of a liquid-like layer at the GB as the chemical composition approaches the solidus line from below.

3.5. Stabilization mechanisms revisited

We next revisit the issue of stabilization mechanisms, including the notoriously complex relationship between the thermodynamic and kinetic factors of stabilization. As mentioned above, the Zener pinning of GBs by atomic clusters in highly immiscible alloys is a clear case of kinetic stabilization. In all other cases, two or more stabilization mechanisms can operate concurrently. The dominant mechanism, if there is one, may change with temperature, chemical composition, and many other factors. A few examples of competing stabilization mechanisms were discussed in the previous chapter. Nevertheless, understanding the *individual* mechanisms is highly desirable on fundamental grounds and for developing alloy design strategies.

At present, segregation-induced stabilization is the most common approach. GB segregation of solute components causes a reduction in the GB free energy and simultaneously increases the resistance to GB motion due to the solute drag. Because of the strong coupling between the two effects, isolating one of them for a separate study is highly challenging. We are not aware of convincing experimental evidence demonstrating a clear separation. Whenever grain growth suppression was achieved by alloying, the effect could be either due to a decreased GB free energy or a reduced GB mobility (or both). We envisage that a successful separation will first be achieved by specifically designed computer modeling. It should be possible to choose a binary system with a simple phase diagram whose thermodynamic functions and lattice/GB diffusivities are known or can be reliably measured and in which GB dynamics can be studied comprehensively. The simulation results could then inspire or guide the design of experimental attempts.

In recent years, computational research has focused on thermodynamic stabilization with less attention to kinetic models. We expect that future efforts will be more balanced. Recent atomistic simulations have shown that GB segregation typically lowers the GB free energy by less than 50 % [107,172,370,374,400]. In contrast, the GB mobility is reduced by orders of magnitude, suggesting that most of the stabilization effect is due to kinetic factors. More systematic studies of thermodynamic stabilization are required, including efforts to push the GB-free energy down as much as possible. The usual tandem of MD and Monte Carlo is an appealing choice. However, such simulations heavily rely on computational power and the availability and reliability of interatomic potentials for the alloy systems. Perhaps a better starting point would be a more general approach, such as kinetic Monte Carlo (KMC), in which the model parameters can be tweaked to enforce the predominance of either GB free energy reduction or the solute drag.

3.6. Zero grain boundary energy?

We have already mentioned the fascinating idea that an appropriate choice of solute can *completely* stabilize NC material. This idea is fundamentally important and warrants a more detailed discussion. Complete stabilization means that a nanocrystal with a *finite* grain size will have a lower total free energy than a single crystal of the same chemical composition. There will be no driving force for grain growth. This state is yet to be demonstrated experimentally. It will be difficult to distinguish the predicted global free energy minimum from a kinetically trapped nanostructure exhibiting little or no grain growth on the experimental time scale. Nevertheless, the idea presents great theoretical interest. The feasibility of complete stabilization of a nanostructure, at least in principle, is an attractive topic for future investigation.

At present, we can only state that some theoretical models predict the existence of a global minimum of free energy at a finite grain size. However, as mentioned above, such models rely on many approximations, and their relevance to real NC materials requires further examination. The models treat the GBs as uniform layers of a fixed thickness with the same thermodynamic properties across the entire nanostructure. It is tacitly assumed that spontaneous local deviations of the nanostructure from the minimum free energy state preserve or instantly restore the GB/lattice equilibrium under the closed-system constraint, leading to an increase in the total free energy. Satisfying this condition requires infinitely fast solute diffusion. In reality, the solute diffusion rate is finite and cannot instantly respond to the chemical potential gradients arising due to spontaneous GB displacements. For example, a GB can spontaneously break away from the segregation atmosphere, which will increase its free energy γ and create a driving force for continued motion. The moving GB can then break the tension balance with the neighboring boundaries and cause them to separate from their atmospheres, triggering (possibly abnormal) grain growth. In other words, it is not immediately obvious that the presumed fully stabilized state would be stable against fluctuations away from equilibrium.

Even without considering the fluctuations, it is unclear how all GBs in a NC material could be stabilized simultaneously. For a single GB, the fully stabilized state is achieved when the GB free energy becomes zero, $\gamma = 0$. Achieving this condition requires a particular combination of the chemical composition and temperature specific to the given GB crystallography. In a polycrystalline assembly, the GB network is characterized by a broad spectrum of GB energies and structures with different interactions with the solute atoms. Furthermore, some GBs can be above the roughening transition while others are below; some GBs could have undergone a particular phase transformation (e.g., premelting) while others have not. It seems unlikely that all GBs in a polycrystalline sample can reach the $\gamma = 0$ condition simultaneously. Recent KMC simulations [143] suggest that the $\gamma = 0$ state is not a state of static equilibrium. Instead, this is a state of dynamic equilibrium between grain growth and grain refinement with small fluctuations around a constant total GB area. It was also confirmed that fast solute diffusion is required to maintain this dynamic equilibrium. Slow diffusion drives the system

into a metastable or kinetically trapped unstable state. However, these simulations were performed within a highly idealized 2D KMC model with only two lattice orientations.

It is essential to better understand the nature of the intriguing GB state with $\gamma = 0$ required for the complete stabilization. Although the $\gamma \leq 0$ condition is not prohibited by thermodynamics, the question of what happens to the interface when this condition is met has a long and winding history going back to Gibbs [102]. In an open system, the amount of the GB phase with $\gamma \leq 0$ is expected to increase without bounds (assuming that γ is curvature-independent [404]). For fluid–fluid interfaces, Gibbs [102] predicted that the interface area would spontaneously grow. This argument is often extended to GBs, claiming that the $\gamma \leq 0$ condition will trigger spontaneous grain refinement instead of grain growth [125]. To our knowledge, this prediction has yet to be confirmed experimentally. An alternative scenario is that the thickness of the fully stabilized GB phase will spontaneously grow with little change in the GB area. This would be equivalent to wetting the GB with a solute-rich phase that may or may not exist in a bulk form. These and other possible scenarios must be thoroughly investigated in the future, as they are highly relevant to the nano-stabilization problem.

3.7. Entropic stabilization of grain boundaries

Some bulk phases exhibit improved thermodynamic stability due to entropic effects. Examples include high-entropy metallic alloys [405] and entropy-stabilized oxides [406], in which the high entropy arises due to configurational effects in the presence of multiple principal components. By extension, configurational entropy could contribute to the thermodynamic stabilization of GBs in NC alloys. Even if the solute concentration in the grains is small, it can be much higher in GBs, increasing their configurational entropy. In multicomponent alloys, GBs can be enriched with several chemical components in nearly equal amounts, increasing the GB excess entropy. Recent experiments [407] and thermodynamic modeling [407,408] indicate that the "high-entropy GBs" [408] can stabilize nanocrystals more effectively than GB segregation in binary alloys. Note that the grains need not be high-entropy alloys to reach a high-entropy GB state. They can even be dilute solutions. Tailoring chemically complex NC alloys to maximize the GB entropy is a promising research direction worth exploring. The challenge is to keep the GBs structurally disordered. Any ordering/patterning reduces the configurational effects. It is also essential to avoid precipitation of new phases in the GBs or inside the grains during high-

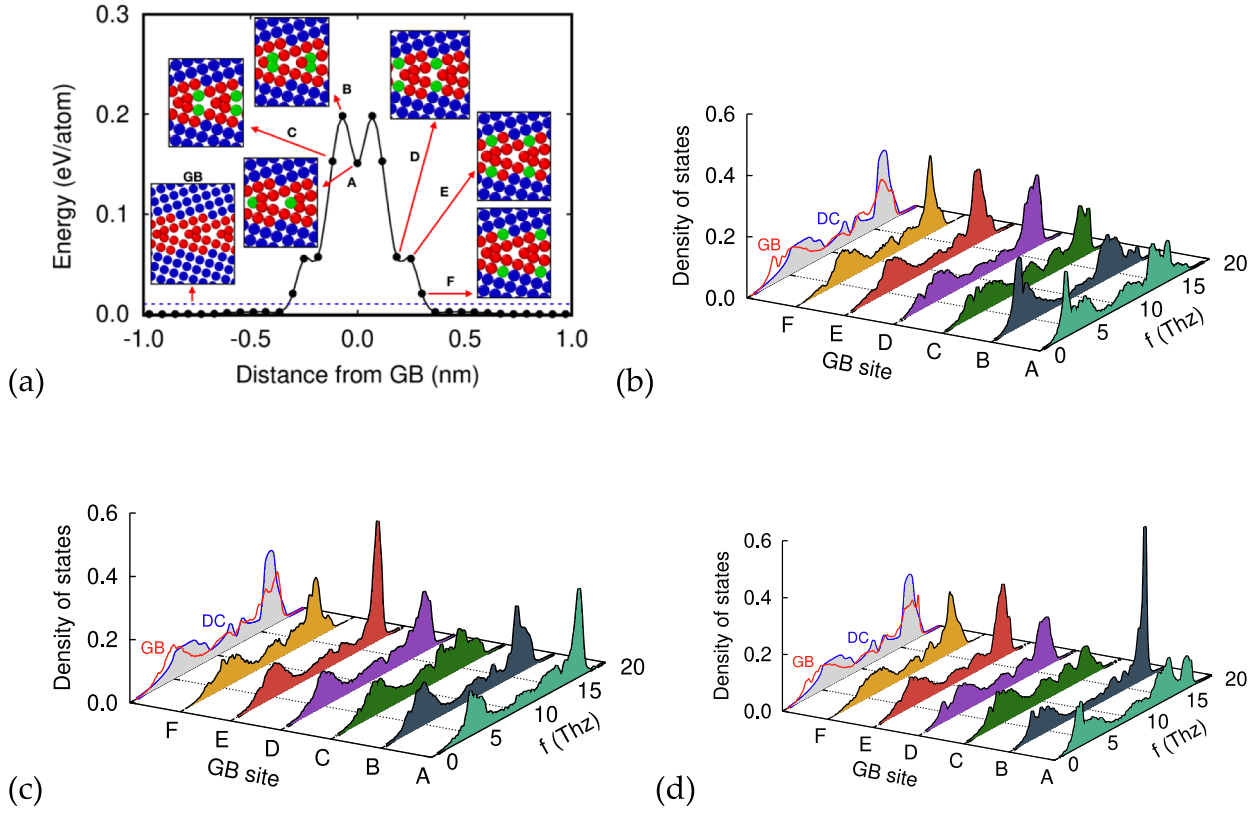

Fig. 12. (a) Selected atomic sites (shown in green and labeled A through F) in the symmetrical tilt Σ5 (210) GB in Si from MD simulations at 300 K [419]. The sites are ranked according to the distance from the GB center, and their energy is plotted as a function of this distance. Panels (b), (c), and (d) show the vibrational DOS of selected GB sites in the *x*, *y*, and *z* directions, respectively. The *y*-axis is normal to the GB plane. The projection on the DOS-frequency plane shows the overall DOS of the GB in comparison with that for diamond cubic (DC) Si. The DOS plots demonstrate significant distortions of the vibrational spectrum in the GB region with new peaks in the acoustic range. (For interpretation of the references to color in this Fig. legend, the reader is referred to the web version of this article.)

temperature anneals.

Atomic vibrations can also contribute to GB free energy and improve NC stability. The vibrational entropy is a significant stabilizing factor affecting the thermodynamics of materials [409–412]. Many bulk phases are stabilized by vibrational entropy. In fact, some phases are only stable due to the vibrational free energy. The best-known examples are group IVB metals Ti, Zr, and Hf, which have the HCP structure at low temperatures and transform to the BCC structure at high temperatures. The BCC structure of these metals is mechanically unstable at low temperatures but is stabilized by anharmonic atomic vibrations at high temperatures [413,414].

A temperature-dependent interplay exists between the configurational and vibrational contributions to the entropy. While the vibrational entropy rapidly increases with temperature, the configurational entropy is weakly temperature-dependent, with a relatively slow increase at high temperatures as the short-range order weakens. As a result, low temperatures are dominated by configurational effects, while the vibrational contribution becomes more significant and often dominant at high temperatures [415]. Even in high-entropy materials, in which the configurational entropy is of key significance, atomic vibrations should be taken into account and, in some cases, can be as important as the configurational effects [412,415–417].

The vibrational properties of GBs are different from those of the perfect lattice, especially when the GBs are packed with several segregated components. Due to the significant structural distortions, mass dispersion, and broad distribution of force constants, the vibrational density of states (DOS) in GBs is broader than for lattice vibrations [418,419]. At the same time, the GB DOS can contain sharp peaks (resonances) [418–420] and other unusual features arising from the coexistence of tightly compressed atoms alongside loosely bound atoms in low-density local environments (Fig. 12). The vibrations can be strongly anharmonic and can stabilize the GB structure in a manner similar to the stabilization in high-entropy alloys [421]. These features manifest themselves in the measured and computed vibrational properties of nanomaterials [422–426], which are different from those of coarse-grained polycrystals and single crystals.

The possibility of GB stabilization by atomic vibrations calls for further investigation. This effect is particularly relevant to systems where kinetic pinning, such as Zener pinning, is exceptionally strong. In such alloys, most of the solute is concentrated in nanoclusters, and the concentration of randomly distributed solute atoms in GBs is small. Thus, the excess configurational entropy in GBs is relatively small, shifting the balance towards the vibrational entropy at high temperatures. The stabilizing effect of atomic vibrations can be observed more readily.

Vibrational entropy calculations are computationally expensive, especially for GBs, because they require large system sizes. However, there are no fundamental obstacles, and some work was done in the past [120,418,419,422–426]. Experimental methods to probe the vibrational properties of GBs have also been developed [418].

3.8. Unconventional recrystallization mechanisms

Coarse-grained alloys subjected to cold plastic deformation often undergo recrystallization upon subsequent annealing at temperatures ranging from 0.3 to 0.5 of the melting point [427,428]. In NC alloys, this form of recrystallization rarely occurs because grain growth starts at lower temperatures [96]. Instead, the excess energy of the highly non-equilibrium GBs is reduced by structural relaxation, a process often accompanied by significant strengthening of the material. Separation of the GB relaxation from the concurrently occurring grain growth is challenging but not impossible and has been observed in several NC alloys with improved grain stability [429–432]. The GB relaxation process can play a significant role in microstructurally stable nanomaterials (such as Cu-Ta alloys), which can accumulate a high degree of straining without grain growth. Extreme deformations bring GBs into highly nonequilibrium states, from which they rapidly relax at elevated temperatures. The microstructurally stable nanomaterials thus offer an opportunity to better understand the nature of the GB relaxation process and its effect on the mechanical strength in a broader temperature range than would be possible in conventional alloys.

Another relevant process is grain refinement due to phase transformation, as demonstrated in the binary Fe-Au system [433] (Fig. 13). In this case, grain refinement is driven by a combination of phase a transformation and GB segregation. Experimental results revealed that γ-Fe, formed after the α → γ transformation, stabilizes at a smaller grain size (~115 nm) at 1000 °C, compared to α-Fe (~130 nm) at 800 °C. Even at 1100 °C, γ-Fe was found to maintain a grain size (~130 nm), consistent with the stability map's prediction. In situ XRD experiments revealed that Au precipitated from α-Fe, allowing α-Fe grains to grow. Upon heating past the transformation temperature, Au dissolved and diffused into atomically small γ-Fe grains, which nucleated at α-Fe GBs and triple lines. These γ-Fe grains, upon reaching the thermodynamically described state, stabilized at smaller sizes than the parent α-grains, refining the microstructure by allowing Au to segregate to the GBs and provide stability. Upon cooling past the transition, α-Fe grains nucleated and grew as Au re-precipitated from the solution, leaving the GBs of the γ-Fe grains and forming secondary phases within the matrix of the new α-Fe grains, disrupting the thermodynamic equilibrium and resulting in a coarser microstructure. This process was shown to be repeatable, cycling between maintaining a stable NC microstructure and a larger grain size. Thus, the phase transformation functions similarly to recrystallization, leading to new, smaller grains compared to those in the α-Fe phase. The stabilization mechanism, along with the shift in Au's stability on the phase diagram, was shown to cause a deviation from conventional grain growth behavior, where grain size remains reduced at elevated temperatures.

Another possible recrystallization mechanism was suggested by computer simulations of an NC Cu-6.5at.%Ta alloy [206]. At temperatures above 1100 K (0.8–09 T_m of Cu), some of the smaller grains spontaneously melted and subsequently re-solidified into a new crystallographic orientation. The latter often continued the orientation of a neighboring grain or was close to that orientation and separated from that grain by a low-angle GB. Such intermittent local melting events coarsened the average grain size. At temperatures close to the melting point (e.g., 1200 K), the liquid pocket could survive for tens of nanoseconds before it finally solidified. The process is clearly driven by the interface free energy reduction. Although at $T < T_m$ the liquid grain has a higher bulk free energy than the solid

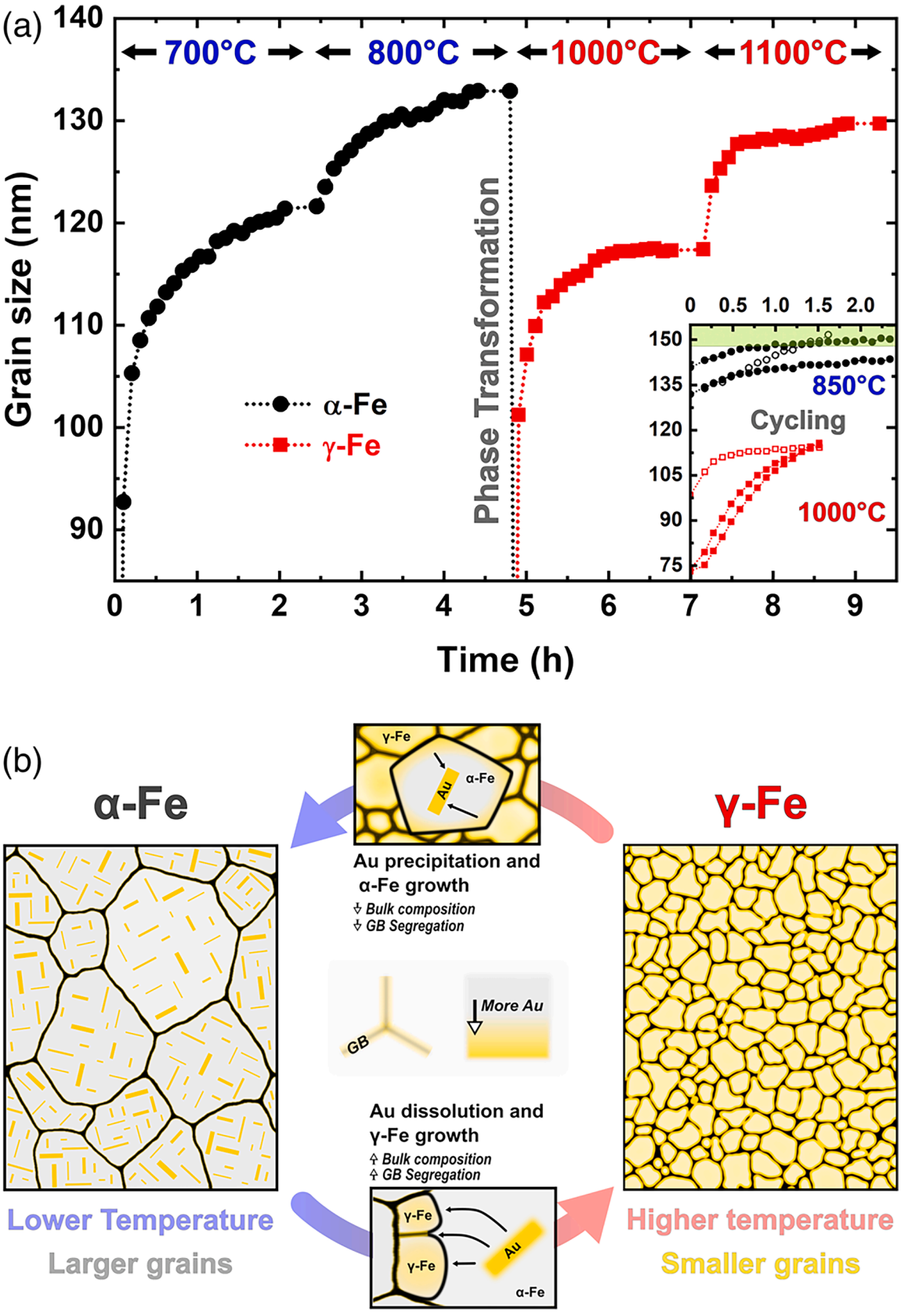

(caption on next page)

Fig. 13. In situ grain growth and phase transformation in NC $Fe_{95}Au_5$ alloy [433]. (a) Grain size evolutions in α-Fe (at 700 and 800 °C) and γ-Fe (at 1000 and 1100 °C). The inset shows the grain size after several cycles between 850 and 1000 °C. (b) Schematic illustration of α-Fe microstructure with Au nanoscale precipitates and its transformation into γ-Fe.

solution, the total free energy of the solid–liquid interfaces separating the liquid grain from its neighbors can be smaller than the total excess free energy of the GBs surrounding the solid grain. Thus, if the grain can overcome the transformation barrier, its melting reduces free energy. The process is similar to the size-dependent melting of free nanoparticles and embedded clusters [434–440]. Once the GBs are replaced by solid–liquid interfaces, the neighboring grains can grow into the liquid pool and solidify it, eliminating the initial grain.

We hypothesize that the intermittent grain melting can be another recrystallization mechanism in NC materials during high-temperature anneals. The strain energy stored inside the cold-deformed grains and the excess free energy of the highly non-equilibrium GBs can increase the driving force for the grain melting and thus reduce the temperature at which the melting-solidification events can occur. Since the newly solidified grain regions are dislocation-free, the recrystallization mechanism described here could be effective at relatively high temperatures. We emphasize that this mechanism is unique to the microstructurally stable NC materials. It would not operate in unstable nanomaterials because of the rapid grain growth at high temperatures. So far, intermittent grain melting has only been observed in a single simulation study [206]. Future research can validate this mysterious phenomenon by further simulations and specifically designed experiments involving, for example, high-temperature in situ TEM.

3.9. Casting NCs from the liquid state?

We conclude this section by discussing another "think-outside-the-box" idea. In highly immiscible alloy systems, such as Cu-Ta and Cu-Nb, the liquid phase is highly heterogeneous on the nanoscale. For example, atomistic simulations have revealed that the liquid solution Cu-Ta with a relatively small Ta concentration consists of nanoscale Ta clusters embedded into the liquid Cu matrix [404]. Remarkably, the size of the clusters in this nano-colloidal liquid is nearly independent of the chemical composition and temperature. Even more remarkably, extensive simulations have shown that the nano-colloidal liquid is the thermodynamic *ground state* of the liquid phase. This structure resists both coarsening and coalescence of the Ta clusters. A uniform distribution of Ta atoms in liquid Cu quickly evolves into the nano-colloid. A large Ta particle embedded in liquid Cu breaks into nanoclusters. A planar Cu/Ta interface between the two liquids disintegrates, forming a nano-colloid. In short, the nano-colloid is the final state of any simulation starting from any initial distribution of the Ta atoms [404].

This highly unusual thermodynamic stability of Ta nanoclusters is explained by the negative free energy of the Cu/Ta interfaces, which are stabilized by a strong curvature dependence [404]. Note that the situation differs from the previously discussed negative GB free energy. In the latter case, the GB curvature can be treated as a second-order effect. Interfaces stabilized by spontaneous curvature are known in biological systems, such as vesicles, but are highly unusual in metallic materials. We should emphasize the difference between the thermodynamically stable metallic nano-colloid discussed here and the various types of nano- and micro-emulsions [441–448]. In the latter case, the system can remain dispersed for a long time but is not thermodynamically stable. It eventually evolves towards a more stable state by coalescence and sedimentation.

Simulations [404] have also shown that the nano-colloidal state of the Cu-Ta liquid can be quenched into a solid state, forming an NC structure with Ta nanoparticles embedded into the FCC Cu matrix.

It is tempting to suggest that the Ta-stabilized NC Cu alloys can be obtained by rapid solidification as an alternative to the powder metallurgy (PM) route used to synthesize them today. It is understood that the cooling rates implemented in the simulations are orders of magnitude faster than in the experiments. On the other hand, the behavior of the Ta nanoclusters in the experimental Cu-Ta samples is amazingly similar to that in the Cu-Ta liquid phase observed in the simulations. The Ta clusters in the NC Cu-Ta alloys have about the same size, which is only weakly dependent on the alloy composition and temperature [45,67,184,206,224,225,227,229,242]. The extraordinary resistance of the Ta clusters to coarsening, coalescence, or any significant size change suggests that they are likely governed by the same stabilization mechanism as the nanoclusters in the liquid nano-colloid. This similarity motivates future pursuits of microscopically stable immiscible NC alloys obtained by a suitable rapid solidification technique.

4. Properties of unstable NC materials: (from 1981 to ~ 2014)

4.1. Discovery by Gleiter and start of timeline for mechanics properties of NC materials

Since 1981, Gleiter's pioneering work established NC materials as a unique class with the potential to transcend the performance limits of conventional materials [449]. This foresight was built on earlier concepts, including Feynman's famous 1959 speech that envisioned novel phenomena at the nanometer scale [450]. Gleiter's categorization of nanostructured materials—spanning zero-, one-, two-, and three-dimensional architectures—provided a foundational framework for subsequent research [2].

At the atomic level, the dense network of interfaces in NC structures promised transformative macroscopic behaviors. The interfaces facilitated the manipulation of atomic arrangements, defect densities, and electronic properties, unlocking new possibilities for enhancing the strength while controlling deformation mechanisms. However, realizing these promises hinged on producing high-quality, fully dense NC materials with uniform grain sizes [451]. Since traditional PM techniques faced significant limitations—particularly because achieving full density required high-temperature processing that led to substantial grain growth,

undermining the nanostructured starting materials [452,453]—early research was primarily redirected toward investigating physical properties such as magnetism, electrical conductivity, and diffusion in NC metals, areas less dependent on full densification.

By the late 1980s and early 1990s, advances in the synthesis and testing of NC materials began revealing their mechanical potential. Reports on NC Cu, Ni, and Pd demonstrated significant increases in hardness and validated the Hall-Petch relationship, linking grain size to strength[454–457]. For grain sizes below 25 nm, however, a deviation from this relationship was observed, with negative Hall-Petch slopes indicating a transition to mechanisms such as GB sliding and diffusion-dominated plasticity [13,458–460].

Shortly thereafter, miniaturized mechanical testing techniques were employed to evaluate mechanical properties [461]. These techniques were adopted from those used to evaluate the high-temperature creep behavior of thermal barrier coating (TBC) materials developed mainly by Sharpe [462–464]. Weertman published some of the earliest works on tensile properties and creep, utilizing samples with only a few millimeters in gauge length and width [457]. These samples were produced through IGC of pure elements such as Cu, Pd, and Ag, and then compacted at room temperature under 1.4 GPa of pressure for 90 s, achieving densities of approximately 85–95 % of the theoretical values. Creep behavior was analyzed based on previous research indicating increased diffusion in NC metals.

4.1.1. Rise of miniaturized testing borrowed from the nuclear industry

In the late 1990s and early 2000s, testing methods, such as miniaturized disk bending [465,466], small punch [467] or shear punch testing [468], automated ball indentation [469,470], impression creep [471,472], miniature tensile/compression and later nano-indentation [473], along with micro- and nano-pillar [474,475]/tensile testing were developed [464], that revolutionized the assessment of mechanical properties beyond simple hardness measurements. These methods were originally developed in the nuclear industry to evaluate radiation-damaged materials, where limited sample volumes necessitated innovative approaches.

Miniaturized methods offered several advantages, including the ability to process a large number of samples rapidly and cost-effectively. High-throughput capabilities allowed researchers to systematically evaluate mechanical properties across a wide range of compositions and processing conditions, improving statistical robustness. Additionally, the compact geometries of these tests enabled precise control of strain and stress states, facilitating detailed studies of deformation mechanisms.

Bulk NC metals synthesized via electrodeposition complemented these techniques. These materials, typically in the form of thin coupons with full density, provided ideal specimens for studying conventional mechanical properties such as tensile strength, hardness, and creep resistance. Electrodeposition also allowed precise control over grain size and chemical composition, enabling the systematic exploration of microstructural effects.

Despite their benefits, non-standard testing methods presented challenges, particularly in strain measurement accuracy. Techniques such as digital image correlation (DIC) and laser interferometry addressed these issues by providing high-resolution strain mapping, ensuring reliable measurements even for small and highly deformable specimens [476–478]. Proper validation of these methods remains critical to their reliability and reproducibility.

The synergy between high-throughput miniaturized testing and the growing availability of bulk NC samples accelerated the pace of discovery in the field. These approaches facilitated the identification of rare phenomena, such as the transition from dislocation-mediated plasticity to GB sliding at nanoscale grain sizes. They also enabled the rapid screening of novel material systems, advancing both fundamental understanding and practical applications.

As the development of NC materials continues, the integration of innovative testing methodologies with advanced synthesis

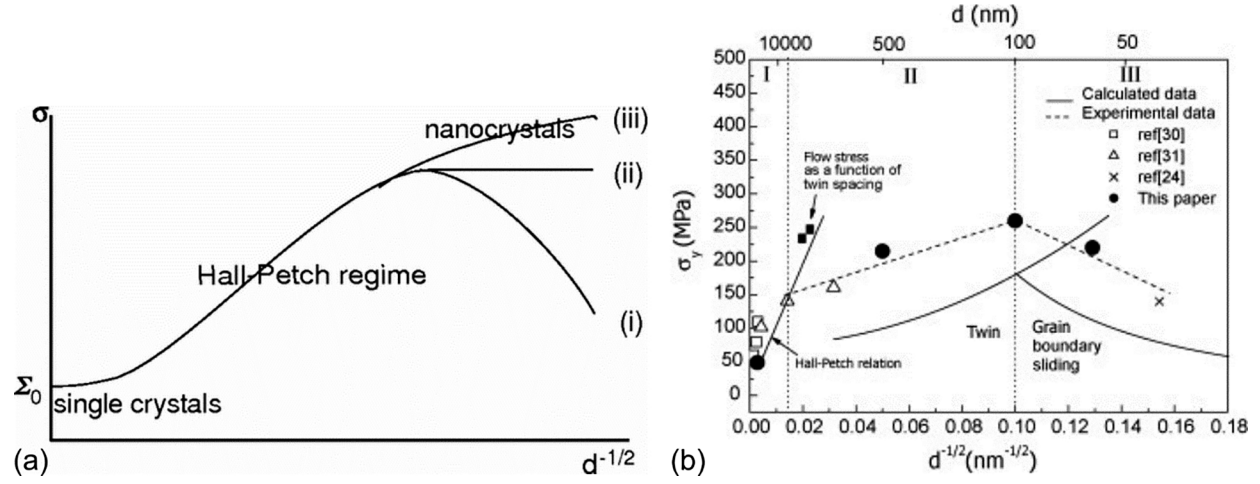

Fig. 14. (a) Schematic trends of the yield stress vs. $d^{-1/2}$: from the single crystal limiting case Σ_o, the yield stress increases as $d^{-1/2}$ in the Hall-Petch regime. At nanoscales, the Hall-Petch breakdown leads to three possible behaviors, depending on whether dislocations are nucleated at quadruple junctions (i), at triple junctions (ii), or at GBs (iii) [483]. (b) Grain size dependence of the strength of magnesium. The solid black squares represent the flow stresses after 0.1 and 0.15 of compressive strains for the magnesium specimens [493]. Ref. [30] in this Fig. is by Yamashita et al. [494], [31] is by Somekawa and Mukai [490], and [24] by Hwang et al. [495].

techniques will remain essential. The ability to probe mechanical behavior at increasingly small scales, combined with the robust statistical analysis offered by high-throughput methods, ensures that the field will continue to yield transformative insights and breakthroughs.

4.2. Understanding of un-stable NC response

4.2.1. The Hall-Petch relation

The Hall-Petch relation, a fundamental observation in materials science, was independently proposed by Hall in 1951 [479] and Petch in 1953 [480]. Over the past six decades, several reviews have celebrated its significance [59,65,82,481,482]. It should be noted that the Hall-Petch linear relation is purely empirical, defined as

$$\sigma = \sigma_0 + k_{H-P} d^{-\frac{1}{2}} \tag{3}$$

where σ is the yield/flow strength of the metal, σ_0 is the lattice friction, $k_{H\text{-}P}$ the Hall-Petch coefficient depending on factors such as lattice structure, texture, stacking fault energy (γ_{SF}), etc., and d the grain size in the materials. Cordero et al. compiled Hall-Petch plots for a wide range of metals, including BCC (Fe, V, Nb, Ta, Cr, Mo, W), FCC (Cu, Ag, Au, Ni, Al), and HCP metals (Ti, Zr, Hf, Co, Be, Mg, Zn, Cd) [65].

Several mechanisms have been proposed to explain the Hall-Petch relation. The various mechanisms have been analyzed in recent review articles [59,65,483]. The first mechanism was suggested by Petch based on dislocation pile-ups against GBs [484]. However, as Li [485,486] and later Ashby [487] pointed out, the drawback of this model is the lack of convincing experimental evidence supporting the notion of dislocation pile-ups against GBs, especially in pure metals where the Hall-Petch relation was well-established. In their 2016 review, Cordero et al. [65] outlined over five mechanisms, including dislocation pile-ups, GBs acting as sources and sinks for dislocations [485], geometrically necessary dislocations (GNDs) [487], and composite models treating GBs and grain interiors as distinct [488,489]. Other models, such as dislocation avalanche and collective dislocation dynamics [483], have also been proposed. Fig. 14 (a) is based on the dislocation avalanche model by Louchet et al. [483]. The model results branch in the NC regimes depending on the location of the dislocation nucleation.

A common feature across these models is their reliance on the Taylor strain hardening model, where the flow stress is directly related to the square root of the dislocation density during plastic deformation. Fig. 14a schematically illustrates the trend of yield stress versus $d^{-1/2}$, showing that if dislocations are nucleated only from GBs, no inverse Hall-Petch effect should be observed. Instead, a decreased Hall-Petch slope is expected. However, this prediction is at odds with convincing experimental results [82] shown in Fig. 14 (b). Also, it is hard, if not impossible, to pin down the exact dislocation nucleation mechanisms in NC materials under mechanical stress.

For low melting point metals, such as Al and Mg, the Hall-Petch breakdown can be attributed to GB-mediated plasticity as the experimentally measured activation volume for plastic deformation is on the order of a few $\sim b^3$ (b is the magnitude of the Burgers vector) [490–492]. The work of Choi et al. [493] illustrated in Fig. 14b based on Mg in the grain size spectrum from nano- to micrometer showed a normal Hall-Petch effect for grain size about 1 μm. Below 1 μm, an inverse Hall-Petch effect was observed [493].

Recently, Figueiredo and Longdon [496] proposed a model based on GB sliding to provide a unified framework explaining the mechanical behavior from large grain size to NC materials, including the Hall-Petch effect, and strain rate sensitivity. Their model is based on two observations or assumptions. First, strain hardening capacity is usually diminished for materials with ultrafine-grained and NC microstructure. This is especially true at relatively high homologous temperatures, or at room temperature for metals with low

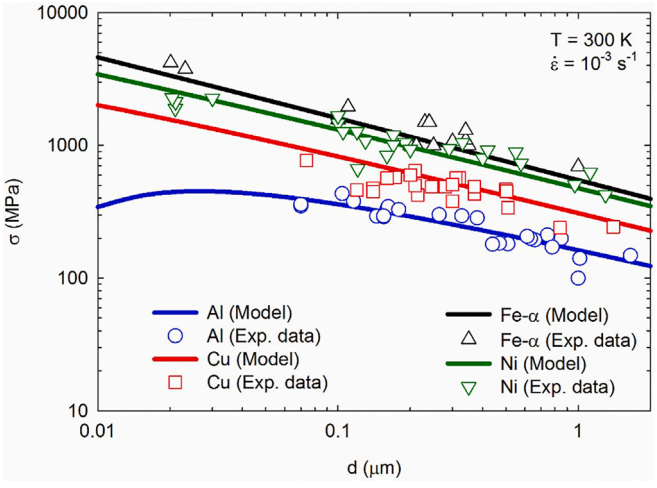

Fig. 15. Double-logarithmic plot of flow stress versus grain size for Al, Cu, α-Fe and Ni along with experimental results. For the source of the experimental results, refer to [496]. The solid lines are based on the model, and the symbols represent experimental data points.

melting points such as Al, Mg, etc., where a dynamic equilibrium can be established between dislocation multiplication and annihilation due to recovery/recrystallization. Second, the authors believe that it is an accepted notion in the materials science community that GB sliding plays a role in the plastic deformation of UFG/NC metals including Al, Cu and Mg. For this to occur, GB diffusion becomes very important. Based on those observations or assumptions, the authors derived the following equation to describe the stress as a function of factors such as strain rate, grain size, temperature, etc.

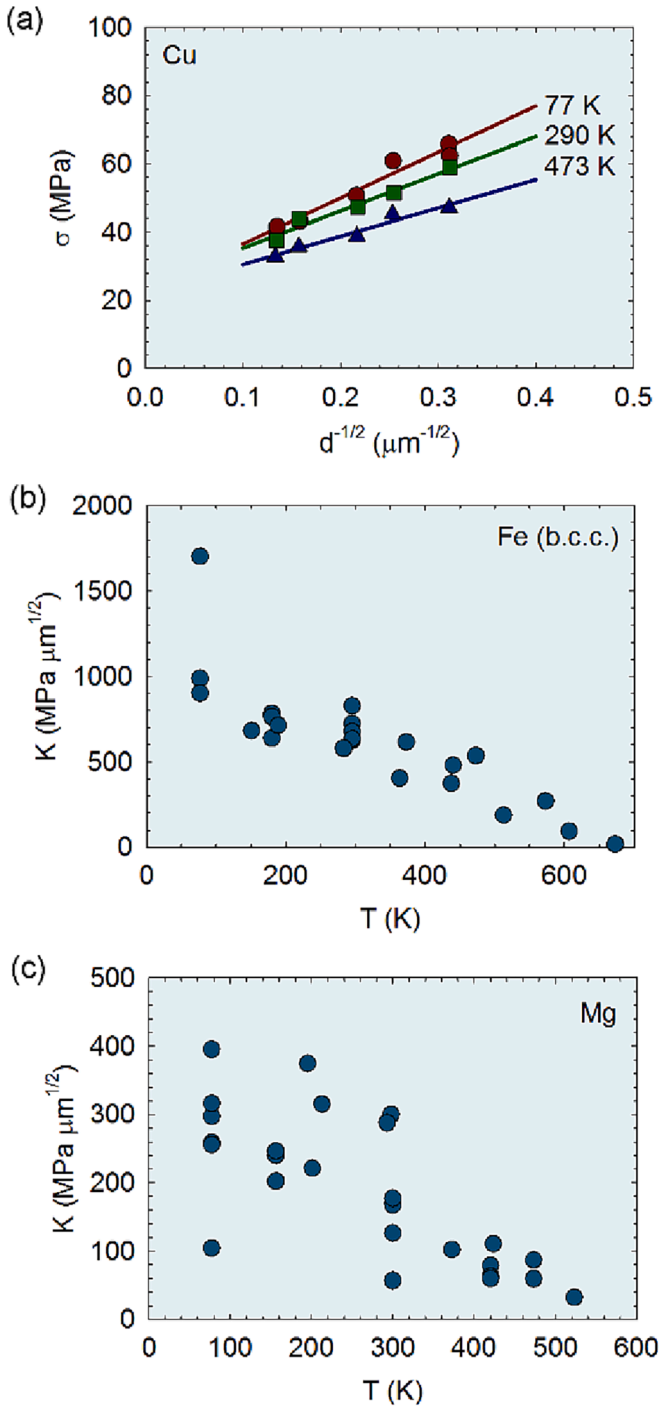

Fig. 16. Effect of temperature on the Hall-Petch effect for Cu, Fe, and Mg. The general trend is that as the temperature increases, $k_{H\text{-}P}$ decreases. These plots were compiled by Figueredo et al. [482] (see their overview paper for the sources of the data presented in the plots).

$$\sigma \approx \sqrt{\frac{3GkT}{2db^2} ln\left(\frac{d^3\dot{\varepsilon}}{10\delta D_{GB}} + 1\right)} \tag{4}$$

In the above equation, G is the shear modulus, k is the Boltzmann constant, T is the temperature in Kelvin, δ is the width of the GB, D_{GB} is the GB diffusivity, $\dot{\varepsilon}$ is the strain rate, and d is the grain size in the material. Fig. 15 is a double-logarithmic plot of the equation for a number of metals, and comparison with experimental results. The slopes of the solid lines from the model calculations are 0.5, signaling the Hall-Petch relation. The exception is Al for very fine grains (NC grains), indicating a Hall-Petch break-down to be discussed in what follows.

It is worth pointing out that Equation (4) does not contain any fitting parameters. As such, the agreement between the model and the experimental results is remarkable, at least for the metals chosen for the analyses. However, the performance of the model for metals with high melting points (or at low homologous temperatures) needs to be further evaluated. There is another caveat associated with the Hall-Petch relationship. Ideally, one should only vary the grain size of the material when discussing the grain size effect while keeping other factors unchanged, such as the chemical composition or second-phase particles. In reality, this is far from the case, which often causes confusion in this area.

Many research efforts have been focused on factors that affect the Hall-Petch coefficient of $k_{H\text{-}P}$, including texture, temperature, stacking fault energy, and plastic strain. It has been recognized that temperature has a strong effect on $k_{H\text{-}P}$, especially at relatively high homologous temperatures ($T/T_m > 0.25$). This is not surprising as dislocation dynamics is a strong function of temperature. However, most literature models of the Hall-Petch effect do not incorporate the temperature effect. One of the few exceptions is the model proposed by Figueiredo and Langdon [496] (see Eq. (4) above). As temperature increases, the Hall-Petch coefficient decreases. This is shown in Fig. 16, which illustrates the results for Cu, Fe and Mg as compiled by Figueredo et al. [482].

Not much can be found in the literature regarding the effect of strain rate or loading rate on the Hall-Petch effect, especially in the UFG and NC regions. For example, Astafurov et al. [498], examined the effect of strain rate on the Hall-Petch coefficient $k_{H\text{-}P}$ for two austenitic stainless steels with coarse grains. It was found that while strain rate may affect the term σ_0 in the Hall-Petch equation, its effect on $k_{H\text{-}P}$ was only marginal. For example, for two decades of increase in strain rate ($1.0 \times 10^{-4}\ s^{-1}$ to $1.0 \times 10^{-2}\ s^{-1}$), only minor changes in $k_{H\text{-}P}$ were observed (322–327 MPa.$\mu m^{0.5}$) for 316 steel.

There has been strong interest in the texture dependence of $k_{H\text{-}P}$ for practical reasons, especially in metal forming. This is particularly the case for materials such as Mg and its alloys with strong plastic anisotropy. A significant texture dependence has been established for the Hall-Petch coefficient of such materials [499–503]. Yu et al. published a brief but critical review on the Hall-Petch effect in Mg and Mg-alloys [499]. It was also found that alloying Mg with rare earth elements can mitigate the texture dependence of the Hall-Petch effect [504].

Grain size effect on $k_{H\text{-}P}$ manifests itself when the grain size d is refined into the UFG/NC regimes, particularly at moderate and high homologous temperatures when GB sliding becomes significant, which will be discussed in the following section. When the grain size of a metal is refined into the NC regime, especially around 20 nm or smaller, the Hall-Petch slope levels off and may eventually become negative. This breakdown of the Hall-Petch relation has been widely termed the inverse Hall-Petch effect. For example, Fig. 17 shows the compilation by Razavi et al. [505] for prismatic slip in AZ31 Mg alloy, including the authors' own data and data from the literature. Since the grain size of the AZ31 Mg alloy was reduced by the "top-down" method (SPD) and no volume defects (such as those from powder consolidation) are of concern, the $k_{H\text{-}P}$ values can be trusted.

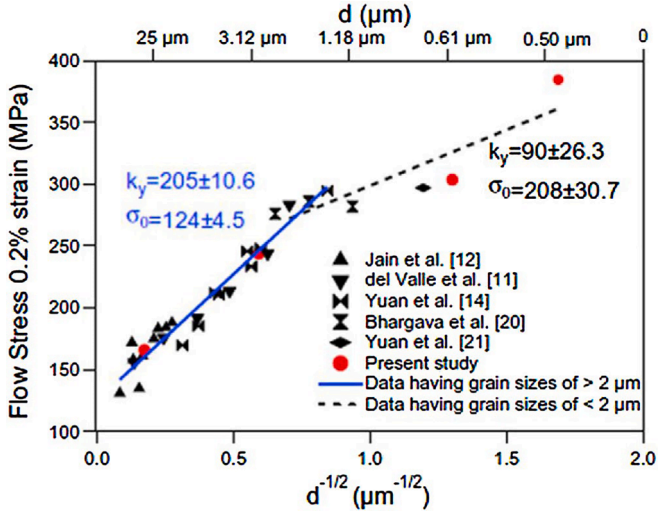

Fig. 17. Hall-Petch plot for prismatic slip in AZ31 Mg alloy, compiled by Razavi et al. [505]. Refer to the original article for the source of data in the plot.

There have been challenges in confirming the inverse Hall-Petch effect. First, early experimental results suffered from artifacts caused by the materials processing routes, especially powder metallurgy, or bottom-up methods involving two-step processes. Such effects as poor inter-particle bonding, contamination, and residual porosity may give rise to spurious grain size effects [42,455]. The second challenge is the ubiquitous stress-driven grain growth observed in pure metals, even at low homologous temperatures [506,507]. The third challenge lies in the difficulty in singling-out the grain size effect when other factors, such as compositional and microstructural changes, are also involved. As such, early experimental results are subject to debate [42]. Even later results for the inverse Hall-Petch effect are debatable due to the possible processing artifacts, grain growth effects, and errors associated with the conversion of hardness to yield strength in NC materials [82].

Predictions from MD simulations [31,508–514] have suggested the inverse Hall-Petch effect for extremely small grain sizes. The proposed mechanisms include the lack of dislocation storage in NC metals during plastic straining, GB sliding, grain rotation, and GB diffusion. Experimental validations of the MD simulations are still a challenge. Other models and mechanisms have also been proposed to explain the inverse Hall-Petch effect, such as the dislocation-based model [509,515], diffusion-based models [460,516], GB shearing models [13], and two-phase-based models [517]. At ultrafine grain sizes, the GB sliding mechanism is often assumed to be rate-controlling, further contributing to the observed weakening. Under this mechanism, as the grain size decreases, the material strength diminishes due to the increased role of GB sliding over the dislocation-driven mechanisms [482,496,518–520].

4.2.2. *Strain rate sensitivity and activation volume*

Many articles have been published since the early 2000s on the strain rate sensitivity (SRS) and activation volume of NC metals and alloys [26,41,521,522]. It has been established that the trend in SRS as a function of grain size depends on the crystalline structure of

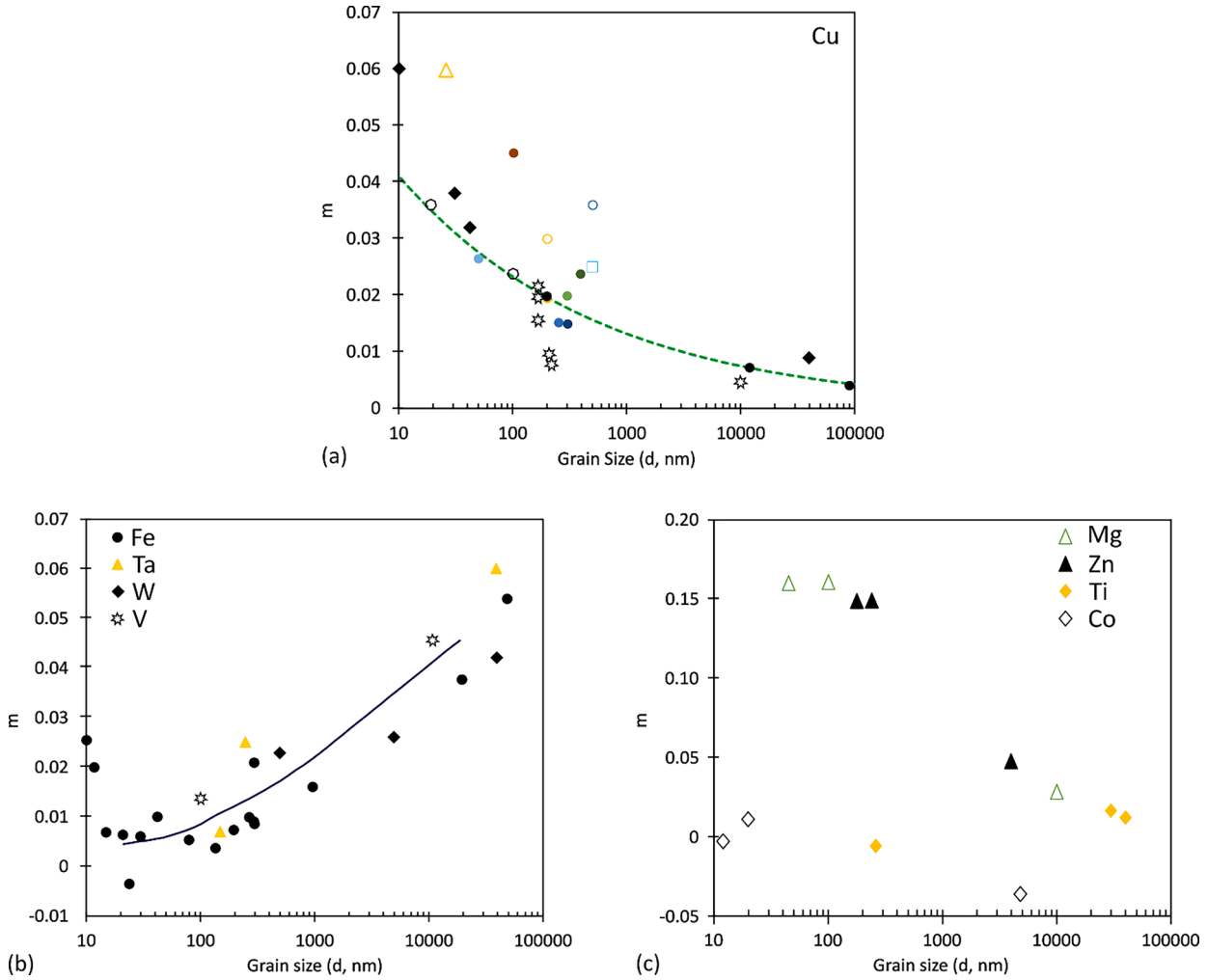

Fig. 18. (a) Strain rate sensitivity parameter (m) of copper as a function of grain size (d) [41]. (b) Strain rate sensitivity of BCC metals. The solid curve was calculated based on the model presented in Ref. [35] of the original paper [41]. (c) Strain rate sensitivity of HCP metals as a function of grain size.

the metal. For FCC materials, earlier work showed that SRS increases with decreasing grain size and increasing plastic strain [523]. The SRS of NC FCC metals can be one order of magnitude higher than that of the coarse-grained counterparts. Fig. 18a shows the trend of SRS parameter m as a function of grain size for FCC Cu [41].

The trend in SRS of BCC metals (Fig. 18b) as a function of grain size is drastically different from that for FCC Cu—it decreases with decreasing grain size, except for NC tantalum, as shown by MD simulations recording a remarkable SRS value attributed to GB-mediated plasticity. Another MD simulation of NC Ta films reported SRS values close to the experimental results [524]. Similar MD results were reported for NC BCC iron but with a much lower SRS value [103]. New data [525,526] after the publication of Fig. 18b for BCC metals did not add new observations but confirmed the established trend [41]. Some experimental results on sputter-deposited high-purity Ta showed increased SRS in the NC regime [527]. However, it should be noted that Ta thin films fabricated by physical deposition, such as direct current magnetron sputtering, can exhibit a tetragonal or BCC structure, or a mixture of both [527]. Wang et al. [528] even reported a negative SRS based on indentation measurements on sputter-deposited Ta, presumably caused by the β-α transformation induced by the pressure under the indenter. Considering that BCC metals, including Ta, are very sensitive to interstitial impurities, the effects of interstitials on the SRS trend in the NC regime need more research.

The data on SRS of HCP metals as a function of grain size is quite scarce. No convincing trend has been established in this case. Fig. 18c shows some sporadic data for different HCP metals. However, the general trend for magnesium and its alloys is that as the grain size is reduced, SRS increases along with a reduction in plastic anisotropy and strain hardening rate, significantly improving the tensile ductility of Mg and Mg-alloys [491–493,529,530]. These recent experimental results have confirmed the earlier observations by Hwang et al. [495,531]. Choi et al. [493] fabricated Mg with grain sizes ranging from 60 nm to a few micrometers and observed increased SRS in the nano-regime. Fig. 19 displays the results for SRS and activation volume as a function of the the grain size in Mg [493]. Fig. 19 (a) shows that the SRS of Mg nearly follows the Hall-Petch trend with the inverse square root of the grain size as shown in Fig. 19(b). Accordingly, the activation volume for plastic deformation decreases. Wang and coworkers produced NC Mg by ball milling followed by SPS and measured an SRS of 0.17 [532]. These authors attributed the extremely large compressive strain (~120 %) to the exceptionally high SRS. Since the mechanical testing was performed under compression, it would be interesting to see how the samples behaved under tension. "Superplasticity under compression" as stated by the authors in their paper [532], is a misnomer. Recent work by Yu and co-workers on the creep behavior of an NC Mg–Gd–Y–Zr alloy using instrumented nanoindentation reported a negative SRS and the authors attributed the results to deformation twinning [533]. The work by Wan et al. [534] on a similar NC Mg alloy did not report a negative SRS. However, from the stress–strain curve and the high strength and strain hardening, a negative SRS would not be convincing [534].

Asaro and Suresh [535] proposed a mechanistic model to explain the small activation volumes and enhanced SRS of FCC metals with NC grains and nano-scale twins. A significant part of their explanation is based on Rice's model [536] for the emission of dislocations at a crack tip due to stress concentration. The model also considers the emission of partial dislocations and the contribution of mechanical twinning, which has been observed experimentally in some FCC metals. Their model gives activation volumes in the range of 3–10 b^3. However, as pointed out by Swygenhoven et al. [537], the model is based on purely athermal, mechanically-driven nucleation and propagation of dislocations from GBs. Zhu et al. [538], based on MD simulations, proposed a mechanistic framework to predict the strain rate sensitivity of NC metals with profuse twins. They showed that slip transfer reactions mediated by twin boundaries are the rate-controlling mechanisms of plastic flow. Their work was aimed at understanding the exceptional combination of high strength and good ductility of nano-twinned Cu [48].

For BCC metals, the activation volume decreases to a nearly constant value when the stress is increased to a moderate level [539,540]. This phenomenon can be readily understood by considering the double-kink nucleation process as the rate-controlling mechanism for BCC metals at low homologous temperatures. Dorn and Rajnak's analyses [540] showed that the critical length of the double kink, or the spread width between the two kinks, would be ~ 1.0 μm. Below this, the activation volume decreases with stress

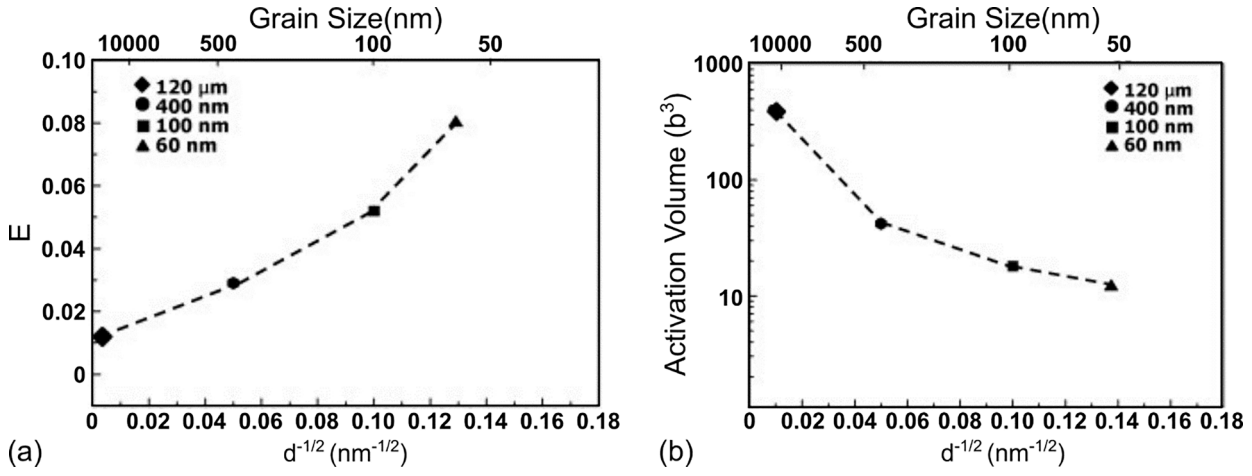

Fig. 19. Plots of (a) strain rate sensitivity and (b) activation volume as a function of grain size of magnesium [493].

only very slowly. However, the stress still follows the Hall-Petch relation. The Hall-Petch coefficient is usually independent of strain rate and temperature, and the grain size to a large extent [541] The decrease of SRS with the reduction of grain size in BCC metals can be explained by the increasing prevalence of GB strengthening while the rate-controlling mechanism stays the same, namely, nucleation of double kinks. It is uncertain if double-kink nucleation is still the rate-controlling mechanism when the grain size falls below 50 nm. Available experimental data on samples of fully dense BCC metals have only been available for the smallest grain size of ~ 40 nm [526]. Whether GB-related mechanism affects even smaller grain-size metals is an open question. Because most BCC metals are refractory metals with high melting points, their production as bulk NC materials is extremely difficult. Other unconventional mechanical testing techniques, such as micro-compression [475], may need to be utilized to probe the rate effect on small specimens. New models may be required if experimental results contradicting the present observations become available.

For HCP metals, a model for the grain size dependence of SRS is still lacking. Zheng et al. [542] examined the origin of SRS over a decade range of strain rates (10^{-5} to 10^{5} s^{-1}) considering three mechanisms: dislocation nucleation, time of flight (dislocation mobility), and thermally activated escape of pinned dislocations. Their work was based on discrete dislocation simulations, even though HCP titanium was used as the model material. How the work can be extended to include the effect of grain size or other length scale parameters is uncertain.

Armstrong examined the literature data for strain rate sensitivity and proposed that SRS and the reciprocal of activation volume followed Hall-Petch relation when plotted again the inverse square root of grain size [59]. Fig. 20 (a) displays the inverse activation volume versus the inverse square root of the grain size (l), and Fig. 20 (b) is the double-logarithmic plot of the inverse activation volume versus the grain size.

Similar Hall-Petch effect of activation volume and strain rate sensitivity was observed and elaborated by Figueiredo et al. [482,496]. However, such trends could only be established for FCC metals. BCC metals do not follow the trend, as seen from the previous discussions. Whether HCP metals follow such a trend is still an open question.

4.2.3. Creep behavior of NC materials

Creep is a fundamental property describing the mechanical behavior of materials at high temperatures, which plays a crucial role in the operational life of many engineering components. In coarse-grained materials (with an average grain size greater than 1000 nm), the creep deformation mechanisms are well-known [543] and are dominated by dislocation climb and lattice diffusional flow. These mechanisms have been combined in a classical macroscopic treatment, wherein the steady-state creep rate $\dot{\varepsilon}$ under an applied stress σ is given by [543]:

$$\dot{\varepsilon} = AD_0 exp\left(-\frac{Q}{kT}\right)\left(\frac{Gb}{kT}\right)\left(\frac{b}{d}\right)^{p}\left(\frac{\sigma}{\mu}\right)^{n} \tag{5}$$

where A is a dimensionless constant, D_0 is the frequency factor, Q is the activation energy for creep, T is the temperature, μ is the at-temperature shear modulus, p is the grain size exponent, and n is the stress exponent. The value of the stress exponent n can be used to distinguish between the dominant mechanisms: $n = 1$ implies a stress-directed diffusion-dominated Coble and Nabarro-Herring creep mechanisms, while $n \geq 3$ implies a dislocation-mediated creep mechanism.

Fig. 21 visually represents a simple relationship (based on Eq.(5)) between steady-state creep and applied stress for two-grain sizes. As the grain size decreases, particularly approaching the NC range, GB diffusion creep becomes increasingly dominant and significant even at lower temperatures and moderate stress levels. This observation has been experimentally confirmed [14,544–552], as the diffusion-based mechanisms of Nabarro-Herring and Coble creep generally exhibit a smaller stress exponent and a stronger dependence on grain size compared to dislocation-based mechanisms [553]. Consequently, Coble creep prevails in materials with finer grain sizes, such as those within the NC regime, facilitated by GB diffusion at relatively lower temperatures, leading to higher steady-state creep rates [554]. Notably, many pure NC materials, characterized by grain sizes below 100 nm, exhibit steady-state creep rates four to five orders of magnitude higher than those observed in coarse-grained materials [17,544,555].

Despite their excellent properties at room and cryogenic temperatures [21,33,42,62], NC materials exhibit somewhat inferior creep behavior compared to coarse-grained materials, which is primarily attributed to the high diffusivities in NC materials. For instance, Gleiter reported significantly higher diffusivities in NC Cu than in conventional Cu [2]. Chokshi et al. [455] attributed the inverse Hall-Petch effect in NC Cu to rapid diffusion creep (Coble creep) at room temperature, but the inverse cube dependence of strain rate on grain size could not be experimentally verified. Further, an early investigation focused on NC Cu at room temperature [556] revealed that NC Cu exhibits a higher steady-state creep rate than its coarse-grained counterpart. The NC Cu synthesized using IGC and consolidated at room temperature, had an average grain size of 25 nm, as determined through XRD measurements.

While no definitive conclusions were drawn regarding the rate-controlling mechanisms during creep in NC Cu, an important observation was that a significant enhancement in creep rate does not occur as grain size decreases. Similarly, Wang et al. [545] studied the high-temperature creep behavior of NC Ni-P alloys produced by crystallizing amorphous ribbons. They focused on the stress exponent and activation energy, examining NC Ni-P samples with grain sizes of 28 nm and 257 nm under a tension-based setup at 573 K with an applied load of 146 MPa. Analysis of the creep curves showed instant high strains and an initial stage showing a decreasing creep rate, with the 28-nm sample exhibiting a significantly higher creep rate than the 257-nm sample. These findings suggest a change in creep mechanisms as grain size decreases.

Sanders et al. [557] extensively investigated the creep properties of NC Cu with varying grain sizes in the temperature range of 0.24–0.48 T_m. In the low-temperature region, NC Cu exhibited slow creep rates following the logarithmic or exhaustion creep relationship. However, the measured creep rates were notably slower than those predicted by the Coble creep theory [554]. Similarly, Cai

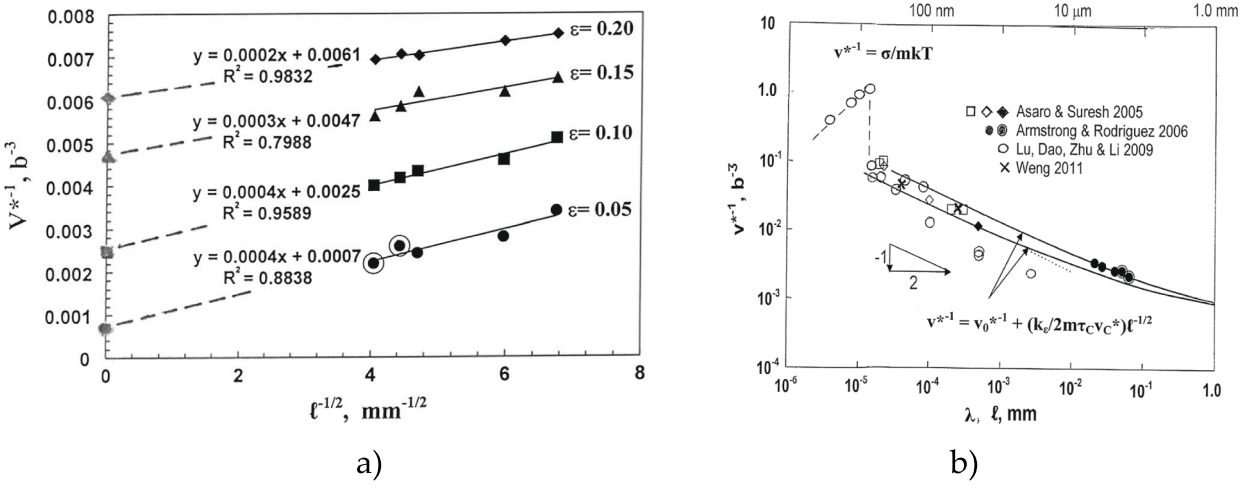

Fig. 20. (a) Hall-Petch plot of reciprocal activation volume for nickel, and (b) double-logarithmic plots of reciprocal activation volume for Cu and Ni versus grain size for Cu and Ni, compiled by Armstrong in celebrating six decades of Hall-Petch effect [59]. See the papers by Armstrong for the literature data sources.

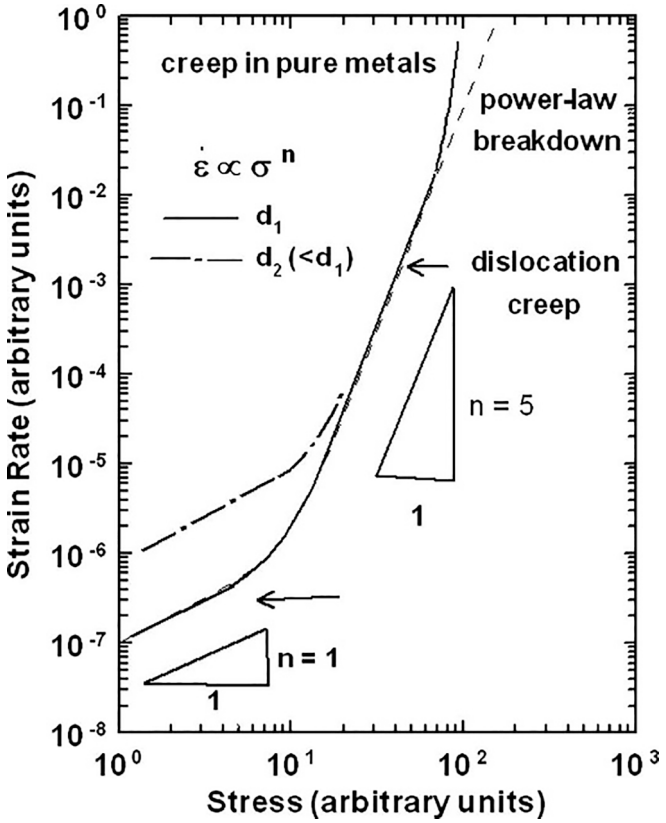

Fig. 21. Illustration of a simple relationship between steady-state creep and applied stress for two-grain sizes [544].

et al. [546] observed a GB diffusion-based mechanism during the tensile creep of pure NC Cu at around room temperature (0.22 T_m – 0.24 T_m). In the case of high-strength materials such as Ni, Wang et al. [545] investigated the influence of grain size on the room temperature steady-state creep rate of NC Ni, which was processed using an electrodeposition technique. Their finding suggests that the effect of grain size on creep behavior aligned with the model of GB sliding controlled by GB diffusion. Further, they observed faster creep rates for smaller grain sizes, and the total creep strains measured in the experiments were less than 0.01, which may not be sufficient to confirm the presence of steady-state creep. Similarly, Yin et al. [548] conducted a tensile creep test on NC Ni at room temperature. They measured the stress exponent, which was found to be one (1), confirming the creep rate associated with diffusional Nabarro-Herring or Coble creep, exhibiting a linear dependence with the true applied stress [553].

The studies discussed above have generally found that as grain sizes approach the NC range, GB diffusion creep becomes increasingly dominant and significant at low temperatures (e.g., room temperature) and moderate stress levels. However, the lack of TEM characterization of post-deformed samples in these studies makes it challenging to determine the controlling creep mechanism(s) definitively. Various factors, such as difficulty with sample preparation, and sample size and geometry may contribute to the lack of TEM characterization. Additionally, some of the consolidated NC samples used in these studies have been too small to undergo conventional, large-scale mechanical tests.

In recent years, the indentation method has emerged as an effective approach to studying the creep deformation of NC materials [17,558–563]. Most of the nanoindentation creep studies have indicated mixed diffusional mechanisms [561]. However, it is essential to consider the state of stress in nanoindentation, as some reports have observed dislocation nucleation and high creep rates under high stresses induced by the indenter tip [560,563,564]. Despite the progress made with nanoindentation, studies on the creep behavior of NC metals and their alloys at elevated temperatures remain limited, even for bulk-scale samples [67,230,560,562].

Alongside experimental investigations, atomistic modeling, such as MD simulations, has played a crucial role in understanding creep behaviors and the underlying mechanisms of NC materials. For instance, Swygenhoven et al. [27,35,39,565,566] have conducted MD simulations on various NC materials, including NC Ni, at low temperatures and found that creep deformation in these materials could be attributed to GB sliding, grain rotation, and GB motion. Gleiter and co-workers studied various aspects of deformation mechanisms, including diffusion creep in Si and Pd at high temperatures. The creep behavior in these cases is controlled by GB diffusion and described quantitatively by Coble creep [31,283,510,547]. More recently, using atomistic simulations, Wang et al. [567] suggested that the creep mechanism in NC materials can transition from Coble creep to GB sliding to dislocation-base plasticity. Unfortunately, high strain rates and the short time scale limit the broader applicability of MD simulations since lattice diffusion and solute hopping that occur at low temperatures are nearly frozen on the MD time scale. Nevertheless, these atomistic simulations have

been instrumental in providing insights into the complex creep behavior of NC materials.

While the experimental studies have provided valuable insights, certain limitations must be acknowledged. One major challenge arises from the relatively small total creep strains measured, usually not exceeding 0.05, making it difficult to distinguish between gradual creep rate decreases and the attainment of steady-state creep [568]. Moreover, the lack of sufficient data on the grain size dependence of creep rate makes it hard to definitively determine the dominant creep mechanism. The absence of post-TEM characterizations of deformed samples further compounds the issue, as it hinders the understanding of rate-controlling mechanisms in NC materials. Concurrent deformation processes and microstructural changes during prolonged creep tests can lead to wide variations in reported steady-state creep rates and controlling mechanisms [17,544,546,548,569]. For instance, in some studies on NC Ni, stress exponent values have been reported in the range of 1 to 40 for approximately the same average grain size [545,548,570–572]. This discrepancy can be attributed to concurrent grain growth during creep deformation, as thermo-mechanically induced microstructure instability has been observed at both room and high temperatures [17,544,546,548,569]. For example, NC Ni displays grain growth during creep deformation [571]. At moderate temperatures, NC Cu displays a continuous decrease in creep rate even after prolonged testing, accompanied by grain growth from 25 nm to several hundred nanometers [557]. Similarly, almost a five-fold increase in grain size was observed during room temperature creep of NC Ni by Wang et al. [560], as seen in Fig. 22.

While refining microstructure in pure metals and alloys through nano-crystallization holds promise, microstructural instability can hinder practical applications of bulk NC materials (with overall grain size not exceeding about 100 nm). Therefore, the suitability of NC materials for structural applications is yet to be thoroughly evaluated. The observed variations in stress exponent values can be attributed to factors such as concurrent grain growth, impurities, level of creep strains, testing conditions, and sample geometry. Nonetheless, these findings underscore the significant influence of grain structure on the creep behavior of NC materials, with a decrease in grain size leading to an increase in the creep rate.

4.2.4. Fatigue properties of NC materials

Cumulative damage due to cyclic loading is a leading cause of structural failure in many technologically critical applications. During cyclic loading, the local microstructure in highly stressed areas evolves, eventually leading to the nucleation and growth of small surface cracks near impurity sites, persistent slip bands (PSBs), or GBs that interact and interlink. Ultimately, these microstructural changes can result in catastrophic failure [573,574]. Viable ways to improve fatigue resistance include enhancement in tensile strength, reduction in initial damage, and dispersion of accumulated damage (as opposed to strain localization) during cyclic loading [575]. In coarse-grained materials, the fatigue strength is typically enhanced by increasing the tensile strength through solute additions, heat treatment, or reduction in grain size [49,576,577]. The underlying mechanisms for such improvement in fatigue strength point toward competition between crack initiation and damage accumulation [21]. Typically, solute additions improve fatigue strength by stabilizing the microstructure, altering the stacking fault energy and dislocation cross-slip behavior, and/or retarding crack advancement [578].

Several recent studies have indicated enhanced fatigue behavior of NC metallic materials and hierarchical gradient nanostructure materials compared to their coarse-grained counterparts [579–584]. This is attributed primarily to greater resistance to crack initiation [21,49,585,586] and strain localization [587–589]. Thus, NC materials present a viable alternative to coarse-grained equivalents for cyclic load-bearing structural applications. Despite the great potential of NC alloys, very few studies have addressed their microstructural evolution under fatigue loading when the grain size remains stable during cyclic loading.

It is well-established that, under similar conditions, the endurance limit of initially smooth-surfaced specimens generally correlates with the material strength, which tends to increase as the grain size decreases. Recent studies have revealed that NC/UFG metals subjected to cyclic fatigue loading exhibit heightened crack initiation thresholds and accelerated crack propagation rates, contributing to enhanced fatigue lifetimes [579–583]. The improved fatigue resistance is primarily attributed to the combination of higher yield strength and smaller grain size in NC/UFG materials compared to conventional coarse-grained counterparts [21,49,585,586]. In essence, the suppression of dislocation activity in NC materials effectively increases the strength [35]. Consequently, NC materials demonstrate superior resistance to fatigue crack initiation (due to strain delocalization) and higher fatigue endurance limits during stress-controlled high-cycle fatigue tests.

For instance, investigations by Hanlon et al. [581,582] into the fatigue behavior of cryo-milled Ni at a load ratio (R) of 0 have revealed an increased fatigue endurance limit with grain size reduction, as depicted in Fig. 23. Additionally, smaller grain-size materials exhibited significantly higher crack initiation resistance at a lower load ratio than their coarse-grained materials. Similarly, the S-N behavior of pure electrodeposited Co under both NC and coarse-grained regimes at an R-value of 0.25, as shown in Fig. 23b [590], underscores the strong dependence of fatigue behavior on grain size. The cyclic loading resistance of electrodeposited pure Co is notably higher in the NC state than in the coarse-grained state. Similar enhancements in fatigue life have also been observed in alloy systems, such as Ni-Fe and Ni-Mn, under $R = -1$ loading conditions [585]. However, it is important to note that grain refinement does not universally guarantee improved fatigue life, as experimental results have shown variation within the same material systems with similar grain sizes. For example, Cavaliere et al. [590] demonstrated that NC Ni samples with closely matched microstructures (average grain sizes of 20 nm and 40 nm) at $R = 0.25$ exhibited markedly different fatigue behaviors, indicating that fatigue life did not consistently correlate with grain refinement. Additionally, Fan et al. [591,592] found that fatigue life in NC Ni-Fe with an average grain size of 18 nm for $R = 0.1$ was comparable to coarse-grained materials, in contrast to the findings by Boyce et al. [585]. These divergent outcomes (Fig. 23) emphasize the effects of sample preparation and material quality, consistency, and variability, and the need for a systematic approach to determine the fatigue behavior of NC materials while accounting for other extraneous effects.

In NC materials, high fatigue life is attributed to an increase in the number of cycles required for crack nucleation since the small grain size makes nucleation of lattice dislocations and their propagation difficult [537]. On the other hand, GB processes govern most

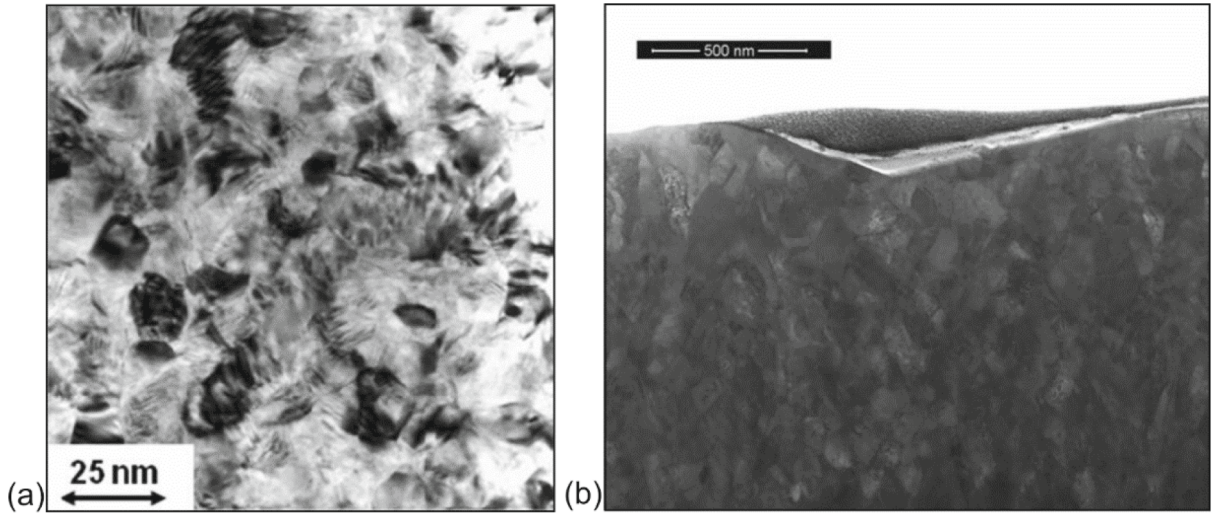

Fig. 22. Bright-field TEM image of as-deposited Ni, showing an average grain size of about 14 nm. Bright-field STEM image of Ni indentation creep at 448 K showing the grain structure is uniform and the size is about 77 nm [560].

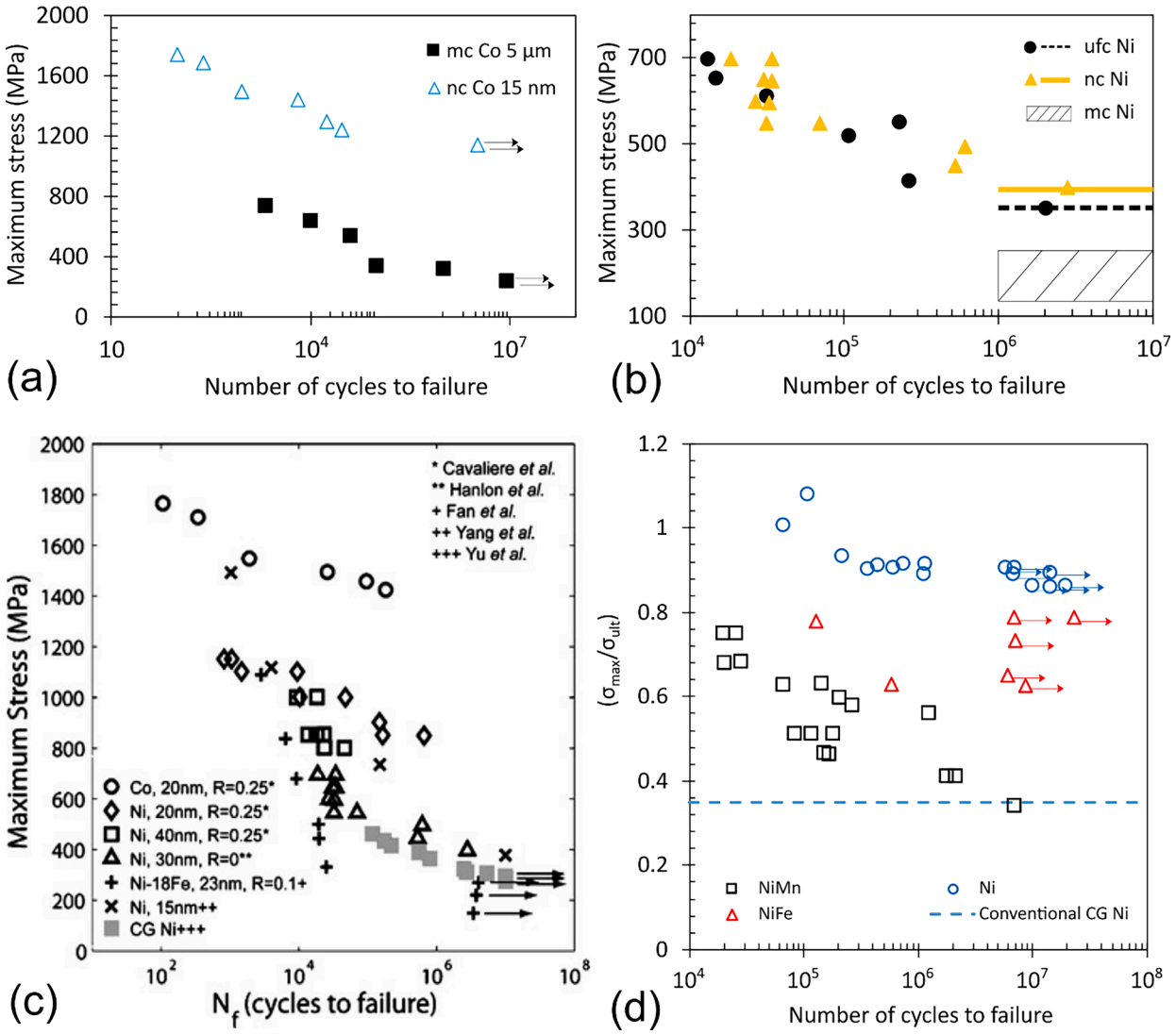

Fig. 23. (a-d) Plots of applied stress versus number of cycles to failure (N_f) for Co and Ni with different grain sizes [573,581,585].

of the mechanical properties of NC materials. Therefore, fatigue crack initiation in NC materials has been associated with subsurface nucleation at internal defects and/or surface extrusions. However, the exact mechanisms of surface extrusions are unclear since the average grains in these NC materials are too small to form PSBs, as in the case of coarse-grained materials. Through atomistic simulations in NC Al [537], nucleation of dislocations from GBs and their propagation through the grain interior by a pinning-depinning mechanism have been observed. These dislocations glide across the adjacent or opposite GBs until being fully absorbed into the GBs. The formation of PSBs is impossible. One possible scenario would be where the crack initiation that results in higher fatigue life is preceded by the formation of coarse grains enabling PSB mechanisms, i.e., localized grain growth [585] (see Fig. 24). In fact, mechanically driven recrystallization and grain growth have been observed under both monotonic and cyclic conditions in NC and UFG materials [49,507,593,594]. Grain geometry is also said to influence growth, where the elastic mismatch increases the elastic driving force and causes local variations in GB mobility [585,595].

Overall, the substantial variability in the reported fatigue life of NC materials can be attributed to differences in loading conditions, impurities, sample preparation techniques, sample dimensions/geometry, and the evolving microstructure as a function of cyclic loading. Importantly, since many NC metals exhibit deformation-induced grain growth [585], gaining a comprehensive mechanistic understanding of their fatigue behavior remains challenging.

The analyses of crack resistance and the growth of stable crack behavior are critical to many engineering applications. Generally, fatigue crack growth behavior is evaluated for single-edge notch material specimens with pre-existing cracks under constant cyclic load experiments. As such, the mechanism for crack resistance, i.e., resistance to subcritical fatigue fracture and growth mechanisms, can be inferred. In materials with a coarse-grained structure, certain mechanisms contribute to the increased range of the stress in-

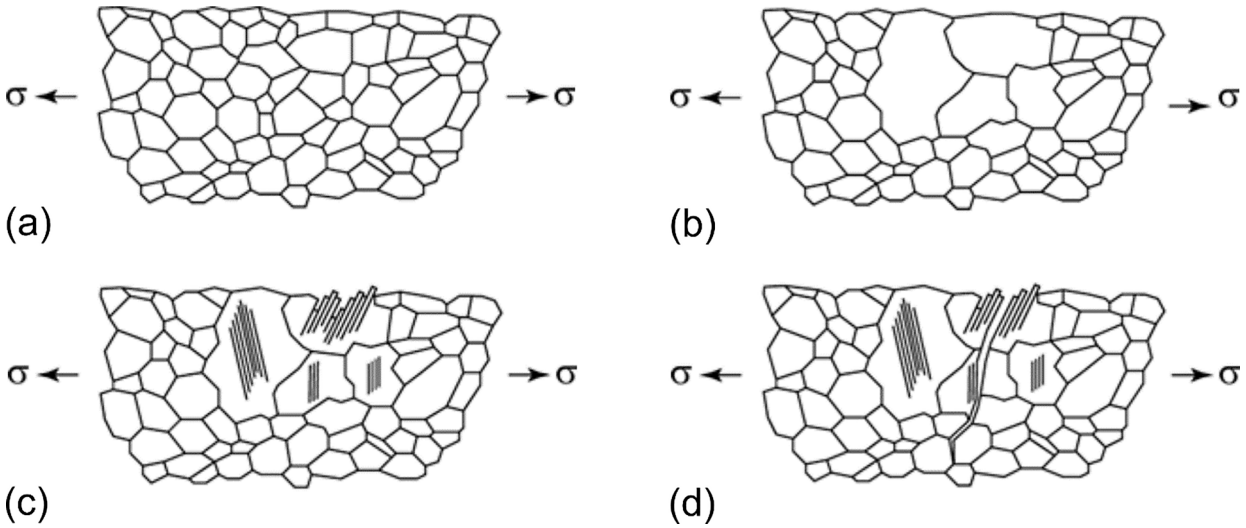

Fig. 24. Plausible crack initiation mechanisms in NC metals (after [585]): (a) initial state, (b) initial grain growth, (c) enabling PSB mechanisms, and (d) crack initiation due to interaction of PSBs with the free surface.

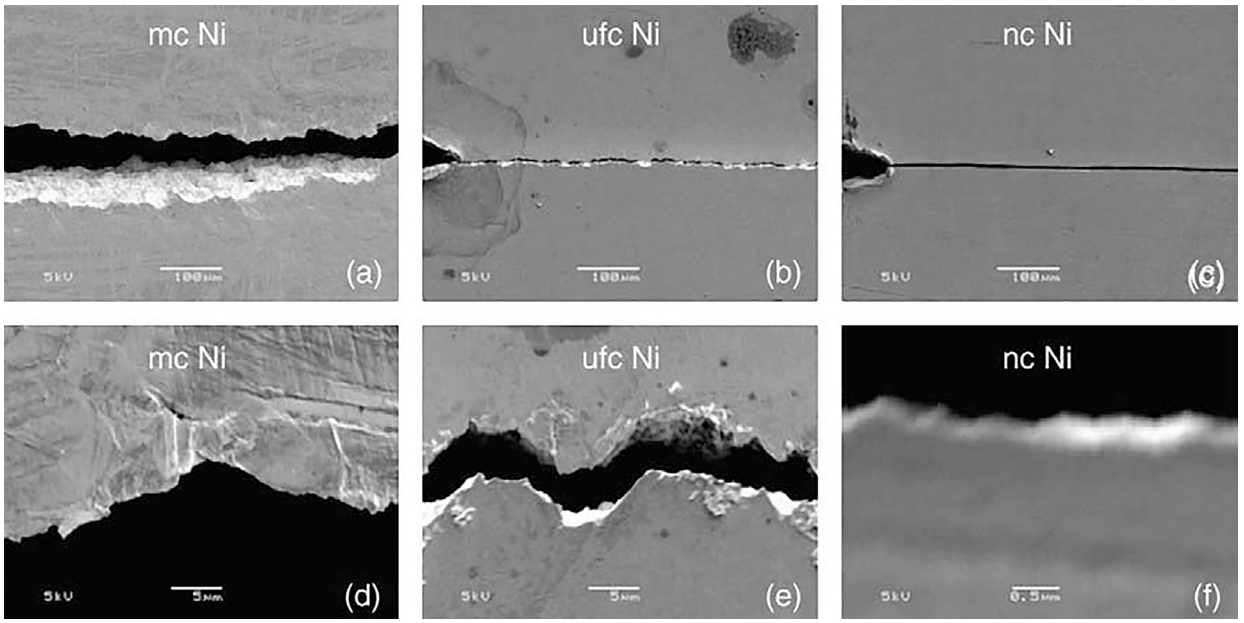

Fig. 25. Scanning electron micrographs of (a, d) microcrystalline (mc), (b, e) UFG, and (c,f) NC Ni [582] showing varying levels of plastic deformation, crack tip blunting, and crack growth.

tensity factor threshold of the fatigue crack. These mechanisms involve strain localizations and periodic deflections of the fatigue crack path at GBs during crystallographic fracture. These result in enhanced resistance to fatigue crack growth, facilitated by plastic deformation, crack-tip blunting, and the intricate crack path observed in both coarse-grained and UFG materials [21,575,582], as shown in Fig. 25. Further, in coarse-grained materials, the enhancement in strength due to a reduction in the average grain size leads to enhanced fatigue life (N_f) disregarding other structural influences. Here, the fatigue life is dominated by the crack nucleation as the grain refinement reduces the extent of crack path tortuosity (Fig. 25). However, isolating the exclusive impact of grain size on fatigue response in coarse-grained materials is often challenging due to the influence of other structural factors such as second phases, impurities, crystallography, initial defect density, etc.

Fig. 26 shows fatigue crack growth data for various NC materials as well as some coarse-grained and UFG materials. The reduction in grain size from coarse-grained to NC range is in line with expectations, leading to a distinct decrease in threshold (ΔK_{th}) and a

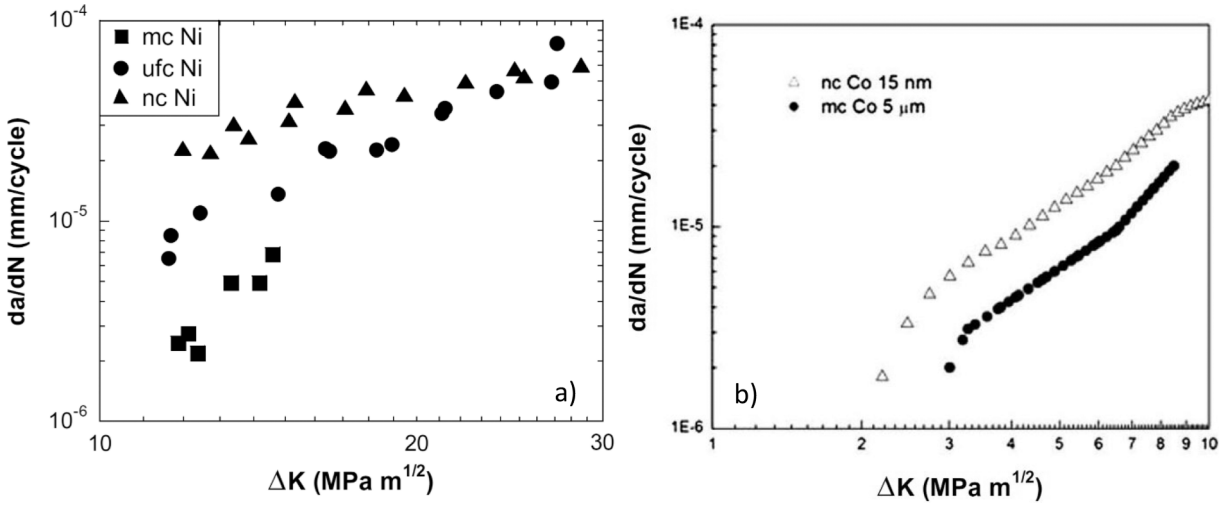

Fig. 26. Variation of fatigue crack growth rate, da/dN, as a function of the stress intensity factor range, Δ K, for (a) Ni and (b) Co with various grain sizes [49,581,582].

significant rise in the rate of fatigue crack growth from the threshold point to the ultimate failure. In other words, experimental results show that with grain size reduction, the resistance to crack propagation also diminishes. Accordingly, the fatigue crack growth curves shift to the upper left on a da/dN and ΔK log-log plot [582], Fig. 26. This trend is consistent across various materials and processing conditions [582,590]. It's worth noting that the presence of impurities, such as hydrogen or oxygen, introduced during the processing of NC materials, as well as potential grain growth, can significantly contribute to this observed behavior. However, the existing literature often lacks comprehensive data on such factors, making the precise mechanisms and trends harder to ascertain. Nevertheless, the limited toughening in NC materials can be ascribed to the interplay of crack-tip plasticity and the crack path, involving microcrack bridging and the diversion of the crack trajectory. Once the crack grows, it propagates through the NC region with a straight path [582] instead of a tortuous path seen in coarse-grained and UFG materials [21,575,582] due to limited crack tip plasticity (also in part due to limited ductility under tension). The occurrence of flat, non-tortuous fatigue crack paths becomes evident with the progression of grain refinement, ultimately influencing the fatigue crack growth resistance adversely, as shown in Fig. 25 (c).

To further illustrate the issue, Hanlon et al. plotted the change in crack length as a function of the number of fatigue cycles for pure Ni with various average grain sizes. As shown in Fig. 27, the crack growth rate in NC Ni is significantly higher than that in the UFG and coarse-grained counterparts [49,581,582]. Other researchers have also demonstrated similar behavior: their experimental work on fatigue of NC metals shows higher fatigue crack growth rates than those in coarse-grained alloys [49,581,582]. The observed increases

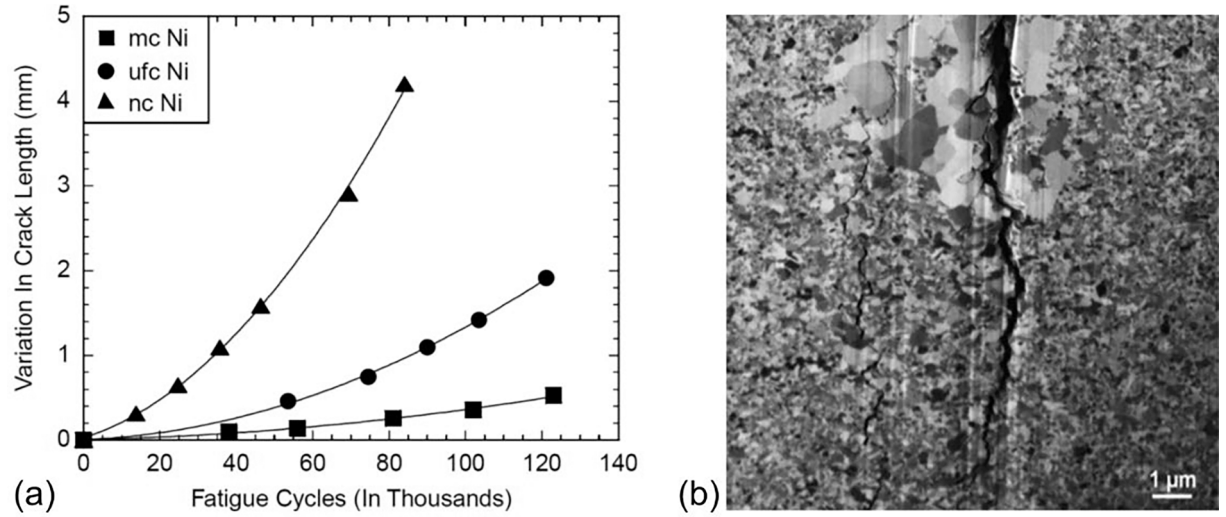

Fig. 27. (a) Variation in crack length as a function of the number of fatigue cycles for Ni [49,581,582], and (b) Ion-channeling image showing cyclic deformation induced micron-scale grain growth in NC Ni-Mn [49].

in fatigue crack growth rates indicate the possibility of different crack tip deformation/closure behaviors in NC metals compared to coarse-grained metals. While some trends in fatigue behavior in NC metals show the existence of grain size dependence, there is still a lack of fundamental understanding of the critical microstructural characteristics of NC metals (e.g., grain size heterogeneities) and their subsequent effects on fatigue crack growth mechanisms (e.g., cyclic plasticity). It is again worth repeating that in fatigue crack growth studies performed to date, NC metals have strongly exhibited deformation-induced grain growth [49] (Fig. 27b). Grain stability is an essential factor that will affect the crack initiation and propagation process in NC materials.

Overall, the fatigue behavior of NC materials can be understood through the following expression [596,597]:

$$N_f = N_{nuc} + N_{lc} \tag{6}$$

where N_{nuc} is the number of cycles to nucleate a crack, and N_{lc} is the number of cycles for long crack growth within the Paris regime. Generally, N_{nuc} depends on microstructure and has an inverse relation with the average grain size d [598]: $N_{nuc}\alpha 1/d$. Thus, the finer the grain size, the more cycles are needed to nucleate a crack, which is primarily a surface phenomenon. Hence, in NC material, most of the fatigue life is spent nucleating a crack, unlike that in coarse-grained materials. For NC materials, the stress amplitude versus N_f plot typically shows a right shift with refined grain size [581]. However, inconsistent results from the literature complicate our understanding of the effects of relevant operative length scales on fatigue crack nucleation processes. Nevertheless, grain growth or microstructural instability contributes significantly to N_{nuc}. Thus, microstructural stability and damage delocalization are important parameters controlling N_{nuc} in NC materials. On the other hand, N_{lc} might not solely rely on microstructural characteristics, as it is primarily regulated by plasticity, typically diminished in NC materials. In essence, after the fatigue crack traverses through grains that have coarsened during cyclic deformation, its continued propagation becomes unobstructed due to restricted crack-tip plasticity and reduced tortuosity. Therefore, strength–ductility combinations can be used to enhance NC materials' N_{lc}.

4.2.5. High strain rate deformation

First, it is useful to define the strain rate ($\dot{\varepsilon}$) range utilized in scientific research and engineering practice [599]. Static experiments, such as creep dominated by viscoelastic/viscoplastic material response, correspond to strain rates $\leq 10^{-5}$ s^{-1}. Quasi-static strain rate corresponds to the range of up to $\sim 10^{0}$ s^{-1} utilizing conventional hydraulic, servo-hydraulic, or screw-driven test machines. The medium or dynamic strain rate regime utilizes high-velocity hydraulic or pneumatic machines producing strain rates from 10^{1} s^{-1} to 10^{3} s^{-1}, where inertial forces become important. Dynamic high strain rate regime corresponds to $\dot{\varepsilon}$ up to $5x10^{4}$ s^{-1}, and ultra-high strain rates involving high-velocity impact-producing shock waves correspond to strain rates above 10^{5} s^{-1} [599].

Accurate evaluation of the mechanical behavior of materials within the medium dynamic strain rate range remains challenging. The most utilized experimental technique for dynamic high-strain rate behavior is the Kolsky bar (or Split-Hopkinson Pressure Bar) technique, which can load specimens at high strain rates under torsion, compression, and tension [599]. Among the three modes, loading under compression is most investigated. Many articles, and even books, can be found about the working principles, design, manufacturing, operation and data processing, and interpretation of Kolsky bar systems for various materials [600–602]. Miniature Kolsky bar systems have also been designed, manufactured, tested, and analyzed [603,604].

To understand the dynamic high strain rate behavior of NC materials, it is essential to first grasp strain rate sensitivity across the static to high-impact velocity regimes. Fig. 28 illustrates the flow stress of oxygen-free high thermal conductivity (OFHC) copper across three regions [603,604]: 1) the thermal activation region, where plastic deformation is dominated by thermally activated slip mechanisms, 2) the transition region, influenced by microstructure and lattice properties, and 3) the upturn phonon drag region, where lattice vibrations (phonons) dominate dislocation drag.

At low to moderate strain rates, plastic deformation occurs as dislocations overcome energy barriers from the material's intrinsic lattice resistance, as defined by the energy barrier model by Kocks et al. [607]:

$$\Delta G = \Delta G_0 \left[1 - \left(\frac{\sigma}{\sigma_0} \right)^{p} \right]^{q} \tag{7}$$

where ΔG_0 is the activation energy at 0 K (for which $\sigma = 0$), σ is the applied stress, σ_0 is the thermal component of the stress, and p and q are experimentally determined parameters. At higher strain rates, energy from plastic deformation turns into heat, causing adiabatic localized heating, which the Zerilli-Armstrong model [608] accounts for. However, this model does not include the dislocation drag at high strain rates.

The Johnson-Cook model [609] provides a widely used empirical expression for strain rate dependence of flow stress, while the Zerilli-Armstrong model accounts for adiabatic heating but omits dislocation drag. The upturn in flow stress due to dislocation drag was first observed in Cu by Follansbee et al. [610] and modeled by Follansbee and Kocks [611], with further refinements by Fan et al. [612] for BCC materials and Huang et al. [613] for FCC materials. Despite these advances, a comprehensive understanding of all dislocation barriers remains incomplete.

Dislocation drag arises from interactions between dislocations and lattice excitations (electrons, phonons, or magnons), with the drag force F proportional to dislocation velocity v:

$$F = Bv \tag{8}$$

where B is the drag coefficient [599]. This coefficient combines contributions the from electron (B_e), phonon (B_{ph}), and magnon (B_m) drag. The dislocation velocity increases with the strain rate $d\gamma/dt$ according to Orowan's equation $d\gamma/dt = \rho_m.b.v$ [614], where ρ_m is the

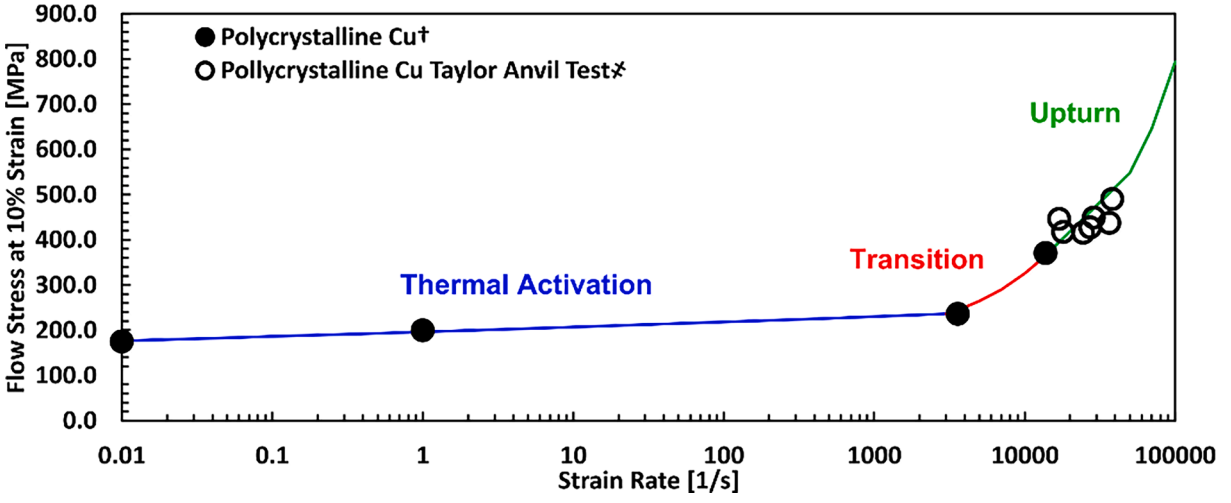

Fig. 28. Flow stress as a function of strain rate for polycrystalline Cu. Experimental results are from Jordan et al. [605] on static tests (†) and House et al. [606] on Taylor Anvil tests (⊁). The thermal activation, transition, and upturn regions are marked with blue, red, and green lines, respectively. (For interpretation of the references to color in this Fig. legend, the reader is referred to the web version of this article.)

density of mobile dislocations and *b* is the magnitude of the Burgers vector. Phonon drag, particularly significant at high temperatures and strain rates, results from interactions between fast-moving dislocations and phonons, and can increase the flow stress. To enhance ductility at high strain rates, obstacles are introduced to slow the dislocation glide and prevent phonon drag from leading to failure. At elevated temperatures, the drag force increases as phonon occupation numbers rise, with other defects like twin boundaries also influencing the dislocation motion and the drag effects. Recent atomistic studies have shown that decreasing grain size in pure NC metals enhances both low- and high-frequency phonon DOS [605,615,616]. The lower atomic density in GB regions enhances the low-frequency vibrational modes and promotes the general broadening of the phonon DOS due to disorder. In contrast, internal stresses within NC grains shift the phonon DOS to higher frequencies [616]. In addition to scattering and absorption of phonons, GBs and nanoclusters can delay the transition to the drag regime by acting as barriers that pin and slow down the defect propagation.

In addition to phonon scattering, the average dislocation velocity plays an essential role in the phonon drag and its effect on the flow stress. When a dislocation travels through the lattice without encountering obstacles, the drag force limits the dislocation to travel at the maximum velocity. When obstacles such as GBs or precipitates interrupt dislocation motion, the dislocation velocity can be

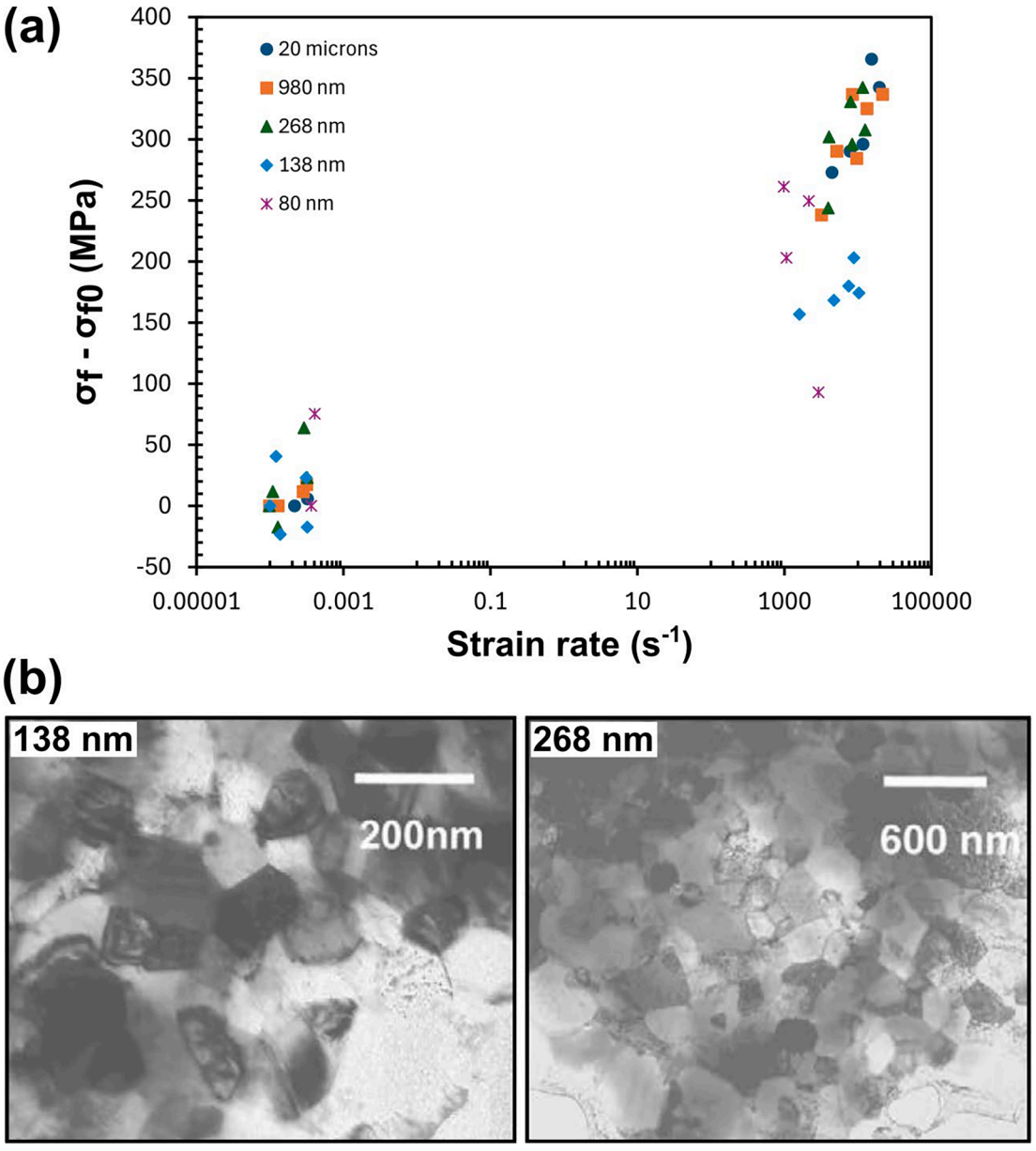

Fig. 29. (a) Change in the flow stress versus stress–strain rate for pure iron of multiple grain sizes [541]. A dramatic increase in flow stress is observed as grain size decreases, and as the strain rate increases above $10^3\ s^{-1}$. (b) Initial microstructure for the 138 nm and 268 nm cases. The only noticeable features are the GBs and a few preexisting dislocations.

slowed below the velocities at which the phonon drag is relevant. The average dislocation velocity is measured as the average distance between obstacles divided by the time for the dislocation to become free from the obstacle ($\Delta t_{obstacle}$) and travel across the open lattice (Δt_{ph}):

$$v = \frac{L}{\Delta t_{obstacle} + \Delta t_{ph}} \tag{9}$$

where

$$\Delta t_{obstacle} = \Delta t_0 exp\left(\frac{(\tau_{max} - \tau)V}{kT}\right) \tag{10}$$

$$\Delta t_{ph} = L\sqrt{\left(\frac{B}{\tau b}\right)^2 + \left(\frac{1}{c_t}\right)^2} \tag{11}$$

In these equations, L is the average length between the obstacles, Δt_0 is an adjustable parameter indicating the time for a single attempt for the dislocation to unpin from the first obstacle, τ_{max} and τ are the maximum and applied critical shear stresses, respectively, V is the activation volume, and c_t is the approximate transverse wave speed in the lattice [617]. According to these equations, if the distance between dislocation barriers is sufficiently small, the time spent by the dislocation traveling through the lattice will be reduced, decreasing the phonon drag effect. This provides the basis for investigating the dynamic mechanical behavior of materials that maintain a stable NC structure.

Some authors have proposed alternatives to the classical idea that dislocation drag causes an upturn in flow stress. For example, Zerilli and Armstrong [608] indicate that a model they previously developed to account for the phonon drag did not accurately predict the strain experienced by the sample. Instead, they proposed that a sudden increase in the number of dislocations causes the flow stress upturn. Microstructural characteristics significantly impact the flow stress as the strain rates increase. As mentioned above, obstacles such as GBs, twin boundaries, and precipitates reduce the dislocation velocities and delay the onset of the drag regime, thereby affecting the flow stress at higher strain rates.

Grain Size effects on the flow stress upturn, require testing a material that is free from other microstructural characteristics that may also be influential. For example, pure iron (BCC) has been investigated by Jia et al. [541] at grain sizes ranging from 80 nm up to 20 μm. The change in the flow stress, i.e., 10 % stress at quasi-static to high strain rates, is plotted as a function of strain rate in Fig. 29a. A power-law fit can then be applied to observe the upturn in the flow stress. It can be seen that as grain size increases, the upturn occurs at lower strain rates. The microstructure of pure iron of two different grain sizes, both before and after deformation, is free from precipitates or twins (Fig. 29b). Hence, the upturn can be attributed only to the effects of grain size on the dislocation drag.

The effect of grain size on the flow stress upturn can also be seen in alpha titanium (HCP) tested in tension [618], as shown in Fig. 30a. Ti does not exhibit a dramatic drag effect as the grain size is changed. Ti is prone to twin formation, and twins can strengthen the material [618]. However, as seen in the image of the fracture surface in Fig. 30b, failure results from void coalescence, which indicates dislocation motion rather than twin formation.

Twinning is another alternative mode of plastic deformation, especially in HCP and some BCC metals and alloys. Twins can act much like GBs in slowing dislocations. AZ31 is a magnesium-based (HCP) alloy prone to twinning during plastic deformation [900]. Results from Tucker et al. [619] and Ulacia et al. [620] are presented in Fig. 31. The stress–strain curve shows two points where plastic

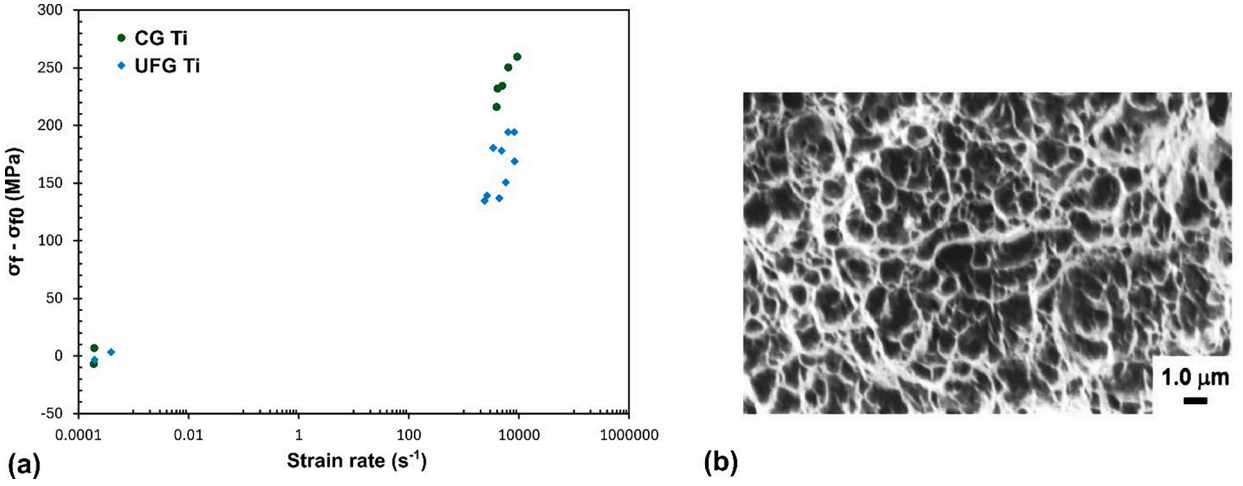

Fig. 30. (a) Change in the flow stress – from quasi-static to high strain rate for pure titanium in the UFG and microcrystalline regimes [618]. (b) Fracture surface image showing a highly ductile dimpled surface indicative of void nucleation and coalescence.

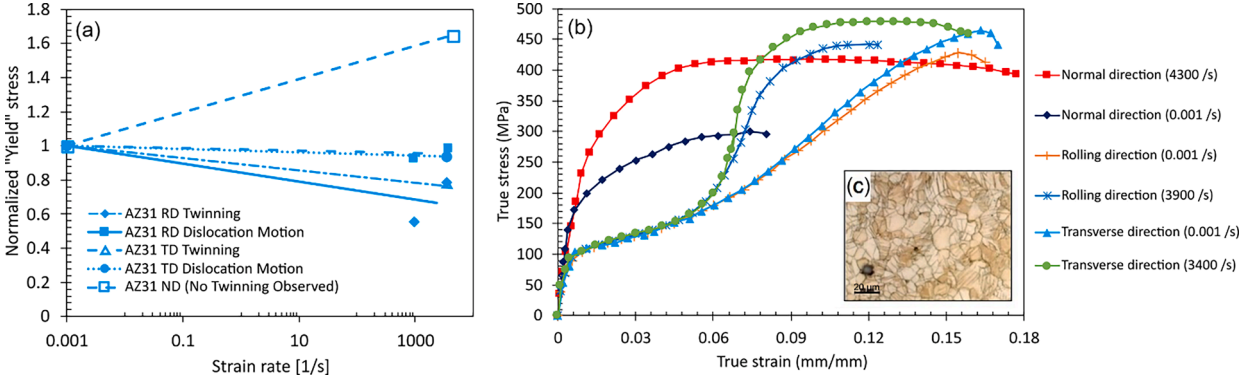

Fig. 31. (a) Normalized flow stress versus strain rate for AZ31 magnesium in the rolling (RD), transverse (TD), and normal directions (ND) of the plate [619,620]. The flow stresses at the onset of yielding and onset of dislocation motion are observed. Twinning causes a reduction in the flow stress in the RD and TD, but the flow stress increases with the strain rate in the ND direction, where twins do not form. (b) Stress–strain curves of the AZ31 material shows a sigmoidal shape for the RD and TD due to twinning. (c) Optical micrographs before testing show the presence of twins.

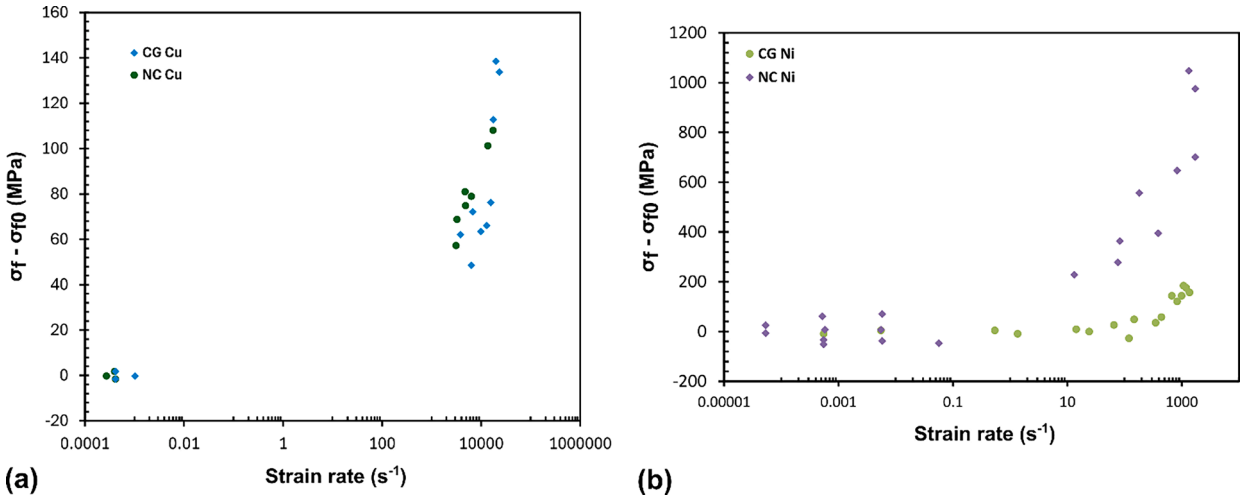

Fig. 32. Change in the flow stress–from quasi-static to high strain rates for (a) Cu [621] and (b) Ni. With a reduction in the grain size and an increase in the strain rate, dislocation drag becomes dominant [19].

deformation by twinning becomes dominant, resulting in a sigmoidal curve shape. The first point occurs at a low stress at which twinning starts. After this point, the material begins to stiffen again as the energy required to move dislocations is accumulated. At the second point, slip-mediated plastic deformation via dislocation motion becomes dominant. Fig. 31b shows the onsets of both twinning and dislocation motion. Note that twinning results in softening as the strain rate increases since it occurs at a lower stress.

In FCC copper, the effect of twinning is less noticeable, as demonstrated by the results from Jia et al. [621] in Fig. 32a. Although the preexistence of twins is known to stabilize the strain rate sensitivity of Cu [521], no softening due to twin formation is noticed. Because copper does not twin as easily as magnesium, the deformation is primarily caused by dislocation motion. Preexisting twins act as obstacles to dislocation motion and stabilize the strain rate-dependent behavior of a material. Fig. 32b highlights changes in the flow stress in Ni as a function of strain rates for two different grain sizes. It is clear from Fig. 32 that both Cu and Ni show a dramatic effect of phonon drag on dislocation motion as the grain size is decreased.

The presence of **precipitates** can also impede dislocation motion. Aluminum 6061-T6 is a prime example of a precipitation-strengthened alloy. Fig. 33 shows results from Jia and Ramesh [603] and Khan and Meredith [622] for 6061-T6 at different grain sizes. Little difference is seen in the flow stress upturn as grain size is increased since dislocations are already significantly slowed down by the presence of precipitates.

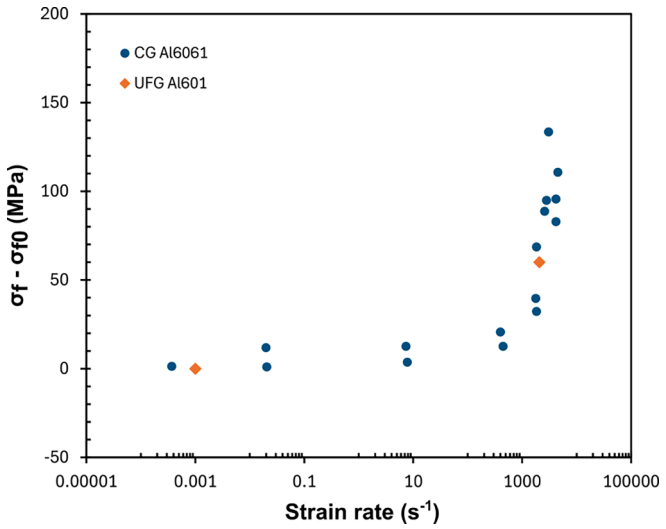

Fig. 33. Change in the flow stress (high rate − quasi-static) versus strain rate for UFG and microcrystalline 6061-T6 aluminum [603,622]. The grain size effect is minimal despite the significant change in the strain rate due to the dislocation pinning by precipitates.

4.2.6. Shock compression of NC materials

Shock compression of materials involves irreversible plastic deformation through mechanisms, such as dislocation generation, slip-twinning transition, strain gradients, void nucleation, and phase transformations. These processes are crucial for understanding material behavior under extreme conditions such as automotive crashes, ballistic impacts, explosive detonation, and laser-material interactions.

High strain rate deformations (exceeding 10^4 s^{-1}) are relevant for applications such as metal forming, machining, cladding, cold spray, and shock consolidation of difficult-to-compact metallic powders. Shock loading differs fundamentally from static conditions, with mass inertia driving deformation via dislocation motion, which is influenced by thermal activation, phonon drag, or relativistic effects [599]. Materials with slip-limiting microstructures, such as those with fine grains, may also deform via twinning or phase transformations [623,624]. Thermal inertia can cause localized softening due to adiabatic heating and temperature inhomogeneity [625,626].

Shock compression experiments, using techniques such as gun- or explosive- or laser-launched plate-on-plate impact, cover a wide range of strain rates from 10^5 to 10^9 s^{-1} [599]. These methods typically use velocity interferometry or stress gauges to measure wave profiles, providing insights into the Hugoniot Elastic Limit (HEL), which corresponds to the dynamic compressive yield strength and the transition stress from elastic to plastic deformation. The HEL can also be derived from velocity data using the formula $\sigma_{HEL} = ½ \rho_o.C_L.u_{HEL}$, where ρ_o is density, C_L is longitudinal sound speed, and u_{HEL} is velocity corresponding to the slope change [627] arising from the elastic to plastic transition.

Dynamic tensile or spall failure strength, σ_{SPALL}, is obtained from the bulk sound speed and pullback signal indicative of spall-induced free surface formation [628]. Other methods, such as high-speed imaging of transient deformation states (e.g., Taylor rod on anvil impact), correlate with physics-based models to define material strength as a function of strain, strain rate, and temperature [618,619]. Instabilities such as Rayleigh-Taylor [629] and Richtmyer-Meshkov instabilities [630], captured in high-pressure experiments, can also provide strength properties [599].

Recent advancements include laser-induced particle impact testing to study size-dependent mechanical behavior. This method measures hardness at strain rates exceeding 10^6 s^{-1} through dynamic indentation. Although dynamic hardness does not directly correlate to a singular strain rate, it provides insight into deformation mechanisms, especially at high strains. Studies have also demonstrated nanotwinning-assisted dynamic recrystallization, offering new processing pathways for high-strength metals and alloys with ultra-fine and NC grains [631].

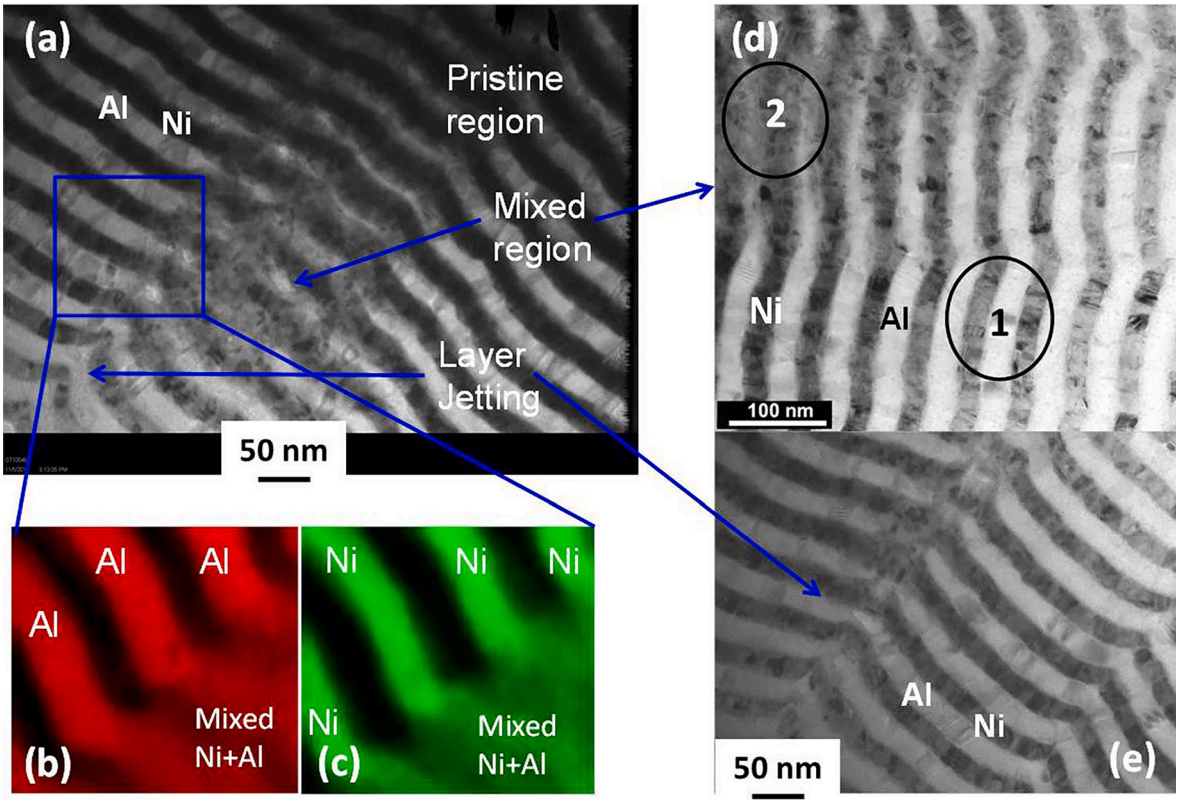

Fig. 34. (a) TEM image of a cross-section of impacted Ni + Al nanolaminate illustrating effects of shock-induced mixing and jetting, which is seen more clearly in higher magnification images in (d) and (e). The compositional maps in (b) and (c) illustrate the presence of Ni and Al constituents in the mixed regions [635].

Past interest in the effects of **grain size on the high strain rate dynamic deformation behavior** of metals has stemmed from the effects of varying influences on the performance of copper-shaped charge liners [632]. Tensile ductility affecting the shaped charge jet break-up times is considerably longer with 20 μm grain size copper-shaped charge liners, compared to that with 90 μm grain size [633]. The smaller grain size is believed to retard tensile instability, leading to a more significant elongation and overall shaped charge performance. In prior work, Meyers et al. [634] showed that decreasing grain size profoundly affects the shock compression response of copper, with excessive twinning observed in 315 μm grain size and no twinning in 9 μm grain size material. The slip-twinning transition shifts to higher stresses with decreasing grain size, leading to more homogeneous plastic deformation, while coarse-grained copper undergoes strain localization and dynamic recrystallization.

Studies of dynamic deformation and shock compression of NC materials and nano-layered structures have generally focused on investigating the effects of GBs and inter-phase boundaries on defect generation and failure [636]. The influence of nano-scale structure on altered characteristics of stress wave propagation has also been investigated, showing, for example, decreased wave-front width with a reduction in grain size or layer thickness [637]. Nano-sized powder particles and their mixtures, as well as nano-laminates, have been investigated to determine the thermodynamic influence of their high surface (or interface) energy on compressibility and energy dissipation in inert [638] and exothermic energy release in reactive systems [639]. The latter effects have been particularly attractive in the case of nanoparticles and nano-laminates of metal–metal, metal-polymer, and metal-oxide reactive mixtures for applications as nano-energetic materials [640,641]. Extensive shock-induced mixing of reactants can occur, particularly due to shear-dominated deformation at pre-existing wave perturbations (heterogeneities), as shown in the TEM images in Fig. 34 of the cross-section of Ni + Al nanolaminate structures [635]. The shear-induced mixing (alloying) can trigger highly exothermic chemical reactions or even fine-scale mixing and alloying of otherwise immiscible components, as shown in Fig. 35 [642].

Nanostructured materials are not immune to defect nucleation caused by shock wave interactions with interfaces modifying the stress states and strain accommodation processes and consequently affecting the overall mechanical behavior. Unlike materials with conventional coarse-grained microstructures, the structural stability of NC materials, or lack thereof, can drastically alter the material response to shock compression and lead to inconsistent effects. Consequently, many studies of the effects of shock compression on mechanical behavior and associated deformation mechanisms in nanostructured materials have been performed through atomistic modeling and MD studies. MD simulations are, in fact, suitable for comparing the predicted responses with laser shock compression

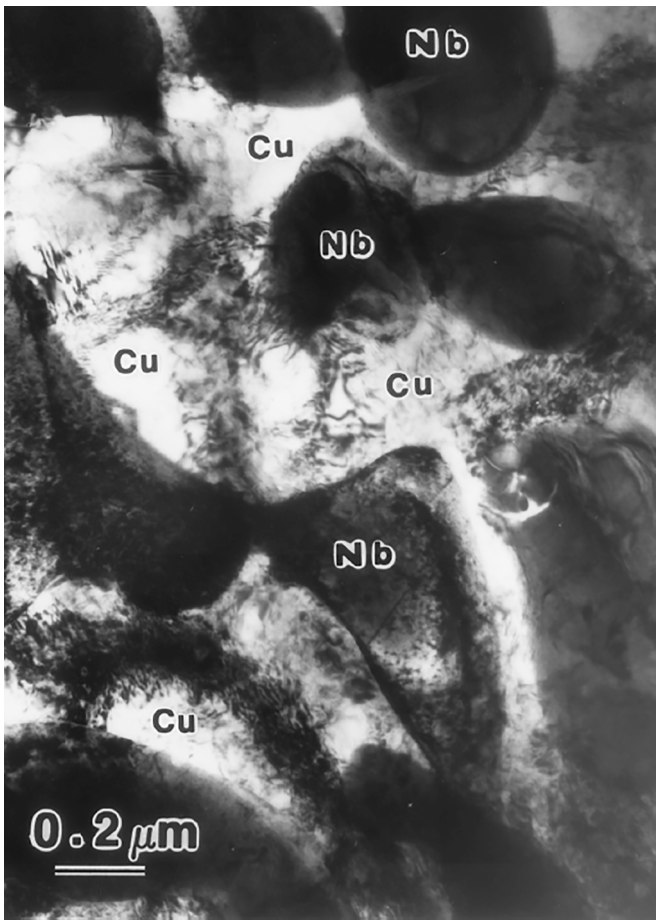

Fig. 35. (a) TEM micrograph showing finely intermixed Cu and Nb precipitate-like phases [642].

experiments due to similarities in spatial and temporal scales. Holian and Germann [643,644] used MD simulations of the shock compression response of Cu to show that Hugoniot properties correlated well with experimental measurements for shock propagation along [001] orientation, with partial dislocation loops emitted along {111} close-packed planes, consistent with Smith's model of dislocation generation. Likewise, MD simulations in monolithic FCC Cu have predicted a pressure of ~ 5 GPa for the transition from slip to stacking faults and a much higher ~ 50 GPa pressure for the transition from slip to twinning, consistent with experimental results. On the other hand, the transition pressure from slip to twinning (~15 GPa) in Ni is lower than that for the transition from dislocation cells to stacking faults (~27 GPa), which is why individual stacking faults are generally not observed in Ni [645]. Differences are also predicted for the responses of FCC and BCC metals under high strain rate loading, with homogeneous nucleation being a common dislocation generation mechanism in FCC metals and dislocation multiplication favored in BCC metals [642].

MD simulations of shock-compressed NC materials predict an order of magnitude higher dislocation density generation than experimentally observed [65,66]. The lack of experimental evidence of high dislocation density is due to their possible annihilation during unloading from the peak shock-pressure state. While GB sliding accounts for the bulk of the strain during shock compression of NC Ni (with slightly less in 5 nm than in 10 nm grain size), MD simulations predict that the strain due to dislocations is governed by partial dislocations with GBs acting as sinks or sources. Simulations also indicate that twinning is more favored with a 5 nm grain size than a 10 nm grain size Ni, similar to the trend observed in NC Cu. The slip-twinning transition pressure in Ni with ~ 30 nm grain size is predicted to be substantially higher (~78 GPa) compared to critical transition pressure in single-crystalline Ni (~15 GPa), which is consistent with the lack of TEM observations of twins in shock compressed Ni at ~ 70 GPa. On the other hand, MD simulations predict a lower transition pressure of ~ 16 GPa for NC (~10 nm grain size) Ni–W, which is also consistent with experimental observations. Generally, the threshold for slip-twinning transition stress decreases with increasing grain size, more so for pure Ni than Ni–W alloy, as shown in Fig. 36 [646].

The high density of GBs in NC materials can significantly suppress slip-mediated dislocation motion during shock compression, resulting in ultra-high-strength and hardness. However, strength degradation and inverse Hall-Petch behavior are also possible as GB-mediated plasticity can take over with increasing volume fraction of GBs [647]. BCC tantalum exhibits complex effects revealing conflicting trends under shock compression with decreasing grain size. Coarse-grained Ta has been shown by Hsiung and Lassila [648] to exhibit twinning upon explosive shock loading at a pressure of ~ 45 GPa, while NC Ta has shown no evidence of twinning upon laser shock loading at a pressure of 145 GPa [649]. Similar conflicting trends have been observed with dynamic XRD using laser shock compression with twinning-dominated plastic deformation at 40–80 GPa [650,651] decreasing at higher pressures [652]. In recent work, Wu et al. [653] used large-scale non-equilibrium MD and showed that the response of 5–60 nm grained Ta at shock velocities of 500 to 1500 m/s strongly depended on the shock strength and the grain size. In particular, the influence of grain size on the shock wave structure, the onset of plasticity, and the slip/twinning deformation mechanism, are affected by weak, strong, and ultra-strong shock compression conditions.

Under weak shock conditions, the dominant deformation mechanism changes from GB-mediated plasticity to combined slip and twining to slip-dominated deformation with increasing grain size, which also influences the elastic–plastic wave from being single- to double- and back to a single-wave structure. Competing deformation mechanisms are also observed, with slip-mediated deformation being the more dominant mechanism than twinning in materials with grain size exceeding 30 nm, as shown in the plot of dislocation

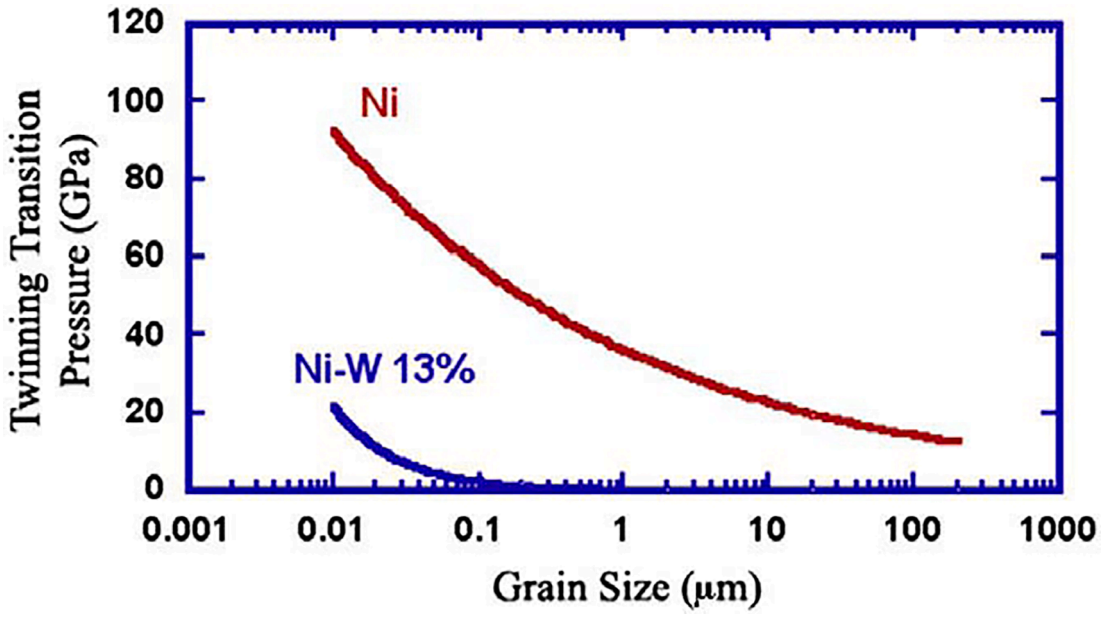

Fig. 36. Plot showing the difference in twinning transition threshold pressure decreasing with increasing grain size for Ni compared to Ni–W alloy from a few nanometers to > 100 μm scale [646].

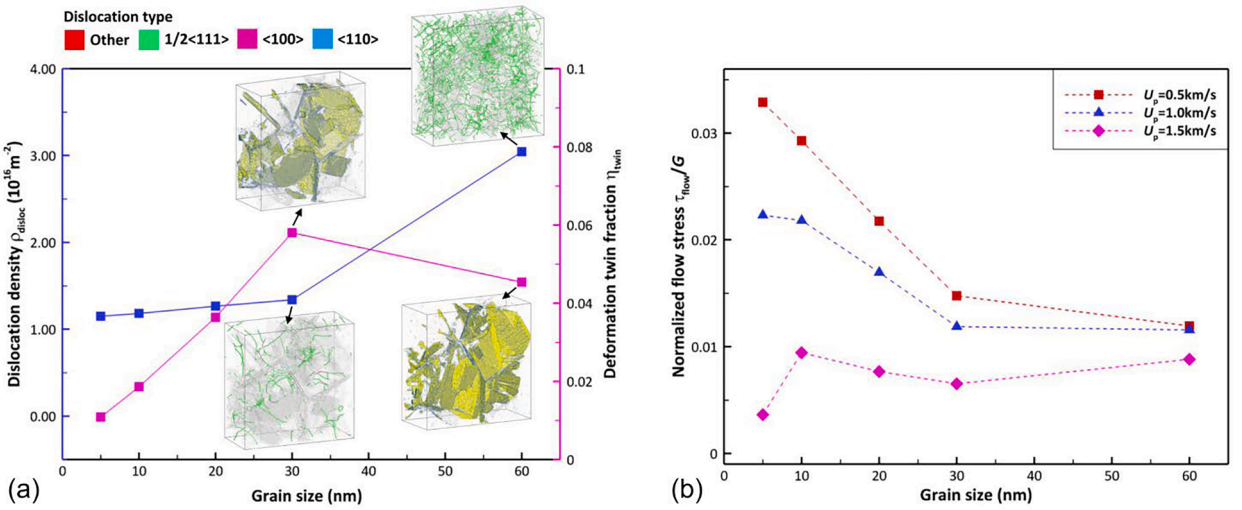

Fig. 37. (a) Variation of dislocation density and deformation twin volume fraction as a function of grain size for shock compression at a velocity of 0.5 km/s. (b) Normalized flow stress as a function of grain size under three different shock compression conditions: 0.5 km/s, 1.0 km/s, and 1.5 km/s [653].

density and twin fraction versus grain size in Fig. 37a [653]. The authors identify the twinning versus slip transition based on the observation that the critical shear stress for perfect dislocation emission is lower than that for partial dislocation emission from GBs with grain size increasing beyond ~ 33 nm. Strong and ultra-strong shock compression conditions show a weak influence of the grain size on the wave structure and deformation mechanisms, with twinning-detwinning for strong shocks and amorphization-recrystallization processes for ultra-strong shocks leading to the single plastic wave structure. Flow stress dependence on the grain size follows the Hall–Petch relation under weak shock conditions, while an inverse Hall–Petch relationship is observed under ultra-strong shock compression conditions and with ultra-small and very large grain sizes, as shown in Fig. 37b.

4.2.7. Radiation resistance of NC materials

Materials exposed to intense radiation, such as in nuclear reactors, are subjected to displacement damage as the high energy radiation knocks off atoms from their lattice sites, creating a primary knock-on atom (PKA). The PKA initiates a displacement cascade until the energy of the displaced atoms becomes less than the threshold displacement energy, at which point the atoms settle at interstitial positions. Several theories have been proposed for the radiation damage cascades (Fig. 38), their impact on mechanical properties, and ways of measuring the damage [654,655]. Radiation-induced displacement cascades generate a high density of vacancies and interstitials (Frenkel pairs), which eventually can coalesce to form defect clusters such as interstitial dislocation loops, voids, and stacking fault tetrahedra. As the concentration of these extended defects increases, combined with helium generated as a result of the transmutation reaction, the effects of radiation can pose five major threats summarized as hardening and embrittlement, phase instabilities from radiation-induced precipitates, radiation creep, volumetric swelling from void formation, and high-temperature helium embrittlement [656], thus leading to a reduction in the material's performance and lifetime [657]. Hence, efficient operation and extended lifetime of future nuclear reactors depend on the performance of structural materials in such an extreme radiation environment [658].

GBs and phase boundaries are efficient sinks to annihilate defects produced during irradiation. Prior research has focused on designing and processing materials with large concentrations of point-defect sinks to mitigate radiation damage (Fig. 39). The state-of-the-art materials for reactor applications are Reduced-Activation Ferritic-Martensitic (RAFM) and ODS steels. ODS steels are of great interest due to their superiority in defect sink efficiency and high-temperature properties attributed to fine oxide dispersions [660]. However, they are not entirely immune to radiation hardening at considerably high doses [661,662]. Also, the stability of the oxide phases (dissolution, growth, and amorphization) is poorly understood, which is reflected in the inconsistency of published results [663]. Research on other advanced materials, such as nano-layered composites, has shown that improving the interface density (e.g., reducing the spacing of nanolayers) creates overlapping void-denuded zones, which is critical to achieving a void-free structure [664–666].

NC materials exhibit considerable promise as potential candidates for mitigating radiation-induced defects owing to their abundant interface sink concentration, including grain and inter-phase boundaries [667–675]. However, the susceptibility of these materials to microstructural and phase instability resulting from the high-energy displacement damage, encompassing phenomena such as ballistic mixing and Ostwald ripening, reduces the interface defect-absorption ability and density, thus constraining their potential [676]. Nevertheless, noteworthy results have emerged from investigations of nanolayered composites and bulk NC materials, showcasing exceptional radiation resistance [668,677,678]. For instance, as depicted in Fig. 40, radiation hardening is a significant issue influencing the embrittlement of structural reactor components. At low temperatures and displacement per atom (dpa) below 2, materials

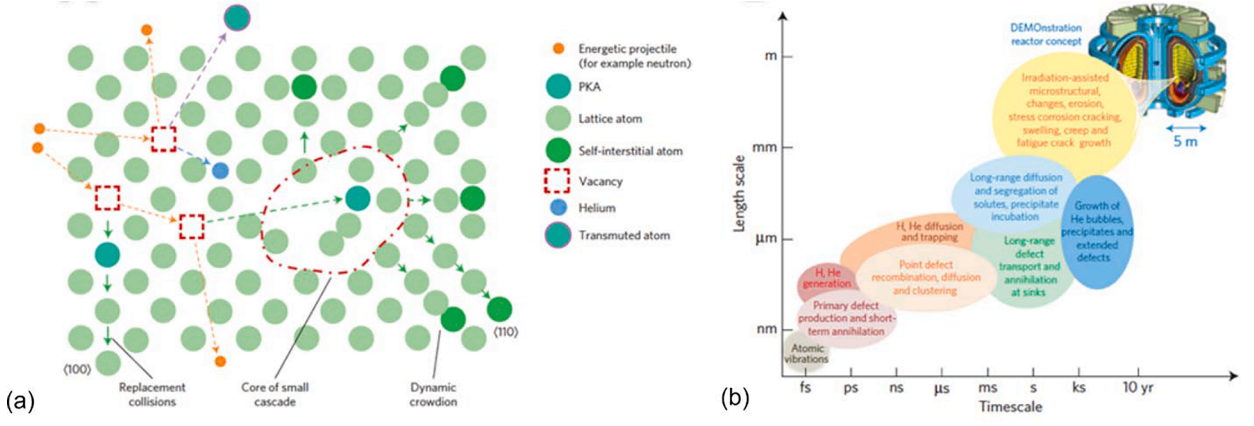

Fig. 38. (A) Radiation damage evolution at lattice scale and (B) time and length scales of the multiscale damage processes responsible for microstructural changes and property degradation during high-energy neutron irradiation of plasma-near in-vessel materials [659]. The plot in (B) shows the microstructural changes (yellow and blue ellipses) and their effects on defect nucleation and growth at the nanoscale. (For interpretation of the references to color in this Fig. legend, the reader is referred to the web version of this article.)

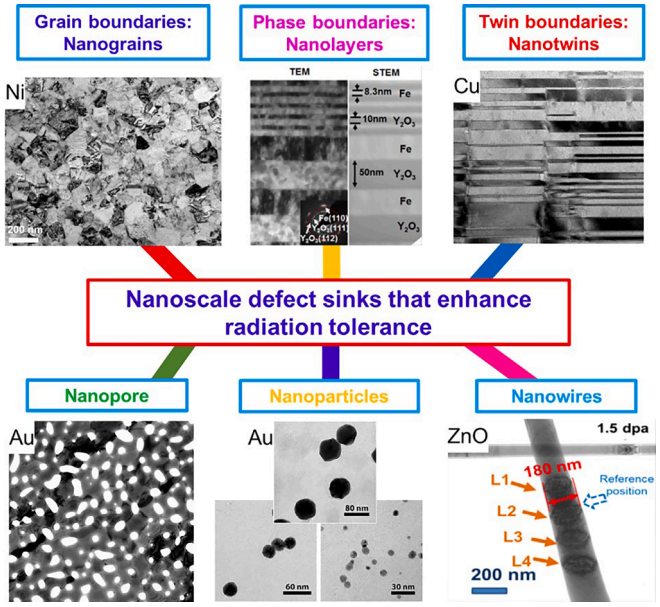

Fig. 39. Key engineering strategies to alleviate radiation damage through the incorporation of nanoscale defects such as GBs, phase boundaries, nanopores, etc. which enhances radiation tolerance of base materials. [667].

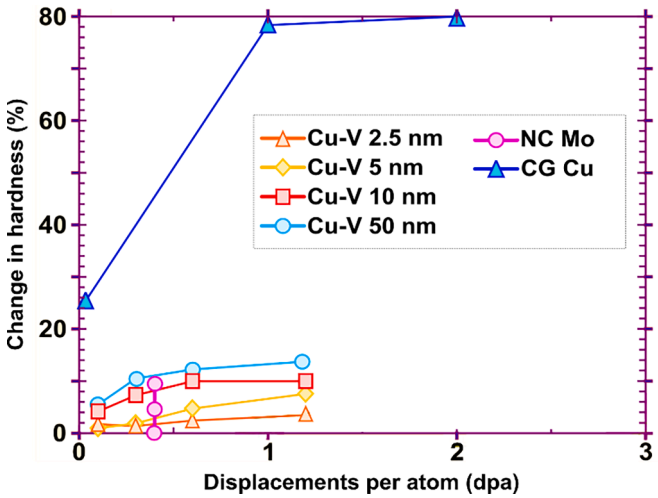

Fig. 40. Percentage of radiation hardening for various materials at different doses irradiated at 298 K [661,662,668,677–686].

generally experience radiation-induced hardening. In the case of coarse-grained pure copper, hardening increases by ~ 80 % (with a 24 % rise at an extremely low dose of 0.034 dpa) [677], whereas in nano-layered composites, this increase is around ~ 15 % [678]. Similarly, for pure Mo, radiation-induced hardening reaches 60 % compared to nearly zero hardening in NC Mo with an average grain size of 25 nm irradiated at room temperature using 200 keV helium ions with a total fluence of 1.4×10^{17} ions/cm^2 [668]. Such improvement in hardening behavior in NC materials has been attributed to GB accommodation of radiation defects [668,677,678].

Experimental evidence has shown that refining grain size down to the nanometer range can significantly improve radiation tolerance [687], provided the microstructure is stable. Metallic nanolayered (e.g., Cu-Nb, Cu-Mo, and Cu-V) composites have validated the importance of interface density in effectively suppressing radiation-induced defects and helium bubble swelling [664,688]. Specifically, immiscible and semi-coherent (e.g., fcc/bcc) interfaces have been proclaimed to offer promising radiation tolerance compared to their miscible (e.g., Al/Nb, Fe/W) and coherent (e.g., fcc/fcc: Ag/Ni) counterparts due to the presence of a large concentration of misfit dislocations at their interfaces [689–692]. Apart from this, immiscible nano-alloyed systems have shown great potential for developing thermally stable nanostructures through kinetic pinning mechanisms [178]. Furthermore, immiscible NC systems such as Cu-Nb, Cu-V, Cu-Mo, Ni-Ag, Ag-Fe, Ag-Cu, etc., driven far from equilibrium through mechanical ball milling or irradiation, have been of great interest since their response to SPD/radiation is unique. This is in comparison to their miscible

counterparts (or those with low heat of mixing) due to the competition between ballistic mixing and thermodynamically driven kinetics such as decomposition and phase separation [184,693,694].

Radiation-induced phase instabilities are also an important concept encompassing a range of mechanisms, including ballistic dissolution, Ostwald ripening, radiation-enhanced diffusion, and inverse Ostwald ripening [663,695–697]. For instance, in coarse-grained materials, Chen et al. observed the contraction and dissolution of oxide particles in 12Cr ODS materials [698], while Lescoat et al. noted the growth of oxides in ferritic ODS steels [699]. Furthermore, intense defect accumulation and chemical disordering at incoherent interfaces can be caused by dense cascades, resulting in increased free energy and promoting amorphization [700]. Computational investigations have indicated that such an amorphization process is due to shear-induced chemical mixing at precipitate-matrix interfaces in NC materials, especially in Cu-Nb (4 at.%) and Cu-V (8 at.%) systems, with amorphization increasing linearly with atomic radius [701].

Semi-coherent interfaces are found to be more stable and resistant to amorphization. Sauvage et al. [702] have reported amorphous interfaces resulting from nanowire drawing of Cu-Nb, which are linked to the fine mixing of copper and niobium. Apart from this, the phenomenon of dissolution and re-precipitation of second-phase particles due to recoils was postulated by Russell [703], who found that finer particles gradually replaced larger dissolved particles during continuous irradiation. Chen et al. and Lu et al. [698,704] observed such dissolution of larger particles and the precipitation of fine dispersoids in ODS alloys after high-dose self-ion irradiation and helium pre-implantation irradiation, respectively. Certain et al. [705] also observed the dissolution of nanoclusters in 14YWT at low temperatures, although these nanoclusters remained stable at high temperatures. The effect was attributed to the diffusion of dissolved solute back to the parent cluster, preventing new precipitation. Several computational and experimental studies have explored the role of compositional self-organization in binary alloys with a positive heat of mixing, observed within specific temperature and shearing rate ranges, to maintain a refined microstructure during extended high-temperature irradiations or ball milling processes [706–708]. Chee et al. [709] reported the maximum temperature of the patterning regime (T_{max}) for various copper-based NC alloys, with systems having a high positive heat of mixing, such as Cu-Nb and Cu-V, experiencing higher T_{max} values (>773 K). A high density of sinks has been predicted to positively influence the stabilization of irradiation-induced patterning [710].

The prevailing view is that reducing grain size diminishes the increase in hardness following irradiation. This trend arises from producing defects, such as dislocation loops and helium bubbles, at a low density and small size in NC materials during irradiation. However, the presence of microstructural instabilities (such as grain growth, as illustrated in Fig. 41) in intense radiation environments

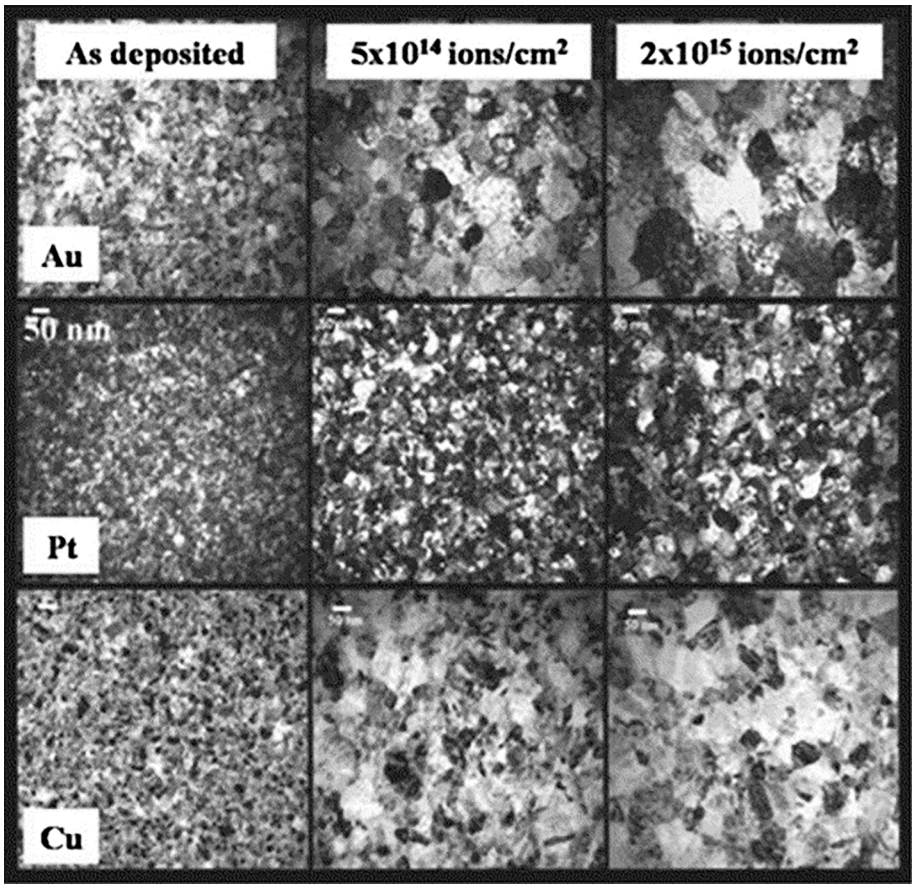

Fig. 41. Microstructural instability in NC materials with irradiation [667].

complicates the interpretation of grain size effects [676,711,712]. These instabilities lead to a reduced sink concentration and efficiency, thus limiting their potential to mitigate radiation-induced effects. For example, significant grain growth has been observed in NC Cu, with grain sizes increased from approximately 48 to 800 nm at 1 dpa [677], and in NC Cu-0.5Al_2O_3 composites, where grains grew in size from 180 to 495 nm at 0.9 dpa [667]. Various other NC alloys and composites have exhibited grain growth under ion irradiation [221,670,713,714].

In addition to grain growth, introducing impurities during processing, variations in sample geometry and size, and different loading conditions further complicate a comprehensive understanding of grain size effects and the potential applications of NC alloys. For instance, self-ion irradiation is commonly employed to replicate displacement cascades, while helium ions are directly implanted to simulate transmutation reaction products. However, previous studies have shown that pre-implantation of helium ions before self-ion irradiation does not yield the same microstructure as simultaneous ion irradiation [715–717]. Consequently, investigations focusing on in-situ irradiation followed by isochronal annealing are crucial for gaining deeper insights into damage accumulation, defect evolution, and precipitate dynamics. Such real-time observations can reveal previously unexplored nano-scale mechanisms that, in theory, can confer irradiation tolerance. If stabilization of grains in nanostructured materials can be achieved, a novel class of materials with enduring sinks and radiation-resilient structures (self-healing ones) could emerge, paving the way for enhanced radiation resistance.

4.2.8. *Oxidation resistance of NC materials*

Oxidation of NC alloys designed to sustain extremely corrosive and mechanical environments has attracted considerable research interest in recent years. An advantageous and essential consequence of grain size refinement is the enhanced diffusivity of atoms in such alloys [718–721]. This behavior makes NC alloys candidates for high-temperature and other advanced applications (such as engine pistons, turbines, liners, etc.) for which a combinatory arsenal of enhanced mechanical properties, high-temperature microstructural and thermal stability, and improved corrosion resistance is crucial [722–724].

NC alloys are particularly susceptible to corrosion during processing and applications. During processing, introducing impurities and oxidation-prone alloying elements is unavoidable, leading to an increased affinity for oxidation. Moreover, owing to their excellent properties, NC alloys often find use in high-temperature oxygen-rich environments, where they may be subjected to extreme, sustained mechanical and corrosive conditions. A detailed study and understanding of the oxidation resistance of the alloy is crucially important if an NC alloy is to be employed for withstanding the extreme conditions in which it must operate in [725,726]. Understanding the origin of the oxidation resistance of NC alloys is the key to improving and developing NC alloys for use in next-generation applications and technologies [725,726].

Several studies have explored the oxidation resistance of established NC alloy systems compared to their coarse-grained counterparts. The most common method to measure the extent of oxidation is by performing thermo-gravimetric weight measurements using a high-quality microbalance [727–729]. Raman et. al. [729] studied the oxidation behavior of NC Fe-10Cr alloys in comparison with microcrystalline Fe-10Cr at 300 ℃ and found the weight gain in microcrystalline Fe10Cr to be nearly seven times greater than that in NC Fe-10Cr. Interestingly, the rate constant of microcrystalline Fe-10Cr was found to follow parabolic law throughout the oxidation time. In contrast, the rate constant of NC Fe-10Cr followed parabolic kinetics only for the first 240 min of oxidation. This significant departure from the parabolic kinetic behavior was attributed to the insignificant weight gain in NC Fe-10Cr beyond 240 min of oxidation. Fig. 42 shows the oxidation kinetics of microcrystalline Fe10Cr compared to NC Fe-10Cr.

The deviation from parabolic behavior in NC Fe-10Cr was attributed to a greater GB oxidation at the initial stages due to the dominant GB diffusion effect. This, in turn, led to the faster formation of a passive Cr_2O_3 layer and prevented further oxidation of NC Fe-10Cr. Kumar et. al. [730] also studied the oxidation behavior of NC and microcrystalline FeCrAl alloys and found that this system exhibited the same behavior as outlined above for the FeCr alloy. Fig. 43 shows the oxidation kinetics of NC and microcrystalline FeCrAl at three temperatures. As in the case of the FeCr alloy, the NC structure facilitates the increased and selective formation of a passivating Cr_2O_3 layer, whereas the microcrystalline structure forms a compound scale of Cr_2O_3 and Al_2O_3 owing to similar diffusion coefficients of Al and Cr in the microcrystalline structure.

The most comprehensive study of the ternary NiCrAl system was performed by Liu et al. [731], who showed that NC NiCrAl alloys have a superior oxidation resistance to their microcrystalline counterparts. Fig. 44 shows results for one such system, Ni-20Cr-2Al, processed via different routes. The improvement in oxidation resistance was attributed to the selective formation of a highly protective Al_2O_3 scale, which was promoted due to the NC structure. Short circuit diffusion of Al along GBs facilitated selective oxidation.

Xie et al. showed that adding small amounts of Y to the NC NiCrAl alloy could further improve the oxidation resistance, demonstrating a beneficial effect of this reactive element on oxidation [732]. Fig. 45 shows the oxidation mass-gain curves for NC and coarse-grained Ni-30Cr-5Al and Ni-30Cr-5Al-Y.

Yang et. al conducted perhaps the most systematic, detailed study on the oxidation behavior of the Ni-xCr-yAl ternary alloy system and reported remarkable findings [733]. The nature of the final oxide scale developed was heavily composition-dependent, with the (Cr + Al) content and Cr/Al ratio determining whether the final oxide scale was external chromia or alumina, or a complex scale of compound oxides. Fig. 46 shows the oxidation mass gain curves for four tested compositions, which can be summarized as follows [733]: 1) (Cr + Al) $<$ 10 wt% caused the formation of complex NiO, Cr_2O_3, Al_2O_3 and Ni($CrAl_2$)O_4 spinels; 2) (Cr + Al) $>$ 10 wt% and Cr/Al $<$ 1.5 caused the formation of exclusive external alumina; and 3) (Cr + Al) $>$ 10 wt% and Cr/Al $>$ 1.5 caused the formation of exclusive external chromia. Yang et al. [733] also established that reducing the grain size of Cr in the NC alloy from $\sim$ 85 nm to $\sim$ 17 nm drastically reduced the critical content of Cr required to facilitate the exclusive formation of external, protective chromia scales (Fig. 46b).

Han et al. [734] extensively studied the oxidation behavior of NC Cu compared to coarse-grained Cu and concluded that the

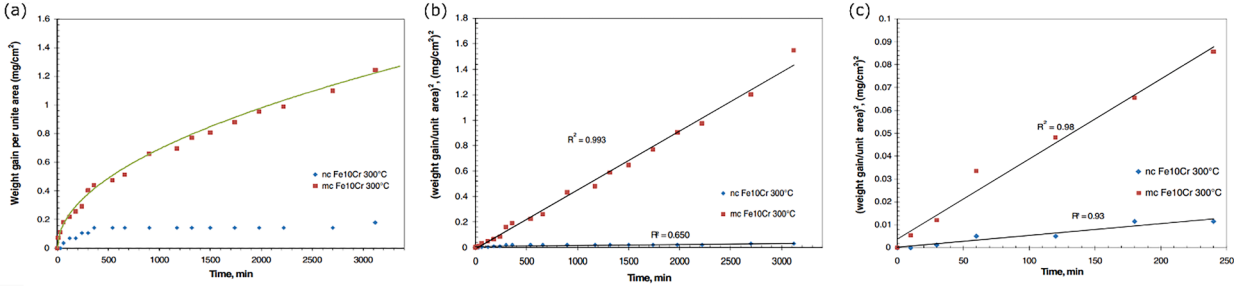

Fig. 42. Oxidation kinetics of NC and microcrystalline (mc) Fe-10Cr alloy oxidized at 300 ℃ [729]. (a) Weight gain (ΔW) vs. time plots up to 3120 min. (b) ΔW^2 versus time plots indicating the parabolic behavior of microcrystalline Fe-10Cr and departure from the parabolic behavior of NC Fe-10Cr alloy at higher temperatures. (c) ΔW^2 versus time plots (up to 240 min) indicating parabolic kinetics of both NC and microcrystalline Fe-10Cr alloy.

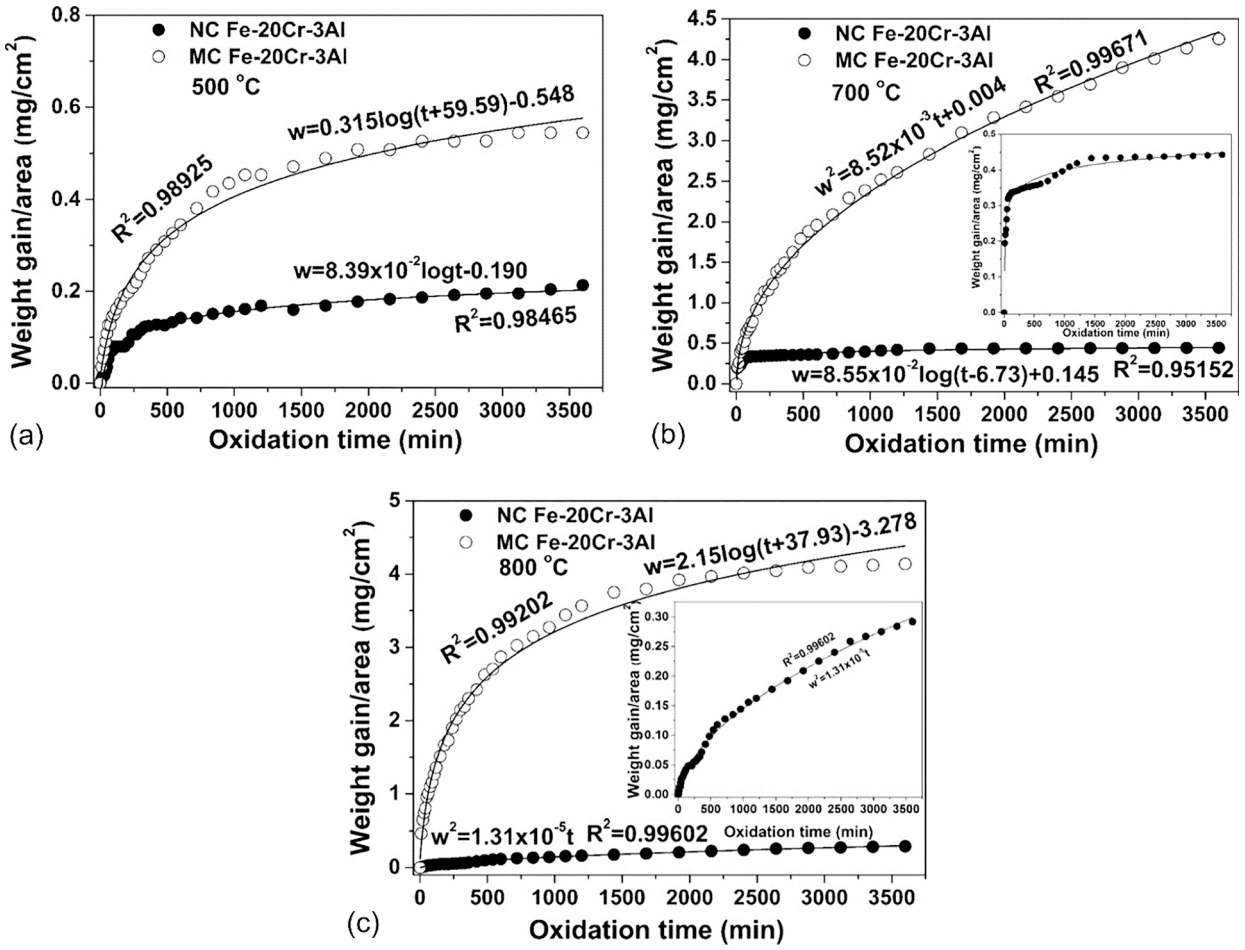

Fig. 43. The oxidation kinetic of NC and microcrystalline (MC) FeCrAl alloys at (a) 500 ℃, (b) 700 ℃, and (c) 800 ℃ [730].

oxidation rate in NC Cu far exceeded the oxidation rate of coarse-grained Cu. This behavior deviates from the alloy system examples shown above, where the oxidation rates of NC structures were lower than those of microcrystalline or coarse-grained structures. By directly measuring the weight gain of the oxidized samples at different temperatures as a function of time, Han et al. [734] determined the oxidation rate constants of NC and coarse-grained structures. As seen in Fig. 47, the weight gain increases linearly with temperature above 700 ℃ in both cases. Between 300 and 700 ℃, the weight gain ΔW follows the parabolic law $\Delta W^2 = K_p t + C$, where K_p is the parabolic rate constant, and t is oxidation time (Fig. 48). Table 1 lists the rate constant values between 300 and 600 ℃, showing that NC Cu corrodes more rapidly than coarse-grained Cu over the entire tested temperature range.

This deviation from previously studied alloy systems was attributed to the enhanced diffusion of copper and oxygen in both the metal and the oxide scale. Faster outward diffusion of copper leading to rapid external oxidation and significant inward diffusion of oxygen atoms along the GBs in the scale led to rapid recession of Cu in the bulk metal, lowering the oxidation resistance of NC Cu as compared to coarse-grained Cu. Fig. 49 schematically depicts the distinction between internal and external oxidation based on the rates of inward diffusion of oxygen versus outward diffusion of metal atoms.

On the other hand, Fu. et al. [735] showed the opposite behavior in the Cu-Cr system: grain size refinement enhanced the oxidation resistance of an NC CuCr alloy compared to coarse-grained CuCr (Fig. 50). The coarse-grained CuCr was processed via powder metallurgy, exhibiting a grain size of 50–150 μm (PM-CuCr), while the NC CuCr was synthesized via mechanical alloying (grain size: 50–300 nm, MA-CuCr) and magnetron sputtering (grain size: 5–10 nm, MS-CuCr). The coarse-grained CuCr produced complex oxide scales of CuO and Cu_2O with some amount of $Cu_2Cr_2O_4$ and Cr_2O_3, whereas the NC CuCr produced a simple, continuous, protective scale of external Cr_2O_3. The presence of Cr atoms promoted the selective oxidation of Cr due to enhanced Cr diffusion along the GB pathways in the metal and oxide scale. The decrease in the alloy grain size favored the exclusive external oxidation of the most reactive component, chromium, promoting the formation of an external chromia scale. The latter prevented the base alloy from further oxidation, considerably decreasing the oxidation reaction rate.

As evidenced by the above examples, oxidation of NC alloys can be influenced by (i) grain size effect and (ii) alloying elements. Most studies establish that reducing grain size improves oxidation resistance [734–739]. Nano-crystallization increases the density of

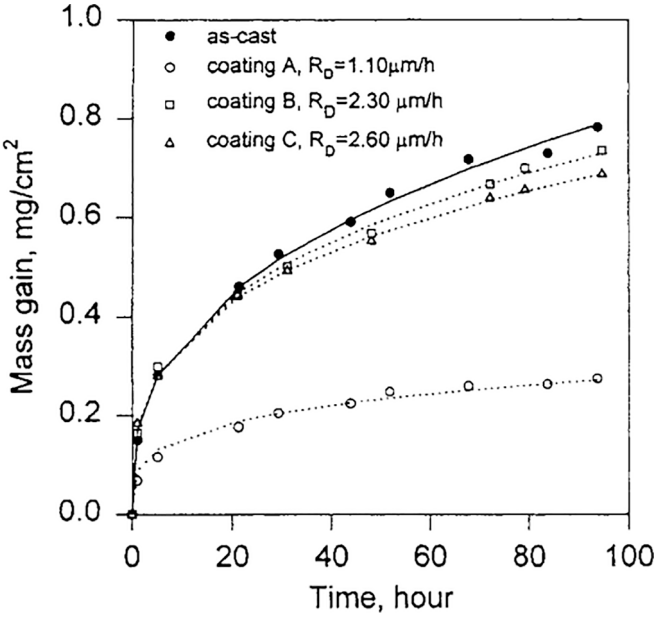

Fig. 44. Mass gain versus time plots for Ni-20Cr-2Al as-cast alloy and sputter deposited coatings with different deposition rates and grain sizes oxidized at 1000 ℃ for 100 h [731]. Grain sizes: coating A: ~60 nm, coating B: ~370 nm, and coating C: ~250 nm.

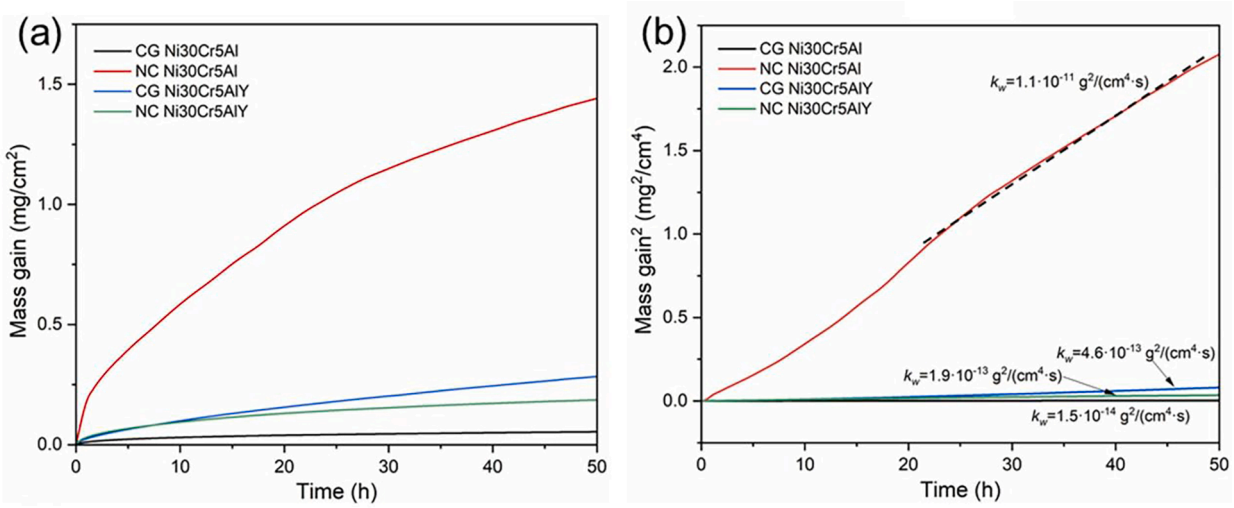

Fig. 45. (a) Isothermal oxidation kinetic curves and (b) corresponding parabolic behavior in the air at 1000 °C [732].

GBs and other interfaces, accelerating atomic diffusion during the oxidation process, and can promote the selective formation of protective oxide scales, provided that the atomic composition of the NC alloy allows for the formation of such a scale. Wagner's analysis [740–742] of diffusion-controlled oxidation gives the equation

$$\frac{dX}{dt} = \frac{\Omega}{X}\frac{2\delta}{d}D_{gb}\Delta c \tag{12}$$

Here, the term dX/dt is the oxidation reaction rate based on the change in thickness X of the oxide scale, Ω is the volume of oxide formed per unit quantity of diffusing metal species, d is the grain diameter, δ is the GB width, D_{gb} is the GB diffusion coefficient, and Δc is the time-invariant concentration gradient during the oxidation.

Although numerous other factors must be considered while studying the oxidation kinetics of NC alloys, Eq. (12) demonstrates that the short-circuit diffusion of elements accelerates the oxide growth rate. The grain size refinement in NC alloys increases solute diffusivity through the NC system [718]. In alloys where the solute is an oxide former that allows for the selective formation of a

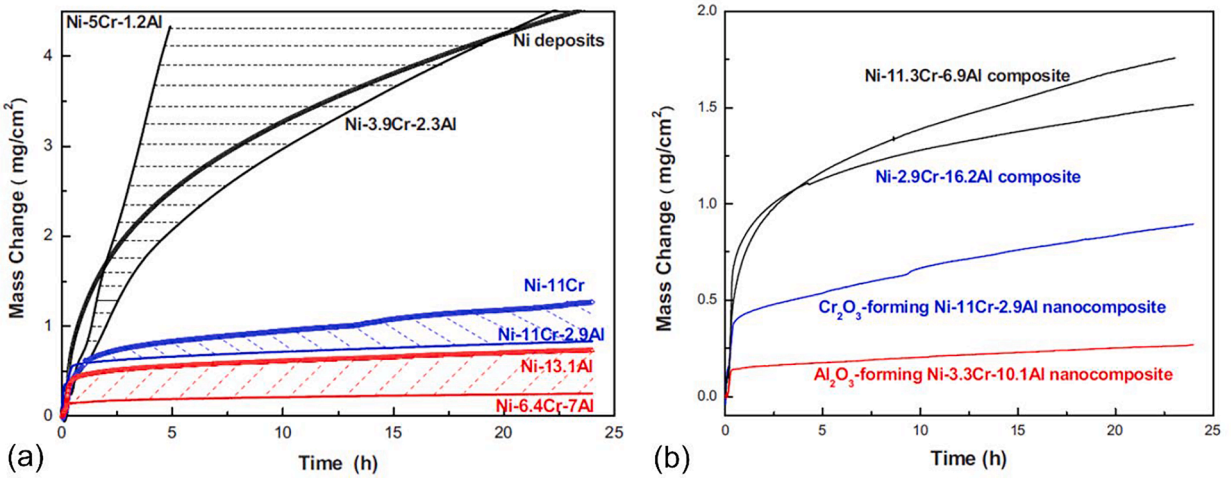

Fig. 46. Oxidation mass gain curves for four different Ni-xCr-yAl alloy compositions [733].

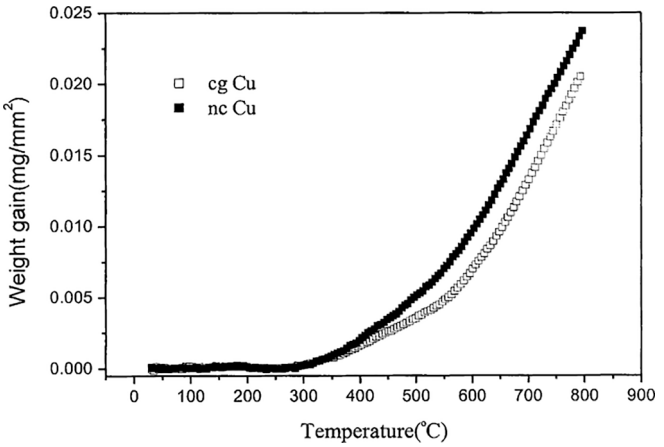

Fig. 47. Thermogravimetric curves for coarse-grained and NC Cu at constant heating rate and in 1 atm of oxygen [734].

protective scale, the enhanced diffusivity results in faster growth rates, protecting the substrate alloy from drastic metal recession and internal oxidation. The selective formation of a protective external oxide scale is also promoted by alloying elements with a higher affinity for oxidation. However, the microstructural stability of the NC material is the most critical issue as it determines the timescale on which the advantageous properties of the fine-grained structure, increasing oxidation resistance, continue to exist during the oxidation process.

4.2.9. Advancement in characterization

At the end of the timeline from 1981 to ~ 2014, significant advancements in the characterization of NC metals had been made, particularly in GB solute engineering and understanding local chemical changes. The growing recognition of the importance of local chemistry led to the widespread use of focused FIBs, which dramatically enhanced the ability to extract and image microstructures at specific locations. This innovation, coupled with techniques such as aberration-corrected TEM and STEM, coupled to APT, allowed for highly precise analysis of microstructural features at the atomic level, even in samples that were not fully consolidated.

More recently, APT has emerged as a critical tool, providing accurate quantification of GB solute excess and the chemistry of small phases. This has enabled a deeper understanding of how solute excess influences the stability of NC microstructures. In particular, interstitial elements such as carbon, nitrogen, oxygen, and sulfur, which are commonly introduced during processes such as mechanical alloying and electro-deposition, have been found to play a significant role. Even in carefully controlled vapor deposition techniques, trace levels of contamination persist, demonstrating that even small amounts of contamination—on the order of parts per million—can significantly affect GB mobility in coarse-grained materials, contributing to GB embrittlement through decohesion.

The emergence of small clusters, typically coherent with the matrix and only a few nanometers in diameter, further complicates the detection of these features using traditional x-ray diffraction and TEM techniques. These clusters exhibit considerable partitioning of interstitial elements, leading to a reduction in the average atomic number, and adding another layer of complexity to the

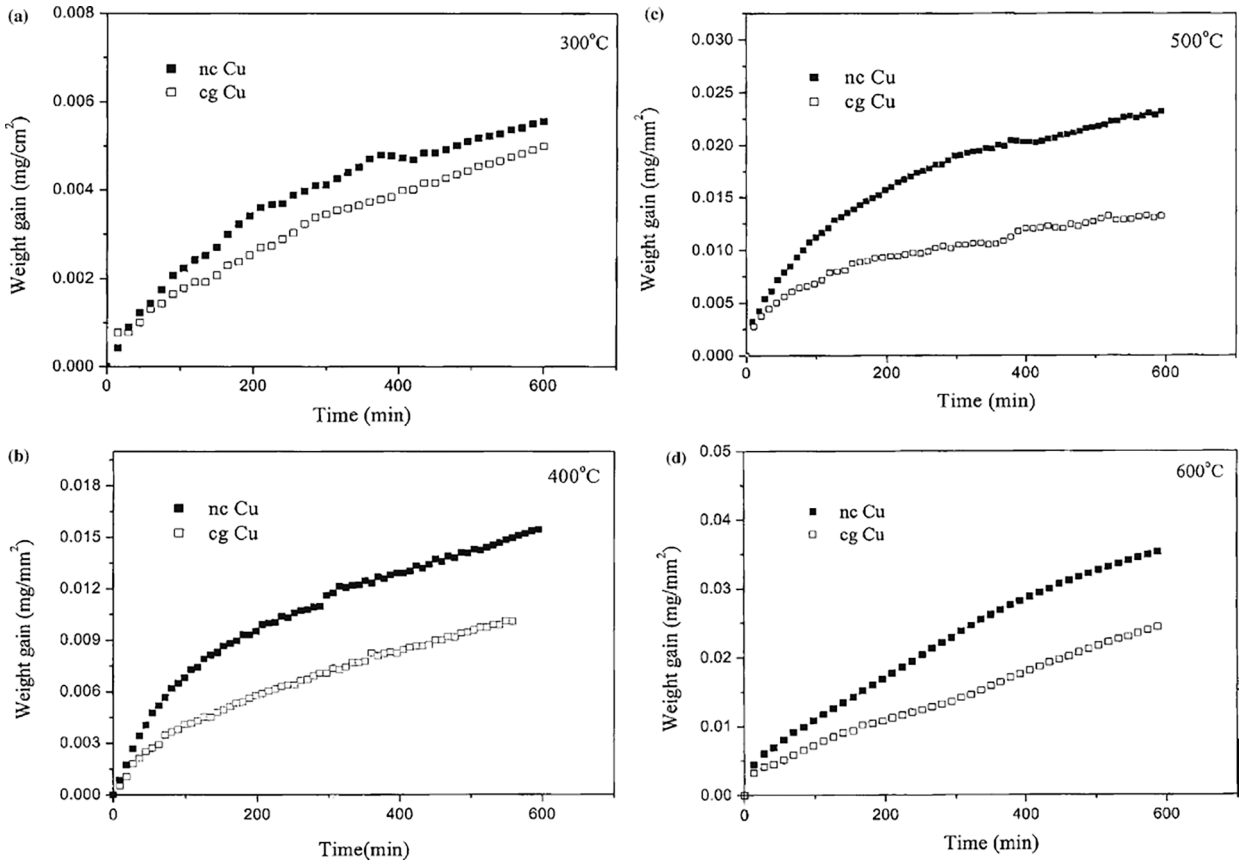

Fig. 48. Oxidation kinetics of NC and coarse-grained Cu at (a) 300 ℃, (b) 400 ℃, (c) 500 ℃, and (d) 600 ℃ in 1 atm of oxygen for 10 h [734].

Table 1
K_p values for NC-Cu and coarse-grained Cu between 300–600 ℃ [734].

Temperature (℃)	K_p(mg²/mm⁴min)	
	NC-Cu	Coarse-grained Cu
300	5.35×10^{-8}	4.23×10^{-8}
400	3.94×10^{-7}	1.86×10^{-7}
500	1.18×10^{-6}	4.35×10^{-7}
600	2.29×10^{-6}	1.2×10^{-6}

characterization of NC materials. At elevated temperatures, short-circuit diffusion can drive transitions between GB-segregated states and GB-precipitated states. More recent studies have also demonstrated that contamination plays a critical role in the formation and transition of amorphous intergranular films, which are often used to stabilize microstructures and inhibit grain growth. These advancements in characterization techniques over the timeline have greatly expanded the understanding of the behavior and stability of NC materials, providing a much clearer picture of the atomic-scale processes governing their properties.

Measuring the grain size in NC materials remains a challenging task due to the extremely small and often heterogeneous nature of the grains (aspect ratio, presence of twins/stacking faults, overlapping grains, and stereographic projections). Various techniques are commonly employed, each with its strengths and limitations. XRD is a widely used method for estimating grain size in NC materials, typically relying on the broadening of diffraction peaks. However, this technique can be inaccurate if the material has phases and other small microstructural features with similar d-spacing [743]. Additionally, for grain sizes between 50–100 nm, the magnitude of instrumental broadening (typically between 0.1 and 0.5 degrees) can add to the measurement uncertainty. TEM offers a higher resolution and direct imaging of individual grains. However, it is often limited by sampling issues and the difficulty of preparing high-quality thin foils of NC materials [744–746]. EBSD and transmission Kikuchi diffraction (TKD) are powerful methods for mapping crystallographic orientations and GBs. However, EBSD often struggles with indexing at very fine grain sizes, and TKD is sensitive to the material's surface preparation and geometry [747]. Therefore, reliable grain size measurement in NC materials typically requires a combination of techniques to overcome the limitations inherent in each method, such TEM combined with precision electron

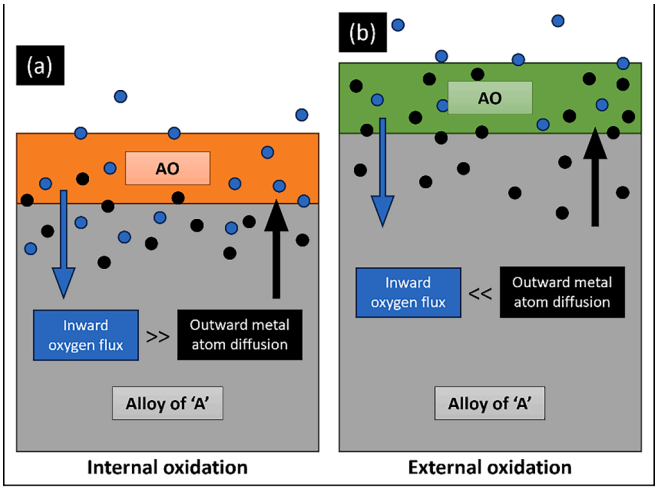

Fig. 49. Internal versus external oxidation behavior in an alloy of atoms A forming an oxide AO.

diffraction or synchrotron XRD (instrumental broadening between typically between 0.005 and 0.05 degrees, [748]) (e.g. [749]).

5. Properties of NC materials: State of the art (~ the past 10 years of advancement)

5.1. Microstructural influences on strength and deformation behavior in stable NC materials

In their 2006 paper, Meyers et al. [33] provided an extensive review on the progress of synthesizing NC materials, noting the remarkable properties these materials can exhibit, such as increased hardness, higher yield strength, improved fatigue crack nucleation stress, and enhanced strain rate sensitivity, particularly in FCC alloys. These properties make NC materials attractive for high-performance applications. However, despite these advantages, NC materials faced several significant limitations. They were particularly susceptible to thermal and stress-induced grain growth, which reduces their overall mechanical properties. Additionally, compared to coarser-grained materials, NC materials often displayed reduced ductility and toughness. The deformation mechanisms of NC materials were known to be strongly influenced by atomic diffusion, compromising their performance under various loading conditions. Unstable NC materials also struggled with resisting creep deformation, fatigue, dynamic loading, shock deformation, and intense radiation exposure. This severely limited their applicability in engineering, even after decades of research.

Furthermore, prior to 2010, the strengthening mechanisms in NC materials were not well understood. It was generally believed that strengthening via solid solution or secondary phase distribution had a limited effect compared to the more significant strengthening observed through grain size reduction. The prevailing consensus was that the contribution from mechanisms other than grain size reduction would only enhance strength to a degree similar to that in conventional polycrystalline alloys. Typically, this strengthening was in the range of a few hundred MPa, depending on the system. When compared to the Hall-Petch strengthening from grain size reduction, the effects from solid solution or secondary phases rarely surpassed ± 35 %, and often fell short of this amount [270,750]. Additionally, the impact of solid solution strengthening was sometimes confounded with grain size reduction, as both lead to matrix hardening [751,752,901].

However, recent research has led to a significant shift in understanding the behavior of thermo-mechanically stabilized NC materials. These materials, which were not well understood during the time of the 2006 review [33], have been found to exhibit mechanical properties, deformation mechanisms, and other physical characteristics that were previously unknown. The stabilization of their nanostructures has resulted in the development of a new class of materials that display far greater stability and unique properties compared to the earlier NC systems. The progress in understanding the thermodynamic and kinetic factors that govern the stability of NC materials, as well as the methods used to stabilize their microstructures, has opened new avenues for further research and application. This shift in understanding has highlighted the unusual properties of the stabilized NC materials and provided new insights that were not previously recognized. For instance, grain size is no longer the primary method of strengthening the material. Recent developments have shown that the spontaneous decomposition of metastable solid solutions to form nanoclusters of immiscible or insoluble elements with particle densities exceeding $10^{23}/m^3$ and average separations below 20 nm can produce unprecedented strengthening effects. These nanoclusters, which are typically smaller than 10 nm in size (often in the range of 2–3 nm) and coherent with the surrounding lattice, resist coarsening due to the reduced diffusion rates, making them particularly effective at pinning GBs and enhancing the strength.

The strength of the stable NC materials is closely tied to the stability of their microstructure. For example, different NC materials, such as Ni–W [][430] and Cu-Ta [242,753] alloys, exhibit distinct strength characteristics due to variations in their microstructural features. In Ni–W alloys, the high strength can be attributed to the formation of GB segregated states, which contribute to enhanced stability (Fig. 51a). Similarly, in Cu-Ta alloys, the stability and strength are linked to the presence of atomic clusters of Ta, which are

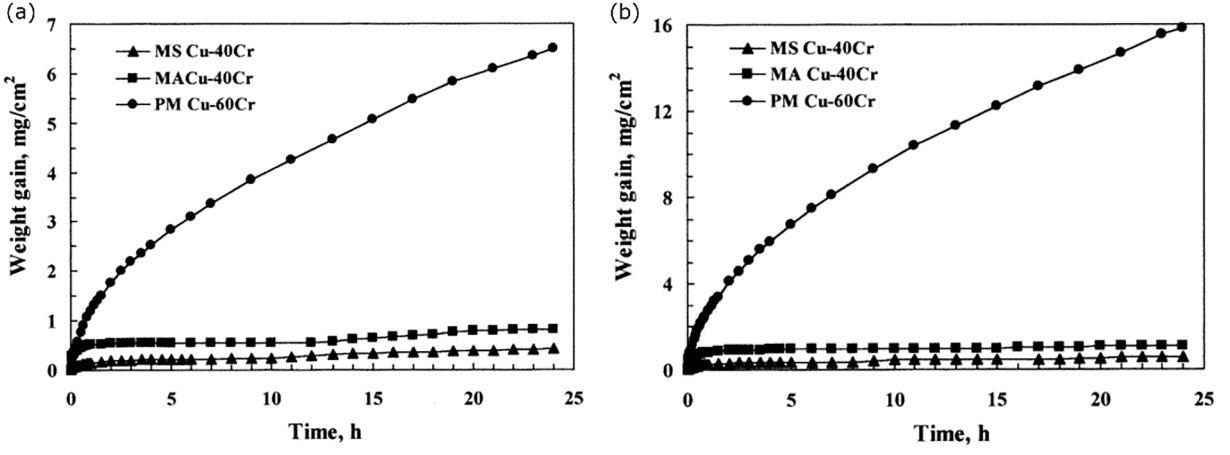

Fig. 50. Oxidation kinetics of the three Cu-Cr systems in 1 atm of pure oxygen at (a) 700 ℃ and (b) 800 ℃ [735].

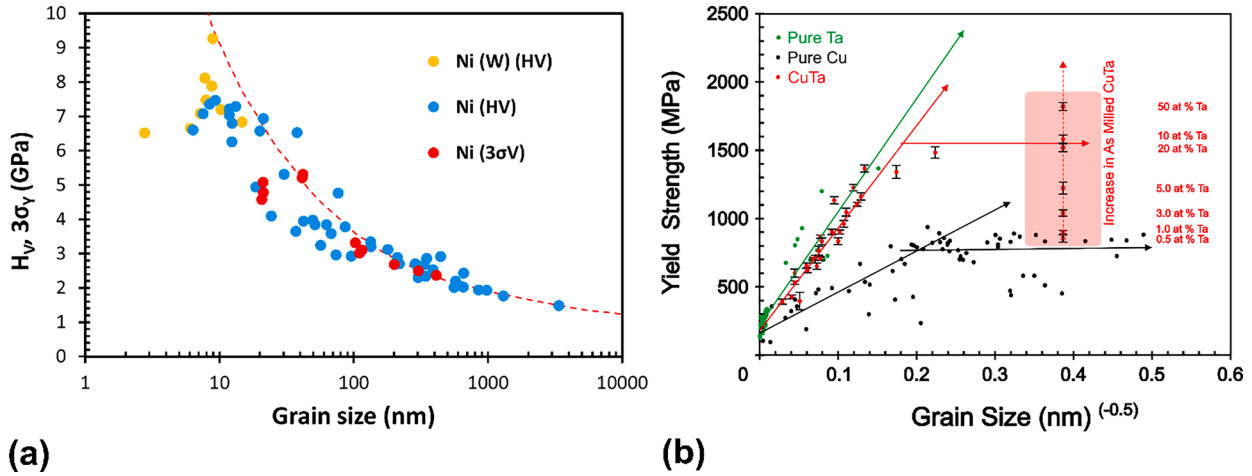

Fig. 51. (a) Hardness versus grain size plot for various Ni alloys [68]. (b) The strength versus grain size plot reveals anomalous strength of Cu-Ta alloys [753]: deviation from the expected rule of mixture strength near theoretical strength limits. The error bar on Cu-Ta points corresponds to one standard deviation resulting from 10 hardness tests.

distributed throughout the grain interior and along the GBs. Despite these differences, studies (Fig. 51) show that even highly stable NC materials demonstrate grain size-dependent strengthening up to a certain critical threshold. Beyond this threshold, further grain size reduction does not result in the expected improvements in strength. This complex behavior reveals the important role played by inter-granular regions, which behave differently from GBs.

In elucidating the need to constrain or strengthen GB, a recent STEM bright-field imaging study on Cu-Ta alloys [753] revealed that an abrupt transformation occurs in the transgranular regions of as-milled material following annealing at 600 °C. These regions, which are highly strained and consist of thickened semi-amorphous material, transform into more equilibrium structures featuring equiaxed high-angle GBs with an average grain size of 35 nm. Below 600 °C, the grain size increased from approximately 7 nm at 100 °C to about 20 nm at 400 °C. This grain size range (7 to 20 nm) corresponds to the Hall-Petch plateau region for pure Cu and Cu-Ta alloys (Fig. 51), where hardness is no longer a function of grain size. Similar observations were made in Ni–W alloys [43], where a breakdown in strength scaling occurred at a grain size of 10–20 nm, accompanied by a transition to shear banding and inhomogeneous flow.

Thermo-mechanically stabilized alloys, such as Cu-Ta, exhibit strong resistance to GB deformation, including sliding, grain rotation, and viscous flow, even at grain sizes close to the NC limit [184,230]. These findings suggest that the breakdown in strength scaling in NC alloys (Fig. 51b) is linked to the transition to amorphous, highly strained regions, which are less resistant to deformation than crystalline regions [753]. Consequently, in thermo-mechanically stabilized NC materials, the thickened disordered inter-granular regions are likely not constrainable like typical relaxed GBs in a more crystalline state. Aifantis et al. [754,755] considered GBs a distinct phase with a finite thickness that might exhibit differing hardness compared to the grain interior. They expanded on previous research by enabling the interfacial energy of the GB to be a function of the GB yield stress [754,755]:

$$\sigma_y = \sigma_0 + k_{HP} d^{-\frac{1}{2}} + \frac{\gamma}{2ad} \tag{13}$$

where a is the faction of the gain size and γ is the GB free energy.

The deformation mechanisms and mechanical properties of thermally stable alloys remain an active area of research, particularly regarding the stability of NC grains under mechanical loading. Quantifying the various strengthening mechanisms in the stabilized systems is challenging due to the complex interplay of microstructural features. As processing parameters change, the interconnectedness of the grain size and inter-granular region makes it difficult to isolate the effects of individual mechanisms. Additionally, dislocation nucleation from GBs is a dominant deformation mechanism for NC materials, with uncertainties regarding the role of segregants and different GB phases in dislocation nucleation or boundary cohesion [306,308,309,342,756–758]. Dislocation processes, such as nucleation and glide in the presence of solutes, are also complicated. The mismatch in atomic sizes and thermal expansion coefficients between GBs and the lattice can introduce residual strains, which further complicate the strengthening mechanisms [759]. Recent MD simulations and other computational techniques have provided insights into these effects, leading to the development of more robust and stable NC microstructures, which can be quantified under varying temperature conditions [206].

For instance, at ambient temperatures and quasi-static strain rates (10^{-4} - 10^{1} s^{-1}), tensile, compressive, and shear loadings in unstable microstructures show predictable behavior. However, as stabilized systems are subjected to more extreme conditions, deviations in properties and performance arise. For example, in coarse-grained Cu [225,231], which follows classical strength-temperature behavior, i.e., the strength versus temperature data shows abrupt slope changes, reflecting shifts in the deformation mechanism [240]. However, stabilized NC Cu-Ta alloys exhibit a nearly linear decrease in flow stress over a wide temperature range [240]. This behavior suggests that dislocation-mediated mechanisms persist even at high temperatures, consistent with the Zener-Hollomon plot. At very high homologous temperatures, Cu-Ta alloys show slight deviations from linearity due to the stable grain

size and microstructure, which delay transitions between deformation mechanisms. The apparent linear temperature dependence over a large temperature window likely results from a complex interplay of several strengthening mechanisms, including grain size, dispersion of ultrafine Ta particles, coherent Ta-rich clusters, and the presence of Ta solute atoms along GBs and within the Cu-rich matrix.

5.2. Strength-ductility trade-off in stable NC materials

The trade-off between strength and ductility is another key challenge in NC materials. An optimal grain size of approximately a few micrometers has been identified as the point where the strain energy density (the product of strength and uniform elongation) reaches its maximum [75,760,902]. In the grain size range of 100–500 nm, the deformation mechanisms are similar to those in traditional fine-grained materials. In the grain size range of 100–500 nm, the deformation mechanisms are similar to those in traditional fine-grained materials. However, as the grain size decreases below 50 nm, partial dislocation emission and twinning become the dominant deformation mechanisms, leading to an increase in strength but a decrease in tensile ductility. When the grain size is reduced to below 20 nm, GB sliding becomes the primary mechanism, and tensile ductility is almost nonexistent. This trade-off between strength and ductility has long been a barrier to the practical application of NC materials. Stable NC materials have shown that it is possible to achieve high strength at relatively large grain sizes (150–300 nm) compared to pure NC Cu alloys with grain sizes less than or equal to 5 nm (Figs. 51 and 52). This result suggests that the controlled decomposition of forced solid solutions to form nanostructured materials can offer a way to enhance material strength without sacrificing ductility, thus overcoming the traditional limitations of the strength-ductility trade-off in NC materials.

5.3. Materials response under extreme stimuli

5.3.1. Thermal stability and grain growth resistance in stabilized NC materials under intense and prolonged heat

To develop materials that can endure significant thermal energy over long periods, it is crucial to design microstructures that resist vacancy flux and diffusion processes. In particular, maintaining stable GBs and phase boundaries under such conditions is essential.

Sharma et al. studied the microstructural evolution of Ni-Y-Zr ternary alloys after heat treatment at temperatures from 200 °C to 1200 °C for one hour [764]. At 600 °C, the grain growth in the alloy resembled that in pure NC Ni at 100 °C, indicating similar growth mechanisms but at much higher temperatures. At 800 °C, the grains remained NC (≤100 nm), but as the temperature increased to 1200 °C, a bimodal grain size distribution developed. Most grains remained around 350 nm, while a few exhibited abnormal growth and contained annealing twins. Additionally, microstructural analysis revealed the formation of Y and Y–Zr oxides as well as nitrides at higher temperatures. The presence of the cuboidal precipitates was attributed to contamination from liquid nitrogen during cryogenic ball milling.

Cai et al. produced 14YWTZ alloy powders (Fe–14Cr–3 W–0.4Ti–0.8Zr–0.3Y2O3) prepared by mechanical alloying and heat-treated at temperatures from 500 to 1300 °C [765]. Below 800 °C, the grain size remained around 50 nm, increasing slightly to 59 ± 16 nm at 900 °C. Vickers hardness tests showed stability at 800 °C for up to 250 h, indicating grain size stability around 50 nm. After annealing at 1000 °C for 1 h, the grain size increased to 75 ± 23 nm, demonstrating high thermal stability. However, above 1000 °C,

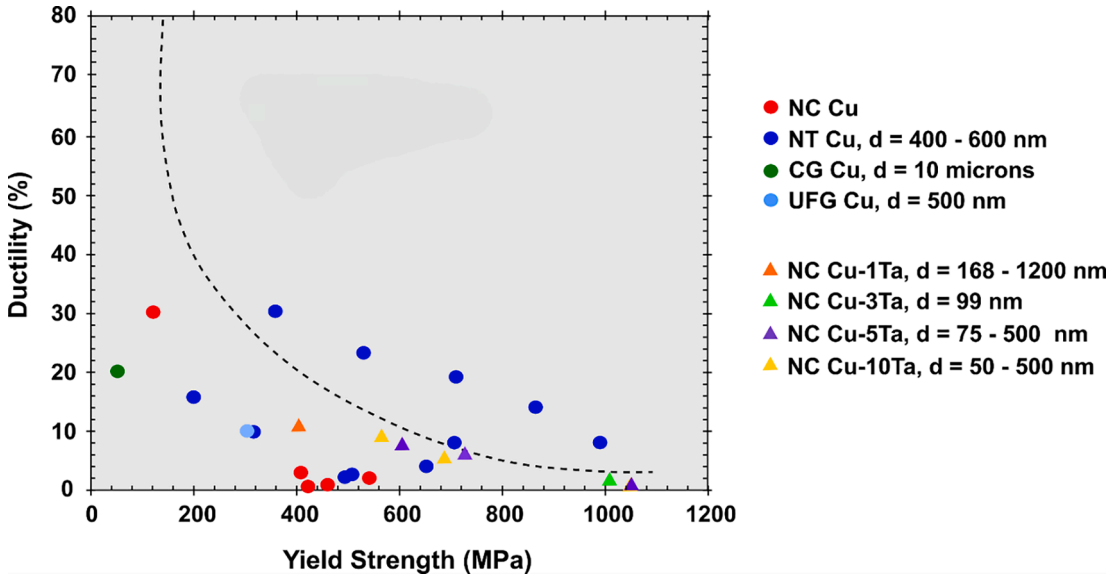

Fig. 52. Tensile ductility as a function of yield strength for different compositions of NC Cu-Ta alloys along with literature data for pure Cu with grain sizes ranging from NC to CG [20,454,461,761,762], nano-twinned Cu, and UFG Cu from [48,763], and CG Cu from [48].

grain growth accelerated, significantly reducing hardness. Nanoclusters (~3.18 nm, ~3 × 10^{24} $m^{-}3$) were uniformly distributed throughout the microstructure, with GBs showing W, C, and Mn segregation. The alloy's stability was determined to be thermodynamic due to co-segregation at GBs and Zener pinning by Zr–Ti–Y–O-enriched clusters, which limited grain growth during annealing.

Similarly, Li et al. [766] reported on the microstructure of 14YT-4Sc alloy after long-term annealing at 1000 °C for up to 60 h. The average grain size of the alloy after annealing for 10, 15, 24, and 60 h was found to be 0.4, 0.52, 0.63, and 1.18 μm, respectively. TEM analysis showed that while the average grain size stayed within the ultrafine-grained regime, the matrix remained largely nanoscale, with only slight grain growth over time (growth exponent n = 0.29). Furthermore, EDS mapping of the sample revealed the presence of Sc–Ti–Y–O-enriched nano-oxide particles, with sizes below 10 nm. The retention of the nanostructure was attributed to the stabilizing effect of these complex nano-oxide particles.

The thermal stability of the NC Cantor alloy (CrMnFeCoNi) was studied under long-term annealing to investigate phase decomposition at low temperatures [767]. Previous work showed that Ni and Mn co-segregated at GBs after 0.5 h of annealing at 100 °C, without phase decomposition. In this study, the annealing time was extended to over 300 h at 100 °C to see if prolonged segregation would lead to phase decomposition. APT results after 30 and 302 h confirmed that Cr, Co, and Fe remained homogeneously distributed, while Ni and Mn co-segregated at the GBs. Despite increased segregation over time, phase decomposition did not occur as the concentration of Ni and Mn at the GBs remained below 47 at. %, preventing decomposition. However, annealing at 250 °C for 5 h caused phase decomposition, with Ni and Mn concentrations at the GBs approaching equilibrium between 1 and 5 h. APT analysis of the 1-hour annealed alloy at 300 °C revealed phase separation into Cr-rich, FeCo-rich, NiMn-rich, and Cr-containing phases. These findings support the discussion in Section 3.4 by demonstrating that GB segregation can undergo a spinodal decomposition and form chemically heterogeneous GB structures.

Lu et al. [768] investigated the grain growth kinetics and thermal stability of Pt.90Au.10 and pure Pt thin films through annealing experiments. Grain growth occurred in films annealed at 500 °C and 700 °C, corresponding to the homologous temperatures of ~ 0.4 and 0.5 Tm, respectively. Both alloy and pure Pt films had an initial grain size of ~ 7.3 nm. Upon annealing at 500 °C, the Pt.90Au.10 alloy exhibited significantly slower grain growth compared to pure Pt. The grain structure in the alloy stabilized after a few hours of annealing, while the pure Pt film showed continued and abnormal grain growth, including rapid growth of a few large grains that consumed smaller ones. At 700 °C, the Pt.90Au.10 alloy showed minimal grain size increase, stabilizing at around 46 nm, while pure Pt experienced continuous abnormal grain growth. Detailed STEM-EDS analysis revealed that Au preferentially segregated to high-energy GBs, forming a stable structure that slows down abnormal grain growth. The Au segregation was more homogeneous at higher annealing temperatures, reducing the heterogeneity observed at 500 °C. The thermal stability was supported by theoretical models of GB solute segregation, which indicated that temperature affects both the thermodynamic and kinetic aspects of GB mobility and solute segregation. At higher temperatures, the entropic effects reduced the segregation energy, while solute drag slowed GB motion, collectively enhancing the alloy's stability.

NC W and W-Ti [769] alloys were processed by high-energy mechanical alloying, resulting in NC structures with average grain sizes of 22 nm for the W-Ti alloy and 17 nm for unalloyed W. After annealing at 1100 °C for one week, unalloyed W exhibited significant grain coarsening, with the average grain size increasing to 600 nm. In contrast, the W-20 at.% Ti alloy retained a much finer average grain size of 24 nm, demonstrating a 25-fold difference in grain growth. TEM, STEM, and EDS analyses revealed a highly inhomogeneous Ti distribution in the W-Ti alloy after annealing, with Ti segregating around the W-rich grains while remaining dilute in the grain interiors. Atom probe tomography confirmed this segregation pattern. Kinetic analysis of diffusion indicated that the one-week annealing time allowed for microstructure relaxation over scales much larger than the grain size, suggesting that the nanostructure stability was influenced by thermodynamic factors. This was further supported by Monte Carlo simulations, which visualized the Ti segregation zone around W-rich grains.

Rupert and coworkers [312,770] studied NC Cu-Zr-Hf alloys created by mechanical alloying to examine their thermal stability and ability to form amorphous intergranular films or (AIFs). The microstructures of these alloys were compared to binary Cu-Hf and Cu-Zr alloys to understand the role of each dopant element [312,770].

All ternary alloys demonstrated excellent thermal stability, maintaining grain sizes between 50–65 nm after two weeks of annealing at 950 °C, well within the NC regime. In contrast, pure Cu grew beyond XRD resolution within the first hour, and binary Cu-Hf alloys exceeded XRD resolution by the end of the tests. The thermal stability was primarily due to thick AIFs and a minor contribution from HfC and ZrC precipitates at the GBs [311]. The ternary Cu-4Hf-1Zr alloy, despite having the same dopant concentration as binary Cu-5Zr, formed thicker AIFs, indicating that the addition of a second dopant reduces the energy penalty for AIF formation. The ternary alloys exhibited the thickest AIFs observed in metallic materials. Previous studies also reported AIF formation in Cu-Zr alloys under similar conditions, supporting the findings of this study.

Further work explored the thermal stability and AIF formation of three quinary NC alloys, based on Cu–Zr–Hf but doped with Mo, W, Nb, and Ti. The Cu–Zr–Hf–Nb–Ti alloy [382] showed the best thermal stability, retaining a grain size of 63 nm after annealing at 950 °C for a week. This stability was attributed to the formation of thick multi-principal element amorphous AIF, which were 44 % thicker than those in Cu–Zr and 32 % thicker than in Cu–Zr–Hf alloys. Processing challenges, including second-phase formation and C contamination, reduced dopant efficacy by forming carbides, which limited the availability of dopants for GB segregation. Similar results were found for various Al alloys [771].

The structural stability of NC aluminum-manganese (Al-6.5 at.%. Mn) alloys was studied in the temperature range of 200 to 400 °C [772]. TEM observations revealed that the presence of Mn effectively suppresses grain growth, allowing grain sizes of 100 nm or finer to be retained at 200 and 300 °C, even after 1 month of annealing. However, the primary instability mechanism in the alloy was found to be the precipitation of the equilibrium Al6Mn phase, which formed rapidly at both 300 and 400 °C.

In NC Cu-Ta alloys, grain coarsening was minimal even after 10,000 h at 800 °C (~80 % T_m), with only a 1 nm increase in grain size

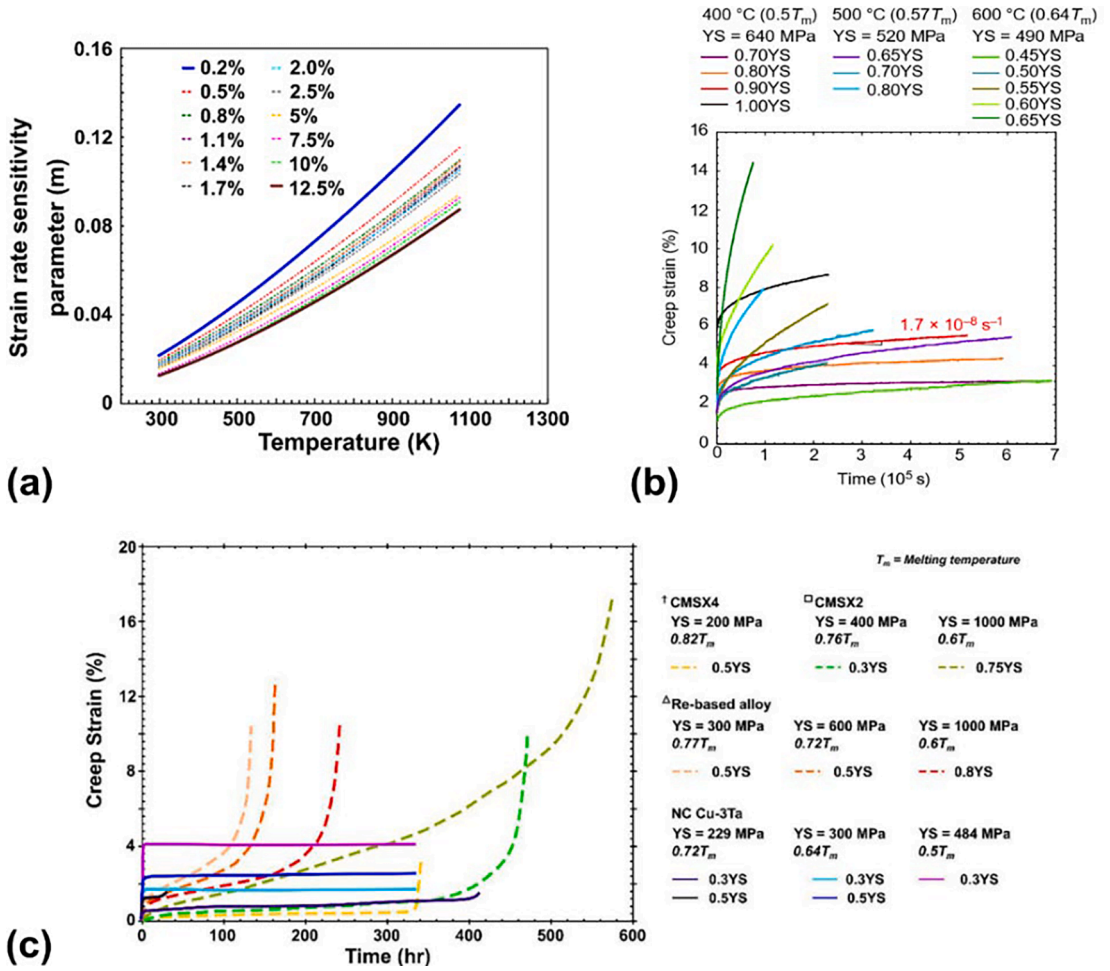

Fig. 53. (a) Effect of temperature on strain rate sensitivity of NC Cu-Ta at different strain levels measured from experiments. (b) Conventional compressive creep strain versus time curves for various applied temperatures and constant stress conditions, (c) Tensile creep strain versus time for NC Cu-3at.%Ta at different fractions of the melting temperature (T_m) plotted along with data for Ni-based superalloys from the literature [775–777].

per 100 h. The stability can be quantified by the vacancy flux, calculated as 6.6 x 10^{17} vacancies per m^2/s in the initial Cu-Ta microstructure having an average grain size of ~ 65 nm. Over 10,000 h, the total number of vacancies absorbed by a given GB would then be approximately 3.2 x 10^{11}. Despite the capillary pressure that would normally induce grain growth, the grain size increased only modestly to 165 nm. This resistance to coarsening is attributed to the Zener pinning force from Ta-nanoclusters, which prevents significant coarsening and stabilizes the GBs. The Ta nanoclusters, approximately 3 nm in diameter, act as diffusion barriers for Cu atoms. As a result, NC Cu-Ta alloys maintain improved hardness and yield strength (about 33 % higher at 800 °C) compared to pure NC Cu, which typically experiences rapid grain growth at lower temperatures over short timescales. The stability was pushed further by the addition of Li to the Cu-Ta alloy [773]. STEM comparison imaging after 10,000 h at 800 °C shows that the Cu-3Ta alloy experiences abnormal grain growth, more than doubling the average grain size, while in the Cu-3Ta-0.5Li alloy, the grain size increases from 35 nm to 91 nm [773]. This corresponds to a growth rate of 0.035 Å per hour, three times slower than the Cu-3Ta alloy. The improved grain stability in the Cu-Ta-Li alloy was attributed to the coherence of Cu3Li clusters with the matrix and electronic contributions from a Ta atomic bilayer.

Collectively, it is found that the stabilization of NC alloys at high temperatures is primarily influenced by GB pinning mechanisms, such as the presence of nanoclusters or thermodynamic mechanisms via solute segregation and/or the formation of AIFs. However, in the latter case, phase instability can arise from second-phase formation (such as carbides) or fast-diffusing interstitial elements, which reduce the availability of dopants for GB segregation and promote grain coarsening. GB phase transformations, including spinodal decomposition, can lead to chemically heterogeneous GB structures. Such structures can reduce the GB mobility and stabilize the grain size, especially if precipitates of a new GB phase act as pinning points in a manner similar to the Zener particles.

5.3.2. Creep response

The complex and interrelated strengthening mechanisms described in the earlier sections play a significant role in determining the

SRS of stable NC materials. These mechanisms also correlate with several important material properties, such as creep resistance. Unlike conventional materials, the SRS of NC materials can depart significantly from typical expectations due to the unique characteristics of their microstructure. One key factor in this behavior is the microstructural stability, which plays a crucial role in governing the SRS. Evidence suggests that thermo-mechanically stable NC materials can mitigate or limit the extent of SRS exhibited at elevated temperatures, leading to improved material performance under high-stress conditions.

The SRS parameter m is inversely proportional to the apparent activation volume v^*, which measures the average volume of the material involved in the deformation process. v^* is critical for determining the rate-controlling mechanisms of plastic deformation. As shown in Fig. 53a, the evolution of the rate-controlling mechanisms with strain and temperature for a stabilized NC alloy reveals a significant increase in the SRS parameter m with temperature (starting at around 0.025 at room temperature). This increase is particularly pronounced at lower strains, as demonstrated by the five-fold increase in the spread of m values between 0.2 % and 12.5 % strain. This behavior suggests that thermally activated strain hardening mechanisms play a more prominent role at the early stages of deformation. This is especially true for NC materials, where the dislocation storage capacity is exhausted within the first few percent strain, leading to a more rapid activation of thermally driven mechanisms.

Although m increases with temperature, as shown in Fig. 53a, it does not surpass the typical threshold of 0.3, which is commonly observed in materials dominated by GB processes, such as those experiencing creep. In fact, a survey of over 184 coarse-grained alloys based on Zn, Sn, Mg, Al, Cu, Fe, Ni, and Ti [774] has demonstrated that alloys with stable grain sizes (ranging from 1 to 20 μm) exhibit deformation mechanisms associated with GB processes, resulting in mm values between 0.3 and 0.8 at homologous temperatures of 50–80 % of the melting temperature T_m [774]. This comparison suggests that thermo-mechanically stabilized NC materials exhibit superior creep resistance relative to coarse-grained samples.

As discussed in Chapter 4, the diffusion-based mechanisms of the Nabarro-Herring and Coble creep generally exhibit a smaller stress exponent and a stronger dependence on grain size than dislocation-based mechanisms [86,553,778,779]. Consequently, Coble creep prevails in materials with finer grain sizes, such as those within the NC regime, due to the amplified GB diffusion at relatively lower temperatures, leading to higher steady-state creep rates [554]. Notably, many pure NC materials with grain sizes below 100 nm exhibit steady-state creep rates four to five orders of magnitude higher than those observed in coarse-grained materials [17,544,555]. Generally, such behavior is associated with a high SRS and an activation volume of less than $\sim 10b^3$.

In this context, GB engineering plays a critical role in enhancing the creep resistance of mechanically stabilized NC materials. By strategically introducing segregated solutes and promoting the formation of solute clusters at the GBs, the GB mobility can be significantly reduced. This reduction helps prevent excessive grain growth, limits diffusion-driven creep mechanisms, and makes the GBs more resistant to sliding and migration under high-stress conditions. Moreover, the geometric structure of the GB network, including the relaxation and stabilization of GBs through mechanisms such as partial dislocation motion, further contributes to the mechanical stability of NC materials. The engineered GBs, with tailored chemical and structural characteristics, serve as barriers to dislocation and vacancy motion, thereby enhancing the overall creep resistance of the material. This approach offers a promising strategy for developing high-performance NC metals for high-temperature applications.

For instance, Zhang et al. [780] showed that stabilization of GBs in NC NiCoCr alloy is possible through structural relaxation triggered by severe plastic deformation, resulting in low-energy $\sum$CSL (coincidence-site lattice) boundaries, interlocked with a high density of twin boundaries that resist migration and sliding. This configuration of stable GBs suppresses diffusion, thereby maintaining the alloy's strength at high temperatures. The GB relaxation facilitated by partial dislocations during grain refinement, hinders the GB-mediated deformation processes such as sliding and migration, enhancing creep resistance. These mechanically stabilized GB networks, analyzed along the [110] axis, revealed that over 50 % of the boundaries were faceted, featuring segments of {1 1 1} atomic planes connected by steps. The stabilized GB configurations exhibited remarkable creep resistance, with the alloy achieving a steady-state creep rate of approximately 10^{-7} $s^{-}1$ under gigapascal-level stress at 700 °C. This performance significantly surpasses that of traditional superalloys. Post-creep microstructural evaluation revealed negligible grain growth and texture changes, confirming the alloy's stability. Huang et al. [781] also demonstrated that the restructuring of GBs significantly enhances the creep resistance of NC Fe-Ni alloys, primarily due to a diffusional phase transformation occurring at TJs and along GBs. The diffusional phase transformation involves the formation of nanoscale secondary FCC phases (~8 vol%), particularly through a chemical reordering of Ni at and near the GBs. This transformation drastically reduces the stored dislocation density (~97 %) through low-temperature annealing at 300 °C, which improves creep resistance. The reduced dislocation density rendered the nucleation of new dislocations necessary, increasing the stress required for dislocation-based creep deformation and thereby enhancing creep resistance. As a result, the nucleation of full or partial lattice dislocations with a Burgers vector characteristic of the BCC grain interior became less likely and/or required higher local resolved shear stresses.

Recent studies have shown that GBs can be stabilized against incipient deformation process through the use of small nanoclusters. For instance, creep tests in compression [67] and tension [230] have shown that the primary creep in NC Cu-Ta is followed by an unusual steady-state creep regime (Fig. 53b-c) in which the creep rate becomes nearly zero (horizontal portion in the curves). The tests were stopped after two weeks of testing if no failure occurred. An extended primary creep regime was observed for the test temperature of 973 K (0.72Tm) and various applied stresses, similar to the one seen at lower temperatures. However, at this temperature, the steady-state creep behavior was different in that it had a non-zero slope and was followed by a short tertiary creep and, ultimately, failure. The steady-state creep rate at 973 K was on the order of 10^{-8} s^{-1}. In all cases, the time to failure depended on the magnitude of the applied stress. By contrast, coarse-grained Ni-based superalloys show traditional creep rate versus time curves with three distinct regimes corresponding to the primary, secondary, and tertiary creep under all test conditions [775–777] (Fig. 53c). The tensile creep behavior exhibited by the NC alloy at temperatures up to $0.64T_m$ is highly unusual for an NC material, especially one that was processed through powder metallurgy.

In the above examples, the primary creep rates of the stabilized NC material were usually high. To gain further insights, the primary creep strains for all test conditions were fitted with a power law, revealing a cubic-root relationship between the strain and time, consistent with the Andrade β-flow theory for stable NC materials [782]. It was determined that certain microstructure regions, such as GBs and TJs, gave rise to stress concentrations exceeding the applied global stress but fell below the threshold for local yielding. Consequently, the microstructure could undergo relaxation to counter the localized stress buildup, which gradually decelerated with time. This relaxation mechanism explained the observed primary creep deformation in the stable NC material [230]. Kale et al. [230] validated this explanation by a loading and re-loading experiment, in which the sample was crept at 873 K (0.64Tm) for 1.5 weeks and exhibited a reduced primary creep strain during re-loading due to prior relaxation in the initial creep test. This insight suggests a potential approach to mitigate the initial considerable instantaneous strain by annealing under stress, which could reduce or eliminate this strain.

Furthermore, an initial transition to tertiary creep was observed despite suppressing several deformation mechanisms in a stable NC material. Although the strain accumulated during this stage was minimal, it signifies the microstructure's capability for this transition. Atomistic simulations have shed light on the mechanisms behind this unique creep behavior in NC alloys [230]. The simulation studies revealed the role of solutes/nanoclusters, which can hinder/alter dislocation movements and GB diffusion. This leads to elongation and tensile creep deformation, clarifying the distinction between diffusion-driven Coble creep and dislocation-based mechanisms. However, a deeper understanding is needed to engineer a more stable response during the final stages of deformation and failure in creep. More studies of other stable NC alloys are also required to explore the limitations of their creep resistance and the underlying mechanisms.

Shan et al. [783] showed that nanoscale precipitates in NC Fe-5at.% Zr steel, likely enriched with zirconium, interact with dislocations and GBs to stabilize the microstructure. Similarly, Xu et al. [784] reported that Y-Ti-Zr-O-enriched nanoparticles in an NC 14YWTZ alloy effectively pin dislocations and inhibit GB coarsening through Zener pinning mechanisms along with multi-component GB co-segregation. The nanoscale clusters reduced GB mobility and suppressed the Coble and Nabarro-Herring diffusional creep mechanisms, ensuring that dislocation-based deformation, particularly dislocation climb, became the dominant mechanism. As a result, the materials exhibited superior creep resistance under high applied stresses and elevated temperatures.

Other forms of GB engineering have aimed to understand and enhance the creep resistance and thermal stability of NC materials by reducing vacancy mobility, suppressing vacancy nucleation and absorption at GBs through atomic-level modifications, such as introducing nanotwin boundaries or solute segregation, or inhibiting diffusion-driven processes and dislocation activity. For instance, the work of Qian et al. [785] on NC and nanotwinned copper reveals the critical role of nanoscale twin boundaries in reducing vacancy mobility and suppressing diffusion processes, which are primary contributors to creep deformation in NC Cu. It was found that twin boundaries act as barriers to dislocation motion, effectively stabilizing GBs and reducing nonaffine displacements during creep. Smaller twin thicknesses further enhance the stabilization, leading to lower steady-state creep rates and better creep resistance due to increased resistance to dislocation nucleation from GB sources. Similarly, the study of high-entropy alloys (HEAs), such as NC CrCoNi and CrMnFeCoNi, has emphasized the role of GBs and dislocation behavior [786]. Both alloys exhibited equiaxed nano-grains (~10–50 nm) with significant contributions from stacking faults (SFs) and nano-twins. The alloys demonstrated superior hardness and creep resistance compared to coarse-grained metals. The creep resistance was further enhanced by the suppression of GB-mediated creep mechanisms at high stress, with dislocation nucleation from GB sources becoming the dominant mechanism at higher stresses. The study highlighted the importance of SFs, nano-twins, and stable GBs in enhancing the mechanical properties and creep resistance of these alloys.

Wani et al. [787] showed the effect of solute segregation on threshold stress for vacancy emission and absorption at GBs using the Mohamed model [788]. The ability of Zr solute atoms to modify the local GB structure and energetics, thereby reducing vacancy concentration and mobility to impede GB sliding and dislocation motion, was a focus of the evaluation. To identify solute atoms capable of simultaneously enhancing grain size stability and creep resistance, the thermodynamic framework proposed by Murdoch and Schuh [129] was employed in conjunction with the Hondros and Henderson equation [789]. In NC Cu-Zr the binding energy and normalized threshold stress were found to decrease with temperature, reflecting weaker solute–solvent bonding at higher thermal conditions. Activation energy analysis confirms Coble creep as the primary mechanism, with Zr increasing vacancy diffusion resistance. The theoretical analysis of solute segregation in NC materials demonstrated that solute atoms reduce vacancy formation and mobility, thereby increasing the activation energy of creep. This mechanism was suggested to impede the GB-mediated deformation processes, including sliding and migration, while strengthening the GBs and enhancing resistance to dislocation motion.

5.3.3. *High strain rate behavior*

Controlling high-strain-rate plasticity in NC materials can be envisioned by the constitutive relationship ($\dot{\varepsilon} = \rho b v$, where b is the magnitude of the Burgers vector), providing two variables to control the response, namely, dislocation velocity (v) and mobile dislocation density (ρ). However, active microstructural control or manipulation of v, *and* ρ as a function of strain rate has not been accomplished to date. Accordingly, there is a direct correlation between the rise in strain rate and the increase in flow stress through dislocation velocity dependence on the applied stress. Stable NC materials are expected to exhibit reduced SRS values, especially at or near the ambient conditions. This is especially true within the quasi-static strain rate regime, in which the change in the flow stress as a function of strain rate should be minimal, given the relative value of the SRS parameter, m. Indeed, recent research conducted by Rajagolapan et al. [234] on a stabilized NC material substantiates that quasi-static rates exert negligible effects on the flow stress response up to 600 °C. In more extreme scenarios, such as those involving strain rates between 10^3 and 10^4 s^{-1} when the relaxation effects are too restricted to reach equilibrium, the dynamics of dislocation velocity, including the drag effects, may become significant factors. Consequently, these conditions can lead to notable changes in the flow stress.

Considering the relations $\sigma = C\dot{\varepsilon}^m$ and $\dot{\varepsilon} = \rho b v$, the drag effects and dislocation density potentially wield a significant influence over the increase in flow stress. As the loading rate increases to a critical point ($\sim 10^4$ s^{-1}), most materials undergo a rapid up-turn in their flow stress [599]. In different materials [599], the strength increases by several hundred percent as the deformation rate increases [19,541,618,790]. For instance, Follansbee et al. [610] experimentally observed that the flow stress upturn in FCC Cu at room temperature increased six times at $\sim 4.0 \times 10^3$ s^{-1} compared to the quasi-static conditions. Likewise, for similarly applied strain rates in coarse-grained Ni, the flow stress was found to experience an approximately 55 % increase compared to the quasi-static flow stress [19]. Although the exact mechanism of this dynamic transition has not been established, it has often been associated with the transition from the thermally activated to drag-dominated dislocation motion, primarily brought about by interactions with phonons in the lattice [484,599]. The contribution of drag effects to dislocation motion becomes significant as the deformation rate increases [599].

Furthermore, variation in the extent of increase in the flow stress at high strain rates has also been attributed to the effective dislocation mass under acceleration and the dislocation interaction with microstructural elements such as GBs and precipitates, which depend on the applied temperature [612]. Such theories are primarily based on atomistic simulations and modeling. Gaining experimental evidence for phenomena such as phonon drag is challenging [791,792]. Recently, Lea et al. experimentally demonstrated that the flow stress upturn in polycrystalline materials is driven mainly by a mechanism involving self-organization of dislocations [793]. In conventional polycrystalline materials, plasticity is mediated through self-organization and avalanches of dislocations, referred to as self-organized criticality (SOCs). Maintaining such self-organization at a high strain rate is constrained by the time available, resulting in multiple short dislocations instead of causing high-rate strengthening. In both theories (phonon drag and time-limiting SOCs), the flow stress upturn is controlled mainly by changes in the dislocation structure and behavior at high rates compared

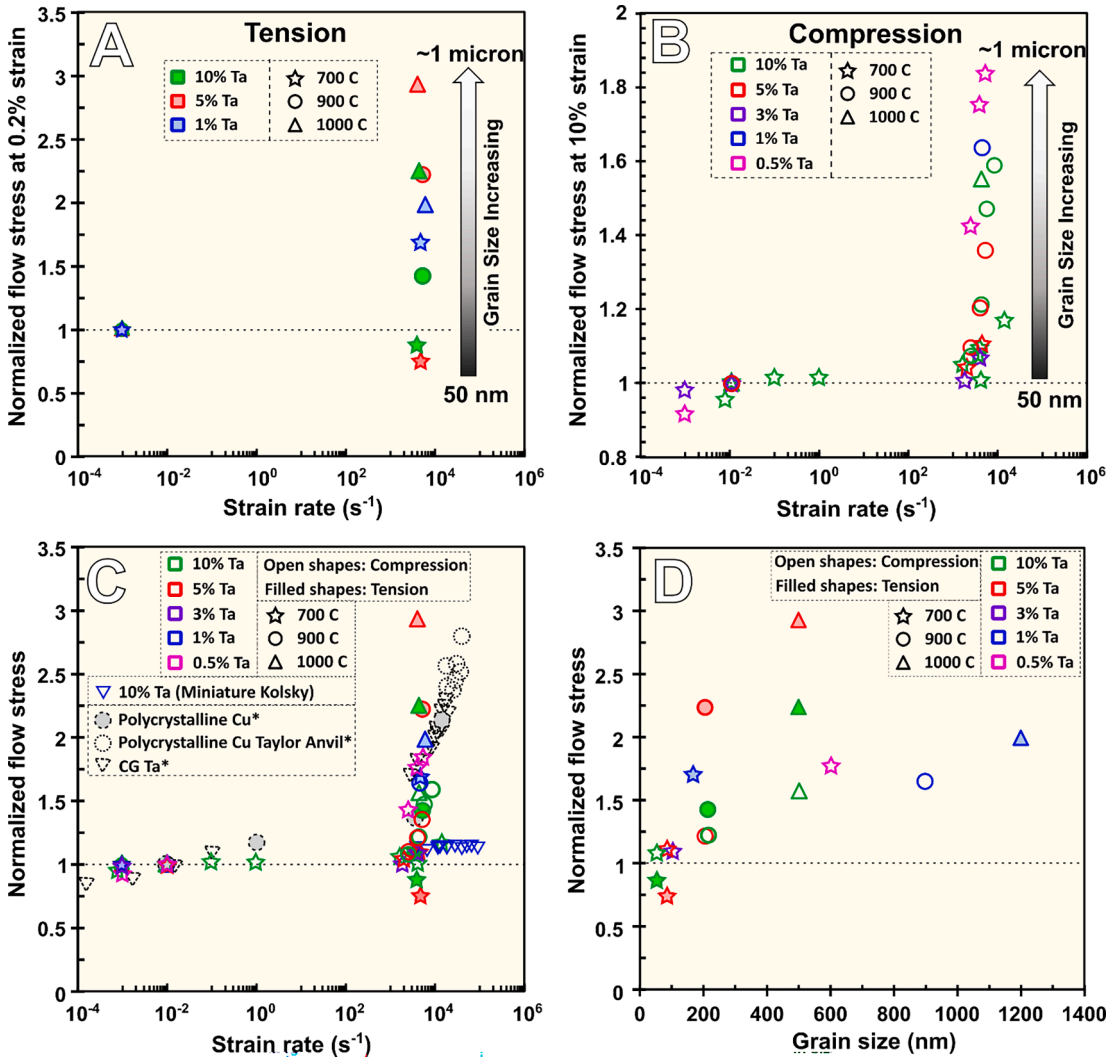

Fig. 54. Normalized flow stress as a function of (A) strain rate in tension and (B) strain rate in compression. (C) Combined plot of tension (0.2 %) and compression (10 %) for various Cu-Ta samples (with literature data points for coarse-grained Cu and Ta [225,231]). (D) Grain size for compression and tension at a similar strain rate (~4000 /s).

to that under quasi-static conditions.

In the quantum–mechanical description, phonons obey the Bose-Einstein statistics, and their mean occupation numbers increase with temperature. In stable NC materials, the high density of barriers, such as grain/twin boundaries and other interfaces, causes phonon scattering, absorption, and transmission, increasing the local phonon DOS. Recent simulation work on stabilized NC systems has indicated a shift of phonon modes toward lower frequencies with increasing temperature, which is typical of thermal expansion and anharmonicity [225]. Such findings suggest that a higher phonon density in stable NC materials results in a higher drag coefficient. The increased energy for generating and propagating dislocations and an increase in phonon drag coefficient require significantly greater stress than at quasi-static states to get further deformation compared to coarse-grained systems. Thus, a stable NC material should be more sensitive to phonon drag and experience it at lower strain rates than conventional materials. It should be noted that such changes in the phonon DOS with increasing temperature during plastic deformation are only possible because of the stable microstructure that resists coarsening.

Thus, tailoring the microstructure to control the dislocation activity through v *and* ρ can provide an avenue for controlling the flow stress upturn at high strain rates. Namely, the perturbations of a moving dislocation caused by interactions with microstructural elements can alter the flow stress upturn. Unfortunately, in most crystalline materials, the available mean free dislocation path between microstructural elements is too large to restrict the dislocation self-organization or the average dislocation velocity below the inherent threshold required for the phonon drag effects. For instance, a moving dislocation in Cu requires only $\sim$ 15 nm to accelerate to a steady-state velocity [225]. Thus, the traditional microstructural length scales have not been sufficient for damping out of the phonon drag effect or the time-limiting SOCs.

It may be hypothesized that if the dislocation mean free path between microstructural elements could be reduced below a certain point, then the phonon drag can be constricted owing to the inability to attain a critical velocity. Similarly, the SOCs will lose their role in the flow stress upturn due to insufficient space required for their formation even at nominal strain rates. For instance, the recent work by Turnage et al. [225] and Casem et al. [241] on microstructurally stable NC materials showed negligible changes in the room temperature compressive flow stress up to 10^6 s^{-1} (no flow stress up-turn), by contrast to the coarse-grained counterparts [225]. A high upturn, similar ones exhibited by coarse-grained pure Cu at 298 K were observed only at a high homologous temperature (0.55 T_m) in a stable NC material, as reported by Turnage et al. [225]. It was suggested that the initial mechanism for such behavior was related to a reduced dislocation velocity associated with damping out through a pinning interaction with a critical length scale of stable atomic clusters. As the drag coefficient is temperature-dependent, this mechanism was ultimately overcome at high homologous temperatures.

To further elucidate the effect of strain rate on flow stress, Srinivasan et al. performed experiments in tension and compression by systematically varying the grain size and cluster spacing [231]. The goal was to determine the length scale effects on dislocation motion and subsequent flow stress upturn by altering v. The plot illustrates their work, which includes the high tensile strain rate at 0.2 % flow stress normalized with the corresponding quasi-static strain rate stress for the same material and condition. For the compression behavior, the flow stress values were taken for each strain rate at 10 % plastic strain. Fig. 54 shows the normalized flow stress as a function of strain rate and grain size for each specimen and condition. For the tension data, despite taking stress values from correspondingly low strain, where questions of attaining equilibrium during testing may arise, the correlations made are consistent with compression, where these concerns do not exist.

The results in Fig. 54 reveal that alloys with both NC grain size and moderate-to-high Ta concentrations exhibit the lowest rise in the flow stress as the strain rate (tensile or compressive) increases. Further, for each concentration, as the processing temperature increases, causing grain size to increase, the normalized flow stress also increases. This indicates the importance of GBs in the nucleation and pinning of dislocations. Interestingly, although Cu-10at.%Ta processed at 900 °C has a slightly larger grain size than Cu-1at.%Ta processed at 700 °C, the rise in the flow stress is greater for the Cu-1at.%Ta processed at 700 °C. This behavior indicates the role that Ta nanoclusters play in limiting the effects of dislocation drag and grain size at higher Ta concentrations.

Furthermore, consistent with the previous work [67], Cu-10at.%Ta processed at 700 °C and other alloys with NC grains showed no tension–compression asymmetry. However, as the processing temperature (grain size) increased and the Ta concentration decreased, tension–compression asymmetry became evident. This is seen from plots A and B in Fig. 54, where the magnitude of the flow stress increase is higher in tension compared to compression in coarse-grained alloys. This asymmetry was not previously reported by the authors, as dynamic deformation studies were limited to nanograined Cu-Ta alloys only. Overall, the data presented in Fig. 54 illustrates the importance of controlling/tuning grain size and Ta nanocluster spacing for the flow stress behavior. This work suggests that stable NC Cu-Ta can absorb high-energy loading very efficiently. Thus, it is possible to design a material that deforms with a consistent flow stress even under extreme conditions of high pressure and high loading rates. To achieve this, the material's plastic response must remain unchanged across various loading rates, much like the linear flow stress response with temperature, indicating the persistence of dislocation-mediated slip mechanisms over a wide temperature range.

To make this behavior a reality, it is crucial to prevent the phonon drag mechanism, which typically leads to an increase in flow stress (often leading to brittle failure). Realizing such a material opens the door to creating a new class of tough, high-impact-energy-absorbing materials.

5.3.4. Shock healing

The preceding discussion underscored the possibility of manipulating the dislocation velocity in NC materials, thereby influencing their mechanical behavior, especially high-rate deformation and energy storage capabilities. The next topic concerns the evolution of dislocation density. The question is whether it is plausible to suppress the increase in dislocation density by reducing the accumulation of dislocations or self-healing, particularly in stable NC materials.

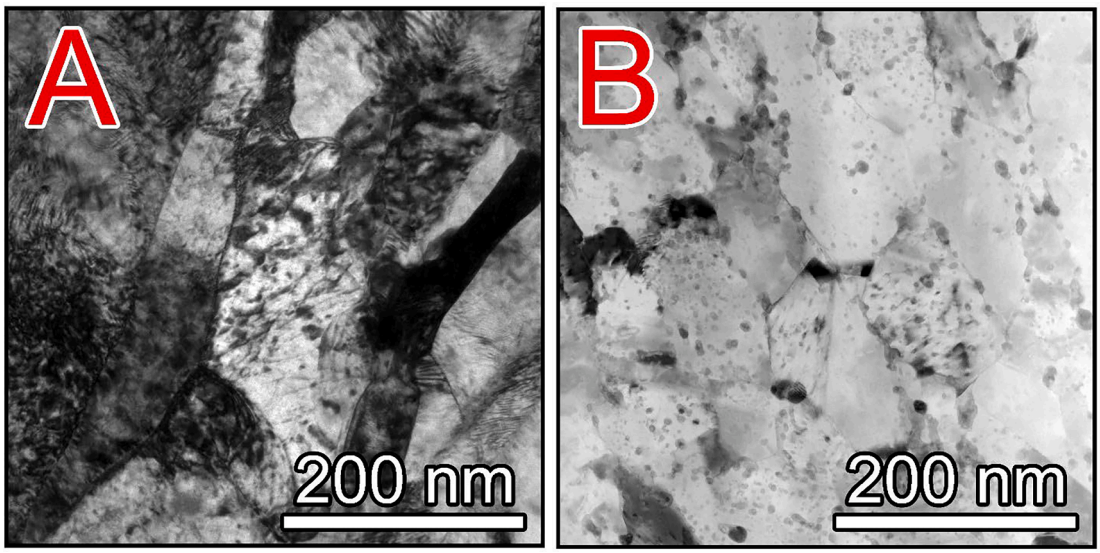

Fig. 55. Bright field images. (A) Steel sample after single shock at 15 GPa versus (B) Cu-3Ta shocked twice at 15 GPa [].

In various engineering scenarios, such as those involving shock loading and fatigue, the accumulation of dislocations can potentially culminate in catastrophic failure. The microstructure of stable NC materials offers the potential to govern dislocation accumulation through GB reabsorption. In stable NC materials, GBs serve as sites for dislocation nucleation. Importantly, once nucleated, dislocations can be "pinned" by precipitates. Subsequently, the same GB or neighboring GBs can reabsorb these pinned dislocations. As discussed earlier, the stability of microstructure in pure NC metals is unfeasible. Adding solutes can provide dislocation-pinning mechanisms (dislocation-solute interactions or dislocation-precipitate interactions).

The recent work by Hornbuckle et al. [604,749] observed such behavior under shock loading. To emphasize this fact and the distinctiveness of a stabilized NC alloy, Fig. 55 illustrates the striking differences in the post-shocked microstructures of steel after a single exposure to shock loading at 15 GPa, illustrating high levels of dislocation activity versus the complete absence of dislocations in a stable NC alloy shocked twice to the same maximum 15 GPa pressure. Due to the nature of standard bright-field imaging [794], the dark or black contrast in these images can be attributed to the enhanced scattering and absorption of the electron beam caused by crystallographic defects such as dislocations, stacking faults, and microbands. In the steel sample, non-equilibrium defects (Fig. 55A) appear predominantly black compared to the stable NC microstructure shown in Fig. 55B.

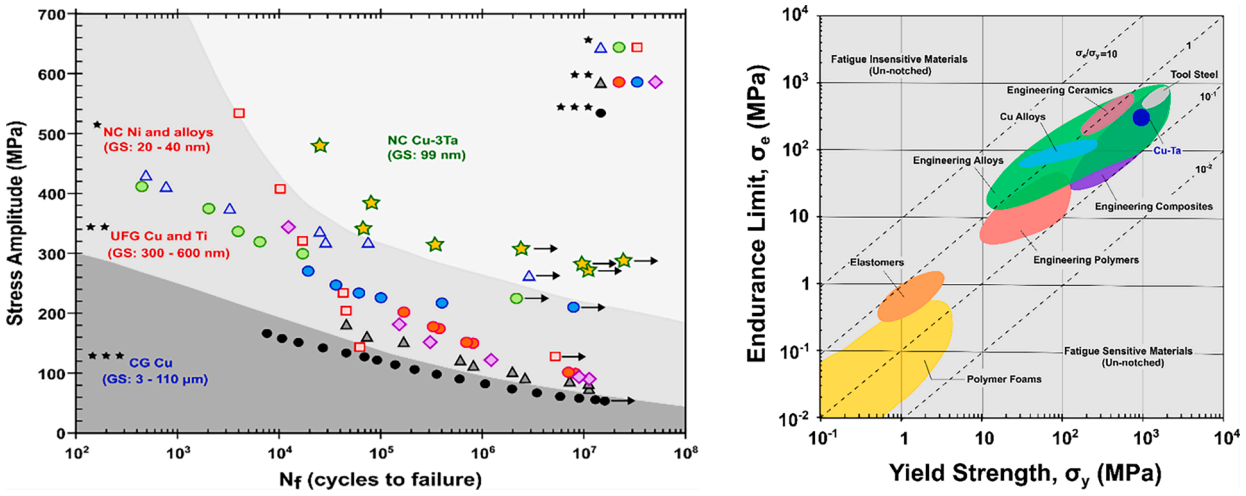

Fig. 56. (a) Stress amplitude plotted versus the number of cycles to failure for NC Cu-3Ta, along with the data for other NC and UFG materials. Literature data were taken from studies performed at different R-ratios and under various stress states other than Cu-Ta. A datum point marked by an arrow denotes the test was terminated when the sample survived more than 10^6 cycles. (b) Ashby-type map showing endurance limit (σ_e) plotted against the yield strength (σ_y) for different engineering materials alongside NC Cu-3Ta data. The σ_e is defined as the strength at which failure does not occur (typically $\geq 10^6$ cycles) [87].

This behavior has an important implication, which could be understood by comparing the hardness behavior. For conventional coarse grain materials, the magnitude of the residual hardness deviation is 1.5 to 2.4 times the initial unshocked hardness values [604]. Given that conventional materials follow the accepted relationships with shock pressure/strain rate, it is rather peculiar that the hardness value of 291 ± 4.84 VHN for a stable NC material (refer to [604]) following repeat shock loading changes minimally (by −4.5 %) relative to the pre-shock hardness of 304 ± 9.73 VHN. This slight variation is within the margin of measurement error, suggesting that the hardness remains virtually unchanged. Furthermore, the result aligns with the absence of any preserved dislocation activity in the microstructure of the stable NC material. Therefore, the notion that dislocation density evolution can be suppressed is critical.

Note that dislocation nucleation is still an active mechanism accommodating deformation, but dislocation reabsorption is the key. In other words, the stable microstructure of NC materials provides an active self-healing mechanism. Namely, the non-equilibrium concentration of defects typically observed in materials when subjected to high-pressure shock compression states can self-heal to preserve the original state. Smaller grain sizes increase the number of GBs, which serve as effective barriers to dislocation motion and facilitate their reabsorption during mechanical deformation. In-situ x-ray diffraction studies performed using the high energy sources at the Advanced Photon Source (APS) have shown that dislocation absorption in NC Cu-Ta alloys occurs in just a few hundred nanoseconds, a process significantly slower in materials with larger grain sizes [749]. Atomistic simulations have confirmed the mechanisms of dislocations interacting with the Ta nanoclusters, becoming pinned by them and then reabsorbed at GBs, thereby effectively reducing stored strain energy 749.

5.3.5. Fatigue damage and healing

Accumulated damage caused by cyclic loading is a prevalent factor in the failure of structures in various critical applications. Mitigating/controlling and healing fatigue damage requires a microstructure that reduces strain localization via dislocation pile-ups. As discussed previously, reducing or controlling the dislocation density can enhance fatigue resistance. In recent work by Kale et al. [87] using a stable NC Cu-3Ta as a model material system, exceptional fatigue strength was observed as compared to other NC materials reported in the literature and an endurance limit on par with tool steels (Fig. 56). Postmortem characterization combined with atomistic simulations revealed the underlying mechanism of the improved fatigue performance, which was linked to diffuse damage accumulation. Namely, multiple grains participated in the deformation processes during cyclic loading, resulting in a more homogenous damage distribution across the microstructure than typically observed in coarse-grained materials. Atomistic simulations also revealed a drastically suppressed damage accumulation and its more uniform distribution across the microstructure. By optimizing grain size, further increases in fatigue resistance can be achieved. Current studies aim to extend the fatigue limit of Cu-Ta alloys and bring it closer to their yield strength (~1 GPa), potentially pushing the material's durability to new extremes. However, investigations on prolonged dislocation interactions with GBs could affect the material's mechanical behavior and fatigue performance.

Since stabilized NC materials exhibit diffuse damage accumulation, the focus shifts to the role of GBs and TJs in the self-healing akin to cold welding of fatigue cracks. The high density of GBs and TJs influences the local strain field near these defects, causing self-healing of a nucleated crack. Recent work by Xu and Demkowicz [795] examined the phenomenon of stress-driven GB migration (SDGBM) as a novel mechanism for crack healing in NC metals. Their MD simulations revealed that when a symmetric tilt GB moves toward a pre-existing nano-crack, it induces a compressive stress field through disclination interactions, leading to crack closure. Conversely, GB migration away from the crack generates tensile stresses, promoting crack opening. Finite element method simulations further confirm the importance of disclination-induced image stresses in crack healing. Xu and Demkowicz [795] suggested that SDGBM could significantly improve the ductility of NC materials by promoting crack healing even under tensile loading, with implications for fracture-resistant design. Similar results were obtained by Meraj and Pai [796], who studied creep behavior and crack healing in NC Ni with an average grain size of approximately 7 nm.

Barr et al. [797] confirmed the concept of GB-mediated crack healing, while focusing on high-cycle fatigue in NC platinum (Pt). The TEM observations and atomistic simulations revealed that, under cyclic loading, a fatigue crack in a 40 nm thick foil underwent healing through a cold-welding-like process near triple junctions. This healing was observed to occur autonomously under continuous tensile stresses without the need for external compression or elevated temperatures. Simulations indicate that localized stresses at the crack tip, induced by GB migration, facilitate crack closure and healing. Such a phenomenon, observed at ambient temperatures, suggests that intrinsic microstructural features, such as the fine grain size and boundary-mediated plasticity inherent to NC materials, can enable self-healing without reliance on external environmental factors. This conclusion was supported by additional simulations of Ag, Al, and prior experimental work on Cu, which indicated that this healing mechanism is not unique to Pt and highlighted the potential for designing fatigue-resistant NC materials with enhanced mechanical performance.

5.3.6. Radiation healing

Recent advancements in stable NC materials have shown promise for preventing damage accumulation under shock loading and fatigue, making them ideal candidates for radiation healing in nuclear industries. However, in NC materials with high sink densities, irradiation-induced point defects primarily interact with and accumulate at interfaces (GBs and phase boundaries), potentially affecting structural stability. The defect accumulation can lead to grain growth [798], dissolution, disordering, or coarsening of second-phase particles [663], depending on the nature and sink efficiency of the interfaces [799]. To design materials resistant to radiation-induced damage, it is essential to develop microstructures capable of withstanding or recovering from point defects—such as vacancies, interstitials, and substitutional atoms—created by high-energy particles such as neutrons or ions. These defects destabilize the material, causing grain growth and property degradation, particularly at high temperatures, where radiation can exacerbate thermal-driven grain coarsening and trigger phase instability through mechanisms such as ballistic dissolution and radiation-enhanced

diffusion.

In coarse-grained materials, Russell [703] demonstrated the dissolution and re-precipitation of second-phase particles due to recoils, with finer particles replacing larger ones under continuous irradiation. Similarly, studies by Chen et al. and Lu et al. [698,704] showed the dissolution of larger particles and the precipitation of fine dispersoids in ODS alloys after high-dose self-ion and helium pre-implanted self-ion irradiations, respectively. Additionally, Certain et al. [705] observed the dissolution of nanoclusters in the 14YWT alloy at low temperatures, with the clusters remaining stable at high temperatures due to the diffusion of dissolved solute back into the parent clusters without new precipitation. In stable NC materials, incorporating second-phase particles and utilizing ballistic dissolution during radiation exposure can effectively promote the re-precipitation of smaller phases, thereby restoring the material's original microstructure. This strategy not only addresses the issue of microstructural stability under irradiation but also mitigates concerns about grain growth, which can be controlled through solute additions that segregate to and pin the GBs. Ultimately, the overall behavior of these systems depends on the stability and behavior of the second-phase particles, which play a crucial role in maintaining the material's integrity. Mechanisms of phase stability (e.g., forced atomic mixing, ballistic dissolution, Ostwald-ripening, inverse Ostwald-ripening, etc.) in systems driven far from equilibrium either through processing or through high energy irradiation have been discussed theoretically and experimentally in various alloys [696,703,800,801].

To understand this extraordinary resistance to radiation hardening of stable NC alloy, consider post-irradiation microstructural analysis at various damage conditions. Fig. 57 shows low and high-magnification bright field STEM images tested at different fluences at room temperature and 573 K, revealing several significant features. The average grain size is maintained in the nano regime even at such a high dose, in comparison to the massive grain growth observed in NC Cu from ~ 48 to 800 nm at 1 dpa [677] and NC composite of Cu-0.5Al_2O_3 from 180 to 495 nm at 0.9 dpa [667]. In other words, minimal grain growth and microstructural evolution in stable

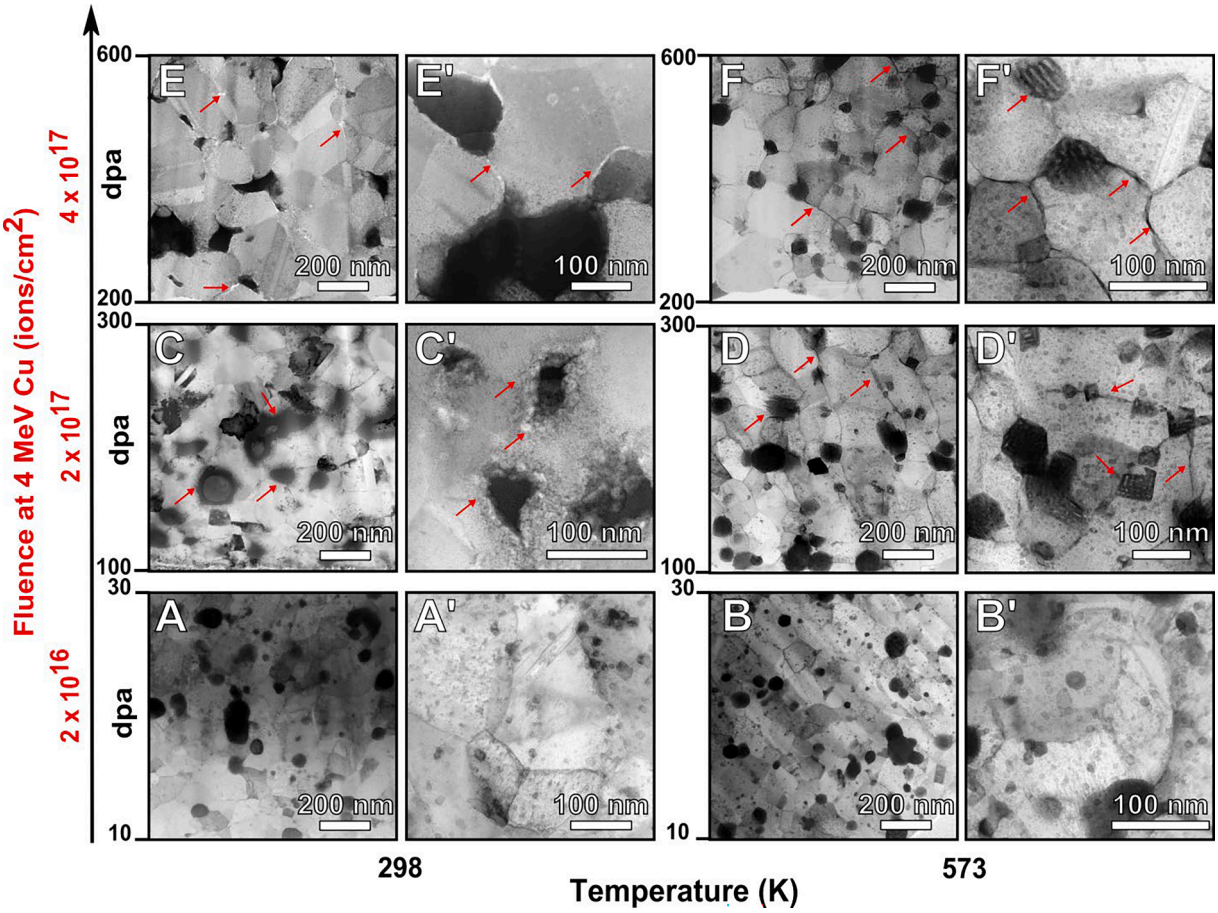

Fig. 57. Cross-section bright field STEM images of NC Cu-Ta from the irradiated surface (bottom of each low mag image) to the peak damage region (refer to Fig. 2 in [88]), where the brighter grains are NC Cu and the darker grains/precipitates are Ta, of samples irradiated at Room temperature to (A, A') 10 dpa showing the stable microstructure and dislocation activity, (C, C') 100 dpa, highlighting amorphous ring and voids around Ta, respectively (red arrows) and (E, E') 200 dpa revealing voids along GBs and Ta interfaces and larger tantalum dissolution; and 573 K to (B, B') 10 dpa with relatively unaffected microstructure with minimum grain growth, (D, D') 100 dpa and (F, F') 200 dpa indicating ballistic dissolution of larger Ta phases and their short circuit diffusion along the GBs (red arrows). The corresponding dpa value along the irradiated surface at the bottom and peak damage at the top of low mag images are indicated on their left (A-F). Images (A'-F') are high magnification views of the conditions corresponding to (A-F) [88]. (For interpretation of the references to color in this Fig. legend, the reader is referred to the web version of this article.)

alloys show that the stabilized GBs act as persistent sinks, thereby annihilating the irradiation-induced defects.

Another critical observation is the dissolution of sacrificial phases in stable NC materials, which could further enhance radiation tolerance and microstructural stability. As discussed earlier, using a second phase to stabilize NC materials might be the most forward-looking approach to developing NC materials for advanced structural applications. The Nelson, Hudson, and Mazey (NHM) model describes precipitate dissolution at a displacement rate k due to the scattering of atoms from precipitates of radius r_p, number density ρ, and solute concentration C_p, through the following equation [800,801]

$$\frac{dr_p}{dt} = -yk + \frac{3DC}{4\pi r_p C_p} - r_p^2 D\rho, \tag{14}$$

where C is the total solute concentration, D is the solute diffusion coefficient, and y is a constant representing the thickness of atom layers scattered from the precipitate per dpa. Using this model, one can identify sacrificial phases that could be used to design radiation-tolerant NC materials. For example, considering the sputtering of Ta atoms, the NHM model suggested a y-value of 10^4 cm/dpa, which was utilized for the calculation. Using the above equation for a Ta particle of average radius 25 nm (from TEM), a negative rate of change was calculated ($dr/dt < 0$), indicating the dissolution of large Ta particles. Srinivasan et al. [88] used those phases and showed that the dissolution of the larger particles led to a local enrichment with Ta solute (Fig. 57(E, E', F, and F')) in surrounding lattice regions, which enhances the microstructural stability.

The main point is that under irradiation, the tendency to form Ta nanoclusters may be similar to the formation of stable nano-emulsions found in liquid Cu–Ta alloys stabilized by a negative and strongly curvature-dependent tension of the Cu-Ta interfaces [404]. This analogy is supported by the high degree of intense cascading effects saturating the structure with point defects. This disordered state offers a "liquid-like" environment for nanocluster formation and provides a pathway for local short-circuit diffusion leading to Ta redistribution in the lattice. Analogous to the stabilized nano-emulsions of Cu-Ta [404], these newly generated Ta-based clusters also resist coarsening despite the intense irradiation and temperature exposure, retaining an average diameter of < 10 nm.

Marwick suggested that the segregation of slow-diffusing solute elements (inverse Kirkendall effect) to the sinks is due to differences in the diffusion coefficients of the alloy components [802]. Solute atoms with large atomic radii diffuse along GBs faster and eventually precipitate as nanoclusters, resulting in a high cluster density near GBs (Fig. 57D' and 57F').

More specifically, the strategic design of alloys incorporating phase-separating elements and sacrificial phases can be key to developing radiation-tolerant materials. This approach significantly increases the number of available interfaces that act as potent and stable sinks. Computational and experimental methods can further explore the role of compositional self-organization in NC alloys, which occurs at specific temperature and shearing rates, in maintaining refined microstructures during high-temperature irradiations or prolonged ball milling.

For example, Chee et al. [709] reported the maximum temperature of a patterning regime (T_{max}) for various Cu-based alloys, with systems having high positive heat of mixing, such as Cu-Nb and Cu-V, exhibiting a higher T_{max} (>773 K). Additionally, the high density of sinks has been predicted to stabilize irradiation-induced patterning. No evident coarsening of clusters in stable NC alloys, as observed by Srinivasan et al. [88], could suggest a significant patterning regime due to the high sink density and positive enthalpy of mixing—an area that warrants further exploration. Furthermore and more recently studies of NC-Cu-Ta alloys under various irradiation conditions, including Cu ions, He++ ions, and protons, have shown that these alloys exhibit minimal radiation-induced hardening or softening, maintaining significantly greater stability than other metals and alloys. For instance, the residual hardness measured indicates negligible changes post-radiation. Fig. 58 shows the change in post-irradiated hardness at 298 K and 573 K for various irradiated alloys compared to Cu-V and NC Cu-Ta alloys. In the case of radiation hardening at 298 K (Fig. 58A), the percentage

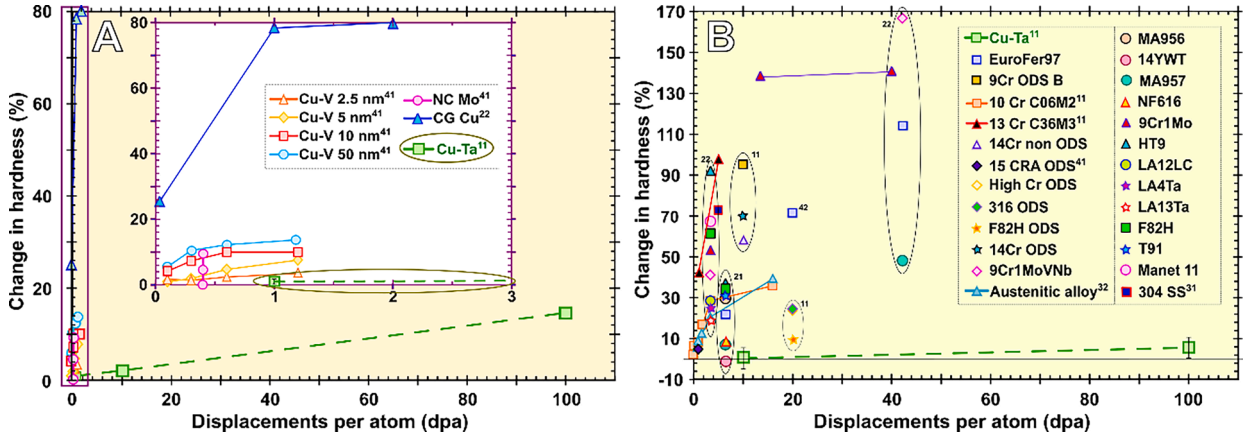

Fig. 58. Percentage irradiation hardening for stable NC Cu-Ta and various materials from literature at different doses irradiated at (A) 298 K and (B) 573 K [661,662,668,677–686]. Note that numbers in the superscripts (on legends and data points) represent irradiation ion type, and testing method carried out for calculating hardening respectively; where 1- Heavy/self-ion, 2- neutron, 3-proton, and 4-helium ion, in the first letter of superscript and 1- Indentation and 2- Tension test, in the second letter of superscript [88].

change in hardness from as-received (0 dpa) to 1 and 10 dpa in stable NC alloys is negligible. By contrast, for similar dpa levels, the radiation hardening of coarse-grained pure Cu is about ~ 80 % (24 % at a very low dose of 0.034 dpa) [677], and that for nano-layered composites is about ~ 15 % [678]. More specifically, at 100 dpa, NC Cu-Ta alloys shows a hardening of a mere ~ 15 %, which is similar to the radiation hardening observed in other materials at 1–2 dpa (Fig. 58A). Thus, a stable NC alloy has a high level of tolerance to radiation hardening at 298 K. Likewise, hardening comparison at 573 K (Fig. 58B) shows that materials such as the ferritic ODS steels and ferritic martensitic steels experience a steep increase in hardness post-radiation at low to moderate damage levels. For instance, MA 957 shows hardening of 7 % at 6.5 dpa and 48 % at 42 dpa [661,683]. However, a stable NC alloy only exhibits insignificant change in hardness at dose levels of 10 and 100 dpa at 573 K. Thus, a stable NC alloy retains its hardness up to considerably high dose levels reached in generation IV reactors, indicating exceptional resistance to radiation hardening. Microstructural analysis further reveals that the grain size in NC Cu-Ta alloys remains stable even at high dpa values. The resilience of NC Cu-Ta alloys under irradiation is attributed to the ability of Ta-nanoclusters to pin GBs and absorb vacancies, preventing radiation-induced swelling.

6. Properties of stable NC materials: Future opportunities

Until recently, the scientific community's primary objective has been to demonstrate the ability of specific alloys to withstand elevated temperature conditions or various processing states. However, recent studies on NC materials have shed light on a crucial technological advancement beyond merely retaining a small grain size. The key lies in engineering GBs and inter-granular regions that are thermo-mechanically stable. Recent developments indicate the emergence of a new frontier in foundational exploration. Within this realm, there are opportunities to surpass the previously perceived mechanical thresholds, which have been a focal point in this scientific field. Specifically, the emphasis should shift toward achieving mechanical stability, as it has become the most relevant topic in this domain. Significant future technological advancements will hinge on the deliberate design of thermo-mechanically stable GBs, inter-granular regions, and other length-scale features, departing from the sole preservation of grain size.

This section aims to initiate the onward journey into the intricate domain of mechanically stable structures in NC materials. The goal is to decipher the interplay among mechanical stability, microstructural evolution, material properties, and design. The rationale for why the direction of this progression is crucial will be offered through an exploration of a wide array of topics that illuminate roles in shaping material responses to diverse external stimuli, including thermal and mechanical stresses. This comprehensive assessment, coupled with forward-thinking discussions, will indicate a realization in surpassing the presumed constraints of conventional NC materials and provide a cohesive narrative that sets the foundation for exploring future concepts.

The broader applications of nanomaterials are hampered by at least four challenges that will continue to be the subject of future research:

1. In many NC materials, the increase in strength with grain size refinement predicted by the Hall-Petch relation [33,43,65] plateaus or even starts decreasing. There appears to be a limit to strength increase, or is there?
2. Despite the high strength, many NC materials suffer from insufficient ductility. Dislocation pileups can no longer form in small grains, and the deformation mode switches to GB-dominated processes such as GB sliding, GB migration, and grain rotation. Are there novel approaches to addressing this longstanding issue?
3. From an energy perspective, is it possible to develop strategies that prevent instability, enabling the material to absorb energy and maintain its structural integrity even under the most extreme conditions? how far can this stabilization be pushed and what might be observed?
4. Designing more complex microstructures while maintaining thermodynamic stability is likely to become an increasingly difficult challenge. Achieving further improvements in alloy performance without compromising stabilization will demand highly precise microstructural engineering. Future progress will hinge on the development of innovative alloy compositions and processing techniques capable of balancing GB engineering with performance optimization, a task that will remain technically demanding and resource-intensive

6.1. Mechanical stability of structurally stabilized NC alloys

6.1.1. Defect-free materials vs. NC materials: Understanding strength limitations and mechanisms

The relationship between the absence of defects in materials and extreme property enhancement is unequivocal. Indeed, perfect single crystals, single-crystal whiskers, and other flawless materials have established a benchmark of strength, creep resistance, and other mechanical properties. This remarkable performance is attributed to their impeccably organized atomic structures and the absence of GBs and other flaws [803,804,876,903].

NC materials are on the opposite side of the spectrum of defects. They have been extensively studied due to their unique deformation mechanisms and extreme strength-to-weight ratios compared to their coarser-grained counterparts. NC materials approaching the limits of crystallinity can achieve strength or hardness values tenfold or greater than conventional polycrystalline materials. For instance, various NC metals such as Cu, Ni, Fe, Ta, Mo, and W have exhibited yield stresses ranging from 0.7 to 4 GPa [65]. However, these strength levels remain significantly lower than those achieved by single-crystal whiskers of the same, 3.5 to 25.0 GPa. Can this limit be reached in stable NC metals [804–807]?

While much work has been done to investigate this phenomenon, controversy over the exact mechanisms preventing a continual increase in strength must be resolved. As pointed out in a previous section, the various fundamental mechanisms proposed by different

authors explaining the Hall-Petch effect are based on dislocation processes. According to the literature, the primary mechanisms responsible for the Hall-Petch breakdown include GB activities such as sliding, shuffling, grain rotation [808], diffusion, and GB amorphization [809].

Asaro and coworkers [810] attempted to provide a "unified" theoretical framework for the grain size effect on strength and strain rate sensitivity in the NC regime. While their model explains FCC NC metals, its applicability to BCC and HCP metals still awaits verification. For example, how the double-kink mechanism in the NC grains of BCC metals stops operating has not been addressed. This question is valid as the activation volume associated with double-kink nucleation in BCC metals might be in the sub-nanometer scale. Furthermore, no convincing experimental evidence has been obtained for the operation of the double-kink mechanism as it is beyond the resolution limit of currently available microscopic techniques.

Nevertheless, from a technological point of view, if the mechanisms that render the inverse Hall-Petch effect can be suppressed, one should anticipate fabricating NC materials with strength approaching the theoretical limit (~G/20 to G/10, where G is the shear modulus of the metals [484]). This could parallel the high strengths seen in single crystals due to their lack of defects and defect sources. This has indeed been realized recently, at least in a preliminary sense.

6.1.2. Nano-grained and nano-twinned materials: A departure from the inverse Hall-Petch effect

Some NC materials defy the inverse Hall-Petch effect by maintaining high strength as the grain size reduces to several nm. For example, the nano-grained and nano-twinned forms of diamond synthesized at high pressures from graphite [811,812] are harder than single-crystalline diamond. Nano-grained diamond shows a downward deviation from the Hall-Petch relation [813], but the nano-twinned diamond does not: its strength continues to increase with decreasing twin thickness down to a few nm [811,812]. Another ultrahard nanomaterial is cubic boron nitride (cBN), synthesized from the hexagonal BN [814–816]. Both nano-grained and nano-twinned forms of cBN are hard, thermally stable, and oxidation-resistant. The reported Vickers hardness of nano-twinned cBN reaches 108 GPa,[1] far exceeding the hardness of single-crystalline cBN (30–40 GPa) [816]. Importantly, this material does not follow the inverse Hall-Petch effect. Its hardness continues to increase with decreasing twin thickness down to 3.8 nm (Fig. 59). The absence of softening suggests that the GB sliding and migration processes are not activated. The exact mechanism responsible for the departure of the nano-twinned structures from the inverse Hall-Petch behavior remains the subject of research [819–822]. If understood, this knowledge could be transferred to the design of metallic nanomaterials.

Several FCC metals produced by SPD, such as surface grinding and HPT, exhibit an unusual combination of structural stability and ultrahigh strength. The deformation is performed in liquid nitrogen and produces a highly non-uniform NC structure with pockets/colonies/filaments of extremely small (a few nm in size) grains surrounded by larger nano-grains (tens of nm) [823,824]. Fig. 60 shows an example of this microstructure in Cu. The smallest grains have truncated octahedron shapes and are packed in a Kelvin structure [825,826] minimizing the GB area. Surprisingly, this structure exhibits extraordinary structural stability with only a slight increase in grain size when heated to high temperatures up to the melting point of the metal (for example, ~9 degrees below T_m of Cu) (Fig. 61(a)). Upon annealing or plastic deformation, the faceted grains gradually transform into continuously curved structures resembling a Schwarz crystal [823,827–829], which is characterized by zero mean curvature. The nanoindentation hardness of the small grains was found to be 4.7 GPa, which exceeds the hardness of NC copper with larger grains. The shear stress estimated from the hardness (1.57 GPa) is comparable with the ideal shear strength when temperature effects are considered [830]. No inverse Hall-Petch softening is observed. The strength increases as the grain size decreases to ~ 10 nm (Fig. 61(b)).

The mechanism underlying the thermal stability and strength of the severely deformed Kelvin/Schwarz structures is not fully understood. While such structures minimize the GB area relative to other grain shapes, the absolute value of the GB area per unit volume in a 10 nm-grain structure is huge, creating an enormous driving force for coarsening. It has been suggested [823,824] that the thermal stability is due to a structural "relaxation" of the GBs. Understanding the nature of this "relaxation" and why it does not occur at larger grain sizes requires further research. The grain growth can be prevented by mechanical constraints imposed by a rigid framework of TJs and coherent twin boundaries. The suppression of GB sliding and migration and avoiding the Hall-Petch softening in a single-component NC metal is an unusual effect that calls for an explanation in the future.

The work by Hu et al. [497] also highlights the critical role of the mechanical and thermal stability of GBs. This stability is inherently influenced by the GB type (e.g., high-angle vs. low-angle GBs) and plays a crucial role in the deformation behavior of nanograined alloys. They utilized the concepts of solute GB engineering and thermodynamic stabilization of GBs to enhance GB stability in Ni-Mo alloys. It was demonstrated that low-temperature annealing promoted GB stability through relaxation and Mo segregation, which hindered GB migration and enhanced partial dislocation activities. Mo was suggested as a thermodynamic stabilizing agent for grain size, enhancing GB stability and helping to suppress grain growth. This shift from GB-mediated deformation mechanisms to dislocation-mediated deformation led to increased hardness, breaking the plateau/negative trend in hardness observed in pure Ni samples. As a result, microhardness values of approximately 11 GPa were achieved, corresponding to a potential yield stress of 3.67 GPa for grain sizes smaller than 10 nm [497]. Moreover, Ni-Mo samples in the "as-synthesized state," which lacked relaxation and stabilization of the GB regions, followed the conventional hardening and softening trends found in the literature for Ni and Ni alloys. These results seem to indicate that annealing of the as-deposited Ni-Mo samples induced Mo enrichment at GBs and depletion of nano-sized Ni (Mo) grains. The results also suggest that the segregation of impurities at GBs may be induced through thermal annealing. Although precipitates were not detected under detailed HRTEM observations and XRD analysis, early-stage precipitation or

[1] The validity of the reported hardness of the nano-twinned cBN [817] was subject to debate [818,819].

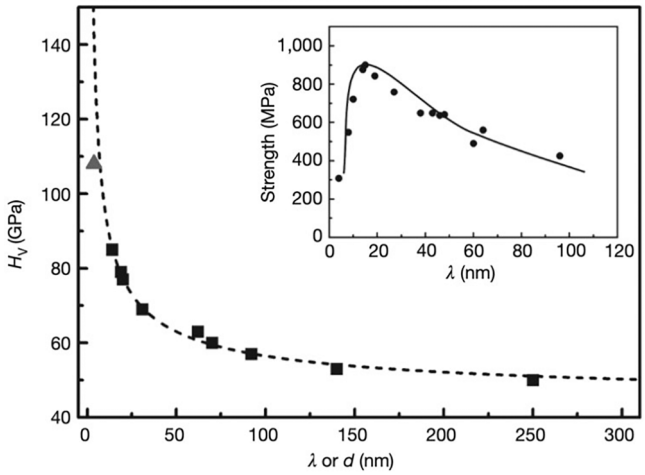

Fig. 59. Vickers hardness H_V as a function of average grain size (d) or twin thickness (l) for nano-grained (squares) and nano-twinned (triangle) cBN [816]. For comparison, the inset shows the yield strength as a function of l for nano-twinned Cu [48].

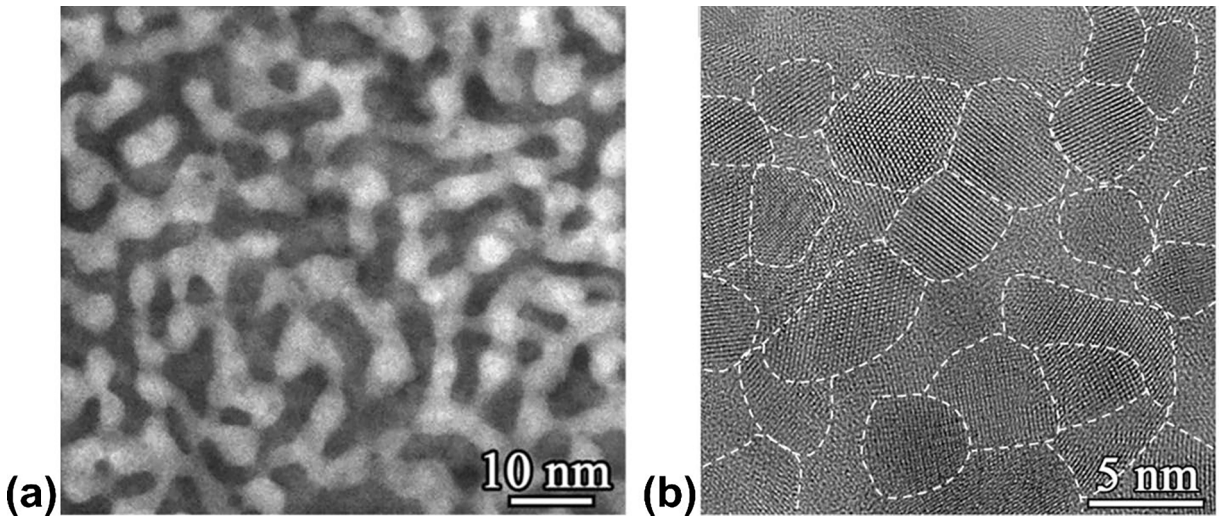

Fig. 60. (a) Bright-field TEM image of severely deformed Cu [823,824]. The brighter regions forming a penetrating framework are aggregates of tiny nanograins (a few nm in size). (b) HRTEM image showing the extremely small nanograins. Dashed lines outline the GBs.

clustering at GBs could not be ruled out in the highest Mo content alloy.

Cu-Ta alloys with varying Ta content and grain size, produced by powder metallurgy, illustrate another example of enhanced GB strengthening. The pinning effect of coherent Ta clusters on Cu GBs plays a significant role in reinforcing the material. The Hall-Petch slope of Cu-Ta alloys was found to be 2.5 times greater than that of pure Cu, indicating a much stronger GB strengthening effect. This led to an impressive yield strength of approximately 1.5 GPa, higher than that of electroplated nano-twinned Cu [753]. The mechanisms responsible for such a high strength are likely similar to those in Ni-Mo alloys, namely, the constraining of GBs and the presence of Ta clusters, which disrupted GB-mediated deformation mechanisms (e.g., sliding and grain rotation). Such mechanisms become more active at grain sizes below 100 nm. Unfortunately, this GB strengthening could not be sustained beyond a certain grain size. Further reduction in grain size resulted in the formation of a thickened quasi-amorphous state at the GBs, necessitating further investigation to explain this behavior. It is interesting to note that the grain size at which this transition occurs in Cu-Ta alloys is very similar, if not identical, to that in pure Cu. The discussed studies of Ni-Mo and Cu-Ta underscore the critical relationship between grain size, GB stability, and deformation mechanisms.

If the strategies used in the above examples can be further advanced, it could lead to the development of microstructurally stable NC materials, overcoming the challenges of Hall-Petch breakdown. Undoubtedly, such efforts will face challenges, but the potential to achieve single-crystal whisker-like strength in bulk materials remains a compelling goal. This calls for innovative, out-of-the-box approaches in designing novel materials.

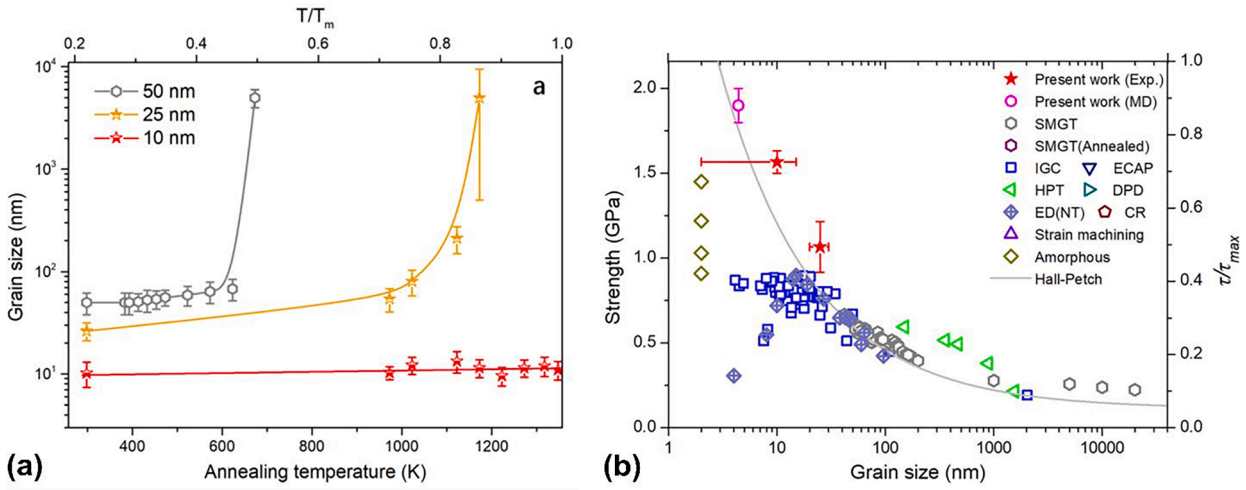

Fig. 61. Thermal stability and strength of NC copper with extremely small grains [823,824]. (a) Grain size as a function of annealing temperature (for 15 min) for three samples with initial average grain sizes of 50, 25, and 10 nm. Note that the grain refinement improves thermal stability. 10 nm grains do not practically grow up to the melting temperature. (b) Plot of yield strength versus grain size. Different symbols represent literature data from different preparation methods. The samples prepared in Ref. [823,824] follow the Hall-Petch trend, while samples prepared with all other techniques exhibits the inverse Hall-Petch effect. The point obtained by MD simulations (pink open circle) is also included. The right-hand-side scale shows the shear strength of the material τ normalized by the theoretical shear strength of Cu τ_{max}. (For interpretation of the references to color in this Fig. legend, the reader is referred to the web version of this article.)

6.2. *Redefining material performance: The future of NC metals in energy resilience and thermodynamics*

Recent advancements in the understanding of materials science have identified NC materials as key opportunities for promising solutions in energy absorption and transference challenges. Traditionally, materials have been designed to resist specific energy types, requiring years of development [831]. However, as seen in Section 5, NC materials have emerged as stable materials capable of withstanding multiple energy sources such as thermal, irradiation, and mechanical stress. Unlike single-crystal Ni-based superalloys, which are engineered for thermo-mechanical loading, thermo-mechanically stabilized NC metals offer a more unified and efficient approach [803]. These materials not only mitigate damage from different energy sources but also address defect accumulation and energy state excitation in a convergent manner, enhancing durability and performance in extreme environments.

A key development in NC materials is the resilience and persistence of stabilized GBs and other microstructural elements. NC immiscible alloys are prominent examples of this innovation. These alloys have demonstrated an impressive ability to resist various forms of energy, resulting in unique properties, including the persistent absorption of different defect types. The stabilization of GBs plays a crucial role in maintaining these properties, including the material's ability to withstand thermal, mechanical, and radiation-induced stresses.

The deep metastability of the stabilized GBs, particularly in phase-separating immiscible alloys, enables the material to remain in a stable configuration up to high temperatures and resist diverse energy impacts. Some thermodynamic aspects of the strongly pinned GBs are unique to this class of NC materials. The microstructures stabilized by the pinning particles are kinetically trapped in a deep metastable state surrounded by extremely high energy barriers separating this state from all other states. The barriers can be so high that the material would rather melt and re-solidify into a new structure than change its microstructure. This resistance to charge endows the stabilized NC materials with the extraordinary ability to maintain their microstructures under extremely high energy fluxes of virtually any nature, from mechanical impacts (such as shock waves) to irradiation with energetic particles. The unique thermodynamics of deeply trapped nonequilibrium states is poorly understood and should be the subject of future fundamental research.

6.3. *Exploring phase transformations for enhanced stability and alternate plastic deformation avenues*

6.3.1. *Grain size and phase transformation mechanisms*

The effect of the nano-scale grain size on phase transformations is a well-studied phenomenon. As with the previously discussed microstructure stability (Sections 2, 3 and 6.2.1), thermodynamic and kinetic factors are responsible for the effect. When the specific GB area is high, GBs make a substantial contribution to the total free energy of the material. This contribution alters the alloy thermodynamics, shifting the lines on phase diagrams and stabilizing new phases that do not appear on the equilibrium phase diagrams. Kinetically, GBs and TJs provide additional heterogeneous phase nucleation sites, affecting the phase transformation pathways. GBs can also significantly accelerate the diffusion rates of the alloy components compared to single-crystalline phases and coarse-grained polycrystals. The enhanced atomic diffusion can impact the phase transformation kinetics and, thus, the phase selection during the growth rate competition [832].

As a prominent example, Al-Mg [833] and Al-Zn [824] alloys were produced by cryogenic HPT processing as metastable single-phase Al-based FCC solid solutions with a grain size of about 10 nm. The nano-grains formed a Schwarz-crystal structure [823,827–829] with high thermal stability against grain growth. While the Al-Mg alloys with ~ 50 nm grains underwent the expected phase transformations (such as precipitation of the Al_3Mg_2 intermetallic phase), the 10 nm NC alloy remained a homogeneous solid solution maintaining about the same grain size during high-temperature anneals up to the solidus temperature (760 K) [833]. Similarly, significant departures from the phase diagram were found in an Al-21.7at.%Zn alloy with a grain size of about 9 nm [824]. Al-Zn is a typical spinodal alloy with a wide miscibility gap. Surprisingly, the NC Al-Zn alloy retained its homogeneous solid solution state and about the same grain size within the miscibility gap. The spinodal decomposition was suppressed entirely. Its onset could only be observed at larger grain sizes exceeding ~ 16 nm. The expected increase in the spinodal decomposition temperature with the grain size due to the accelerated GB diffusion was only observed at grain sizes above ~ 100 nm. The suppression of phase transformations in 10 nm-grained alloys was attributed to drastically reduced diffusivity. The mechanism of the reduced diffusivity is yet to be understood.

6.3.2. Interplay between phase transformations and deformation

Studies of diffusionless phase transformations, including allotropic, polymorphous, and martensitic transformations in NC materials, were reviewed by Rong in 2005 [834]. The general observation is that non-equilibrium conditions significantly influence phase transformations and phase stability in NC materials during fabrication. The martensite-start temperature M_s decreases with decreasing particle size, which has been a classical contribution by Cech and Turnbull in small particle experiments [835]. NC martensitic alloys with the shape memory effect (SME) have been studied in the context of enhanced strength and shape-memory properties [836,837].

Simultaneous plastic deformation can influence the interplay between phase transformations and grain size. An FCC-BCC phase transformation has been found by cryogenic rolling of NC nickel with an initial grain size of around 20 nm characterized by X-ray diffraction and HRTEM [838]. The new metastable BCC phase was found to form via the Kurdjumov-Sachs martensitic transformation mechanism. The intensity of the XRD peaks corresponding to the BCC phase weakened with time when the rolled NC nickel was kept at room temperature. This study indicates that a martensitic transformation can accommodate the plasticity of hard-to-deform materials, such as NC metals and alloys, at large plastic strains. The formation of BCC nickel precipitates was also observed in a fast-quenched nickel-doped magnesium oxide [839], presumably due to the significant stresses arising during the fast-quenching process. BCC nickel can be formed via MBE deposition, but it is only stable up to 6 atomic layers (less than 3 unit cells) due to the intrinsic mechanical instability of the stress-free BCC structure [840]. Only the stress-stabilized BCC phase provides an alternative avenue for the plastic deformation of NC materials.

Phase transformations have been found during the HPT treatment of some materials, including Ti-Nb [841], pure titanium [842], zirconium [843], and even ceramics such as zirconia [844], and Cu-based alloys [845]. Nanoindentation of covalent single crystals, such as Ge and Si, can also induce phase changes [846–848]. Ductile machining via diamond turning of intrinsically brittle materials, such as silicon carbide, single crystalline Ge, and other single-crystal semiconductors, has been demonstrated [849–851]. Future research should explore the possibility of exploiting deformation-induced phase transformations during the fabrication of NC materials for achieving a trade-off between strength and ductility.

Some strategies for the strengthening and toughening of NC materials could be borrowed from traditional wisdom, such as TRIP

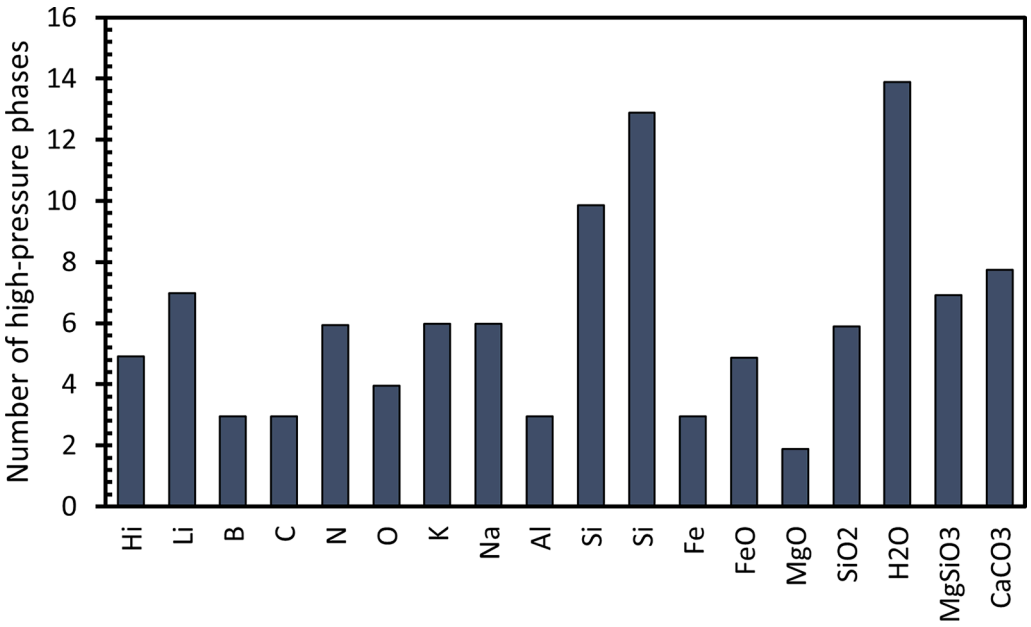

Fig. 62. Histogram showing the number of high-pressure phases for selected elemental, binary, and ternary solids [854].

steels [852]. For example, a composite NC material may be produced with SME nanoparticles embedded within an NC matrix. Stress-induced phase transformation upon mechanical loading may accommodate the strain and divert or blunt the cracks, leading to toughening of the material. To apply this methodology, various factors must be considered, including the effect of the SME nanoparticles on the microstructural stability.

6.4. Dislocation, grain, and phase engineering for NC plasticity

Additional phase changes in stable NC materials can be induced by applying static or dynamic high pressures (tens of GPa) [853–856]. Like the presence of GBs, the high pressure can destabilize some phases and stabilize other phases. The physical mechanism of the effect is primarily electronic. The high pressure brings atoms closer together and causes a redistribution of the electron density. The nature of chemical bonding can shift from covalent to metallic or in the opposite direction. This change in the bonding alters the thermodynamic functions of the phases. High-pressure experiments have been a powerful tool for discovering new materials inaccessible at atmospheric pressure. Fig. 62 demonstrates the multitude of new phases revealed by high-pressure experiments [854].

6.4.1. Thermodynamic and kinetic stabilization of dislocations

The preceding sections discussed the mechanisms of nanostructure stabilization by solute segregation at GBs or by pinning GBs with an array of second-phase particles. Dislocations constitute another critical component of nanostructures and are equally important, especially considering their direct link to mechanical behavior. Both mechanical properties and NC stability depend on the thermodynamic and kinetic properties of dislocations. Similar to GBs, solute segregation or discrete pinning (or both) can control these properties. Success in controlling the dislocation processes depends on further progress in the fundamental understanding of dislocation-solute and dislocation-particle interactions. Such interactions have been extensively studied in the general context of classical materials science [484,857] for many years but not in the context of NC stability. Furthermore, certain aspects of the dislocation-solute/precipitate interactions are specific to the nano-scale confinement in stabilized NC materials and have not received much attention.

One feature of NC materials is the existence of significant image forces arising due to the weaker shear resistance of GBs compared to the perfect lattice. The image forces are superimposed on the dislocation strain fields and can affect their mutual interactions and interactions with other elements of the microstructure. This creates a complex interplay between GB segregation and dislocation behavior. For example, GB segregation can alter the GB resistance to shear and, thus, the image forces, which can affect the dislocation behavior. On the other hand, GB segregation is influenced by the dislocations inside the nano-grains, which provide efficient short-circuit diffusion pathways [858–861] for the solute supply to the GBs. Dislocations can also be absorbed by GBs, changing the GB structure and the segregation capacity. Another effect specific to nanostructures is the fast solute supply to dislocation segments attached to GBs. The solute atoms segregated at GBs can travel a short distance along the dislocation lines to maintain the solute atmospheres at the dislocations or deplete such atmospheres. Both processes can affect the dislocation mobility.

The thermodynamic mechanism of GB stabilization can also operate for dislocations. Segregation atmospheres (also known as Cottrell atmospheres [862–865]) affect the line tension of the dislocations (free energy of the dislocation core per unit length) and thus dislocation line shapes (e.g., the ease of forming full or partial loops) and dislocation reactions. The thermodynamics of segregation atmospheres is more complex than the thermodynamics of GB segregation due to the long-range elastic strain field [863,864]. As a result, despite previous efforts [863,864], the thermodynamics and dislocation atmospheres remains less developed compared with GB thermodynamics. Similarly, the impact of solute drag on the dislocation dynamics is less understood than the solute drag by GBs. The same applies to the dislocation pinning theories [866] versus the Zener pinning theory for GBs. Filling these gaps could be an exciting research direction within the general effort to control NC stability.

6.4.2. Dislocation absorption and nucleation mechanisms

Geometrically, a dislocation density of $1x10^{19}$ m^{-2} results in a spacing of roughly 3 Angstroms, which approaches the theoretical limit for packing given that most metal unit cells have interatomic spacings of 0.36 ± 0.6 nm. We are neglecting the size of the defect cores, and hence, the real value would be lower, more likely about 1 $x10^{18}$ m^{-2}. It has been predicted that in Cu-Ta, dislocations can be nucleate and be reabsorbed instantaneously at a certain spacing [225]. This raises the intriguing question of whether we might observe instantaneous dislocation densities well beyond the theoretical packing limit. Currently, plasticity is constrained by the maximum dislocation velocity, which is capped by the shear wave speed, leading to phonon drag and brittle-like failure at high velocities. However, if nucleation and absorption occur almost instantaneously, the density might not be limited, offering a new mechanism to enhance and sustain high-rate plasticity beyond the dislocation glide mechanism constrained by the velocity and energy dissipation and controlled by dislocation nucleation. Indeed, dislocation density is sensitive to strain rate, while dislocation velocity under constrained conditions may not be [867,868].

GBs in materials often act as barriers to dislocation motion, often pinning or trapping dislocations. Ballistically driven dislocations, for which the pressure from nucleation, acceleration, or deceleration play a key role, have been shown to alter the dislocation density and distribution in stable NC metals [225,231]. For example, in NC materials, dislocations may need to traverse multiple GBs. The pressure generated by the dynamic behavior of dislocations has been shown to activate the nucleation and interaction processes across multiple grains, potentially leading to a homogeneous dislocation distribution rather than localized dense networks within individual grains [869]. This pressure, which is associated with nucleation, acceleration/deceleration, and absorption, can be influenced by the size, shape, and distribution of GBs and precipitates—regions that nucleate, absorb, and pin dislocations. By engineering these microstructural features, it may be possible to control the dislocation behavior and, consequently, the distribution and density of

dislocations throughout the material.

6.4.3. Grain size engineering and recovery mechanisms for enhanced plasticity in NC materials

Much remains to be understood about the dynamic recrystallization of stable NC materials. One of the open questions is related to the recrystallization mechanisms, which can differ from those in coarse-grained materials. In addition to the conventional continuous and discrete recrystallization modes that may still operate, the GRDX process is of particular interest in the context of NC materials. GDRX presents a promising mechanism to enhance ductility and plasticity in stable NC materials. By facilitating microstructural recovery during deformation, GDRX enables these materials to dissipate accumulated strain energy effectively and maintain their structural integrity under extreme conditions. This process, occurring at elevated temperatures and high strains, leverages the inherent stability of NC systems to rejuvenate the microstructure while resisting grain coarsening. GDRX mechanics are influenced by strain rate, temperature, and initial grain size [870].

Typically occurring in materials with higher stacking fault energy and subjected to extremely high strains [427,870–872], such as those achieved during machining, extrusion, torsion, and other forms of SPD [229,238], GDRX is characterized by dominant dynamic recovery processes [873]. Does GDRX operate actively in NC materials in the absence of discontinuous dynamic recrystallization (DDRX) or continuous dynamic recrystallization (CDRX)? In NC materials, high-angle GBs act as effective barriers against recrystallization, due to their reduced mobility and potential to enhance strain localizations. Efficient recovery processes in GRDX require substantial strain accumulation for initiation [870,874]. The ability of NC materials to undergo GDRX underscores their exceptional workability due to significant plasticity and resistance to grain coarsening. Furthermore, controlling dislocation absorption in NC materials can amplify the localized strain required to initiate the GDRX process. As discussed earlier, dislocation velocity can be controlled, for example, through nanocluster addition (impedes dislocation motion). If nanoclusters obstruct dislocations attempting to glide across nano-grains, this can lead to sub-grain formation. The sub-grains, once formed, act as templates, becoming pinned and re-stabilized repeatedly.

Consequently, GDRX emerges as a potential rejuvenation process within NC materials. Recent research [875] involving distinct NC alloy compositions and processing techniques demonstrates that stabilized NC or near-nano materials can undergo repetitive processes akin to conventional coarse-grained materials. Notably, GDRX activation was found to occur in the absence of DDRX or CDRX, as traditionally fine-grained materials lack the microstructural stability for such rejuvenation events. Their observations indicate that clusters arrest dislocations within textured elongated grains, leading to a non-uniform dislocation distribution. Regions with high dislocation density originated from serrated boundaries in elongated grains, while adjacent regions exhibited lower dislocation density. This resulted in dislocations reconstructing into a wall that separated high and low-density domains in differently reoriented grains. The stable clusters within grain interiors, derived from prior processing, served as templates during the SPD to restore the microstructure through a rejuvenation process, yielding a refined microstructure through GDRX. Similar findings were reported for alloys subjected to SPD by machining (up to 250 % strain) [229]. The experiments revealed a significant grain size reduction despite the 350 °C increase in temperature during the deformation process. Characterizations of the deformed samples and complementary atomistic computer simulations have shown that grain growth during the deformation was blocked by Ta nanoclusters pinning the GBs and arresting lattice dislocations. As a result, a high dislocation density was created inside the nano-scale grains, causing dynamic recrystallization with the formation of smaller grains by a grain fragmentation mechanism. These observations suggest that GRDX was at work. If future experiments confirm the hypothesis, this will be another experimental demonstration of the possibility of GRDX in nanomaterials and the first example of atomistic simulation of the GRDX process. Other unconventional recrystallization mechanisms potentially useful for increasing plasticity were discussed in Section 3.8.

6.5. Achieving single-crystal performance in stable NC materials: Enhancing spall strength, creep resistance, and damage tolerance

6.5.1. Spall strength and creep resistance: The role of defect-free structures

The resilience of materials to extreme conditions, such as shock loading and high-temperature environments, is significantly influenced by the type and concentration of defects present within their structure [876]. Shock-induced spallation, or spall failure, occurs when rarefaction waves produce tension within a material, causing it to fracture. The damage tolerance of materials subjected to shock loading depends largely on defects such as GBs, which act as sites for void nucleation. As a shock wave travels through the material, these defects are further distorted during the compressive phase. New defects are generated, leading to material failure. Fracture begins through the nucleation, growth, and coalescence of voids, typically along the planes where tension is most concentrated. Since GBs and other interfaces tend to be the weakest sites, void formation and coalescence can occur more readily at these locations rather than within the perfect crystal lattice [877–879].

In contrast, an ideal single crystal, free from defects, represents the theoretical maximum spall strength, serving as an upper boundary for material resilience under shock loading [876]. Experimental investigations of single-crystal specimens across various crystal structures consistently show that their spall strength is two to four times greater than that of conventional materials, which contain defects like GBs [876]. These findings highlight the significance of a defect-free structure in maximizing resistance to shock-induced failure.

Similarly, the absence of defects, particularly GBs, contributes to the exceptional creep resistance in materials subjected to high temperatures. For applications such as turbine blades in high-performance aircraft and gas turbines, the removal of intrinsic defects such as GBs has proven crucial for enhancing the material performance. In turbine blades, which operate under extreme conditions of high temperatures, pressures, and mechanical stresses, defects can lead to failure by increasing creep deformation, where coordinated grain sliding and rotation along GBs accelerate steady-state creep rates and shorten rupture life. To address this, the microstructure of

turbine blades has evolved from fine-grained structures to directionally solidified and, eventually, to single-crystal configurations [775]. The absence of GBs in single crystals significantly reduces the time to rupture and greatly improves creep resistance.

As in spallation, the accumulation of defects in a material under cyclic loading can lead to fatigue failure. Accumulation of defects results in crack nucleation and growth, which can ultimately result in catastrophic failure. By eliminating these defects, the fatigue resistance of turbine blades can be markedly enhanced, further underscoring the importance of defect-free structures in extending the material's lifespan and performance under extreme conditions.

6.5.2. Advancing stable NC materials: Approaching single-crystal performance through microstructural stabilization

In the 50 years of dedicated research on shock and creep deformation of materials, there has been little or no evidence that similar gains could be made by moving in the opposite direction, creating more defects by shrinking the grain size to the nanometer range. However, if the GBs and interfacial regions in NC materials can be stabilized and strengthened, their presence in a high-volume fraction could be negated entirely. Accomplishing this would require stable NC materials that 1) slow down diffusional processes, 2) strengthen weak points within the crystalline lattice, and 3) persistently absorb linear or other defects. By doing so, NC materials should be able to approach or even exceed the response of single crystals in several related areas, not just in extreme environments of shock compression or creep.

Recent developments reviewed in this paper suggest that this goal can be achieved: microstructurally stabilized NC materials may have more in common with the single-crystal performance than their coarse-grained counterparts. As discussed in Section 5, stabilized NC materials demonstrate remarkable energy-absorbing and damage-mitigating capabilities when subjected to intense irradiation. The stabilized GBs serve as effective sinks absorbing defects during the deformation or irradiation. The stabilized NC materials can avoid the detrimental effects of shock hardening by healing the increased concentration of dislocations generated by the shock. This unique behavior stems from the stability of the microstructure. It offers a pathway for overcoming the kinetic barriers that typically hinder the removal or absorption of excess free energy associated with shock-induced high concentrations of defects. This remarkable characteristic is absent in unstable NC materials, as their microstructures tend to destabilize under the applied forces. Similarly, in conventional coarse-grained materials, dislocations are trapped at significant distances from GBs, making the diffusional length scales too long for complete reabsorption to occur.

These exceptional capabilities of stable NC materials result from an interplay between microstructural length scale and the stabilization of GB structure, two aspects that cannot be separated. The ability to heal damage and reduce phonon drag, along with increased strain rate sensitivity and reinforcement of GBs, contribute to the spall strength in stabilized Cu-Ta alloys being 2–2.5 times higher compared to their coarser-grained counterparts [227,228,604,749]. This value is approximately 50 % of the single crystal spall strength [876]. It was consequently hypothesized that by employing higher fidelity synthesis methods to eliminate larger, incoherent Ta particles, combined with the overall microstructure stabilization and local grain reorientation, even greater ductility and higher spall strengths could be achieved [604].

Strategies to enhance creep resistance in NC metals have included stabilizing GBs through severe plastic deformation, promoting secondary phase formation, and encouraging solute segregation [67,230,783,784,880]. Low-energy CSL boundaries and high-density twin boundaries resist migration and sliding, suppressing diffusion and maintaining strength at high temperatures. Nanoscale precipitates and solute segregation reduce dislocation density, hindering nucleation and increasing stress resistance. Additionally, nanotwin boundaries and solute atoms can reduce vacancy mobility and prevent GB coarsening, promoting dislocation climb as the dominant deformation mechanism. These approaches provide effective solutions for designing NC alloys with superior creep resistance in many cases increasing resistance to creep by several orders of magnitude.

Recent work demonstrates a potential for additional improvements to position stable NC materials on par with single crystal performance, provided further advancements in microstructure engineering can be realized [67,230]. Many questions remain, such as to what extent the stabilized GBs can absorb dislocation and point defects without undergoing detrimental transformations. Is there a limit to which phonon drag can be damped out? Can tertiary creep be sustained when GB sliding, and rotation are shut down? These questions and many more should be the focus of research efforts in the future.

6.6. Evolution of nanocrystalline alloys: Pioneering the design of internal structures for enhanced alloy performance

6.6.1. Moving beyond grain size: Designing internal microstructural features

Until recently, the primary focus in bulk NC alloys has been on grain size as a critical microstructural feature, with less attention to designing other microstructural features. With substantial progress in stabilizing the grain size, the next development phase will involve engineering both the GB and grain interior regions, as discussed above. The design approaches previously applied to advanced polycrystalline alloys [831] can be utilized, but this time at a much smaller length scale. In addition, the experience with non-stabilized NC materials can be transferred to stable systems to enhance mechanical performance and other physical properties. Such efforts may result in the design of the first-ever NC-based superalloys.

One of the challenges in the design of high-temperature alloys has been to create and maintain, under service conditions, coherent interfaces between the matrix and precipitates. Successful examples of engineering alloys following this principle include age-hardened Al alloys for automotive engines, Ni-based superalloys predominantly used in advanced gas turbines, and, more recently, nano-oxide ODS alloys developed for next-generation nuclear reactors [831]. In these examples, the precipitate chemistry has been manipulated and perfected through progressive research efforts focused on engineering a stable coherent relationship with the matrix. For example, the precipitation of Guiner-Preston (GP) zones in Al-Cu alloys is significantly altered by additions of Zn and Mg, leading to the development of the 7000 series aluminum alloys. Changing their chemistry through solute additions increases the density of GP

zones, resulting in extremely low interfacial energy [831].

Ni-based superalloys exemplify another system with remarkable strength and resilience by engineering coherent precipitates (γ' and γ'' precipitates from the γ matrix) through controlled chemistry. The evolution of Ni-based superalloys from the 1940 s to the 1970 s primarily focused on optimizing the volume fraction of γ' precipitates and altering their morphology from spherical to cubic. Specific alloying elements (such as Ti, Nb, Mo, and Ta, among others) were selected for their ability to promote improved precipitate morphology, stability, number density, and, most importantly, their coherent relationship with the Ni-based lattice. This resulted in alloys with exceptional thermo-mechanical strength and creep resistance [831].

6.6.2. Engineering within stability limits: Evolving bulk NC alloys for enhanced performance

More recently, research efforts to strengthen alloys via coherent particles have led to the discovery of complex nano-oxide dispersion-strengthened steels. By incorporating specific solutes (such as Y, Ti, Zr, and Cr), it is possible to engineer complex nano-scale oxide precipitates with shell-like structures [200,215,253,697,705,881,882]. The composition and structure of the shell layer play a pivotal role in inhibiting oxide cluster coarsening while maintaining coherency with the lattice even under extreme conditions of high-temperature irradiation [882].

In these cases, previous research efforts have played a crucial role in advancing scientific understanding and setting the stage for the next technological advancements in their respective fields of application, just as the serial nature of scientific exploration and progression has led to the emergence of modern-day superalloys. The same principle applies to stable NC metals and alloys. For example, we discuss below a new category of faceted nanoscale clusters, hereafter referred to as nano-sized superlattice clusters (NSS clusters). This category represents a natural progression in line with the historical development of alloy technologies. Once a stable base is established, attention can shift towards designing other microstructural aspects, see Fig. 63..

Assisted by oxygen and further enhanced by lithium doping, a new variety of faceted yet nanoscale particles was created through ball milling. Adding Li promoted a morphological evolution from spherical clusters to cuboidal NSS clusters in the spatially optimized Cu-3Ta alloy, similar to γ' particles in Ni superalloys. The clusters have an average size of >5 nm and a high number density of $\sim 6 \times 10^{23}/m^3$ [773,883]. It has been determined that Ta exists as a segregated bilayer between the NSS cluster and the matrix, forming a shell structure similar to that observed in ODS alloys [773,883]. The clusters have the ordered $L1_2$-type structure and exhibit enhanced coherency with the Cu matrix in comparison to their spherical predecessors (Fig. 63). This enhanced coherency contributes to the retention of high strength/hardness and grain size after long-term exposure of more than 1 year at a high homologous temperature of 80 % T_m. To highlight the stability of Cu-3Ta-0.5Li, it should be noted that after the exposure to 800C ($0.8T_m$) for 10,000 h (~14 months), the Cu-matrix grain size of 56 nm only increased by 35 nm, and the yield strength decreased by only a 3 % (from 983 MPa to 947 MPa) [773,883].

This is an example of how the engineering of internal structure in a stabilized NC material can push the performance to an extreme level; in this case, retaining the high strength/hardness and grain size after prolonged exposure very close to the melting point. To accomplish this, significant thought was given to preserving the fundamental reasons for stabilizing the alloy. Leveraging the inherent stability of the base alloy (Cu-Ta), lithium (Li) was selected due to its unique capacity to dissolve in the Cu matrix while remaining immiscible with Ta in the clusters [884,885]. Li also possesses the remarkable ability to reduce oxides of both Cu and Ta [886,904]. Given that oxygen is typically found within Ta-based clusters, it was hypothesized that Li atoms would migrate from the matrix to the core of the Ta clusters, causing a restructuring given the immiscibility between the two elements [[884,885]]. Furthermore, incorporating Li into the Cu lattice has been shown to alter the stacking fault energy, imparting enhanced high-temperature creep resistance to the alloy [887,888].

Other considerations involve the addition of Ni to Cu. Cu and Ni exhibit an isomorphous phase diagram, with Ni elevating the melting point of Cu and providing reasonable solid solution strengthening at elevated temperatures [885]. It is worth noting that Ta can be dissolved in Ni up to approximately 3 at% [885]. By maintaining Ta at or below this concentration, Ni could remain in a solid solution with Cu and not precipitate as a Ni-Ta intermetallic compound. Moreover, while Cu and Ni can dissolve in each other completely, the disparity in atomic sizes between Cu and Ni leads to localized stresses, which form the basis for strengthening the crystalline structure. This effect likely further impedes the diffusion of Ta, contributing to even greater resistance against the coarsening of Ta-based clusters at higher temperatures. These strategic examples of working within the framework of the alloy's inherent stability to enhance its capabilities represent the next step in evolutionary development for bulk NC alloy design.

7. From labs to markets: Journeying stabilized bulk nanostructured materials in industry

7.1. Challenges and opportunities in the transition from traditional to stabilized NC metals for industrial adoption

For the past forty-two years, the traditional "unstable" bulk NC materials have been the subject of concurrent scientific exploration and technological development. However, despite some success by several companies, the push for their commercialization was perhaps premature. The rise of stabilized NC materials has created new opportunities for scientific discoveries and more advanced applications that seemed impossible because of the severe limitations of traditional NC materials. Nevertheless, the previous initiatives in examining the technical viability, optimizing manufacturing procedures, identifying shared market opportunities, setting the baseline for intellectual property protection, and laying the foundation for manufacturing infrastructure will catalyze the upcoming new phase of commercialization.

Widespread adoption of the new materials is contingent upon developing a processing technology for *bulk* NC materials suitable for the market. A bulk material is understood as one that has a theoretical density and can be produced in large quantities measured in

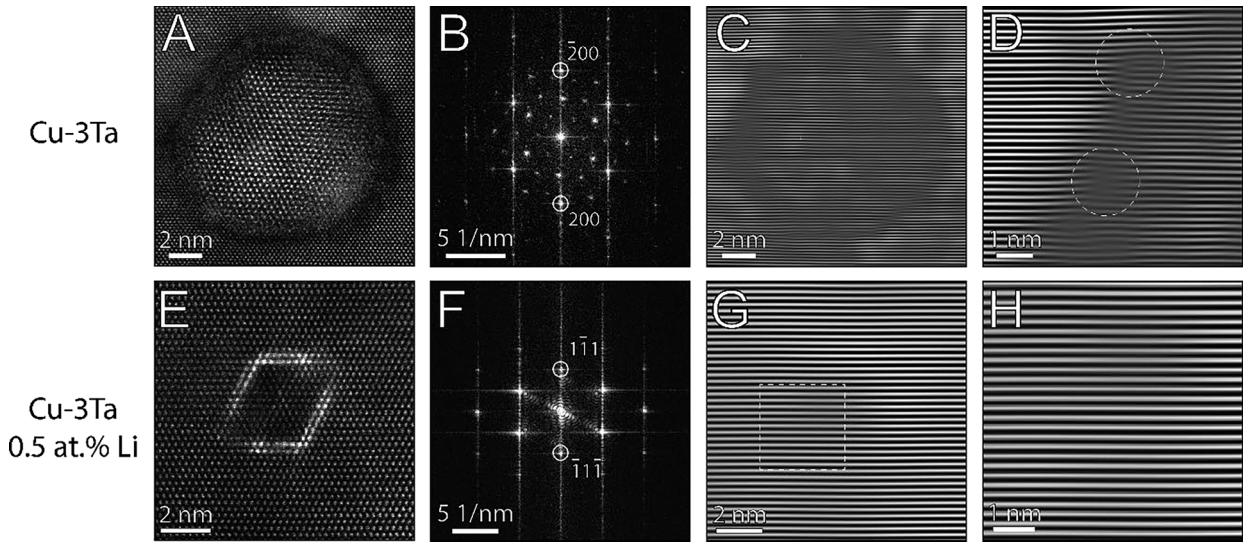

Fig. 63. (A,D) STEM-HAADF images of nanoscale particles in binary Cu-3Ta and ternary Cu-3Ta 0.5Li alloys annealed at 900 °C for 1hr, respectively. (B,F) Fast Fourier Transforms (FFTs) taken from the [110] crystallographic directions of the FCC matrix grains for both alloys. (C,D,G,H) Filtered atomic-resolution images show misfit dislocations surrounding the core–shell particle in (A) and the absence of dislocations surrounding the faceted particle in (E). Filtered images were constructed using the (200) and (1–11) reflections from the FFTs of the Cu-rich matrix in (A) and (E), respectively. Yellow dashed boxes in (C,G) denote the magnified regions in (D, H). Dashed yellow circles in (D) mark the location of dislocation cores. (For interpretation of the references to color in this Fig. legend, the reader is referred to the web version of this article.)

centimeters and kilograms rather than microns and milligrams. Most of the current metal manufacturing industry relies on equilibrium processing due to its advantages over non-equilibrium methods. Equilibrium processing involves heating a metal to a high temperature, holding it at that temperature for some time, and then cooling it down (which often involves quenching), followed by heat-treating for aging and phase reprecipitation. These procedures have enabled the current manufacturing industry to establish a knowledge base for controlling grain size, crystal structure, composition, and other properties. In addition, such methods are simpler and more cost-effective than non-equilibrium methods, which demand specialized equipment and techniques. This explains why the equilibrium processing methods are currently more accessible and practical for large-scale industrial manufacturing.

In contrast, NC metals can only be produced by non-equilibrium methods, most of which were developed in academia. The science behind them is still relatively new and needs to be fully understood. This can create challenges for researchers and engineers seeking to optimize the processing parameters and integrate them into industrial production. Additionally, the lack of standardization makes it difficult to compare results across different studies or establish reliable quality control measures, creating uncertainty that limits the adoption in the industry.

Collaboration between academia and industry is required for successful commercialization. Many, if not all, current industries for producing bulk NC metals have come through channels such as industry partnerships, entrepreneurship programs, licensing, startups, or congressional and other government programs such as the Small Business Innovative Research or Small Business Technology Transfer initiatives. The partnerships, programs, and events provide valuable opportunities for collaboration, networking, and technology transfer between researchers, entrepreneurs, and industry experts. These relationships form the foundation for developing the necessary manufacturing knowledge for NC metals, a knowledge base that is currently lacking in the current metals manufacturing industry.

During the component production, new NC materials can undergo diverse combinations of multiaxial stress states, fluctuating quasistatic or dynamic loading rates, and varying degrees of strain and deformation. Such conditions occur during various manufacturing operations, including creating foils through rolling, wire drawing, deep drawing, forging, and bending, which are commonly used in industrial part manufacturing. It is unclear how the stabilized NC materials coming to the market will respond to such complex stress and deformation states. They can have property sets never seen before, including high thermo-mechanical strength, high elastic limits, extreme hardness, and enhanced or altered strain rate sensitivities. Many of these properties are in the early stages of their understanding through academic studies. Additionally, some limitations may necessitate a departure from traditional manufacturing methods utilized in the current manufacturing of parts.

The road to industrial adoption may not be smooth. The prior pessimistic view of the performance potential of the traditional NC materials might give rise to misconceptions and mistrust about the performance of this new class of stabilized NC materials. Furthermore, the resistance to change in preference for established materials and processes in many industries and markets can make it challenging for stabilized NC materials to gain acceptance and market share. These materials will often be subjected to regulatory approvals and safety standards before they can be used in products or processes. Meeting these requirements can be a significant hurdle, especially for materials with unique properties or poorly understood applications. In some cases, the regulatory approvals or

specifications must be changed, which can take time. Despite these hurdles, we believe that the innovative NC materials emerging today will open new market opportunities that were previously unimaginable.

7.2. Scaling up: Ball milling for bulk NC materials in commercial applications

One of the biggest challenges associated with commercialization of NC materials in the past, which will remain in the future, is the difficulty in producing new materials in large quantities and at a low cost. As discussed in this paper, several methods have been developed to synthesize bulk NC metals, including mechanical alloying, electrodeposition, various vapor precipitation/deposition, and powder densification techniques. Each of these methods has advantages and limitations, and the choice depends on the material's specific application and desired properties. Of these methods, SPD methods, such as mechanical alloying, have been one of the most widely utilized and hold the most promise for bringing about the commercialization of bulk NC materials for structural engineering applications.

Mechanical alloying involves relatively short processing times, often completed in just a few hours, and can be cost-effectively scaled up to produce large quantities of the material. From a commercialization standpoint, the economics of ball milling depend on several factors, including the cost of equipment, grinding media, raw materials, and energy consumption. The cost of equipment increases with the scale and complexity of the process. Energy consumption is a critical factor in the economics of ball milling as it can be energy-intensive, and the cost of electricity or other energy sources can be significant. Choosing the appropriate grinding media can help optimize the milling process and reduce costs. Thus, optimizing the milling process to reduce costs while achieving the desired product quality is an important consideration for any commercial application of ball milling.

In recent years, various milling devices, including several types of ball mills, have been utilized for high kinetic processing techniques, each having advantages and disadvantages depending on the specific application and requirements. The planetary ball mill, shaker mill (SPEX), and small vertical attritors commonly produce mechanically alloyed powders for laboratory purposes. Such mills range in size from the smallest SPEX mill at approximately 0.2 L to the planetary and small vertical attritors, typically less than 10 L in milling volume. They can produce as little as 10 g to about 5–10 kgs of powder and are conducive to alloy design concepts. On the other hand, the horizontal Zoz mill and large attritor mills can be considerably larger at around 1000 L, producing 500 kg of powder per batch. The sufficient production capacity these mills provide enables evaluating scalability, packing, and distribution economics. The significant volumes produced facilitate the assessment of consistency and reproducibility of the quality of the end product. The largest ball mills are the Drum mills, which can reach commercial scales. For instance, the Drum ball mills found at the Toromocho mine in Peru are among the largest in the world. They can process various ores, including copper concentrate and molybdenum oxide, at an estimated rate of 100,000 tons per day. The dimensions of these mills are around 28 feet in diameter and 44 feet in length.

Thus, mechanical alloying has a continuous path from laboratory curiosity to scaled-up synthesis to full industrial production. While ball milling can be an efficient and cost-effective way to process some materials, other materials may require alternative processing methods.

7.3. Advancements in powder metallurgy: Microstructure stabilization and densification strategies

Producing a powder with a stabilized microstructure is only part of the challenge. Equally important is producing a fully densified and strongly bonded monolithic material in which the microstructure is consistently maintained and controlled throughout the process. The most cost-effective powder densification technique depends on the specific application, the required material properties, and the production volume. Some common powder metallurgy techniques include press-and-sinter, metal injection molding (MIM), and HIP. The press-and-sinter technique is a traditional and cost-effective method for producing simple-shaped components. MIM is a more advanced and expensive technique that allows the production of more complex shapes with high precision. HIP is another advanced technique that can produce fully dense components with excellent mechanical properties but requires expensive equipment and high-pressure vessels.

The requirement to preserve the stable microstructure inherently limit the choices of the sintering and densification protocols, which may require the development of new sintering/densification strategies. One example is given by the recently developed accelerated sintering in nanophase separating systems in which the controlling factors (such as surface energy, interfacial energy, and enhanced atomic mobility) lead to rapid sintering to near theoretical density at much lower temperatures than conventionally possible [889]. Current efforts aim to clarify the roles of the alloying elements in stabilizing the nanostructure and accelerating the sintering process. The general guidelines for system selection introduce three criteria: 1) the melting temperature of the matrix must be much higher than that of the selected solute. 2) a miscibility gap must exist, and 3) the solute phase has a high solubility in the matrix phase. From these criteria, W-Cr, W-Ti-Cr Cr-Ni, Mo-Cr, and Mo-W-Cr systems have been identified as strong candidates for accelerated sintering [889–894]. Mo-W-Cr was selected because the components are from two binary systems with a proven/common sintering aid. Difficulties in using the Ni-Fe and Ni-Ag systems and unfavorable conditions for the sintering process were identified, such as burnout of organic materials present and oxide reduction [891,895]. Additive manufacturing to process some of the nanophase sintering samples was explored [896,897]. This type of research is critical because it may pave the way to ensuring large-scale production of parts via pressure-less and pressure-assisted sintering of stabilized NC powders.

7.4. The need for complementary processing for novel materials: Impacts on market integration

The quality and maturity of complementary processes directly impact the production, fabrication, maintenance, and overall life

cycle of a structural system, ensuring its longevity, safety, and functionality. It is the ability to utilize a range of manufacturing methods that makes steel and non-ferrous alloys versatile choices for various applications in different industries. Such practices have been developed over several decades and involve a combination of practical experience, theoretical knowledge, and the ability to integrate various disciplines to create efficient, high-quality, and cost-effective products. However, for a breakthrough technology such as producing thermo-mechanically stablized NC materials, no or minimal complementry processing methods will be available to fabricate a complex system. This scenario often occurs when new, disruptive materials emerge with the potential to create entirely new market opportunities that were previously unimaginable.

A prime example of the need for supporting complementary processing for bulk NC materials or related materials entering a market is illustrated by the recent Funding Opportunity Announcement (FOA) introduced by The Advanced Research Projects Agency–Energy (ARPA–E) [898]. This FOA sought the development of advanced heat exchangers capable of withstanding extreme conditions, including temperatures exceeding 800 °C and pressures exceeding 80 bar. Developing such a groundbreaking technology would be the cornerstone for the next generation of highly efficient modular power generation systems across various industrial sectors.

These sectors encompass traditional and hybrid space and aerospace applications, cutting-edge nuclear and concentrated solar power generation systems, and high-efficiency modular thermo-electric power conversion systems. Current designs of advanced heat exchangers utilize materials such as high-temperature steels and Ni-based alloys such as Inconel despite their much lower thermal conductivity than, say, for Cu, which is 20–25 times higher than for the currently used materials [807]. In fact, copper and Cu-alloys have never been considered viable options for such applications. Despite their significantly lower thermal conductivity, the preference for using steels and other alloys in the construction of advanced heat exchangers and similar systems is rooted in the combination of their physical properties and the ease of fabricating and maintaining such systems that copper alloys do not enjoy. For example, unlike the various steels and Ni-based alloys, the primary strengthening mechanisms of copper alloys involve work hardening and solid solution strengthening. Stress relief temperatures for such alloys occur in a temperature range that is too low (180–460 °C) [831,905]. Solid solution strengthening only increases strength by a few hundred MPa (100–200 MPa) and, therefore, is not a potent strengthening mechanism. Only a few types of copper alloys are age-hardenable by heat treatment, i.e., during low-to-intermediate-temperature treatments (after solution treatment and quenching). These alloys exhibit precipitation-hardening, spinodal-hardening, and order-hardening. Generally, such alloys are solution heat-treated in the range 760 to 955 °C and age-hardened to produce coherent precipitates when aged in the range of 260 to 565 °C [831,905]. As a result, commercially available copper-based alloys lack the inherent strength and stability at the temperatures required for demanding applications.

Although the stabilized NC Cu-based alloys address several of these strength and stability concerns, extensively developed complementary manufacturing methods are needed, unlike those for steel and Ni-based alloys, tailored explicitly for NC alloys. This deficiency encompasses fabrication processes and methods for ensuring durability and longevity, to name a few. Such processes and methods have long been developed for steel and other high-temperature structural alloys. However, very few, if any, studies exist on the machining, joining, and welding of NC alloys. While oxidation and corrosion studies are more common, there is little consistency in the literature on whether NC metals display improved performance [725].

Developing similar processes for thermo-mechanically stable NC alloys will only be possible when they become more readily available on a larger scale. It will take time to develop expertise in working with these novel materials. For example, welding and joining of NC alloys pose challenges due to the inability to melt the microstructure without its destruction. Thus, alternative non-fusion-based methods for joining and repair must be advanced. Many of these joining methods are still undergoing academic research and have not even been discussed for the new class NC materials. Until such alternative methods are developed, market entry will likely occur by individual components or widgets that can stand alone or be added to an existing system but not an entire system.

7.5. Anticipated direction of research in bulk NC metals manufacturing science

As the commercial adoption of bulk NC metals progresses, the focus of research will likely shift toward advancing manufacturing science to support their large-scale integration. Key areas for exploration include the development of effective welding and joining methods. Non-fusion-based joining techniques such as ultrasonic welding, friction stir welding, diffusion bonding, and cold and thermal spray processes will be critical in overcoming these challenges. In addition, research will be needed to optimize sintering processes for maintaining the stabilized microstructure and achieving high-density, monolithic materials over large volumes. Processes such as machining, drawing, forging, bending, and forming, particularly those involving multi-axial stress states, will require further investigation to understand how stabilized NC materials respond to complex deformations. The behavior of grain size under these stresses and strains, as well as the effects of annealing and recrystallization, will be crucial factors influencing the material formability. Corrosion and oxidation prevention strategies must be developed to ensure the longevity and reliability of NC materials in harsh environments. These advancements in manufacturing science will play a central role in ensuring that stabilized NC materials can be effectively processed and integrated into a variety of industries, accelerating their transition from laboratory concepts to commercial products.

7.6. Emerging frontiers: Exploring the commercial trajectory of stable NC materials

Discoveries related to stabilized NC materials are constantly emerging, and these dynamics impact the future of their commercialization. Their genuine commercialization remains pending as a prevailing bulk NC system, which can serve as the foundation for establishing an industrial standard, has yet to be substantiated. These more advanced NC materials will possess many characteristics, making them attractive in markets that traditional nonstabilized NC materials could not access. The ability to have mutually exclusive

and often extreme properties arising in a singular material will ease the adoption and increase the levels of integration into advanced and complex engineered systems.

For example, NC materials with high strength and mechanical stability, high thermal conductivity, and radiation/creep resistance make for an attractive material for integration into next-generation nuclear reactors. As such, these materials are expected to find inroads within several industries, including but not limited to aerospace and aviation, electronics, medical, energy, automotive, construction, defense, and sports equipment. Promotion and marketing will become important when trying to delineate between different levels of the economic value and impact of these materials compared to the non-stabilized NC systems or conventional alloy systems. Consequently, the potential for superior value in these new materials will raise questions about their market entry. This is why marketing will be a critical component of adopting the new technology, as it will help people understand and appreciate its value, overcome resistance to change, acquire the necessary skills and knowledge to use the new technology, and foster a culture of innovation in establishing a market.

Finally, the emergence of stabilized NC materials signifies a new era for innovative fundamental and applied science. Once one such material appears on the market, the industrial entities will try to duplicate the intellectual properties and gain a foothold. At this point, proper commercialization will take place. The commercialization will likely start before the full potential of the new materials is revealed. Premature commercialization may lead to a false sense of completion or satisfaction with the current state of the technology. This can result in decreased funding and interest in further research and development efforts, potentially stifling-innovation and limiting the exploration of new applications and further improvements. Without research into the technology's underlying principles and potential avenues for advancement, there is a risk of missing out on breakthrough discoveries that could significantly enhance the capabilities or lead to entirely new applications. The missed opportunities could hinder the technology from reaching its full potential. If this scenario can be avoided, a second wave of commercialization will likely occur sometime after the initial products become available, resembling a "there and back again" scenario. To fully realize the potential of the game-changing technology, stakeholders need to prioritize ongoing research, collaboration, and transparency. This includes continued investment in fundamental research, robust testing and validation, proactive risk assessment, and open communication about the technology's capabilities and current limitations and prospects. Overall, with ongoing advances in manufacturing and increased collaboration between academia and industry, we can expect to see new applications for these new materials in the near future.

8. Conclusions

In this paper, we have reviewed the challenges and recent breakthroughs in the understanding of the mechanical behavior and physical properties of NC materials, focusing on the problem of structural stability. Prior research struggled due to the unstable microstructures undergoing significant grain growth in the tested samples, which clouded the true mechanical and physical behavior. Recent advances in stabilizing nanostructures have transformed the field. They have enabled the synthesis of stabilized NC materials, revolutionizing our understanding of plastic deformation, fracture mechanisms, and physical behavior at the nanoscale. Overcoming the instability curse has opened new possibilities for observing extraordinary properties in this new class of materials.

The paper has provided a detailed discussion of the emergence and status of the stabilized NC materials, including their synthesis, processing, grain size evolution, GB processes, and extraordinary physical/mechanical properties. It has been shown that the stabilized NC materials exhibit remarkable behaviors, such as the ability to preserve the microstructure at temperatures up to the melting point, in addition to exceptional creep resistance, fatigue endurance, and the ability to absorb various forms of energy fluxes. The stabilized NC materials exhibit novel responses to extreme conditions such as irradiation, high-temperature creep deformation, and shock compression. They reveal previously unseen connections between seemingly disparate properties.

We have also reviewed the computer modeling and simulation efforts that have helped us understand the nano-stabilization mechanisms. The experimental research and simulations have demonstrated the significance of inter-granular and *trans*-granular processes in stabilizing the microstructures and enhancing their properties. We have discussed the intricate interplay between microstructural stability, mechanical stability, and the unusual behavior of NC materials under extreme conditions.

To provide the context, we have traced the historical evolution of the key concepts, models, simulation approaches, and experimental efforts that motivated the pursuit of nanoscale stability and eventually led to the development and progress in the understanding of stabilized nanomaterials. In addition to looking into the past and discussing the state of the art, we have looked into the future, outlining a pathway to overcoming the presumed limitations of the conventional, unstable NC materials and paving the way to future explorations in the field. We believe that the new directions outlined in this paper signify a paradigm shift in the development, understanding, and applications of NC materials.

The specific conclusions of this paper can be summarized as follows.

1. NC materials are intrinsically unstable against grain coarsening because GBs possess excess free energy. This excess free energy creates a thermodynamic driving force for decreasing the total GB free energy by at least three processes: (1) crystallographic reorientations of the grains to lower the GB free energy γ (e.g., grain rotation), (2) replacement of high-energy GBs with low-energy GBs through topological rearrangements in the GB network, and (3) decreasing the total GB area. These processes can operate concurrently. However, the first two are not very sensitive to the grain size d, while the third one is. The decrease in the GB area is driven by the capillary force p, which scales approximately as the inverse power of d ($p \propto 1/d$). In NC materials, the capillary force is extremely large and causes rapid grain growth. In chemically pure NC metals, the grain growth is virtually unstoppable already at moderate homologous temperatures. In many cases, it may even occur at room temperature. Significant stabilization of elemental NC materials seems unfeasible.

2. The most effective way to domesticate the grain growth is by alloying with appropriate solutes. Two approaches to alloy stabilization have been pursued. The *thermodynamic approach* involves alloying the materials with solutes that strongly segregate to GBs, reducing the GB free energy and thus the capillary driving force for grain growth. In recent years, several thermodynamic models have been developed, and the results can be represented by NC stability diagrams guiding the choice of stabilizing solutes. Significant grain growth reduction has been achieved in several alloy systems, although only in a limited temperature range because GB segregation weakens with temperature while the GB mobility increases. Progress in this direction is hampered by competition between GB segregation and bulk phase transformations. Instead of segregating to GBs and lowering their free energy, many solutes prefer reducing the total free energy by precipitating as a new phase either inside the grains or at GBs. In the latter case, the precipitates may pin the GBs, suppressing their migration. However, this is a different, not thermodynamic, stabilization mechanism. The boundaries of the thermodynamic approach can be pushed further by research into the fundamental mechanisms of GB segregation and more reliable computational screening of candidate alloy systems.
3. The *kinetic approach* focuses on reducing GB mobility by one of two mechanisms: (1) solute drag caused by a heavy segregation atmosphere or (2) pinning GBs by a distribution of small particles acting as obstacles to GB migration (Zener pinning). In the second case, the particles can be introduced externally during fabrication, such as oxide particles in ODS alloys, or emerge by second-phase precipitation from a solid solution during thermal processing. Limitations of the kinetic approach are primarily due to the particle coarsening and/or dissolution at high temperatures. The solute drag dynamics and Zener pinning are subjects of active research, which may suggest ways to enhance the effectiveness of the kinetic stabilization further.
4. Separating the thermodynamic and kinetic mechanisms is challenging both experimentally and in simulations. Strongly segregating solutes lower the GB free energy and simultaneously reduce the GB mobility through the solute drag effect with a possible contribution of discrete pinning if the segregation atmosphere is strongly inhomogeneous (which it often is). While understanding the separate roles of the different mechanisms is of fundamental interest, the practical applications move in the opposite direction by looking to combine the thermodynamic and kinetic mechanisms in the same alloy to amplify the stabilization effect.
5. Recent examples of highly stabilized nanomaterials suggest that kinetic stabilization by nanoclusters through the Zener pinning mechanism might offer the most effective pathway forward. An example highlighted in this paper is the kinetically stabilized Cu-Ta alloys, in which the GBs are pinned by Ta nanoclusters precipitated from the metastable solute solution after mechanical alloying of the immiscible components. The Cu-Ta alloys retain nanoscale grain size up to 0.7 of the melting temperature of Cu for long durations, enabling consolidation of the powder and fabrication of bulk samples. The extraordinary properties of these alloys were discussed in detail in the previous sections and will be briefly summarized below.
6. Despite the recent successes in achieving nano-stabilization in specific materials, the fundamental understanding of nanoscale stability is far from complete. Section 3 discussed several unresolved problems in the field. They include the impact of the GB structural and chemical phase transformations on the GB thermodynamics and kinetics, the role of GB diffusion (and diffusion mechanisms) in the GB mobility in alloys (especially in the presence of solute drag), and the role of GB TJs and quadruple points in the gain evolution. Including TJs and quadruple points in future modeling of NC stability is highly desirable. In NC materials capable of preserving the nanoscale grains up to the melting temperature, GB (and generally, defect) premelting can play a prominent role in the grain evolution and mechanical responses (e.g., sliding along premelted GBs). The possible spontaneous melting and re-solidification of individual nanograins as part of the grain evolution is another intriguing phenomenon worth exploring in the future.
7. A thought-provoking idea in NC stabilization is the possibility of creating a truly thermodynamically stable NC alloy with a finite grain size. In this peculiar state, the capillary driving force vanishes, and the total free energy falls below that of uniform, single-crystalline solid solutions of the alloy components.[2] As discussed in sections 2 and 3, the idea remains controversial. So far, a truly stable NC state has not been demonstrated experimentally. Such a state has been predicted by thermodynamic models and Monte Carlo simulations based on such models, which in turn rely on many simplifying approximations. The most drastic of them is the assumption of uniform GB properties. The absolute stability condition predicted by the models is $\gamma = 0$ at all GBs simultaneously. It is also assumed that the solute atoms can instantly redistribute themselves across the entire sample to ensure stability against the system fluctuations away from the $\gamma = 0$ state. Many factors can prevent this state from occurring in practice, including precipitation of bulk phases, a broad distribution of GB structures, energies, segregation capacities, and mobilities in a real polycrystalline sample, and the finite rate of solute diffusion. An intriguing question that warrants further exploration is whether the predicted thermodynamically stable polycrystalline nanomaterials can exist under more realistic conditions, such as the dispersion and anisotropy of GB properties and diffusion-controlled redistribution of the solute atoms in response to fluctuations such as spontaneous local displacements of GBs. Even if the $\gamma = 0$ condition can be achieved simultaneously in all GBs (which is unlikely), what will the polycrystalline structure look like, and will it be truly stable? answering these questions is an exciting research direction.
8. NC materials become stronger with decreasing grain size, a trend that usually follows the empirical Hall-Petch relation between grain size and strength. However, the strength eventually plateaus and then reverses below a critical grain size, setting the upper limit achievable by the material. The nano-grain stability significantly impacts this behavior. The stabilized NC materials defy

[2] Note that even the most stabilized NC materials, such as Cu-Ta alloys, are not thermodynamically stable. They are kinetically trapped in a metastable state. The grains will eventually coarsen, although it may take longer than the timescale of typical laboratory tests and applications.

the inverse Hall-Petch behavior down to lower grain sizes than the unstable NC materials, achieving much higher hardness and strength. This paper demonstrates this behavior with the example of Cu-Ta alloys.

9. Despite their strength, NC materials often suffer from insufficient ductility, limiting their potential for technological applications. In the stabilized NC materials, the GBs are not only dislocation glide barriers but also facilitators of plastic deformation. As such, they can avoid the strength-ductility tradeoff and enhance strength and ductility simultaneously.
10. Stabilized NC alloys can exhibit unconventional recrystallization mechanisms, including the GRDX previously thought impossible in NC materials. For example, after the SPD of Cu-Ta alloys, the GBs remain pinned by the Ta nanoclusters. During recrystallization anneals, the deformed structure undergoes significant dislocation rearrangements and local grain refinement instead of grain coarsening in conventional NC alloys. The intermittent grain melting mentioned above could be another unconventional recrystallization mechanism operating at high temperatures.
11. Kinetically stabilized NC materials, such as Cu-Ta alloys, preserve much of their grain size during high-temperature anneals and when subjected to mechanical stresses. This property opens a unique opportunity to investigate detailed nanoscale deformation mechanisms in stable nanostructures, including high temperatures, unobscured by the concurrent grain growth unavoidable in conventional NC materials. Such investigations could narrow the gap between experiments and MD simulations. The latter primarily deform nanostructures that do not exhibit grain growth on the MD timescale, inviting criticism that the mechanisms observed by MD cannot be compared with mechanisms operating in the ever-changing experimental nanostructures. Of course, the disparity between the experimental and MD timescales continues to exist. However, at least the microstructures studied by both approaches can be reasonably close.
12. Strain rate-sensitive behavior in stable NC materials differs significantly from conventional expectations. Stable nanostructures do not typically cross the threshold of strain rate sensitivity associated with superplastic behavior, which is commonly observed in many coarse-grained alloys at the same temperature. This finding suggests that stabilized NC materials can mitigate (or limit the amount of) the strain rate sensitivity at elevated temperatures. In addition, stable NC materials push the flow-stress upturn caused by the phonon drag towards higher strain rates.
13. Conventional NC materials exhibit higher steady-state creep rates than coarse-grained materials. This behavior suggests a dominant contribution of the Coble mechanism mediated by short-circuit diffusion along GBs. By contrast, stabilized NC materials display higher stress exponents than those associated with diffusional creep and GB-related mechanisms. The steady-state creep rates are significantly lower, and the stress exponents lie primarily in the dislocation climb regime. In addition, initial observations indicate that the primary creep behavior in stable nanostructures follows a cubic-root relationship between strain and time, suggesting microstructure relaxation as a mechanism counteracting the localized stress buildup.
14. Investigations of dislocation density evolution under shock compression of stable NC materials suggest a significant reduction in dislocation buildup due to GB reabsorption. This behavior hints at a potential for these materials to resist damage accumulation in extreme scenarios such as shock, radiation, and fatigue, ultimately displaying a form of self-healing. Materials such as NC Cu-Ta alloys resist plastic deformation and failure under shock loading, exhibiting a higher spall strength and HEL than single crystals. This suggests the possibility of engineering structural materials with enhanced resistance to extreme stimuli. Further exploration across different stable NC alloys is necessary to fully understand these responses.
15. Stable NC materials subjected to fatigue tests display a highly elevated endurance limit on par with highest-performance materials. The improved fatigue performance is attributed to diffuse damage accumulation across multiple nano-grains during cyclic loading. The more homogenous damage distribution contrasts with more localized damage accumulation in typical coarse-grained materials. Atomistic simulations further support this trend, indicating significantly suppressed and evenly distributed damage accumulation. Furthermore, investigations suggest the possibility of damage-healing behavior in stabilized nanomaterials. Coupled with their high endurance limits, this behavior opens an avenue for developing new materials with superior fatigue resistance.
16. Stabilized NC alloys resist radiation-induced hardening, maintaining their hardness up to high doses. This contrasts starkly with coarse-grained materials that experience significant hardening even at low doses. The stable GBs act as effective sinks annihilating irradiation-induced defects. Key research directions for further exploration include understanding the significance of the high sink density in stabilizing irradiation-induced patterning, the role of compositional self-organization in binary alloys with positive heat of mixing, and mechanisms by which the dissolution of sacrificial phases enhances radiation tolerance and microstructural stability, offering promising pathways for developing radiation-tolerant NC materials.
17. The nanoscale grain size profoundly influences phase transformations in materials, which are governed by both thermodynamic and kinetic factors. Due to the large specific GB area, the GBs significantly contribute to the material's free energy, causing shifts in phase diagrams and stabilizing novel phases. Kinetically, GBs and TJs act as heterogeneous nucleation sites and provide high-diffusivity pathways for the growth of new phases. The stabilized NC alloys extend these size effects to higher temperatures. The ability to modify the thermodynamics and kinetics of phase transformations opens avenues for discovering ultrahard nanomaterials similar to nano-polycrystalline diamond and cubic boron nitride. In future research, exploring high-pressure treatments in the material's synthesis may unveil novel NC phases with unprecedented stability and mechanical properties.
18. The exceptional resistance of single crystals to shock-induced spallation and the triumph of defect-free materials in resisting creep at high temperatures have long distinguished them from their polycrystalline counterparts. However, the stable NC alloys exhibit significantly higher spall resistance than coarse-grained materials. They also display compressive and tensile creep resistance similar to that of single crystals, making these materials robust contenders in areas where single crystals have traditionally excelled. Future research should investigate the mechanisms behind the single crystal-like responses and find ways to further narrow the gap between NC and single-crystalline materials.

19. The field of NC materials has historically centered around grain size. The focus should shift towards the microstructure as a whole, with grain size being only one of the structural characteristics. In particular, the distributions and morphologies of precipitates (including nanoclusters) and the precipitate-matrix interfaces should also be the subject of engineering design, as they are in classical systems such as Al-Cu and Ni-based superalloys. In fact, the precipitate design could consider creating two or more different sets of particles. For example, small precipitates of a chemically ordered phase could be added to the existing nanoclusters, creating a stabilized NC superalloy. These and other creative alloy designs could lead to novel NC materials with previously unimaginable properties.
20. Unlike many conventional materials, stabilized NC alloys require non-equilibrium fabrication and processing methods, which complicate industrial adoption due to limited understanding and lack of standardization. Collaborative efforts between academia and industry are crucial to overcome these challenges and establish viable production methods.
21. Market acceptance relies on achieving reliability and scalability of manufacturing processes for the new materials. Because the properties of the stabilized NC materials significantly differ from those of conventional alloys, their response to the diverse stress and deformation conditions arising during the manufacturing processes is a critical area requiring extensive exploration. High-energy ball milling or mechanical alloying shows the most promise in producing bulk structural NC materials for engineering applications. The absence of established machining, joining, welding, and protective measures for the new materials also makes their utilization challenging.
22. The emergence of a standardized, thermo-mechanically stabilized NC alloy on the market will mark a pivotal moment in commercialization, leading to widespread adoption and competition within the market. Advances in manufacturing processes and increased collaboration between academia and industry are expected to drive innovation and expand technological applications for this new class of materials in the coming years.

CRediT authorship contribution statement

K.A. Darling: Conceptualization, primary drafting and overall coordination of the manuscript, Construction of the narrative framework via epistemological grounding, Writing – original draft, (review and editing). **Y. Mishin:** Writing – review & editing, Writing – original draft, Methodology, Investigation. **N.N. Thadhani:** Writing – review & editing, Writing – original draft. **Q. Wei:** Writing – review & editing. **K. Solanki:** Writing – review & editing, Writing – original draft, Supervision, Project administration, Methodology, Investigation, Conceptualization.

Declaration of competing interest

The authors declare that they have no known competing financial interests or personal relationships that could have appeared to influence the work reported in this paper.

Acknowledgements

The work presented in this review article stems from research performed by the authors supported at their various institutions including DEVCOM Army Research Laboratory, George Mason University, Georgia Institute of Technology, University of North Carolina at Charlotte, and Arizona State University. Y.M gratefully acknowledges the financial support of the United States Army Research Office, grant number ARO-W911NF-15-2-0050. N.T. acknowledges the funding provided by the U.S. Army Research Laboratory under contract No. W911NF-21-2-0015 and the U.S. Army Research Office Cooperative Agreement Project No. W911NF-24-2-0116. K.S. acknowledges the support of the US Army Research Laboratory under contract W911NF-15-2-0038 and the National Science Foundation under grants No. 1663287 and 1810431.

Data availability

No data was used for the research described in the article.

References

[1] Gleiter H. Materials with ultra-fine grain sizes. In: Hansen N, Horsewell A, Leffers T, editors. Proceedings of the 2nd Riso International Symposium on Metallurgy and Materials Science; 1981. p. 15.
[2] Gleiter H. Nanostructured materials: basic concepts and microstructure. Acta Mater 2000;48:1–29. https://doi.org/10.1016/S1359-6454(99)00285-2.
[3] Birringer R. Nanocrystalline materials. Mater Sci Eng A 1989;117:33–43. https://doi.org/10.1016/0921-5093(89)90083-X.
[4] Chakravorty D, Giri A. Chemistry of Advanced Materials, edited by CNR Rao. Oxford: Blackwell Sci. Publications; 1992.
[5] Weissmüller J. Alloy effects in nanostructures. Nanostruct Mater 1993;3:261–72. https://doi.org/10.1016/0965-9773(93)90088-S.
[6] Weissmüller J. Alloy thermodynamics in nanostructures. J Mater Res 1994;9:4–7. https://doi.org/10.1557/JMR.1994.0004.
[7] Suryanarayana C. Nanocrystalline materials. Int Mater Rev 1995;40:41–64. https://doi.org/10.1179/imr.1995.40.2.41.
[8] Lu K. Nanocrystalline metals crystallized from amorphous solids: nanocrystallization, structure, and properties. Mater Sci Eng R Rep 1996;16:161–221. https://doi.org/10.1016/0927-796X(95)00187-5.
[9] Koch CC. Synthesis of nanostructured materials by mechanical milling: problems and opportunities. Nanostruct Mater 1997;9:13–22. https://doi.org/10.1016/S0965-9773(97)00014-7.
[10] Murty BS, Ranganathan S. Novel materials synthesis by mechanical alloying/milling. Int Mater Rev 1998;43:101–41. https://doi.org/10.1179/imr.1998.43.3.101.

[11] Suryanarayana C, Koch CC. Nanocrystalline materials – Current research and future directions. Hyperfine Interact 2000;130:5–44. https://doi.org/10.1023/A:1011026900989.
[12] Valiev RZ, Islamgaliev RK, Alexandrov IV. Bulk nanostructured materials from severe plastic deformation. Prog Mater Sci 2000;45:103–89. https://doi.org/10.1016/S0079-6425(99)00007-9.
[13] Conrad H, Narayan J. On the grain size softening in nanocrystalline materials. Scr Mater 2000;42:1025–30. https://doi.org/10.1016/S1359-6462(00)00320-1.
[14] Lu L, Sui ML, Lu K. Superplastic extensibility of nanocrystalline copper at room temperature. Science 2000;287:1463–6. https://doi.org/10.1126/science.287.5457.1463.
[15] Froes FH (Sam), Senkov ON, Baburaj EG. Synthesis of nanocrystalline materials — an overview. Materials Science and Engineering: A 2001;301:44–53. Doi: 10.1016/S0921-5093(00)01391-5.
[16] Suryanarayana C. Mechanical alloying and milling. Prog Mater Sci 2001;46:1–184. https://doi.org/10.1016/S0079-6425(99)00010-9.
[17] Mohamed FA, Li Y. Creep and superplasticity in nanocrystalline materials: current understanding and future prospects. Mater Sci Eng A 2001;298:1–15. https://doi.org/10.1016/S0928-4931(00)00190-9.
[18] Lu L, Sui ML, Lu K. Cold rolling of bulk nanocrystalline copper. Acta Mater 2001;49:4127–34. https://doi.org/10.1016/S1359-6454(01)00248-8.
[19] Dalla Torre F, Van Swygenhoven H, Victoria M. Nanocrystalline electrodeposited Ni: microstructure and tensile properties. Acta Mater 2002;50:3957–70. https://doi.org/10.1016/S1359-6454(02)00198-2.
[20] Wang Y, Chen M, Zhou F, Ma E. High tensile ductility in a nanostructured metal. Nature 2002;419:912–5. https://doi.org/10.1038/nature01133.
[21] Kumar KS, Van Swygenhoven H, Suresh S. Mechanical behavior of nanocrystalline metals and alloys. Acta Mater 2003;51:5743–74. https://doi.org/10.1016/j.actamat.2003.08.032.
[22] Cheng S, Ma E, Wang YM, Kecskes LJ, Youssef KM, Koch CC, et al. Tensile properties of in situ consolidated nanocrystalline Cu. Acta Mater 2005;53:1521–33. https://doi.org/10.1016/j.actamat.2004.12.005.
[23] Liao XZ, Zhou F, Lavernia EJ, He DW, Zhu YT. Deformation twins in nanocrystalline Al. Appl Phys Lett 2003;83:5062–4. https://doi.org/10.1063/1.1633975.
[24] Schuh CA, Nieh TG, Iwasaki H. The effect of solid solution W additions on the mechanical properties of nanocrystalline Ni. Acta Mater 2003;51:431–43. https://doi.org/10.1016/S1359-6454(02)00427-5.
[25] Valiev R. Nanostructuring of metals by severe plastic deformation for advanced properties. Nat Mater 2004;3:511–6. https://doi.org/10.1038/nmat1180.
[26] Wei Q, Cheng S, Ramesh KT, Ma E. Effect of nanocrystalline and ultrafine grain sizes on the strain rate sensitivity and activation volume: fcc versus bcc metals. Mater Sci Eng A 2004;381:71–9. https://doi.org/10.1016/j.msea.2004.03.064.
[27] Van Swygenhoven H, Derlet PM, Frøseth AG. Stacking fault energies and slip in nanocrystalline metals. Nat Mater 2004;3:399–403. https://doi.org/10.1038/nmat1136.
[28] Lu L, Shen Y, Chen X, Qian L, Lu K. Ultrahigh strength and high electrical conductivity in copper. Science 2004. https://doi.org/10.1126/science.1092905.
[29] Bringa EM, Caro A, Wang Y, Victoria M, McNaney JM, Remington BA, et al. Ultrahigh strength in nanocrystalline materials under shock loading. Science 2005;309:1838–41. https://doi.org/10.1126/science.1116723.
[30] Mishra RS, Ma ZY. Friction stir welding and processing. Mater Sci Eng R Rep 2005;50:1–78. https://doi.org/10.1016/j.mser.2005.07.001.
[31] Wolf D, Yamakov V, Phillpot SR, Mukherjee A, Gleiter H. Deformation of nanocrystalline materials by molecular-dynamics simulation: relationship to experiments? Acta Mater 2005;53:1–40. https://doi.org/10.1016/j.actamat.2004.08.045.
[32] Youssef KM, Scattergood RO, Murty KL, Horton JA, Koch CC. Ultrahigh strength and high ductility of bulk nanocrystalline copper. Appl Phys Lett 2005;87. https://doi.org/10.1063/1.2034122.
[33] Meyers MA, Mishra A, Benson DJ. Mechanical properties of nanocrystalline materials. Prog Mater Sci 2006;51:427–556. https://doi.org/10.1016/j.pmatsci.2005.08.003.
[34] Valiev RZ, Langdon TG. Principles of equal-channel angular pressing as a processing tool for grain refinement. Prog Mater Sci 2006;51:881–981. https://doi.org/10.1016/j.pmatsci.2006.02.003.
[35] Van Swygenhoven H, Weertman JR. Deformation in nanocrystalline metals. Mater Today 2006;9:24–31. https://doi.org/10.1016/S1369-7021(06)71494-8.
[36] Ma E. Eight routes to improve the tensile ductility of bulk nanostructured metals and alloys. JOM 2006;58:49–53. https://doi.org/10.1007/s11837-006-0215-5.
[37] Witkin DB, Lavernia EJ. Synthesis and mechanical behavior of nanostructured materials via cryomilling. Prog Mater Sci 2006;51:1–60. https://doi.org/10.1016/j.pmatsci.2005.04.004.
[38] Wang YM, Bringa EM, McNaney JM, Victoria M, Caro A, Hodge AM, et al. Deforming nanocrystalline nickel at ultrahigh strain rates. Appl Phys Lett 2006;88:061917. https://doi.org/10.1063/1.2173257.
[39] Farkas D, Frøseth A, Van Swygenhoven H. Grain boundary migration during room temperature deformation of nanocrystalline Ni. Scr Mater 2006;55:695–8. https://doi.org/10.1016/j.scriptamat.2006.06.032.
[40] Detor AJ, Schuh CA. Grain boundary segregation, chemical ordering and stability of nanocrystalline alloys: Atomistic computer simulations in the Ni–W system. Acta Mater 2007;55:4221–32.
[41] Wei Q. Strain rate effects in the ultrafine grain and nanocrystalline regimes—influence on some constitutive responses. J Mater Sci 2007;42:1709–27. https://doi.org/10.1007/s10853-006-0700-9.
[42] Koch CC. Structural nanocrystalline materials: an overview. J Mater Sci 2007;42:1403–14.
[43] Trelewicz JR, Schuh CA. The Hall–Petch breakdown in nanocrystalline metals: A crossover to glass-like deformation. Acta Mater 2007;55:5948–58. https://doi.org/10.1016/j.actamat.2007.07.020.
[44] Zhilyaev AP, Langdon TG. Using high-pressure torsion for metal processing: Fundamentals and applications. Prog Mater Sci 2008;53:893–979. https://doi.org/10.1016/j.pmatsci.2008.03.002.
[45] Koch CC, Scattergood RO, Darling KA, Semones JE. Stabilization of nanocrystalline grain sizes by solute additions. J Mater Sci 2008;43:7264–72. https://doi.org/10.1007/s10853-008-2870-0.
[46] Lu K, Lu L, Suresh S. Strengthening Materials by Engineering Coherent Internal Boundaries at the Nanoscale. Science 2009. https://doi.org/10.1126/science.1159610.
[47] Trelewicz JR, Schuh CA. Grain boundary segregation and thermodynamically stable binary nanocrystalline alloys. PhysRevB 2009;79:094112. https://doi.org/10.1103/PhysRevB.79.094112.
[48] Lu L, Chen X, Huang X, Lu K. Revealing the Maximum Strength in Nanotwinned Copper. Science 2009. https://doi.org/10.1126/science.1167641.
[49] Ii HAP, Boyce BL. A Review of Fatigue Behavior in Nanocrystalline Metals. Exp Mech 2010;50:5–23. https://doi.org/10.1007/s11340-009-9301-2.
[50] Zhao Y, Zhu Y, Lavernia EJ. Strategies for Improving Tensile Ductility of Bulk Nanostructured Materials. Adv Eng Mater 2010;12:769–78. https://doi.org/10.1002/adem.200900335.
[51] Yu Q, Shan Z-W, Li J, Huang X, Xiao L, Sun J, et al. Strong crystal size effect on deformation twinning. Nature 2010;463:335–8. https://doi.org/10.1038/nature08692.
[52] Greer JR, De Hosson JTM. Plasticity in small-sized metallic systems: Intrinsic versus extrinsic size effect. Prog Mater Sci 2011;56:654–724. https://doi.org/10.1016/j.pmatsci.2011.01.005.
[53] Chookajorn T, Murdoch HA, Schuh CA. Design of Stable Nanocrystalline Alloys. Science 2012;337:951–4. https://doi.org/10.1126/science.1224737.
[54] Zhu YT, Liao XZ, Wu XL. Deformation twinning in nanocrystalline materials. Prog Mater Sci 2012;57:1–62. https://doi.org/10.1016/j.pmatsci.2011.05.001.
[55] Sauvage X, Wilde G, Divinski SV, Horita Z, Valiev RZ. Grain boundaries in ultrafine grained materials processed by severe plastic deformation and related phenomena. Mater Sci Eng A 2012;540:1–12. https://doi.org/10.1016/j.msea.2012.01.080.
[56] Estrin Y, Vinogradov A. Extreme grain refinement by severe plastic deformation: A wealth of challenging science. Acta Mater 2013;61:782–817. https://doi.org/10.1016/j.actamat.2012.10.038.

[57] Langdon TG. Twenty-five years of ultrafine-grained materials: Achieving exceptional properties through grain refinement. Acta Mater 2013;61:7035–59. https://doi.org/10.1016/j.actamat.2013.08.018.
[58] Raabe D, Herbig M, Sandlöbes S, Li Y, Tytko D, Kuzmina M, et al. Grain boundary segregation engineering in metallic alloys: A pathway to the design of interfaces. Curr Opin Solid State Mater Sci 2014;18:253–61. https://doi.org/10.1016/j.cossms.2014.06.002.
[59] Armstrong RW. 60 Years of Hall-Petch: Past to Present Nano-Scale Connections. Mater Trans 2014;55:2–12. https://doi.org/10.2320/matertrans.MA201302.
[60] Tschopp MA, Murdoch HA, Kecskes LJ, Darling KA. "Bulk" Nanocrystalline Metals: Review of the Current State of the Art and Future Opportunities for Copper and Copper Alloys. JOM 2014;66:1000–19. https://doi.org/10.1007/s11837-014-0978-z.
[61] Andrievski RA. Review of thermal stability of nanomaterials. J Mater Sci 2014;49:1449–60. https://doi.org/10.1007/s10853-013-7836-1.
[62] Mathaudhu SN, Boyce BL. Thermal Stability: The Next Frontier for Nanocrystalline Materials. JOM 2015;67:2785–7. https://doi.org/10.1007/s11837-015-1708-x.
[63] Kalidindi AR, Chookajorn T, Schuh CA. Nanocrystalline Materials at Equilibrium: A Thermodynamic Review. JOM 2015;67:2834–43. https://doi.org/10.1007/s11837-015-1636-9.
[64] Hahn EN, Meyers MA. Grain-size dependent mechanical behavior of nanocrystalline metals. Mater Sci Eng A 2015;646:101–34. https://doi.org/10.1016/j.msea.2015.07.075.
[65] Cordero ZC, Knight BE, Schuh CA. Six decades of the Hall–Petch effect – a survey of grain-size strengthening studies on pure metals. Int Mater Rev 2016;61:495–512. https://doi.org/10.1080/09506608.2016.1191808.
[66] Andrievski R, Khatchoyan A. Nanomaterials in Extreme Environments. Switzerland: Springer Int; 2016.
[67] Darling KA, Rajagopalan M, Komarasamy M, Bhatia MA, Hornbuckle BC, Mishra RS, et al. Extreme creep resistance in a microstructurally stable nanocrystalline alloy. Nature 2016;537:378–81. https://doi.org/10.1038/nature19313.
[68] Lu K. Stabilizing nanostructures in metals using grain and twin boundary architectures. Nat Rev Mater 2016;1:natrevmats201619. https://doi.org/10.1038/natrevmats.2016.19.
[69] Ma E, Zhu T. Towards strength–ductility synergy through the design of heterogeneous nanostructures in metals. Mater Today 2017;20:323–31. https://doi.org/10.1016/j.mattod.2017.02.003.
[70] Tian L. A short review on mechanical behavior of nanocrystalline materials. Int J Metall Met Phys 2017;2:1–13.
[71] Peng HR, Gong MM, Chen YZ, Liu F. Thermal stability of nanocrystalline materials: thermodynamics and kinetics. Int Mater Rev 2017;62:303–33. https://doi.org/10.1080/09506608.2016.1257536.
[72] Han J, Thomas SL, Srolovitz DJ. Grain-boundary kinetics: A unified approach. Prog Mater Sci 2018;98:386–476. https://doi.org/10.1016/j.pmatsci.2018.05.004.
[73] Vinogradov A, Estrin Y. Analytical and numerical approaches to modelling severe plastic deformation. Prog Mater Sci 2018;95:172–242. https://doi.org/10.1016/j.pmatsci.2018.02.001.
[74] Cao Y, Ni S, Liao X, Song M, Zhu Y. Structural evolutions of metallic materials processed by severe plastic deformation. Mater Sci Eng R Rep 2018;133:1–59. https://doi.org/10.1016/j.mser.2018.06.001.
[75] Ovid'ko IA, Valiev RZ, Zhu YT. Review on superior strength and enhanced ductility of metallic nanomaterials. Prog Mater Sci 2018;94:462–540. https://doi.org/10.1016/j.pmatsci.2018.02.002.
[76] Spearot DE, Tucker GJ, Gupta A, Thompson GB. Mechanical properties of stabilized nanocrystalline FCC metals. J Appl Phys 2019;126. https://doi.org/10.1063/1.5114706.
[77] Wilde G, Divinski S. Grain Boundaries and Diffusion Phenomena in Severely Deformed Materials. Mater Trans 2019;60:1302–15. https://doi.org/10.2320/matertrans.MF201934.
[78] Bachmaier A, Pippan R. High-Pressure Torsion Deformation Induced Phase Transformations and Formations: New Material Combinations and Advanced Properties. Mater Trans 2019;60:1256–69. https://doi.org/10.2320/matertrans.MF201930.
[79] An XH, Wu SD, Wang ZG, Zhang ZF. Significance of stacking fault energy in bulk nanostructured materials: Insights from Cu and its binary alloys as model systems. Prog Mater Sci 2019;101:1–45. https://doi.org/10.1016/j.pmatsci.2018.11.001.
[80] Cantwell PR, Frolov T, Rupert TJ, Krause AR, Marvel CJ, Rohrer GS, et al. Grain Boundary Complexion Transitions. Annu Rev Mater Res 2020;50:465–92. https://doi.org/10.1146/annurev-matsci-081619-114055.
[81] Wu H, Fan G. An overview of tailoring strain delocalization for strength-ductility synergy. Prog Mater Sci 2020;113:100675. https://doi.org/10.1016/j.pmatsci.2020.100675.
[82] Naik SN, Walley SM. The Hall–Petch and inverse Hall–Petch relations and the hardness of nanocrystalline metals. J Mater Sci 2020;55:2661–81. https://doi.org/10.1007/s10853-019-04160-w.
[83] Schuh CA, Lu K. Stability of nanocrystalline metals: The role of grain-boundary chemistry and structure. MRS Bull 2021;46:225–35. https://doi.org/10.1557/s43577-021-00055-x.
[84] Perrin AE, Schuh CA. Stabilized Nanocrystalline Alloys: The Intersection of Grain Boundary Segregation with Processing Science. Annu Rev Mater Res 2021;51:241–68. https://doi.org/10.1146/annurev-matsci-080819-121823.
[85] Thomas M, Salvador H, Clark T, Lang E, Hattar K, Mathaudhu S. Thermal and Radiation Stability in Nanocrystalline Cu. Nanomaterials 2023;13:1211. https://doi.org/10.3390/nano13071211.
[86] Choi I-C, Kim Y-J, Seok M-Y, Yoo B-G, Kim J-Y, Wang Y, et al. Nanoscale room temperature creep of nanocrystalline nickel pillars at low stresses. Int J Plast 2013;41:53–64.
[87] Kale C, Srinivasan S, Sharma S, Hornbuckle BC, Koju RK, Grendahl S, et al. Exceptional fatigue strength of a microstructurally stable bulk nanocrystalline alloy. Acta Mater 2023;255:119049. https://doi.org/10.1016/j.actamat.2023.119049.
[88] Srinivasan S, Kale C, Hornbuckle BC, Darling KA, Chancey MR, Hernández-Rivera E, et al. Radiation tolerance and microstructural changes of nanocrystalline Cu-Ta alloy to high dose self-ion irradiation. Acta Mater 2020;195:621–30. https://doi.org/10.1016/j.actamat.2020.05.061.
[89] Haubold T, Birringer R, Lengeler B, Gleiter H. Exafs studies of nanocrystalline materials exhibiting a new solid state structure with randomly arranged atoms. Phys Lett A 1989;135:461–6. https://doi.org/10.1016/0375-9601(89)90049-2.
[90] Suryanarayana C, Prabhu B. 2 - Synthesis of Nanostructured Materials by Inert-Gas Condensation Methods. In: Koch CC, editor. Nanostructured Materials (Second Edition). Norwich, NY: William Andrew Publishing; 2007. p. 47–90. https://doi.org/10.1016/B978-081551534-0.50004-X.
[91] Clark D, Wood D, Erb U. Industrial applications of electrodeposited nanocrystals. Nanostruct Mater 1997;9:755–8. https://doi.org/10.1016/S0965-9773(97)00163-3.
[92] Hibbard G, Aust KT, Palumbo G, Erb U. Thermal stability of electrodeposited nanocrystalline cobalt. Scr Mater 2001;44:513–8. https://doi.org/10.1016/S1359-6462(00)00628-X.
[93] Valiev RZ, Estrin Y, Horita Z, Langdon TG, Zechetbauer MJ, Zhu YT. Producing bulk ultrafine-grained materials by severe plastic deformation. JOM 2006;58:33–9. https://doi.org/10.1007/s11837-006-0213-7.
[94] Saito Y, Tsuji N, Utsunomiya H, Sakai T, Hong RG. Ultra-fine grained bulk aluminum produced by accumulative roll-bonding (ARB) process. Scr Mater 1998;39:1221–7. https://doi.org/10.1016/S1359-6462(98)00302-9.
[95] Suryanarayana C, Korth GE. Consolidation of nanocrystalline powders. Met Mater 1999;5:121–8. https://doi.org/10.1007/BF03026041.
[96] Günther B, Kumpmann A, Kunze H-D. Secondary recrystallization effects in nanostructured elemental metals. Scr Metall Mater 1992;27:833–8. https://doi.org/10.1016/0956-716X(92)90401-Y.
[97] Hibbard GD, McCrea JL, Palumbo G, Aust KT, Erb U. An initial analysis of mechanisms leading to late stage abnormal grain growth in nanocrystalline Ni. Scr Mater 2002;47:83–7. https://doi.org/10.1016/S1359-6462(02)00098-2.
[98] Klement U, Erb U, El-Sherik AM, Aust KT. Thermal stability of nanocrystalline Ni. Mater Sci Eng A 1995;203:177–86. https://doi.org/10.1016/0921-5093(95)09864-X.

[99] Malow TR, Koch CC. Grain growth in nanocrystalline iron prepared by mechanical attrition. Acta Mater 1997;45:2177–86. https://doi.org/10.1016/S1359-6454(96)00300-X.
[100] Eswarappa Prameela S, Pollock TM, Raabe D, Meyers MA, Aitkaliyeva A, Chintersingh K-L, et al. Materials for extreme environments. Nat Rev Mater 2023;8:81–8. https://doi.org/10.1038/s41578-022-00496-z.
[101] Sutton AP, Balluffi RW. Interfaces in Crystalline Materials, vol. 51. Clarendon Press; 1995.
[102] Gibbs JW. On the equilibrium of heterogeneous substances. The collected works of J. W. Gibbs, vol. 1, New Haven: Yale University Press; 1948, p. 55–349.
[103] Cahn JW. Thermodynamics of solid and fluid surfaces. In: Johnson WC, Blackely JM, editors. Interface Segregation. Metals Park, OH: American Society of Metals; 1979. p. 3–23.
[104] Frolov T, Mishin Y. Effect of non-hydrostatic stresses on solid-fluid equilibrium 2010.
[105] Frolov T, Mishin Y. Temperature dependence of the surface free energy and surface stress: An atomistic calculation for Cu(110). Phys Rev m B 2009;79:45430–40.
[106] Frolov T, Mishin Y. Thermodynamics of coherent interfaces under mechanical stresses. I Theory Phys Rev B 2012;85:224106. https://doi.org/10.1103/PhysRevB.85.224106.
[107] Frolov T, Mishin Y. Thermodynamics of coherent interfaces under mechanical stresses. II. Application to atomistic simulation of grain boundaries. PhysRevB 2012;85:224107. https://doi.org/10.1103/PhysRevB.85.224107.
[108] Mishin Y, Sofronis P, Bassani JL. Thermodynamic and kinetic aspects of interfacial decohesion. Acta Mater 2002;50:3609–22.
[109] Rice JR, Wang JS. Embrittlement of interfaces by solute segregation. Mater Sci Eng A-Struct Mater Prop Microstruct Process 1989;107:23–40.
[110] Hirth JP, Rice JR. On the thermodynamics of adsorption at interfaces as it influences decohesion. Met Trans A-Phys Met Mater Sc 1980;11:1501–11.
[111] Hondros ED, Seah MP. Segregation to interfaces International Metals Reviews 1977;22:262–301.
[112] Lejcek P. Grain boundary segregation in metals, vol. 136. Springer; 2010.
[113] Hondros ED, Seah MP, Hofmann S, Lejcek P. Physical metallurgy. Netherlands: Elsevier Sci Pub BV; 1983. p. 856.
[114] Wagih M, Schuh CA. Spectrum of grain boundary segregation energies in a polycrystal. Acta Mater 2019;181:228–37. https://doi.org/10.1016/j.actamat.2019.09.034.
[115] Wagih M, Schuh CA. Grain boundary segregation beyond the dilute limit: Separating the two contributions of site spectrality and solute interactions. Acta Mater 2020;199:63–72. https://doi.org/10.1016/j.actamat.2020.08.022.
[116] Wagih M, Schuh CA. Learning Grain-Boundary Segregation: From First Principles to Polycrystals. PhysRevLett 2022;129:046102. https://doi.org/10.1103/PhysRevLett.129.046102.
[117] Wagih M, Schuh CA. Thermodynamics and design of nanocrystalline alloys using grain boundary segregation spectra. Acta Mater 2021;217:117177. https://doi.org/10.1016/j.actamat.2021.117177.
[118] Wagih M, Larsen PM, Schuh CA. Learning grain boundary segregation energy spectra in polycrystals. Nat Commun 2020;11:6376. https://doi.org/10.1038/s41467-020-20083-6.
[119] Tuchinda N, Schuh CA. The vibrational entropy spectra of grain boundary segregation in polycrystals. Acta Mater 2023;245:118630. https://doi.org/10.1016/j.actamat.2022.118630.
[120] Tuchinda N, Schuh CA. Computed entropy spectra for grain boundary segregation in polycrystals. npj Comput Mater 2024;10:1–10. https://doi.org/10.1038/s41524-024-01260-3.
[121] Kirchheim R. Grain coarsening inhibited by solute segregation. Acta Mater 2002;50:413–9. https://doi.org/10.1016/S1359-6454(01)00338-X.
[122] Liu F, Kirchheim R. Nano-scale grain growth inhibited by reducing grain boundary energy through solute segregation. J Cryst Growth 2004;264:385–91. https://doi.org/10.1016/j.jcrysgro.2003.12.021.
[123] Kirchheim R. Reducing grain boundary, dislocation line and vacancy formation energies by solute segregation. II. Experimental evidence and consequences. Acta Mater 2007;55:5139–48.
[124] Krill CE, Ehrhardt H, Birringer R. Thermodynamic stabilization of nanocrystallinity. Int J Mater Res 2005;96:1134–41. https://doi.org/10.1515/ijmr-2005-0196.
[125] Shvindlerman LS, Gottstein G. Unexplored topics and potentials of grain boundary engineering. Scri Mater 2006;54:1041–5.
[126] Murdoch HA, Schuh CA. Estimation of grain boundary segregation enthalpy and its role in stable nanocrystalline alloy design. J Mater Res 2013;28:2154–63.
[127] Kalidindi AR, Schuh CA. Stability criteria for nanocrystalline alloys. Acta Mater 2017;132:128–37. https://doi.org/10.1016/j.actamat.2017.03.029.
[128] Chookajorn T, Schuh CA. Thermodynamics of stable nanocrystalline alloys: A Monte Carlo analysis. Phys Rev m B 2014;89:064102.
[129] Murdoch HA, Schuh CA. Stability of binary nanocrystalline alloys against grain growth and phase separation. Acta Mater 2013;61:2121–32.
[130] Darling KA, Tschopp MA, VanLeeuwen BK, Atwater MA, Liu ZK. Mitigating grain growth in binary nanocrystalline alloys through solute selection based on thermodynamic stability maps. Comp Mater Sci 2014;84:255–66.
[131] Saber M, Kotan H, Koch CC, Scattergood RO. Thermodynamic stabilization of nanocrystalline binary alloys. J Appl Phys 2013;113:065515.
[132] Xing W, Kalidindi AR, Amram D, Schuh CA. Solute interaction effects on grain boundary segregation in ternary alloys. Acta Mater 2018;161:285–94. https://doi.org/10.1016/j.actamat.2018.09.005.
[133] Zhou N, Luo J. Developing thermodynamic stability diagrams for equilibrium-grain-size binary alloys. Mater Lett 2014;115:268–71. https://doi.org/10.1016/j.matlet.2013.09.093.
[134] Saber M, Koch CC, Scattergood RO. Thermodynamic Grain Size Stabilization Models: An Overview. Materials Research Letters 2015;3:65–75. https://doi.org/10.1080/21663831.2014.997894.
[135] Saber M, Kotan H, Koch CC, Scattergood RO. A predictive model for thermodynamic stability of grain size in nanocrystalline ternary alloys. J Appl Phys 2013;114:103510. https://doi.org/10.1063/1.4821040.
[136] Kalidindi AR, Schuh CA. Stability criteria for nanocrystalline alloys. J Mater Res 2017;32:1093–2002.
[137] Abdeljawad F, Lu P, Argibay N, Clark BG, Boyce BL, Foiles SM. Grain boundary segregation in immiscible nanocrystalline alloys. Acta Mater 2017;126:528–39. https://doi.org/10.1016/j.actamat.2016.12.036.
[138] Abdeljawad F, Foiles SM. Stabilization of nanocrystalline alloys via grain boundary segregation: A diffuse interface model. Acta Mater 2015;101:159–71.
[139] Kim SG, Lee JS, Lee B-J. Thermodynamic properties of phase-field models for grain boundary segregation. Acta Mater 2016;112:150–61. https://doi.org/10.1016/j.actamat.2016.04.028.
[140] Kadambi SB, Abdeljawad F, Patala S. A phase-field approach for modeling equilibrium solute segregation at the interphase boundary in binary alloys. Comput Mater Sci 2020;175:109533. https://doi.org/10.1016/j.commatsci.2020.109533.
[141] Alkayyali M, Abdeljawad F. Grain boundary solute drag model in regular solution alloys. Phys Rev Lett 2021;127:175503. https://doi.org/10.1103/PhysRevLett.127.175503.
[142] Kalidindi AR, Schuh CA. Phase transitions in stable nanocrystalline alloys. J Mater Res 2017;32:1993–2002. https://doi.org/10.1557/jmr.2017.188.
[143] Hussein O, Mishin Y. A model of thermodynamic stabilization of nanocrystalline grain boundaries in alloy systems. Acta Mater 2024;281:120404. https://doi.org/10.1016/j.actamat.2024.120404.
[144] Millett PC, Selvam RP, Saxena A. Stabilizing nanocrystalline materials with dopants. Acta Mater 2007;55:2329–36.
[145] Wynblatt P, Chatain D. Anisotropy of segregation at grain boundaries and surfaces. Metall Mater Trans m A 2006;37:2595–620.
[146] Wynblatt P, Chatain D, Peng Y. Some aspects of the anisotropy of grain boundary segregation and wetting. J Mate Sci 2006;41:7760–8.
[147] Wynblatt P, Chatain D. Solid-state wetting transitions at grain boundaries. Mater Sci Eng m A 2008;495:119–25.
[148] Purohit Y, Jang S, Irving DL, Padgett CW, Scattergood RO, Brenner DW. Atomistic modeling of the segregation of lead impurities to a grain boundary in an aluminum bicrystalline solid. Mater Sci Eng A 2008;493:97–100. https://doi.org/10.1016/j.msea.2007.05.128.
[149] Purohit Y, Sun L, Irving DL, Scattergood RO, Brenner DW. Computational study of the impurity induced reduction of grain boundary energies in nano- and bi-crystalline Al–Pb alloys. Mater Sci Eng A 2010;527:1769–75. https://doi.org/10.1016/j.msea.2009.11.034.

[150] Purohit Y, Sun L, Shenderova O, Scattergood RO, Brenner DW. First-principles-based mesoscale modeling of the solute-induced stabilization of ⟨100⟩ tilt grain boundaries in an Al–Pb alloy. Acta Mater 2011;59:7022–8. https://doi.org/10.1016/j.actamat.2011.07.056.
[151] Koju RK, Mishin Y. Relationship between grain boundary segregation and grain boundary diffusion in Cu-Ag alloys. PhysRevMaterials 2020;4:073403. https://doi.org/10.1103/PhysRevMaterials.4.073403.
[152] Koju RK, Mishin Y. Atomistic study of grain-boundary segregation and grain-boundary diffusion in Al-Mg alloys 2020.
[153] Mai HL, Cui X-Y, Scheiber D, Romaner L, Ringer SP. The segregation of transition metals to iron grain boundaries and their effects on cohesion. Acta Mater 2022;231:117902. https://doi.org/10.1016/j.actamat.2022.117902.
[154] Huber L, Hadian R, Grabowski B, Neugebauer J. A machine learning approach to model solute grain boundary segregation. Npj Comput Mater 2018;4:1–8. https://doi.org/10.1038/s41524-018-0122-7.
[155] Hu C, Luo J. Data-driven prediction of grain boundary segregation and disordering in high-entropy alloys in a 5D space. Mater Horiz 2022;9:1023–35. https://doi.org/10.1039/D1MH01204E.
[156] Jin H, Elfimov I, Militzer M. Study of the interaction of solutes with Σ5 (013) tilt grain boundaries in iron using density-functional theory. J Appl Phys 2014;115:093506. https://doi.org/10.1063/1.4867400.
[157] Mishin Y, Asta M, Li J. Atomistic modeling of interfaces and their impact on microstructure and properties. Acta Mater 2010;58:1117–51.
[158] LeSar R. Introduction to Computational Materials Science: Fundamentals to Applications. Cambridge University Press; 2013.
[159] Landau DP, Binder K. A Guide to Monte Carlo Simulations in Statistical Physics. Cambridge University Press; 2005.
[160] O'Brien CJ, Barr CM, Price PM, Hattar K, Foiles SM. Grain boundary phase transformations in PtAu and relevance to thermal stabilization of bulk nanocrystalline metals. J Mater Sci 2018;53:2911–27. https://doi.org/10.1007/s10853-017-1706-1.
[161] Kwiatkowski da Silva A, Ponge D, Peng Z, Inden G, Lu Y, Breen A, et al. Phase nucleation through confined spinodal fluctuations at crystal defects evidenced in Fe-Mn alloys. Nat Commun 2018;9:1–11. https://doi.org/10.1038/s41467-018-03591-4.
[162] Tytko D, Choi P-P, Klöwer J, Kostka A, Inden G, Raabe D. Microstructural evolution of a Ni-based superalloy (617B) at 700°C studied by electron microscopy and atom probe tomography. Acta Mater 2012;60:1731–40. https://doi.org/10.1016/j.actamat.2011.11.020.
[163] Stoffers A, Ziebarth B, Barthel J, Cojocaru-Mirédin O, Elsässer C, Raabe D. Complex Nanotwin Substructure of an Asymmetric $\mathrm{\ensuremath{\Sigma}}9$ Tilt Grain Boundary in a Silicon Polycrystal. PhysRevLett 2015;115:235502. https://doi.org/10.1103/PhysRevLett.115.235502.
[164] Cahn JW. The impurity-drag effect in grain boundary motion. Acta Metall 1962;10:789–98.
[165] Ma N, Dregia SA, Wang Y. Solute segregation transition and drag force on grain boundaries. Acta Mater 2003;51:3687–700.
[166] Toda-Caraballo I, Capdevila C, Pimentel G, De Andrés CG. Drag effects on grain growth dynamics. Comput Mater Sci 2013;68:95–106. https://doi.org/10.1016/j.commatsci.2012.10.012.
[167] Koju RK, Mishin Y. Direct atomistic modeling of solute drag by moving grain boundaries. Acta Mater 2020;198:111–20. https://doi.org/10.1016/j.actamat.2020.07.052.
[168] Hillert M. Solute drag, solute trapping and diffusional dissipation of Gibbs energy. Acta Mater 1999;47:4481–505.
[169] Hillert M, Odquist J, Agren J. Comparison between solute drag and dissipation of Gibbs energy by diffusion. Scripta Mater 2001;45:221–7.
[170] Kim SG, Park YB. Grain boundary segregation, solute drag and abnormal grain growth. Acta Mater 2008;56:3739–53.
[171] Mishin Y. Solute drag and dynamic phase transformations in moving grain boundaries. Acta Mater 2019;179:383–95.
[172] Koju RK, Mishin Y. The role of grain boundary diffusion in the solute drag effect. Nanomaterials 2021;11:2348. https://doi.org/10.3390/nano11092348.
[173] Suhane A, Scheiber D, Popov M, Razumovskiy VI, Romaner L, Militzer M. Solute drag assessment of grain boundary migration in Au. Acta Mater 2022;224:117473. https://doi.org/10.1016/j.actamat.2021.117473.
[174] Svoboda J, Fischer FD, Leindl M. Transient solute drag in migrating grain boundaries. Acta Mater 2011;59:6556–62.
[175] Mishin Y. Stochastic model and kinetic Monte Carlo simulation of solute interactions with stationary and moving grain boundaries. I. Model formulation and application to one-dimensional systems. PhysRevMater 2023;7:063403. https://doi.org/10.1103/PhysRevMaterials.7.063403.
[176] Mishin Y. Stochastic model and kinetic Monte Carlo simulation of solute interactions with stationary and moving grain boundaries. II. Application to two-dimensional systems. PhysRevMater 2023;7:063404. https://doi.org/10.1103/PhysRevMaterials.7.063404.
[177] Li W-B, Easterling KE. The influence of particle shape on Zener drag. Acta Metall Mater 1990;38:1045–52. https://doi.org/10.1016/0956-7151(90)90177-I.
[178] Koju RK, Darling KA, Kecskes LJ, Mishin Y. Zener Pinning of Grain Boundaries and Structural Stability of Immiscible Alloys. JOM 2016:1–9. https://doi.org/10.1007/s11837-016-1899-9.
[179] Manohar PA, Ferry M, Chandra T. Five decades of the Zener equation. ISIJ Int 1998;38:913–24.
[180] Miodownik M, Holm EA, Hassold GN. Highly parallel computer simulations of particle pinning: Zener vindicated. Scripta Mater 2000;42:1173–7.
[181] Nes E, Ryum N, Hunderi O. On the Zener drag. Acta Metall 1985;33:11–22.
[182] Prinzio CLD, Druetta E, Nasello OB. More about Zener drag studies with monte carlo simulations. Model Simul Mater Sci Eng 2013;21:025007.
[183] Zhou J, Li C, Guan M, Ren F, Wang X, Zhang S, et al. Zener pinning by coherent particles: pinning efficiency and particle reorientation mechanisms. Model Simul Mater Sci Eng 2017;25:065008.
[184] Koju RK, Darling KA, Solanki KN, Mishin Y. Atomistic modeling of capillary-driven grain boundary motion in Cu-Ta alloys. Acta Mater 2018;148:311–9. https://doi.org/10.1016/j.actamat.2018.01.027.
[185] Hornbuckle BC, Rojhirunsakool T, Rajagopalan M, Alam T, Pun GPP, Banerjee R, et al. Effect of Ta Solute Concentration on the Microstructural Evolution in Immiscible Cu-Ta Alloys. JOM 2015;67:2802–9. https://doi.org/10.1007/s11837-015-1643-x.
[186] Lücke K, Stüwe HP. On the theory of grain boundary motion. In: Himmel L, editor. Recovery and Recrystallization of Metals. New York: Interscience Publishers; 1963. p. 171–210.
[187] Li J, Wang J, Yang G. Phase field modeling of grain boundary migration with solute drag. Acta Mater 2009;57:2108–20.
[188] Greenwood M, Sinclair C, Militzer M. Phase field crystal model of solute drag. Acta Mater 2012;60:5752–61.
[189] Shahandeh S, Greenwood M, Militzer M. Friction pressure method for simulating solute drag and particle pinning in a multiphase-field model. Model Simul Mater Sci Eng 2012;20:065008.
[190] Grönhagen K, Agren J. Grain-boundary segregation and dynamic solute drag theory — A phase-field approach. Acta Mater 2007;55:955–60.
[191] Mendelev MI, Srolovitz DJ. Impurity effects on grain boundary migration. Model Simul Mater Sci Eng 2002;10:R79–.
[192] Mendelev MI, Srolovitz DJ. Kink model for extended defect migration in the presence of diffusing impurities: theory and simulation. Acta Mater 2001;49:2843–52. https://doi.org/10.1016/S1359-6454(01)00175-6.
[193] Mendelev MI, Srolovitz DJ. Domain wall migration in 3-d in the presence of diffusing impurities. Interface Sci 2002;10:243–50. https://doi.org/10.1023/A:1015888516805.
[194] Sun H, Deng C. Direct quantification of solute effects on grain boundary motion by atomistic simulations. Comp Mater Sci 2014;93:137–43.
[195] Rahman MJ, Zurob HS, Hoyt JJ. Molecular dynamics study of solute pinning effects on grain boundary migration in the aluminum magnesium alloy system. Metall Mater Trans A 2016;47:1889–97.
[196] Suzuki A, Mishin Y. Atomic mechanisms of grain boundary diffusion: Low versus high temperatures. J Mater Sci 2005;40:3155–61.
[197] Mishin Y. An atomistic view of grain boundary diffusion. Defect and Diffusion Forum 2015;363:1–11.
[198] Chesser I, Mishin Y. Point-defect avalanches mediate grain boundary diffusion. Commun Mater 2022;3:90. https://doi.org/10.1038/s43246-022-00314-7.
[199] Meiners T, Duarte JM, Richter G, Dehm G, Liebscher CH. Tantalum and zirconium induced structural transitions at complex [111] tilt grain boundaries in copper. Acta Mater 2020;190:93–104. https://doi.org/10.1016/j.actamat.2020.02.064.
[200] Darling KA, Kapoor M, Kotan H, Hornbuckle BC, Walck SD, Thompson GB, et al. Structure and mechanical properties of Fe–Ni–Zr oxide-dispersion-strengthened (ODS) alloys. J Nucl Mater 2015;467:205–13.
[201] Mula S, Bahmanpour H, Mal S, Kang PC, Atwater M, Jian W, et al. Thermodynamic feasibility of solid solubility extension of Nb in Cu and their thermal stability. Mater Sci Eng A 2012;539:330–6. https://doi.org/10.1016/j.msea.2012.01.104.

[202] Konrad H, Haubold T, Birringer R, Gleiter H. Nanostructured Cu-Bi alloys prepared by co-evaporation in a continuous gas flow. Nanostruct Mater 1996;7:605–10. https://doi.org/10.1016/0965-9773(96)00038-4.

[203] Melmed AJ, Tambakis NC, Lau M, Lavernia EJ. Apfim study of impurities in nanocrystalline Fe-Al alloy. Prog Surf Sci 1998;59:313–21. https://doi.org/10.1016/S0079-6816(98)00057-4.

[204] Perez RJ, Huang B, Lavernia EJ. Thermal stability of nanocrystalline Fe-10 wt.% Al produced by cryogenic mechanical alloying. Nanostruct Mater 1996;7:565–72. https://doi.org/10.1016/0965-9773(96)00020-7.

[205] Vo NQ, Schäfer J, Averback RS, Albe K, Ashkenazy Y, Bellon P. Reaching theoretical strengths in nanocrystalline Cu by grain boundary doping. Scr Mater 2011;65:660–3. https://doi.org/10.1016/j.scriptamat.2011.06.048.

[206] Frolov T, Darling KA, Kecskes LJ, Mishin Y. Stabilization and strengthening of nanocrystalline copper by alloying with tantalum. Acta Mater 2012;60:2158–68.

[207] Rajgarhia RK, Saxena A, Spearot DE, Hartwig KT, More KL, Kenik EA, et al. Microstructural stability of copper with antimony dopants at grain boundaries: experiments and molecular dynamics simulations. J Mater Sci 2010;45:6707–18. https://doi.org/10.1007/s10853-010-4764-1.

[208] VanLeeuwen BK, Darling KA, Koch CC, Scattergood RO, Butler BG. Thermal stability of nanocrystalline Pd81Zr19. Acta Mater 2010;58:4292–7.

[209] Atwater MA, Scattergood RO, Koch CC. The stabilization of nanocrystalline copper by zirconium. Mater Sci Eng A 2013;559:250–6. https://doi.org/10.1016/j.msea.2012.08.092.

[210] Eckert J, Holzer JC, Johnson WL. Thermal stability and grain growth behavior of mechanically alloyed nanocrystalline Fe-Cu alloys. J Appl Phys 1993;73:131–41. https://doi.org/10.1063/1.353890.

[211] Thuvander M, Abraham M, Cerezo A, Smith GDW. Thermal stability of electrodeposited nanocrystalline nickel and iron–nickel alloys. Mater Sci Technol 2001;17:961–70. https://doi.org/10.1179/026708301101510799.

[212] Kotan H, Saber M, Koch CC, Scattergood RO. Effect of annealing on microstructure, grain growth, and hardness of nanocrystalline Fe–Ni alloys prepared by mechanical alloying. Mater Sci Eng A 2012;552:310–5. https://doi.org/10.1016/j.msea.2012.05.045.

[213] Liu F. Grain growth in nanocrystalline Fe–Ag thin film. Mater Lett 2005;59:1458–62. https://doi.org/10.1016/j.matlet.2005.01.003.

[214] Gupta R, Singh Raman RK, Koch CC. Grain growth behaviour and consolidation of ball-milled nanocrystalline Fe–10Cr alloy. Mater Sci Eng A 2008;494:253–6. https://doi.org/10.1016/j.msea.2008.04.019.

[215] Darling KA, VanLeeuwen BK, Koch CC, Scattergood RO. Thermal stability of nanocrystalline Fe–Zr alloys. Mater Sci Eng A 2010;527:3572–80.

[216] Dake JM, Krill CE. Sudden loss of thermal stability in Fe-based nanocrystalline alloys. Scr Mater 2012;66:390–3. https://doi.org/10.1016/j.scriptamat.2011.11.040.

[217] Huang B, Perez RJ, Lavernia EJ. Grain growth of nanocrystalline Fe–Al alloys produced by cryomilling in liquid argon and nitrogen. Mater Sci Eng A 1998;255:124–32. https://doi.org/10.1016/S0921-5093(98)00765-5.

[218] Atwater MA, Roy D, Darling KA, Butler BG, Scattergood RO, Koch CC. The thermal stability of nanocrystalline copper cryogenically milled with tungsten. Mater Sci Eng A 2012;558:226–33.

[219] Zhu M, Wu ZF, Zeng MQ, Ouyang LZ, Gao Y. Bimodal growth of the nanophases in the dual-phase composites produced by mechanical alloying in immiscible Cu–Ag system. J Mater Sci 2008;43:3259–66. https://doi.org/10.1007/s10853-008-2545-x.

[220] Botcharova E, Freudenberger J, Schultz L. Mechanical alloying of copper with niobium and molybdenum. J Mater Sci 2004;39:5287–90. https://doi.org/10.1023/B:JMSC.0000039230.73188.5d.

[221] Vo NQ, Chee SW, Schwen D, Zhang X, Bellon P, Averback RS. Microstructural stability of nanostructured Cu alloys during high-temperature irradiation. Scr Mater 2010;63:929–32. https://doi.org/10.1016/j.scriptamat.2010.07.009.

[222] Tan LK, Li Y, Ng SC, Lu L. Structures, properties and responses to heat treatment of Cu–Y alloys prepared by mechanical alloying. J Alloy Compd 1998;278:201–8. https://doi.org/10.1016/S0925-8388(98)00487-3.

[223] Rafailović LD, Artner W, Nauer GE, Minić DM. Structure, morphology and thermal stability of electrochemically obtained Ni–Co deposits. Thermochim Acta 2009;496:110–6. https://doi.org/10.1016/j.tca.2009.07.007.

[224] Rajagopalan M, Darling K, Turnage S, Koju R, Hornbuckle B, Mishin Y, et al. Microstructural evolution in a nanocrystalline Cu-Ta alloy: A combined in-situ TEM and atomistic study. Mater Des 2017;113:178–85.

[225] Turnage SA, Rajagopalan M, Darling KA, Garg P, Kale C, Bazehhour BG, et al. Anomalous mechanical behavior of nanocrystalline binary alloys under extreme conditions. Nat Commun 2018;9:2699. https://doi.org/10.1038/s41467-018-05027-5.

[226] Hornbuckle BC, Kale C, Srinivasan S, Luckenbaugh TL, Solanki KN, Darling KA. Revealing cryogenic mechanical behavior and mechanisms in a microstructurally-stable, immiscible nanocrystalline alloy. Scr Mater 2019;160:33–8. https://doi.org/10.1016/j.scriptamat.2018.09.035.

[227] Hornbuckle BC, Williams CL, Dean SW, Zhou X, Kale C, Turnage SA, et al. Stable microstructure in a nanocrystalline copper–tantalum alloy during shock loading. Communications Materials 2020;1:1–6. https://doi.org/10.1038/s43246-020-0024-3.

[228] Hornbuckle BC, Dean SW, Zhou X, Giri AK, Williams CL, Solanki KN, et al. Laser shocking of nanocrystalline materials: Revealing the extreme pressure effects on the microstructural stability and deformation response. Appl Phys Lett 2020;116:231901. https://doi.org/10.1063/5.0008107.

[229] Darling KA, Srinivasan S, Koju RK, Hornbuckle BC, Smeltzer J, Mishin Y, et al. Stress-driven grain refinement in a microstructurally stable nanocrystalline binary alloy. Scr Mater 2021;191:185–90. https://doi.org/10.1016/j.scriptamat.2020.09.041.

[230] Kale C, Srinivasan S, Hornbuckle BC, Koju RK, Darling K, Mishin Y, et al. An experimental and modeling investigation of tensile creep resistance of a stable nanocrystalline alloy. Acta Mater 2020;199:141–54. https://doi.org/10.1016/j.actamat.2020.08.020.

[231] Srinivasan S, Sharma S, Turnage S, Hornbuckle BC, Kale C, Darling KA, et al. Role of tantalum concentration, processing temperature, and strain-rate on the mechanical behavior of copper-tantalum alloys. Acta Mater 2021;208:116706. https://doi.org/10.1016/j.actamat.2021.116706.

[232] Srinivasan S, Hornbuckle BC, Darling KA, Kim H, Wang YQ, Solanki K. Helium partitioning to the core-shelled Ta nanoclusters in nanocrystalline Cu-Ta alloy. Scr Mater 2022;208:114344. https://doi.org/10.1016/j.scriptamat.2021.114344.

[233] Hornbuckle BC, Solanki K, Darling KA. Prolonged high-temperature exposure: Tailoring nanocrystalline Cu–Ta alloys against grain growth. Mater Sci Eng A 2021;824:141818. https://doi.org/10.1016/j.msea.2021.141818.

[234] Rajagopalan M, Darling KA, Kale C, Turnage SA, Koju RK, Hornbuckle BC, et al. Nanotechnology enabled design of a structural material with extreme strength as well as thermal and electrical properties. Mater Today 2019;31:10–20. https://doi.org/10.1016/j.mattod.2019.09.024.

[235] Marvel CJ, Hornbuckle BC, Smeltzer JA, Darling KA, Harmer MP. Athermal behavior of core-shell particles in nanocrystalline Cu-Ta. Scr Mater 2020;188:69–73. https://doi.org/10.1016/j.scriptamat.2020.07.014.

[236] Ostlind A, Fudger SJ, Luckenbaugh TL, Roberts AJ, Aniska M, Hornbuckle BC, et al. Scalable synthesis of a bulk nanocrystalline material with a multitude of divergent properties through a traditional manufacturing process. Mater Today Commun 2022;33:104390. https://doi.org/10.1016/j.mtcomm.2022.104390.

[237] Rojhirunsakool T, Darling KA, Tschopp MA, Pun GPP, Mishin Y, Banerjee R, et al. Structure and thermal decomposition of a nanocrystalline mechanically alloyed supersaturated Cu-Ta solid solution. MRS Commun 2015;5:333.

[238] Hammond VH, Luckenbaugh TL, Aniska M, Gray DM, Smeltzer JA, Hornbuckle BC, et al. An Insight into Machining of Thermally Stable Bulk Nanocrystalline Metals. Adv Eng Mater 2018;20:1800405.

[239] Darling KA, Roberts AJ, Mishin Y, Mathaudhu SN, Kecskes LJ. Grain size stabilization of nanocrystalline copper at high temperatures by alloying with tantalum. J Alloy Compd 2013;573:142–50. https://doi.org/10.1016/j.jallcom.2013.03.177.

[240] Darling KA, Huskins EL, Schuster BE, Wei Q, Kecskes LJ. Mechanical properties of a high strength Cu–Ta composite at elevated temperature. Mater Sci Eng A 2015;638:322–8. https://doi.org/10.1016/j.msea.2015.04.069.

[241] Casem D, Ligda J, Walter T, Darling K, Hornbuckle B. Strain-Rate Sensitivity of Nanocrystalline Cu–10Ta to 700,000/s. J Dynamic Behavior Mater 2019. https://doi.org/10.1007/s40870-019-00223-w.

[242] Darling KA, Tschopp MA, Guduru RK, Yin WH, Wei Q, Kecskes LJ. Microstructure and mechanical properties of bulk nanostructured Cu–Ta alloys consolidated by equal channel angular extrusion. Acta Mater 2014;76:168–85. https://doi.org/10.1016/j.actamat.2014.04.074.

[243] Kale C, Turnage S, Garg P, Adlakha I, Srinivasan S, Hornbuckle B, et al. Thermo-mechanical strengthening mechanisms in a stable nanocrystalline binary alloy–A combined experimental and modeling study. Mater Des 2019;163:107551.
[244] Bhatia M, Rajagopalan M, Darling K, Tschopp M, Solanki K. The role of Ta on twinnability in nanocrystalline Cu–Ta alloys. Materials Research Letters 2017;5:48–54.
[245] Darling KA, VanLeeuwen BK, Semones JE, Koch CC, Scattergood RO, Kecskes LJ, et al. Stabilized nanocrystalline iron-based alloys: Guiding efforts in alloy selection. Mater Sci Eng A 2011;528:4365–71.
[246] Odette GR, Alinger MJ, Wirth BD. Recent developments in irradiation-resistant steels. Annu Rev Mater Res 2008;38:471–503. https://doi.org/10.1146/annurev.matsci.38.060407.130315.
[247] Hayashi T, Sarosi PM, Schneibel JH, Mills MJ. Creep response and deformation processes in nanocluster-strengthened ferritic steels. Acta Mater 2008;56:1407–16. https://doi.org/10.1016/j.actamat.2007.11.038.
[248] Miller MK, Parish CM, Li Q. Advanced oxide dispersion strengthened and nanostructured ferritic alloys. Mater Sci Technol 2013;29:1174–8. https://doi.org/10.1179/1743284713Y.0000000207.
[249] de Castro V, Leguey T, Muñoz A, Monge MA, Fernández P, Lancha AM, et al. Mechanical and microstructural behaviour of Y2O3 ODS EUROFER 97. J Nucl Mater 2007;367–370:196–201. https://doi.org/10.1016/j.jnucmat.2007.03.146.
[250] Mao X, Kim TK, Kim SS, Oh KH, Jang J. Thermal stability of oxide particles in 12Cr ODS steel. J Nucl Mater 2012;428:82–9. https://doi.org/10.1016/j.jnucmat.2011.09.011.
[251] Yamashita * S, Ohtsuka S, Akasaka N, Ukai S, Ohnuki S. Formation of nanoscale complex oxide particles in mechanically alloyed ferritic steel. Philos Mag Lett 2004;84:525–9. https://doi.org/10.1080/09500830412331303609.
[252] Hsiung LL, Fluss MJ, Tumey SJ, Choi BW, Serruys Y, Willaime F, et al. Formation mechanism and the role of nanoparticles in Fe-Cr ODS steels developed for radiation tolerance. PhysRevB 2010;82:184103. https://doi.org/10.1103/PhysRevB.82.184103.
[253] Saber M, Xu W, Li L, Zhu Y, Koch CC, Scattergood RO. Size effect of primary Y2O3 additions on the characteristics of the nanostructured ferritic ODS alloys: Comparing as-milled and as-milled/annealed alloys using S/TEM. J Nucl Mater 2014;452:223–9. https://doi.org/10.1016/j.jnucmat.2014.05.014.
[254] Zhang X, Hu T, Rufner JF, LaGrange TB, Campbell GH, Lavernia EJ, et al. Metal/ceramic interface structures and segregation behavior in aluminum-based composites. Acta Mater 2015;95:254–63. https://doi.org/10.1016/j.actamat.2015.05.021.
[255] Ye J, Han BQ, Lee Z, Ahn B, Nutt SR, Schoenung JM. A tri-modal aluminum based composite with super-high strength. Scr Mater 2005;53:481–6. https://doi.org/10.1016/j.scriptamat.2005.05.004.
[256] Zhang H, Ye J, Joshi SP, Schoenung JM, Chin ESC, Ramesh KT. Rate-dependent behavior of hierarchical Al matrix composites. Scr Mater 2008;59:1139–42. https://doi.org/10.1016/j.scriptamat.2008.07.036.
[257] Li Y, Zhao YH, Ortalan V, Liu W, Zhang ZH, Vogt RG, et al. Investigation of aluminum-based nanocomposites with ultra-high strength. Mater Sci Eng A 2009;527:305–16. https://doi.org/10.1016/j.msea.2009.07.067.
[258] Li Y, Zhang Z, Vogt R, Schoenung JM, Lavernia EJ. Boundaries and interfaces in ultrafine grain composites. Acta Mater 2011;59:7206–18. https://doi.org/10.1016/j.actamat.2011.08.005.
[259] Witkin D, Lee Z, Rodriguez R, Nutt S, Lavernia E. Al–Mg alloy engineered with bimodal grain size for high strength and increased ductility. Scr Mater 2003;49:297–302. https://doi.org/10.1016/S1359-6462(03)00283-5.
[260] Fang TH, Li WL, Tao NR, Lu K. Revealing Extraordinary Intrinsic Tensile Plasticity in Gradient Nano-Grained Copper. Science 2011. https://doi.org/10.1126/science.1200177.
[261] Vogt RG, Zhang Z, Topping TD, Lavernia EJ, Schoenung JM. Cryomilled aluminum alloy and boron carbide nano-composite plate. J Mater Process Technol 2009;209:5046–53. https://doi.org/10.1016/j.jmatprotec.2009.02.002.
[262] Amram D, Schuh CA. Interplay between thermodynamic and kinetic stabilization mechanisms in nanocrystalline Fe-Mg alloys. Acta Mater 2018;144:447–58.
[263] Ebrahimi F, Li H. Grain growth in electrodeposited nanocrystalline fcc Ni–Fe alloys. Scr Mater 2006;55:263–6. https://doi.org/10.1016/j.scriptamat.2006.03.053.
[264] Li HQ, Ebrahimi F. An investigation of thermal stability and microhardness of electrodeposited nanocrystalline nickel-21% iron alloys. Acta Mater 2003;51:3905–13. https://doi.org/10.1016/S1359-6454(03)00215-5.
[265] Czerwinski F, Li H, Megret M, Szpunar JA, Clark DG, Erb U. The evolution of texture and grain size during annealing of nanocrystalline ni-45% fe electrodeposits. Scr Mater 1997;37:1967–72. https://doi.org/10.1016/S1359-6462(97)00390-4.
[266] Farber B, Cadel E, Menand A, Schmitz G, Kirchheim R. Phosphorus segregation in nanocrystalline Ni–3.6 at.% P alloy investigated with the tomographic atom probe (TAP). Acta Mater 2000;48:789–96. https://doi.org/10.1016/S1359-6454(99)00397-3.
[267] Pellicer E, Varea A, Sivaraman KM, Pané S, Suriñach S, Baró MD, et al. Grain Boundary Segregation and Interdiffusion Effects in Nickel–Copper Alloys: An Effective Means to Improve the Thermal Stability of Nanocrystalline Nickel. ACS Appl Mater Interfaces 2011;3:2265–74. https://doi.org/10.1021/am2004587.
[268] Talin AA, Marquis EA, Goods SH, Kelly JJ, Miller MK. Thermal stability of Ni–Mn electrodeposits. Acta Mater 2006;54:1935–47. https://doi.org/10.1016/j.actamat.2005.12.027.
[269] Yang X, Liu S, Wei X, Pan B. Effects of annealing on the structure and microhardness of nanocrystalline Ni–Mn electrodeposits. J Alloy Compd 2023;960:170732. https://doi.org/10.1016/j.jallcom.2023.170732.
[270] Rajulapati KV, Scattergood RO, Murty KL, Duscher G, Koch CC. Effect of Pb on the mechanical properties of nanocrystalline Al. Scr Mater 2006;55:155.
[271] Wu ZF, Zeng MQ, Ouyang LZ, Zhang XP, Zhu M. Ostwald ripening of Pb nanocrystalline phase in mechanically milled Al-Pb alloys and the influence of Cu additive. Scr Mater 2005;53:529.
[272] Zhou F, Liao XZ, Zhu YT, Dallek S, Lavernia EJ. Microstructural evolution during recovery and recrystallization of a nanocrystalline Al-Mg alloy prepared by cryogenic ball milling. Acta Mater 2003;51.
[273] Hueller M, Vlcek J, Dinkel M, Hoeppel HW, Goeken M. Hardening and thermal stability of nanocrystalline AlMg4.8 powder. Phil Mag 2008;88.
[274] Zhu CJ, Ma XF, Zhao W, Tang HG, Yan JM, Cai SG. Synthesis and thermal stability of A175W25 alloy obtained by mechanically alloying. J Alloy Compd 2005;393:248.
[275] Fogagnolo JB, Amador D, Ruiz-Navas EM, Torralba JM. Solid solution in AI-4.5 wt% Cu produced by mechanical alloying. Mater Sci Eng A-Struct Mater Proper Microstruct Process 2006;433:45.
[276] Bryden KJ, Ying JY. Electrodeposition synthesis and hydrogen absorption properties of nanostructured palladium-iron alloys. Nanostruct Mater 1997;9:485.
[277] Bryden KJ, Ying JY. Pulsed electrodeposition synthesis and hydrogen absorption properties of nanostructured palladium-iron alloy films. J Electrochem Soc 1998;145:3339.
[278] Bryden KJ, Ying JY. Thermal stability and hydrogen absorption characteristics of palladium-yttrium nanoalloys. Acta Mater 1996;44:3847.
[279] Zhang Z, Guo J, Dehm G, Pippan R. In-situ tracking the structural and chemical evolution of nanostructured CuCr alloys. Acta Mater 2017;138:42–51. https://doi.org/10.1016/j.actamat.2017.07.039.
[280] Moon IH, Ryu S-S, Kim S-W, Won DM, Jang WS. Grain Growth in the Nanocrystalline W–Cu and Cu–Pb Composite Powders Prepared by Mechanical Alloying. Int J Mater Res 2001;92:986–94. https://doi.org/10.1515/ijmr-2001-0177.
[281] Liu KW, Mücklich F. Thermal stability of nano-RuAl produced by mechanical alloying. Acta Mater 2001;49:395–403. https://doi.org/10.1016/S1359-6454(00)00340-2.
[282] Abe YR, Johnson WL. Stability of Nanocrystalline Structures in the Ti-Cu System. Mechanical Alloying, vol. 88, Trans Tech Publications Ltd; 1992, p. 513–20. Doi: 10.4028/www.scientific.net/MSF.88-90.513.
[283] Weissmüller J, Krauss W, Haubold T, Birringer R, Gleiter H. Atomic structure and thermal stability of nanostructured Y-Fe alloys. Nanostruct Mater 1992;1:439–47. https://doi.org/10.1016/0965-9773(92)90076-A.

[284] Terwilliger CD, Chiang Y-M. Size-dependent solute segregation and total solubility in ultrafine polycrystals: Ca in TiO2. Acta Metall Mater 1995;43:319–28. https://doi.org/10.1016/0956-7151(95)90288-0.
[285] Unraveling Thermodynamic and Kinetic Contributions to the Stability of Doped Nanocrystalline Alloys using Nanometallic Multilayers - Cunningham - 2022 - Advanced Materials - Wiley Online Library n.d. https://onlinelibrary.wiley.com/doi/full/10.1002/adma.202200354 (accessed September 16, 2023).
[286] Choi P, da Silva M, Klement U, Al-Kassab T, Kirchheim R. Thermal stability of electrodeposited nanocrystalline Co-1.1at.%P. Acta Mater 2005;53:4473.
[287] da Silva M, Wille C, Klement U, Choi P, Al-Kassab T. Electrodeposited nanocrystalline Co-P alloys: Microstructural characterization and thermal stability. Mater Sci Eng A 2007;445–446:31.
[288] Tsyntsaru N, Cesiulis H, Budreika A, Ye X, Juskenas R, Celis JP. The effect of electrodeposition conditions and post-annealing on nanostructure of Co-W coatings. Surf Coat Technol 2012;206:4262.
[289] Chen H, Zuo J-M. Structure and phase separation of Ag–Cu alloy thin films. Acta Mater 2007;55:1617–28. https://doi.org/10.1016/j.actamat.2006.10.036.
[290] Rouya E, Stafford GR, Bertocci U, Mallett JJ, Schad R, Begley MR, et al. Electrodeposition of Metastable Au-Ni Alloys. J Electrochem Soc 2010;157:D396.
[291] Naka M, Shibayanagi T, Maeda M, Mori M, Mori H. Thermal stability of nanostructured Cr-Ni alloys. Vacuum 2004;73:619.
[292] Alfantazi AM, Page J, Erb U. Pulse plating of Zn-Ni alloy coatings. J Appl Electrochem 1996;26:1225.
[293] Alfantazi AM, Erb U. Microhardness and thermal stability of pulse-plated Zn-Ni alloy coatings. Materials Science and Engineering A-Structural Materials Properties Microstructure and Processing 1996;212.
[294] Abe YR, Holzer JC, Johnson WL. Formation and stability of nanocrystalline Nb-Cu alloys. Symposium on Structure and Properties of Interfaces in Materials, at the 1991 Fall Meeting of the Materials Research Society, vol. 238, Boston, MA: 1991, p. 721.
[295] Zhou X, Darvishi Kamachali R, Boyce BL, Clark BG, Raabe D, Thompson GB. Spinodal Decomposition in Nanocrystalline Alloys. Acta Mater 2021;215:117054. https://doi.org/10.1016/j.actamat.2021.117054.
[296] Priedeman JL, Thompson GB. The influence of alloying in stabilizing a faceted grain boundary structure. Acta Mater 2020;201:329–40. https://doi.org/10.1016/j.actamat.2020.09.085.
[297] Herbig M, Raabe D, Li YJ, Choi P, Zaefferer S, Goto S. Atomic-Scale Quantification of Grain Boundary Segregation in Nanocrystalline Material. PhysRevLett 2014;112:126103. https://doi.org/10.1103/PhysRevLett.112.126103.
[298] Thompson GB, Kapoor M, Kaub T, Boyce B, Clarke B, Darling K, et al. Investigation into solute stabilizing effects in nanocrystalline materials: an atom probe characterization study. Microsc Microanal 2015;21:357–8.
[299] Chen Z, Liu F, Wang HF, Yang W, Yang GC, Zhou YH. A thermokinetic description for grain growth in nanocrystalline materials. Acta Mater 2009;57:1466–75.
[300] Gong MM, Liu F, Zhang K. A thermokinetic description of nanoscale grain growth: Analysis of initial grain boundary excess amount. Scr Mater 2010;63:989–92.
[301] Koch CC, Scattergood RO, Saber M, Kotan H. High temperature stabilization of nanocrystalline grain size: Thermodynamic versus kinetic strategies. J Mater Res 2013;28:1785–91. https://doi.org/10.1557/jmr.2012.429.
[302] Tschopp MA, Hernández-Rivera E, Atwater MA, Solanki KN, Darling KA. A thermodynamic and kinetic-based grain growth model for nanocrystalline materials: Parameter sensitivity analysis and model extension. Comput Mater Sci 2017;131:250–65. https://doi.org/10.1016/j.commatsci.2017.02.002.
[303] Kapoor M, Kaub T, Darling KA, Boyce BL, Thompson GB. An atom probe study on Nb solute partitioning and nanocrystalline grain stabilization in mechanically alloyed Cu-Nb. Acta Mater 2017;126:564–75.
[304] Marvel CJ, Hornbuckle BC, Darling KA, Harmer MP. Intentional and unintentional elemental segregation to grain boundaries in a Ni-rich nanocrystalline alloy. J Mater Sci 2019;54:3496–508.
[305] Marvel CJ, Smeltzer JA, Hornbuckle BC, Darling KA, Harmer MP. On the reduction and effect of non-metallic impurities in mechanically alloyed nanocrystalline Ni-W alloys. Acta Mater 2020;200:12–23.
[306] Rajagopalan M, Tschopp MA, Solanki KN. Grain Boundary Segregation of Interstitial and Substitutional Impurity Atoms in Alpha-Iron. JOM 2014;66:129–38. https://doi.org/10.1007/s11837-013-0807-9.
[307] Solanki KN, Tschopp MA, Bhatia MA, Rhodes NR. Atomistic investigation of the role of grain boundary structure on hydrogen segregation and embrittlement in α-Fe. Metall and Mat Trans A 2013;44:1365–75. https://doi.org/10.1007/s11661-012-1430-z.
[308] Adlakha I, Solanki KN. Structural stability and energetics of grain boundary triple junctions in face centered cubic materials. Sci Rep 2015;5. https://doi.org/10.1038/srep08692.
[309] Rajagopalan M, Adlakha I, Tschopp MA, Solanki KN. Energetics of Hydrogen Segregation to α-Fe Grain Boundaries for Modeling Stress Corrosion Cracking. JOM 2017;69:1398–403. https://doi.org/10.1007/s11837-017-2386-7.
[310] Kaur I, Mishin Y, Gust W. Fundamentals of Grain and Interphase Boundary Diffusion. 3rd ed. Wiley; 1995.
[311] Zhou X, Schuler JD, Grigorian CM, Tweddle D, Rupert TJ, Li L, et al. Influence and comparison of contaminate partitioning on nanocrystalline stability in sputter-deposited and ball-milled Cu–Zr alloys. J Mater Sci 2020;55:16758–79. https://doi.org/10.1007/s10853-020-05135-y.
[312] Grigorian CM, Rupert TJ. Thick amorphous complexion formation and extreme thermal stability in ternary nanocrystalline Cu-Zr-Hf alloys. Acta Mater 2019;179:172–82. https://doi.org/10.1016/j.actamat.2019.08.031.
[313] Xing W, Kube SA, Kalidindi AR, Amram D, Schroers J, Schuh CA. Stability of ternary nanocrystalline alloys in the Pt–Pd–Au system. Materialia 2019;8:100449. https://doi.org/10.1016/j.mtla.2019.100449.
[314] Sikdar K, Mahata A, Roy B, Roy D. Hybrid thermal stabilization of Zr doped nanocrystalline Cu. Mater Des 2019;164:107564. https://doi.org/10.1016/j.matdes.2018.107564.
[315] Bachmaier A, Pfaff M, Stolpe M, Aboulfadl H, Motz C. Phase separation of a supersaturated nanocrystalline Cu–Co alloy and its influence on thermal stability. Acta Mater 2015;96:269–83. https://doi.org/10.1016/j.actamat.2015.05.053.
[316] Gottstein G, Shvindlerman LS. Grain Boundary Migration in Metals. Bota Raton: CRC Press; 1999.
[317] Upmanyu M, Smith RW, Srolovitz DJ. Atomistic simulation of curvature driven grain boundary migration. Interface Sci 1998;6:41–58.
[318] Zhang H, Upmanyu M, Srolovitz DJ. Curvature driven grain boundary migration in aluminum: molecular dynamics simulations. Acta Mater 2005;53:79–86.
[319] Trautt ZT, Mishin Y. Grain boundary migration and grain rotation studied by molecular dynamics. Acta Mater 2012;60:2407–24.
[320] Rohrer GS, Chesser I, Krause AR, Naghibzadeh SK, Xu Z, Dayal K, et al. Grain Boundary Migration in Polycrystals. Annu Rev Mater Res 2023;53:347–69. https://doi.org/10.1146/annurev-matsci-080921-091511.
[321] Bhattacharya A, Shen Y-F, Hefferan CM, Li SF, Lind J, Suter RM, et al. Grain boundary velocity and curvature are not correlated in Ni polycrystals. Science 2021;374:189–93. https://doi.org/10.1126/science.abj3210.
[322] Muralikrishnan V, Liu H, Yang L, Conry B, Marvel CJ, Harmer MP, et al. Observations of unexpected grain boundary migration in SrTiO3. Scr Mater 2023;222:115055. https://doi.org/10.1016/j.scriptamat.2022.115055.
[323] Lyu M, Xu Z, Rohrer GS, Holm EA. Comparing molecular dynamics simulations of grain growth with experimental data. Scr Mater 2025;256:116429. https://doi.org/10.1016/j.scriptamat.2024.116429.
[324] Xu Z, Hefferan CM, Li SF, Lind J, Suter RM, Abdeljawad F, et al. Energy dissipation by grain boundary replacement during grain growth. Scr Mater 2023;230:115405. https://doi.org/10.1016/j.scriptamat.2023.115405.
[325] Li J, Wang J, Yang G. On the stagnation of grain growth in nanocrystalline materials. Scr Mater 2009;60:945–8. https://doi.org/10.1016/j.scriptamat.2009.02.015.
[326] Holm EA, Foiles SM. How grain growth stops: a mechanism for grain-growth stagnation in pure materials. Science 2010;328:1138–41.
[327] Rabkin E, Srolovitz DJ. Grain growth stagnation in thin films due to shear-coupled grain boundary migration. Scr Mater 2020;180:83–7. https://doi.org/10.1016/j.scriptamat.2020.01.019.
[328] Zhang J, Ludwig W, Zhang Y, Sørensen HHB, Rowenhorst DJ, Yamanaka A, et al. Grain boundary mobilities in polycrystals. Acta Mater 2020;191:211–20. https://doi.org/10.1016/j.actamat.2020.03.044.
[329] Homer E.R. ODL Holm EA, Foiles SM. Trends in grain boundary mobility: survey of motion mechanisms. JOM 2014;66:114–20.

[330] Karma A, Trautt ZT, Mishin Y. Relationship between equilibrium fluctuations and shear-coupled motion of grain boundaries. Phys Rev Lett 2012;109:095501.
[331] Baruffi C, Curtin WA. Theory of spontaneous grain boundary roughening in high entropy alloys. Acta Mater 2022;234:118011. https://doi.org/10.1016/j.actamat.2022.118011.
[332] Olmsted DL, Foiles SM, Holm EA. Grain boundary interface roughening transition and its effect on grain boundary mobility for non-faceting boundaries. Scripta Mater 2007;57:1161–4.
[333] Cahn JW. Transitions and phase equilibria among grain boundary structures. J Physique Colloques 1982;43:199–213.
[334] Cahn JW, Mishin Y, Suzuki A. Coupling grain boundary motion to shear deformation. Acta Mater 2006;54:4953–75. https://doi.org/10.1016/j.actamat.2006.08.004.
[335] Upmanyu M, Srolovitz DJ, Shvindlerman LS, Gottstein G. Molecular dynamics simulation of triple junction migration. Acta Mater 2002;50:1405–20.
[336] Chen Y, Schuh CA. Contribution of triple junctions to the diffusion anomaly in nanocrystalline materials. Scripta Mater 2007;57:253–6.
[337] Frolov T, Mishin Y. Molecular dynamics modeling of self-diffusion along triple junctions. Phys Rev m B 2009;79:174110.
[338] Hashibon A, Elsässer C. Approaches to atomistic triple-line properties from first-principles. Scripta Mater 2010;62:939–44.
[339] King AH. Triple lines in materials science and engineering. Scripta Mater 2010;62:889–93.
[340] Olives J. Surface thermodynamics, surface stress, equations at surfaces and triple lines for deformable bodies. J Phys: Condens Matter 2010;22:085005.
[341] Zhao B, Gottstein G, Shvindlerman LS. Triple junction effects in solids. Acta Mater 2011;59:3510–8.
[342] Adlakha I, Solanki KN. Atomic-scale investigation of triple junction role on defects binding energetics and structural stability in α-Fe. Acta Mater 2016;118:64–76. https://doi.org/10.1016/j.actamat.2016.07.026.
[343] Czubayko U, Sursaeva VG, Gottstein G, Shvindlerman LS. Acta Mater 1998;46:5863.
[344] Gottstein G, Ma Y, Shvindlerman LS. Triple junction motion and grain microstructure evolution. Acta Mater 2005;53:1535–44. https://doi.org/10.1016/j.actamat.2004.12.006.
[345] Portavoce A, Chow L, Bernardini J. Triple-junction contribution to diffusion in nanocrystalline Si. Appl Phys Lett 2010;96:214102.
[346] Lacon F, Radetic T, Dahmen U. Stability of the chevron domain at triple-line reconstructions. Phys Rev m B 2004;69:172102.
[347] Fedorov AA, Gutkin MY, Ovid'ko IA. Triple junction diffusion and plastic flow in fine-grained materials. Scripta Mater 2002;47:51–5.
[348] Straumal BB, Kogtenkova OA, Gornakova AS, Sursaeva VG, Baretzky B. Review: grain boundary faceting–roughening phenomena. J Mater Sci 2016;51:382–404. https://doi.org/10.1007/s10853-015-9341-1.
[349] Tuchinda N, Schuh CA. Triple junction excess energy in polycrystalline metals. Acta Mater 2024;279:120274. https://doi.org/10.1016/j.actamat.2024.120274.
[350] Chen Y, Zhu Q, Han J, Huang T, Zhang Z, Wang J. Stress-driven triple junction reconstruction facilitates cooperative grain boundary deformation. Acta Mater 2025;283:120565. https://doi.org/10.1016/j.actamat.2024.120565.
[351] Gottstein G, King AH, Shvindlerman LS. The effect of triple-junction drag on grain growth. Acta Mater 2000;48:397–403. https://doi.org/10.1016/S1359-6454(99)00373-0.
[352] Thomas SL, Wei C, Han J, Xiang Y, Srolovitz DJ. Disconnection description of triple-junction motion. Proc Natl Acad Sci 2019;116:8756–65. https://doi.org/10.1073/pnas.1820789116.
[353] Mattissen D, Molodov DA, Shvindlerman LS, Gottstein G. Drag effect of triple junctions on grain boundary and grain growth kinetics in aluminium. Acta Mater 2005;53:2049–57. https://doi.org/10.1016/j.actamat.2005.01.016.
[354] Zöllner D. Triple junction controlled grain growth in thin films. Comput Mater Sci 2021;187:110104. https://doi.org/10.1016/j.commatsci.2020.110104.
[355] Streitenberger P, Zöllner D. Triple junction controlled grain growth in two-dimensional polycrystals and thin films: Self-similar growth laws and grain size distributions. Acta Mater 2014;78:114–24. https://doi.org/10.1016/j.actamat.2014.06.022.
[356] MacPherson RD, Srolovitz DJ. The von Neumann relation generalized to coarsening of three-dimensional microstructures. Nature 2007;446:1053–5. https://doi.org/10.1038/nature05745.
[357] Schimmele L, Napiórkowski M, Dietrich S. Conceptual aspects of line tensions. J Chem Phys 2007;127:164715. https://doi.org/10.1063/1.2799990.
[358] Frolov T, Mishin Y. Phases, phase equilibria, and phase rules in low-dimensional systems. J Chem Phys 2015;143:044706.
[359] Fortes MA. Stability and dissociation of quadruple junctions in polycrystals. Interface Sci 1993;1:147–55. https://doi.org/10.1007/BF00203604.
[360] Hu N, Huang Y, Wang K, Hu W, Zhu W, Chen J, et al. Roles of triple and quadruple junctions on plasticity by phase-field crystal approach. Phys B Condens Matter 2022;626:413449. https://doi.org/10.1016/j.physb.2021.413449.
[361] Frolov T, Asta M, Mishin Y. Phase transformations at interfaces: Observations from atomistic modeling. Curr Opin Solid State Mater Sci 2016;20:308–15.
[362] Korte-Kerzel S, Hickel T, Huber L, Raabe D, Sandlöbes-Haut S, Todorova M, et al. Defect phases – thermodynamics and impact on material properties. Int Mater Rev 2022;67:89–117. https://doi.org/10.1080/09506608.2021.1930734.
[363] Rottman C. Theory of phase transitions at internal interfaces. J de Physique Colloque 1988;49:313–22.
[364] Frolov T, Olmsted DL, Asta M, Mishin Y. Structural phase transformations in metallic grain boundaries. Nat Commun 2013;4:1899.
[365] Cantwell PR, Tang M, Dillon SJ, Luo J, Rohrer GS, Harmer MP. Grain boundary complexions. Acta Mater 2013;62:1–48.
[366] Frolov T, Divinski SV, Asta M, Mishin Y. Effect of interface phase transformations on diffusion and segregation in high-angle grain boundaries. Phys Rev Lett 2013;110:255502.
[367] Meiners T, Frolov T, Rudd RE, Dehm G, Liebscher CH. Observations of grain-boundary phase transformations in an elemental metal. Nature 2020;579:375–8. https://doi.org/10.1038/s41586-020-2082-6.
[368] Fang Z, Xiao J, Tan S, Deng C, Wang G, Mao SX. Atomic-scale observation of dynamic grain boundary structural transformation during shear-mediated migration. Sci Adv 2022;8:eabn3785. https://doi.org/10.1126/sciadv.abn3785.
[369] Brink T, Langenohl L, Bishara H, Dehm G. Universality of grain boundary phases in fcc metals: Case study on high-angle [111] symmetric tilt grain boundaries. PhysRevB 2023;107:054103. https://doi.org/10.1103/PhysRevB.107.054103.
[370] Frolov T, Asta M, Mishin Y. Segregation-induced phase transformations in grain boundaries. Phys Rev m B 2015;92. 020103 (R).
[371] Frolov T. Effect of interfacial structural phase transformations on the coupled motion of grain boundaries: A molecular dynamics study. Appl Phys Lett 2014;104:211905.
[372] Langenohl L, Brink T, Freitas R, Frolov T, Dehm G, Liebscher CH. Dual phase patterning during a congruent grain boundary phase transition in elemental copper. Nat Commun 2022;13:3331. https://doi.org/10.1038/s41467-022-30922-3.
[373] Zhu Q, Samanta A, Li B, Rudd RE, Frolov T. Predicting phase behavior of grain boundaries with evolutionary search and machine learning. Nat Commun 2018;9:467. https://doi.org/10.1038/s41467-018-02937-2.
[374] Starikov S, Abbass A, Drautz R, Mrovec M. Disordering complexion transition of grain boundaries in bcc metals: Insights from atomistic simulations. Acta Mater 2023;261:119399. https://doi.org/10.1016/j.actamat.2023.119399.
[375] Luo J, Gupta VK, Yoon DH, Meyer HM. Segregation-induced grain boundary premelting in nickel-doped tungsten. Appl Phys Lett 2005;87. https://doi.org/10.1063/1.2138796.
[376] Zhou N, Hu T, Luo J. Grain boundary complexions in multicomponent alloys: Challenges and opportunities. Curr Opin Solid State Mater Sci 2016;20:268–77. https://doi.org/10.1016/j.cossms.2016.05.001.
[377] Peter NJ, Duarte MJ, Kirchlechner C, Liebscher CH, Dehm G. Faceting diagram for Ag segregation induced nanofaceting at an asymmetric Cu tilt grain boundary. Acta Mater 2021;214:116960. https://doi.org/10.1016/j.actamat.2021.116960.
[378] Brown JA, Mishin Y. Dissociation and faceting of asymmetrical tilt grain boundaries: Molecular dynamics simulations for copper. Phys Rev m B 2007;76:134118.
[379] Darurka I, Hamilton JC. Atomistic and Lattice Model of a Grain Boundary Defaceting Phase Transition. Phys Rev Lett 2004;92:246105.
[380] Lee SB. Correlation between greain boundary faceting-defaceting transition and change of grain boundary properties with temperature. Mat Lett 2003;57:3779.

[381] Rupert TJ. The role of complexions in metallic nano-grain stability and deformation. Curr Opin Solid State Mater Sci 2016.
[382] Grigorian CM, Rupert TJ. Multi-principal element grain boundaries: Stabilizing nanocrystalline grains with thick amorphous complexions. J Mater Res 2022; 37:554–66. https://doi.org/10.1557/s43578-021-00459-0.
[383] Darvishi Kamachali R, Kwiatkowski da Silva A, McEniry E, Ponge D, Gault B, Neugebauer J, et al. Segregation-assisted spinodal and transient spinodal phase separation at grain boundaries. Npj Comput Mater 2020;6:1–13. https://doi.org/10.1038/s41524-020-00456-7.
[384] Watanabe T, Kimura SI, Karashima S. The effect of grain boundary structural transformation on sliding in (1010)-tilt zinc bicrystals. Philos Mag m A 1984;49: 845–64.
[385] Broughton JQ, Gilmer GH. Grain-boundary shearing as a test for interface melting. Modelling Simul Mater Sci Eng 1998;6:87–97.
[386] Balluffi RW, Maurer R. On rotating sphere-on-plate experiments and the question of whether high angle grain boundaries melt below bulk meting temperatures. Scripta Metall 1988;22:709.
[387] Hsieh TE, Balluffi RW. Experimental study of grain boundary melting in aluminum. Acta Metall 1989;37:1637–44.
[388] Gupta VK, Yoon DH, Meyer HM, Luo J. Thin intergranular films and solid-state activated sintering in nickel-doped tungsten. Acta Mater 2007;55:3131–42.
[389] Masumura RA, Glicksman ME, Vold CL. Absolute solid-liquid and grain boundary energies of bismuth. Scripta Metall 1972;6:943–6.
[390] Inoko F, Okada T, Muraga T, Nakano Y, Yoshikawa T. Strain induced grain boundary premelting in bulk copper bicrystals. Interface Sci 1997;4:263–72.
[391] Broughton JQ, Gilmer GH. Thermodynamic criteria for grain boundary melting: A molecular-dynamics study. Phys Rev Lett 1986;56:2692–5.
[392] Lutsko JF, Wolf D, Phillpot SR, Yip S. Molecular-dynamics study of lattice-defect-nucleated melting in metals using an embedded-atom-method potential. Phys Rev m B 1989;40:2841–55.
[393] Lutsko JF, Wolf D, Yip S, Phillpot SR, Nguyen T. Molecular-dynamics method for the simulation of bulk-solid interfaces at high temperatures. Phys Rev m B 1988;38:11572–81.
[394] Hoyt JJ, Olmsted D, Jindal S, Asta M, Karma A. Method for computing short-range forces between solid-liquid interfaces driving grain boundary premelting. Phys Rev m E 2009;79:020601R.
[395] Fensin SJ, Olmsted D, Buta D, Asta M, Karma A, Hoyt JJ. Structural disjoining potential for grain-boundary premelting and grain coalescence from molecular-dynamics simulations. Phys Rev m E 2010;81:031601.
[396] Besold G, Mouritsen OG. Grain-boundary melting: A Monte Carlo study. Phys Rev m B 1994;50:6573–6.
[397] Besold G, Mouritsen OG. Competition between domain growth and interfacial melting. Comp Mater Sci 2000;18:225–44.
[398] Williams PL, Mishin Y. Thermodynamics of grain boundary premelting in alloys. \mboxII. Atomistic simulation. Acta Mater 2009;57:3786–94.
[399] Mishin Y, Boettinger WJ, Warren JA, McFadden GB. Thermodynamics of grain boundary premelting in alloys. \mboxI. Phase field modeling. Acta Mater 2009; 57:3771–85.
[400] Hickman J, Mishin Y. Disjoining potential and grain boundary premelting in binary alloys. Phys Rev m B 2016;93:224108.
[401] Straumal BB, Kogtenkova O, Zięba P. Wetting transition of grain-boundary triple junctions. Acta Mater 2008;56:925–33. https://doi.org/10.1016/j.actamat.2007.10.043.
[402] Singh D, Turlo V, Gianola DS, Rupert TJ. Linear complexions directly modify dislocation motion in face-centered cubic alloys. Mater Sci Eng A 2023;870: 144875. https://doi.org/10.1016/j.msea.2023.144875.
[403] Turlo V, Rupert TJ. Prediction of a wide variety of linear complexions in face centered cubic alloys. Acta Mater 2020;185:129–41. https://doi.org/10.1016/j.actamat.2019.11.069.
[404] Frolov T, Mishin Y. Stable nanocolloidal structures in metallic systems. Phys Rev Lett 2010;104:055701.
[405] Miracle DB, Senkov ON. A critical review of high entropy alloys and related concepts. Acta Mater 2017;122:448–511. https://doi.org/10.1016/j.actamat.2016.08.081.
[406] Rost CM, Sachet E, Borman T, Moballegh A, Dickey EC, Hou D, et al. Entropy-stabilized oxides Nat Commun 2015;6:8485. https://doi.org/10.1038/ncomms9485.
[407] Zhou N, Hu T, Huang J, Luo J. Stabilization of nanocrystalline alloys at high temperatures via utilizing high-entropy grain boundary complexions. Scr Mater 2016;124:160–3. https://doi.org/10.1016/j.scriptamat.2016.07.014.
[408] Luo J, Zhou N. High-entropy grain boundaries Commun Mater 2023;4:1–8. https://doi.org/10.1038/s43246-023-00335-w.
[409] Walle A \mboxvan de, Ceder G. The effect of lattice vibrations on substitutional alloy thermodynamics. Rev Mod Phys 2002;74:11–45.
[410] Fultz B. Vibrational thermodynamics of materials. Prog Mater Sci 2010;55:247–352. https://doi.org/10.1016/j.pmatsci.2009.05.002.
[411] Glensk A, Grabowski B, Hickel T, Neugebauer J. Understanding anharmonicity in fcc materials: From its origin to ab initio strategies beyond the quasiharmonic approximation. Phys Rev Lett 2015;114:195901. https://doi.org/10.1103/PhysRevLett.114.195901.
[412] Grabowski B, Ikeda Y, Srinivasan P, Körmann F, Freysoldt C, Duff AI, et al. Ab initio vibrational free energies including anharmonicity for multicomponent alloys. npj Comput Mater 2019;5:1–6. https://doi.org/10.1038/s41524-019-0218-8.
[413] Souvatzis P, Eriksson O, Katsnelson MI, Rudin SP. Entropy Driven Stabilization of Energetically Unstable Crystal Structures Explained from First Principles Theory. PhysRevLett 2008;100:095901. https://doi.org/10.1103/PhysRevLett.100.095901.
[414] Kadkhodaei S, Hong Q-J, van de Walle A. Free energy calculation of mechanically unstable but dynamically stabilized bcc titanium. PhysRevB 2017;95: 064101. https://doi.org/10.1103/PhysRevB.95.064101.
[415] Ma D, Grabowski B, Körmann F, Neugebauer J, Raabe D. Ab initio thermodynamics of the CoCrFeMnNi high entropy alloy: Importance of entropy contributions beyond the configurational one. Acta Mater 2015;100:90–7. https://doi.org/10.1016/j.actamat.2015.08.050.
[416] Huang Y, Widom M. Vibrational Entropy of Crystalline Solids from Covariance of Atomic Displacements. Entropy 2022;24:618. https://doi.org/10.3390/e24050618.
[417] Esters M, Oses C, Hicks D, Mehl MJ, Jahnátek M, Hossain MD, et al. Settling the matter of the role of vibrations in the stability of high-entropy carbides. Nat Commun 2021;12:5747. https://doi.org/10.1038/s41467-021-25979-5.
[418] Hoglund ER, Bao D-L, O'Hara A, Pfeifer TW, Hoque MSB, Makarem S, et al. Direct Visualization of Localized Vibrations at Complex Grain Boundaries. Adv Mater 2023;35:2208920. https://doi.org/10.1002/adma.202208920.
[419] Hickman J, Mishin Y. Thermal conductivity and its relation to atomic structure for symmetrical tilt grain boundaries in silicon. PhysRevMater 2020;4:033405. https://doi.org/10.1103/PhysRevMaterials.4.033405.
[420] Hashimoto M, Ichinose H, Ishida Y, Yamamoto R, Doyama M. The Simulated and Observed Structure of a Σ=11 Tilt Boundary in Gold and the Vibration of Individual Atoms at the Grain Boundary. Jpn J Appl Phys 1980;19:1045. https://doi.org/10.1143/JJAP.19.1045.
[421] Samolyuk GD, Osetsky YN, Stocks GM, Morris JR. Role of Static Displacements in Stabilizing Body Centered Cubic High Entropy Alloys. PhysRevLett 2021;126: 025501. https://doi.org/10.1103/PhysRevLett.126.025501.
[422] Meyer R, Lewis LJ, Prakash S, Entel P. Vibrational properties of nanoscale materials: From nanoparticles to nanocrystalline materials. PhysRevB 2003;68: 104303. https://doi.org/10.1103/PhysRevB.68.104303.
[423] Bozyigit D, Yazdani N, Yarema M, Yarema O, Lin WMM, Volk S, et al. Soft surfaces of nanomaterials enable strong phonon interactions. Nature 2016;531: 618–22. https://doi.org/10.1038/nature16977.
[424] Bonetti E, Pasquini L, Sampaolesi E, Deriu A, Cicognani G. Vibrational density of states of nanocrystalline iron and nickel. J Appl Phys 2000;88:4571–5. https://doi.org/10.1063/1.1311310.
[425] Tang J-F, Li X-S, Long W-Y, Wang Y. Vibrational properties in nanocrystalline nickels: temperature effects and composite model for thermodynamics. Physica Status Solidi (b) 2008;245:1527–33. https://doi.org/10.1002/pssb.200743160.
[426] Lohaus SH, Johnson MB, Ahnn PF, Saunders CN, Smith HL, White MA, et al. Thermodynamic stability and contributions to the Gibbs free energy of nanocrystalline ${\mathrm{Ni}}_{3}\mathrm{Fe}$. PhysRevMater 2020;4:086002. https://doi.org/10.1103/PhysRevMaterials.4.086002.
[427] Doherty RD, Hughes DA, Humphreys FJ, Jonas JJ, Jensen DJ, Kassner ME, et al. Current issues in recrystallization: a review. Mater Sci Eng A 1997;238: 219–74. https://doi.org/10.1016/S0921-5093(97)00424-3.

[428] Humphreys FJ, Hatherly M. Recrystallization and related annealing phenomena. Elsevier; 1995.
[429] Rupert TJ, Schuh CA. Mechanically driven grain boundary relaxation: a mechanism for cyclic hardening in nanocrystalline Ni. Philos Mag Lett 2012;92:20–8. https://doi.org/10.1080/09500839.2011.619507.
[430] Rupert TJ, Trelewicz JR, Schuh CA. Grain boundary relaxation strengthening of nanocrystalline Ni–W alloys. J Mater Res 2012;27:1285–94. https://doi.org/10.1557/jmr.2012.55.
[431] Matsui I, Kanetake M, Mori H, Takigawa Y, Higashi K. Relationship between grain boundary relaxation strengthening and orientation in electrodeposited bulk nanocrystalline Ni alloys. Mater Lett 2017;205:211–4. https://doi.org/10.1016/j.matlet.2017.06.094.
[432] Hu K, Yi J, Huang B, Bian X, Wang G. Grain boundary relaxation induced ultrastrong-and-ductile bulk pure Ni. Appl Mater Today 2022;29:101653. https://doi.org/10.1016/j.apmt.2022.101653.
[433] Amram D, Schuh CA. Higher Temperatures Yield Smaller Grains in a Thermally Stable Phase-Transforming Nanocrystalline Alloy. PhysRevLett 2018;121:145503. https://doi.org/10.1103/PhysRevLett.121.145503.
[434] Lai SL, Guo JY, Petrova V, Ramanath G, Allen LH. Size-Dependent Melting Properties of Small Tin Particles: Nanocalorimetric Measurements. PhysRevLett 1996;77:99–102. https://doi.org/10.1103/PhysRevLett.77.99.
[435] Jiang Q, Zhang S, Zhao M. Size-dependent melting point of noble metals. Mater Chem Phys 2003;82:225–7. https://doi.org/10.1016/S0254-0584(03)00201-3.
[436] Zhang M, Efremov MY, Schiettekatte F, Olson EA, Kwan AT, Lai SL, et al. Size-dependent melting point depression of nanostructures: Nanocalorimetric measurements. PhysRevB 2000;62:10548–57. https://doi.org/10.1103/PhysRevB.62.10548.
[437] Nanda KK. Size-dependent melting of nanoparticles: Hundred years of thermodynamic model. Pramana - J Phys 2009;72:617–28. https://doi.org/10.1007/s12043-009-0055-2.
[438] Zhang Z, Li JC, Jiang Q. Modelling for size-dependent and dimension-dependent melting of nanocrystals. J Phys D: Appl Phys 2000;33:2653. https://doi.org/10.1088/0022-3727/33/20/318.
[439] Sun CQ, Shi Y, Li CM, Li S, Au Yeung TC. Size-induced undercooling and overheating in phase transitions in bare and embedded clusters. PhysRevB 2006;73:075408. https://doi.org/10.1103/PhysRevB.73.075408.
[440] Sheng HW, Lu K, Ma E. Melting and freezing behavior of embedded nanoparticles in ball-milled Al–10wt% M (M=In, Sn, Bi, Cd, Pb) mixtures. Acta Mater 1998;46:5195–205. https://doi.org/10.1016/S1359-6454(98)00108-6.
[441] Budai I, Kaptay G. A New Class of Engineering Materials: Particle-Stabilized Metallic Emulsions and Monotectic Alloys. Metall Mater Trans A 2009;40:1524–8. https://doi.org/10.1007/s11661-009-9857-6.
[442] Kuchibhatla SV, Karakoti AS, Seal S. Colloidal stability by surface modification. JOM 2005;57:52–6. https://doi.org/10.1007/s11837-005-0183-1.
[443] Emulsions BP. Theory and Practiice. Oxford, New York: Oxford University Press; 2001.
[444] Mason TG, Wilking JN, Meleson K, Chang CB, Graves SM. Nanoemulsions: formation, structure, and physical properties. J Phys: Condens Matter 2006;18:R635–66.
[445] Prince LM. A theory of aqueous emulsions I. Negative interfacial tension at the oil/water interface. J Colloid Interface Sci 1967;23:165–73. https://doi.org/10.1016/0021-9797(67)90099-9.
[446] Ruckenstein E. Thermodynamic insights on macroemulsion stability. Adv Colloid Interface Sci 1999;79:59–76.
[447] Shahidzadeh N, Bonn D, mboxAguerre-Chariol O, Meunier J. Spontaneous emulsification: relation to microemulsion phase behaviour. Colloids Surf 1999;147:375–80.
[448] Shahidzadeh N, Bonn D, Meunier J, Nabavi M, Airiau M, Morvan M. Dynamics of Spontaneous Emulsification for Fabrication of Oil in Water Emulsions. Langmuir 2000;16:9703–8. https://doi.org/10.1021/la000493l.
[449] Gleiter H, Hansen N, Horsewell A, Leffers T. Proceedings of the 2nd Riso International Symposium on Metallurgy and Materials Science 1981.
[450] Feynman RP. Plenty of Room at the Bottom. APS annual meeting: Little Brown Boston, MA, USA; 1959. p. 1–7.
[451] Koch CC. Nanostructured Materials: Processing. William Andrew: Properties and Applications; 2006.
[452] Lu K. Sintering of nanoceramics. Int Mater Rev 2008;53:21–38. https://doi.org/10.1179/174328008X254358.
[453] German R. Sintering Theory and Practice | Wiley. John Wiley & Sons, Inc.; 1996.
[454] Sanders PG, Eastman JA, Weertman JR. Elastic and tensile behavior of nanocrystalline copper and palladium. Acta Mater 1997;45:4019–25. https://doi.org/10.1016/S1359-6454(97)00092-X.
[455] Chokshi AH, Rosen A, Karch J, Gleiter H. On the validity of the hall-petch relationship in nanocrystalline materials. Scr Metall 1989;23:1679–83. https://doi.org/10.1016/0036-9748(89)90342-6.
[456] Hughes GD, Smith SD, Pande CS, Johnson HR, Armstrong RW. Hall-petch strengthening for the microhardness of twelve nanometer grain diameter electrodeposited nickel. Scr Metall 1986;20:93–7. https://doi.org/10.1016/0036-9748(86)90219-X.
[457] Weertman JR. Hall-Petch strengthening in nanocrystalline metals. Mater Sci Eng A 1993;166:161–7. https://doi.org/10.1016/0921-5093(93)90319-A.
[458] Carlton CE, Ferreira PJ. What is behind the inverse Hall–Petch effect in nanocrystalline materials? Acta Mater 2007;55:3749–56. https://doi.org/10.1016/j.actamat.2007.02.021.
[459] Koch CC, Narayan J. The Inverse Hall-Petch Effect—Fact or Artifact? MRS Online Proceedings Library (OPL) 2000;634. https://doi.org/10.1557/PROC-634-B5.1.1.
[460] Fu H-H, Benson DJ, Meyers MA. Analytical and computational description of effect of grain size on yield stress of metals. Acta Mater 2001;49:2567–82. https://doi.org/10.1016/S1359-6454(01)00062-3.
[461] Legros M, Elliott BR, Rittner MN, Weertman JR, Hemker KJ. Microsample tensile testing of nanocrystalline metals. Philos Mag A 2000;80:1017–26. https://doi.org/10.1080/01418610008212096.
[462] Sharpe WN, Yuan B, Edwards RL. A new technique for measuring the mechanical properties of thin films. J Microelectromech Syst 1997;6:193–9. https://doi.org/10.1109/84.623107.
[463] Sharpe WN, Bagdahn J. Fatigue testing of polysilicon—a review. Mech Mater 2004;36:3–11. https://doi.org/10.1016/S0167-6636(03)00027-9.
[464] Hemker KJ, Sharpe WN. Microscale Characterization of Mechanical Properties. Annu Rev Mater Res 2007;37:93–126. https://doi.org/10.1146/annurev.matsci.36.062705.134551.
[465] Manahan MP, Argon AS, Harling OK. The development of a miniaturized disk bend test for the determination of postirradiation mechanical properties. J Nucl Mater 1981;104:1545–50. https://doi.org/10.1016/0022-3115(82)90820-0.
[466] Malow TR, Koch CC. Mechanical properties in tension of mechanically attrited nanocrystalline iron by the use of the miniaturized disk bend test. Acta Mater 1998;46:6459–73. https://doi.org/10.1016/S1359-6454(98)00294-8.
[467] Baik J-M, Kameda J, Buck O. Small punch test evaluation of intergranular embrittlement of an alloy steel. Scr Metall 1983;17:1443–7. https://doi.org/10.1016/0036-9748(83)90373-3.
[468] Guduru RK, Wong PZ, Darling KA, Koch CC, Murty KL, Scattergood RO. Determination of activation volume in nanocrystalline Cu using the shear punch test. Adv Eng Mater 2007;9:855–9.
[469] Malow TR, Koch CC, Miraglia PQ, Murty KL. Compressive mechanical behavior of nanocrystalline Fe investigated with an automated ball indentation technique. Mater Sci Eng A 1998;252:36–43. https://doi.org/10.1016/S0921-5093(98)00661-3.
[470] Haggag FM. In-situ measurements of mechanical properties using novel automated ball indentation system. ASTM Spec Tech Publ 1993;1204:27.
[471] Chu SNG, Li JCM. Impression creep; a new creep test. J Mater Sci 1977;12:2200–8. https://doi.org/10.1007/BF00552241.
[472] Sastry DH. Impression creep technique—An overview. Mater Sci Eng A 2005;409:67–75. https://doi.org/10.1016/j.msea.2005.05.110.
[473] Oliver WC, Pharr GM. An improved technique for determining hardness and elastic modulus using load and displacement sensing indentation experiments. J Mater Res 1992;7:1564–83. https://doi.org/10.1557/JMR.1992.1564.
[474] Uchic MD, Dimiduk DM, Florando JN, Nix WD. Sample Dimensions Influence Strength and Crystal Plasticity. Science 2004;305:986–9. https://doi.org/10.1126/science.1098993.

[475] Zhang H, Schuster BE, Wei Q, Ramesh KT. The design of accurate micro-compression experiments. Scr Mater 2006;54:181–6. https://doi.org/10.1016/j.scriptamat.2005.06.043.
[476] Zhao YH, Guo YZ, Wei Q, Dangelewicz AM, Xu C, Zhu YT, et al. Influence of specimen dimensions on the tensile behavior of ultrafine-grained Cu. Scr Mater 2008;59:627–30. https://doi.org/10.1016/j.scriptamat.2008.05.031.
[477] Valiev RZ, Alexandrov IV, Zhu YT, Lowe TC. Paradox of Strength and Ductility in Metals Processed Bysevere Plastic Deformation. J Mater Res 2002;17:5–8. https://doi.org/10.1557/JMR.2002.0002.
[478] Zhao YH, Guo YZ, Wei Q, Topping TD, Dangelewicz AM, Zhu YT, et al. Influence of specimen dimensions and strain measurement methods on tensile stress–strain curves. Mater Sci Eng A 2009;525:68–77. https://doi.org/10.1016/j.msea.2009.06.031.
[479] Hall EO. The Deformation and Ageing of Mild Steel: III Discussion of Results. Proc Phys Soc B 1951;64:747. https://doi.org/10.1088/0370-1301/64/9/303.
[480] Petch N. The cleavage strength of polycrystals. J Iron Steel Inst 1953;174:25–8.
[481] Armstrong RW. Engineering science aspects of the Hall–Petch relation. Acta Mechanica 2014;225:1013–28. https://doi.org/10.1007/s00707-013-1048-2.
[482] Figueiredo RB, Kawasaki M, Langdon TG. Seventy years of Hall-Petch, ninety years of superplasticity and a generalized approach to the effect of grain size on flow stress. Prog Mater Sci 2023;137:101131. https://doi.org/10.1016/j.pmatsci.2023.101131.
[483] Louchet F, Weiss J, Richeton T. Hall-Petch Law Revisited in Terms of Collective Dislocation Dynamics. PhysRevLett 2006;97:075504. https://doi.org/10.1103/PhysRevLett.97.075504.
[484] Hirth J, Lothe J. Theory of Dislocations, 780 pp. New York: McGraw-Hill; 1968.
[485] Li JC. Petch relation and grain boundary sources. Trans Metall Soc AIME 1963;227:239.
[486] Li JCM, Chou YT. The role of dislocations in the flow stress grain size relationships. Metall Trans 1970;1:1145–59. https://doi.org/10.1007/BF02900225.
[487] Ashby MF. The deformation of plastically non-homogeneous materials. The Philosophical Magazine: A Journal of Theoretical Experimental and Applied Physics 1970;21:399–424. https://doi.org/10.1080/14786437008238426.
[488] Meyers MA, Ashworth E. A model for the effect of grain size on the yield stress of metals. Philos Mag A 1982. https://doi.org/10.1080/01418618208236928.
[489] Thompson AW, Baskes MI, Flanagan WF. The dependence of polycrystal work hardening on grain size. Acta Metall 1973;21:1017–28. https://doi.org/10.1016/0001-6160(73)90158-2.
[490] Somekawa H, Mukai T. Effect of grain refinement on fracture toughness in extruded pure magnesium. Scr Mater 2005;53:1059–64. https://doi.org/10.1016/j.scriptamat.2005.07.001.
[491] Somekawa H, Schuh CA. Effect of solid solution elements on nanoindentation hardness, rate dependence, and incipient plasticity in fine grained magnesium alloys. Acta Mater 2011;59:7554–63. https://doi.org/10.1016/j.actamat.2011.08.047.
[492] Figueiredo RB, Poggiali FSJ, Silva CLP, Cetlin PR, Langdon TG. The influence of grain size and strain rate on the mechanical behavior of pure magnesium. J Mater Sci 2016;51:3013–24. https://doi.org/10.1007/s10853-015-9612-x.
[493] Choi HJ, Kim Y, Shin JH, Bae DH. Deformation behavior of magnesium in the grain size spectrum from nano- to micrometer. Mater Sci Eng A 2010;527:1565–70. https://doi.org/10.1016/j.msea.2009.10.035.
[494] Yamashita A, Horita Z, Langdon TG. Improving the mechanical properties of magnesium and a magnesium alloy through severe plastic deformation. Mater Sci Eng A 2001;300:142–7. https://doi.org/10.1016/S0921-5093(00)01660-9.
[495] Hwang S, Nishimura C, McCormick PG. Deformation mechanism of nanocrystalline magnesium in compression. Scr Mater 2001;44:1507–11. https://doi.org/10.1016/S1359-6462(01)00716-3.
[496] Figueiredo RB, Langdon TG. Deformation mechanisms in ultrafine-grained metals with an emphasis on the Hall–Petch relationship and strain rate sensitivity. J Mater Res Technol 2021;14:137–59. https://doi.org/10.1016/j.jmrt.2021.06.016.
[497] Hu J, Shi YN, Sauvage X, Sha G, Lu K. Grain boundary stability governs hardening and softening in extremely fine nanograined metals. Science 2017;355:1292–6. https://doi.org/10.1126/science.aal5166.
[498] Astafurov SV, Maier GG, Melnikov EV, Moskvina VA, Panchenko MY, Astafurova EG. The strain-rate dependence of the Hall-Petch effect in two austenitic stainless steels with different stacking fault energies. Mater Sci Eng A 2019;756:365–72. https://doi.org/10.1016/j.msea.2019.04.076.
[499] Yu H, Xin Y, Wang M, Liu Q. Hall-Petch relationship in Mg alloys: A review. J Mater Sci Technol 2018;34:248–56. https://doi.org/10.1016/j.jmst.2017.07.022.
[500] Yu H, Li C, Xin Y, Chapuis A, Huang X, Liu Q. The mechanism for the high dependence of the Hall-Petch slope for twinning/slip on texture in Mg alloys. Acta Mater 2017;128:313–26. https://doi.org/10.1016/j.actamat.2017.02.044.
[501] Guan B, Xin Y, Huang X, Wu P, Liu Q. Quantitative prediction of texture effect on Hall–Petch slope for magnesium alloys. Acta Mater 2019;173:142–52. https://doi.org/10.1016/j.actamat.2019.05.016.
[502] Yuan W, Panigrahi SK, Su J-Q, Mishra RS. Influence of grain size and texture on Hall–Petch relationship for a magnesium alloy. Scr Mater 2011;65:994–7. https://doi.org/10.1016/j.scriptamat.2011.08.028.
[503] Wang Y, Choo H. Influence of texture on Hall–Petch relationships in an Mg alloy. Acta Mater 2014;81:83–97. https://doi.org/10.1016/j.actamat.2014.08.023.
[504] Xu J, Guan B, Xin Y, Wei X, Huang G, Liu C, et al. A weak texture dependence of Hall–Petch relation in a rare-earth containing magnesium alloy. J Mater Sci Technol 2022;99:251–9. https://doi.org/10.1016/j.jmst.2021.04.076.
[505] Razavi SM, Foley DC, Karaman I, Hartwig KT, Duygulu O, Kecskes LJ, et al. Effect of grain size on prismatic slip in Mg–3Al–1Zn alloy. Scr Mater 2012;67:439–42. https://doi.org/10.1016/j.scriptamat.2012.05.017.
[506] Zhang K, Weertman JR, Eastman JA. Rapid stress-driven grain coarsening in nanocrystalline Cu at ambient and cryogenic temperatures. Appl Phys Lett 2005;87:061921. https://doi.org/10.1063/1.2008377.
[507] Gianola DS, Van Petegem S, Legros M, Brandstetter S, Van Swygenhoven H, Hemker KJ. Stress-assisted discontinuous grain growth and its effect on the deformation behavior of nanocrystalline aluminum thin films. Acta Mater 2006;54:2253–63. https://doi.org/10.1016/j.actamat.2006.01.023.
[508] Schiøtz J, Di Tolla FD, Jacobsen KW. Softening of nanocrystalline metals at very small grain sizes. Nature 1998;391:561–3. https://doi.org/10.1038/35328.
[509] Schiøtz J, Jacobsen KW. A Maximum in the Strength of Nanocrystalline Copper. Science 2003. https://doi.org/10.1126/science.1086636.
[510] Yamakov V, Wolf D, Phillpot SR, Mukherjee AK, Gleiter H. Deformation-mechanism map for nanocrystalline metals by molecular-dynamics simulation. Nat Mater 2004;3:43–7. https://doi.org/10.1038/nmat1035.
[511] Zheng G-P. Grain-size effect on plastic flow in nanocrystalline cobalt by atomistic simulation. Acta Mater 2007;55:149–59. https://doi.org/10.1016/j.actamat.2006.07.034.
[512] Tang Y, Bringa EM, Meyers MA. Inverse Hall–Petch relationship in nanocrystalline tantalum. Mater Sci Eng A 2013;580:414–26. https://doi.org/10.1016/j.msea.2013.05.024.
[513] Yuan F. Atomistic simulation study of tensile deformation in bulk nanocrystalline bcc iron. Sci China Phys Mech Astron 2012;55:1657–63. https://doi.org/10.1007/s11433-012-4830-6.
[514] Chang L, Zhou C-Y, Li J, He X-H. Investigation on tensile properties of nanocrystalline titanium with ultra-small grain size. Comput Mater Sci 2018;142:135–44. https://doi.org/10.1016/j.commatsci.2017.10.017.
[515] Scattergood RO, Koch CC. A modified model for hall-petch behavior in nanocrystalline materials. Scr Metall Mater 1992;27:1195–200. https://doi.org/10.1016/0956-716X(92)90598-9.
[516] Millett PC, Desai T, Yamakov V, Wolf D. Atomistic simulations of diffusional creep in a nanocrystalline body-centered cubic material. Acta Mater 2008;56:3688–98.
[517] Fan GJ, Choo H, Liaw PK, Lavernia EJ. A model for the inverse Hall–Petch relation of nanocrystalline materials. Mater Sci Eng A 2005;409:243–8. https://doi.org/10.1016/j.msea.2005.06.073.
[518] Padmanabhan KA, Dinda GP, Hahn H, Gleiter H. Inverse Hall–Petch effect and grain boundary sliding controlled flow in nanocrystalline materials. Mater Sci Eng A 2007;452–453:462–8. https://doi.org/10.1016/j.msea.2006.10.084.

[519] Padmanabhan KA, Sripathi S, Hahn H, Gleiter H. Inverse Hall–Petch effect in quasi- and nanocrystalline materials. Mater Lett 2014;133:151–4. https://doi.org/10.1016/j.matlet.2014.06.153.
[520] Desai TG, Millett P, Wolf D. Is diffusion creep the cause for the inverse Hall–Petch effect in nanocrystalline materials? Mater Sci Eng A 2008;493:41–7. https://doi.org/10.1016/j.msea.2007.06.097.
[521] Lu L, Schwaiger R, Shan ZW, Dao M, Lu K, Suresh S. Nano-sized twins induce high rate sensitivity of flow stress in pure copper. Acta Mater 2005;53:2169–79. https://doi.org/10.1016/j.actamat.2005.01.031.
[522] Lu L, Li SX, Lu K. An abnormal strain rate effect on tensile behavior in nanocrystalline copper. Scr Mater 2001;45:1163–9. https://doi.org/10.1016/S1359-6462(01)01138-1.
[523] Carreker RP, Hibbard WR. Tensile deformation of high-purity copper as a function of temperature, strain rate, and grain size. Acta Metall 1953;1:654–63. https://doi.org/10.1016/0001-6160(53)90022-4.
[524] Smith L, Zimmerman JA, Hale LM, Farkas D. Molecular dynamics study of deformation and fracture in a tantalum nano-crystalline thin film. Modelling Simul Mater Sci Eng 2014;22:045010. https://doi.org/10.1088/0965-0393/22/4/045010.
[525] Pan Z, Xu F, Mathaudhu SN, Kecskes LJ, Yin WH, Zhang XY, et al. Microstructural evolution and mechanical properties of niobium processed by equal channel angular extrusion up to 24 passes. Acta Mater 2012;60:2310–23. https://doi.org/10.1016/j.actamat.2011.12.019.
[526] Wei Q, Pan ZL, Wu XL, Schuster BE, Kecskes LJ, Valiev RZ. Microstructure and mechanical properties at different length scales and strain rates of nanocrystalline tantalum produced by high-pressure torsion. Acta Mater 2011;59:2423–36. https://doi.org/10.1016/j.actamat.2010.12.042.
[527] Hou Z, Zhang P, Wu K, Wang Y, Liu G, Zhang G, et al. Size dependent phase transformation and mechanical behaviors in nanocrystalline Ta thin films. Int J Refract Metal Hard Mater 2019;82:7–14. https://doi.org/10.1016/j.ijrmhm.2019.03.021.
[528] Wang YM, Hodge AM, Bythrow PM, Barbee TW, Hamza AV. Negative strain rate sensitivity in ultrahigh-strength nanocrystalline tantalum. Appl Phys Lett 2006;89. https://doi.org/10.1063/1.2338006.
[529] Chaudry UM, Sravya Tekumalla T-S-J, Gupta M, Hamad K. Designing highly ductile magnesium alloys: current status and future challenges. Crit Rev Solid State Mater Sci 2022;47:194–281. https://doi.org/10.1080/10408436.2021.1947185.
[530] Somekawa H, Mukai T. Hall–Petch Breakdown in Fine-Grained Pure Magnesium at Low Strain Rates. Metall Mater Trans A 2015;46:894–902. https://doi.org/10.1007/s11661-014-2641-2.
[531] Hwang S, Nishimura C, McCormick PG. Mechanical milling of magnesium powder. Mater Sci Eng A 2001;318:22–33. https://doi.org/10.1016/S0921-5093(01)01767-1.
[532] Wang X, Jiang L, Zhang D, Rupert TJ, Beyerlein IJ, Mahajan S, et al. Revealing the deformation mechanisms for room-temperature compressive superplasticity in nanocrystalline magnesium. Materialia 2020;11:100731. https://doi.org/10.1016/j.mtla.2020.100731.
[533] Yu S, Wan Y, Liu C, Chen Z, Zhou X. Twinning-Induced Abnormal Strain Rate Sensitivity and Indentation Creep Behavior in Nanocrystalline Mg Alloy. Materials 2021;14:7104. https://doi.org/10.3390/ma14227104.
[534] Wan Y, Tang B, Gao Y, Tang L, Sha G, Zhang B, et al. Bulk nanocrystalline high-strength magnesium alloys prepared via rotary swaging. Acta Mater 2020;200:274–86. https://doi.org/10.1016/j.actamat.2020.09.024.
[535] Asaro RJ, Suresh S. Mechanistic models for the activation volume and rate sensitivity in metals with nanocrystalline grains and nano-scale twins. Acta Mater 2005;53:3369–82. https://doi.org/10.1016/j.actamat.2005.03.047.
[536] Rice JR. Dislocation nucleation from a crack tip: An analysis based on the Peierls concept. J Mech Phys Solids 1992;40:239–71. https://doi.org/10.1016/S0022-5096(05)80012-2.
[537] Van Swygenhoven H, Derlet P, Frøseth A. Nucleation and propagation of dislocations in nanocrystalline fcc metals. Acta Mater 2006;54:1975–83.
[538] Zhu T, Li J, Samanta A, Kim HG, Suresh S. Interfacial plasticity governs strain rate sensitivity and ductility in nanostructured metals. PNAS 2007;104:3031–6. https://doi.org/10.1073/pnas.0611097104.
[539] Conrad H. The cryogenic properties of metals. In: Zackey V, editor. High-Strength Materials, Wiley; 1964, p. 436.
[540] Dora JE, Rajnak S. Nucleation of kink pairs and the peierls'mechanism of plastic deformation 1963.
[541] Jia D, Ramesh KT, Ma E. Effects of nanocrystalline and ultrafine grain sizes on constitutive behavior and shear bands in iron. Acta Mater 2003;51:3495–509. https://doi.org/10.1016/S1359-6454(03)00169-1.
[542] Zheng Z, Balint DS, Dunne FPE. Rate sensitivity in discrete dislocation plasticity in hexagonal close-packed crystals. Acta Mater 2016;107:17–26. https://doi.org/10.1016/j.actamat.2016.01.035.
[543] Ashby MF. A first report on deformation-mechanism maps. Acta Metall 1972;20:887–97. https://doi.org/10.1016/0001-6160(72)90082-X.
[544] Chokshi AH. Unusual stress and grain size dependence for creep in nanocrystalline materials. Scr Mater 2009;61:96–9. https://doi.org/10.1016/j.scriptamat.2009.03.009.
[545] Wang N, Wang Z, Aust KT, Erb U. Room temperature creep behavior of nanocrystalline nickel produced by an electrodeposition technique. Mater Sci Eng A 1997;237:150–8. https://doi.org/10.1016/S0921-5093(97)00124-X.
[546] Cai B, Kong QP, Lu L, Lu K. Low temperature creep of nanocrystalline pure copper. Mater Sci Eng A 2000;286:188–92. https://doi.org/10.1016/S0921-5093(00)00633-X.
[547] Yamakov V, Wolf D, Phillpot S, Gleiter H. Grain-boundary diffusion creep in nanocrystalline palladium by molecular-dynamics simulation. Acta Mater 2002;50:61–73.
[548] Yin W, Whang S, Mirshams R, Xiao C. Creep behavior of nanocrystalline nickel at 290 and 373 K. Mater Sci Eng A 2001;301:18–22.
[549] Ogino Y. An effect of deformation of grains on diffusional creep of nanocrystalline materials. Scr Mater 2000;43:149–53. https://doi.org/10.1016/S1359-6462(00)00384-5.
[550] Li X, Cao G, Chen Y, Yue P, Song K, Wang J. Dislocation climb mediated Coble-type grain boundary deformation in gold nanocrystals. Materials Research Letters 2024:1–7. https://doi.org/10.1080/21663831.2024.2418391.
[551] Li YJ, Blum W, Breutinger F. Does nanocrystalline Cu deform by Coble creep near room temperature? Mater Sci Eng A 2004;387–389:585–9. https://doi.org/10.1016/j.msea.2003.11.086.
[552] Estrin Y, Gottstein G, Shvindlerman LS. Diffusion controlled creep in nanocrystalline materials under grain growth. Scr Mater 2004;50:993–7. https://doi.org/10.1016/j.scriptamat.2004.01.002.
[553] Raj R, Ashby M. On grain boundary sliding and diffusional creep. Metallurgical Transactions 1971;2:1113–27.
[554] Coble R. A model for boundary diffusion controlled creep in polycrystalline materials. J Appl Phys 1963;34:1679–82.
[555] Yagi N, Rikukawa A, Mizubayashi H, Tanimoto H. Experimental tests of the elementary mechanism responsible for creep deformation in nanocrystalline gold. Phys Rev B 2006;74:144105.
[556] Nieman GW, Weertman JR, Siegel RW. Mechanical behavior of nanocrystalline Cu and Pd. J Mater Res 1991;6:1012–27. https://doi.org/10.1557/JMR.1991.1012.
[557] Sanders PG, Rittner M, Kiedaisch E, Weertman JR, Kung H, Lu YC. Creep of nanocrystalline Cu, Pd, and Al-Zr. Nanostruct Mater 1997;9:433–40. https://doi.org/10.1016/S0965-9773(97)00096-2.
[558] Zhang K, Weertman JR, Eastman JA. The influence of time, temperature, and grain size on indentation creep in high-purity nanocrystalline and ultrafine grain copper. Appl Phys Lett 2004;85:5197–9. https://doi.org/10.1063/1.1828213.
[559] Ma ZS, Long SG, Zhou YC, Pan Y. Indentation scale dependence of tip-in creep behavior in Ni thin films. Scr Mater 2008;59:195–8. https://doi.org/10.1016/j.scriptamat.2008.03.014.
[560] Wang CL, Zhang M, Nieh TG. Nanoindentation creep of nanocrystalline nickel at elevated temperatures. J Phys D: Appl Phys 2009;42:115405. https://doi.org/10.1088/0022-3727/42/11/115405.
[561] Bhakhri V, Klassen RJ. The depth dependence of the indentation creep of polycrystalline gold at 300K. Scr Mater 2006;55:395–8. https://doi.org/10.1016/j.scriptamat.2006.04.004.

[562] Karanjgaokar N, Chasiotis I. Creep behavior of nanocrystalline Au films as a function of temperature. J Mater Sci 2016;51:3701–14. https://doi.org/10.1007/s10853-015-9687-4.
[563] Wang CL, Lai YH, Huang JC, Nieh TG. Creep of nanocrystalline nickel: A direct comparison between uniaxial and nanoindentation creep. Scr Mater 2010;62:175–8. https://doi.org/10.1016/j.scriptamat.2009.10.021.
[564] Li WB, Henshall JL, Hooper RM, Easterling KE. The mechanisms of indentation creep. Acta Metall Mater 1991;39:3099–110. https://doi.org/10.1016/0956-7151(91)90043-Z.
[565] Van Swygenhoven H, Caro A. Plastic behavior of nanophase metals studied by molecular dynamics. PhysRevB 1998;58:11246–51. https://doi.org/10.1103/PhysRevB.58.11246.
[566] Brandstetter S, Zhang K, Escuadro A, Weertman JR, Van Swygenhoven H. Grain coarsening during compression of bulk nanocrystalline nickel and copper. Scr Mater 2008;58:61–4. https://doi.org/10.1016/j.scriptamat.2007.08.042.
[567] Wang Y-J, Ishii A, Ogata S. Transition of creep mechanism in nanocrystalline metals. Phys Rev B 2011;84:224102.
[568] Weertman J. Creep of indium, lead, and some of their alloys with various metals. Trans Met Soc AIME 1960;218.
[569] Li J, Zhang JY, Liu G, Sun J. New insight into the stable grain size of nanotwinned Ni in steady-state creep: Effect of the ratio of effective-to-internal stress. Int J Plast 2016;85:172–89. https://doi.org/10.1016/j.ijplas.2016.07.009.
[570] Kottada RS, Chokshi AH. Low temperature compressive creep in electrodeposited nanocrystalline nickel. Scr Mater 2005;53:887–92. https://doi.org/10.1016/j.scriptamat.2005.06.035.
[571] Mohamed FA, Chauhan M. Interpretation of the creep behavior of nanocrystalline Ni in terms of dislocation accommodated boundary sliding. Metall Mater Trans A 2006;37:3555–67. https://doi.org/10.1007/s11661-006-1050-6.
[572] Van Petegem S, Brandstetter S, Schmitt B, Van Swygenhoven H. Creep in nanocrystalline Ni during X-ray diffraction. Scr Mater 2009;60:297–300. https://doi.org/10.1016/j.scriptamat.2008.10.034.
[573] Forrest PG. Fatigue of metals. Elsevier; 2013.
[574] Laird C, Smith G. Initial stages of damage in high stress fatigue in some pure metals. Phil Mag 1963;8:1945–63.
[575] Suresh S. Fatigue of Materials. Cambridge University Press; 1998.
[576] Roland T, Retraint D, Lu K, Lu J. Fatigue life improvement through surface nanostructuring of stainless steel by means of surface mechanical attrition treatment. Scr Mater 2006;54:1949–54.
[577] Ye C, Suslov S, Kim BJ, Stach EA, Cheng GJ. Fatigue performance improvement in AISI 4140 steel by dynamic strain aging and dynamic precipitation during warm laser shock peening. Acta Mater 2011;59:1014–25.
[578] Feltner C, Laird C. Cyclic stress-strain response of FCC metals and alloys—II Dislocation structures and mechanisms. Acta Metall 1967;15:1633–53.
[579] Agnew SR, Weertman JR. Cyclic softening of ultrafine grain copper. Mater Sci Eng A 1998;244:145–53. https://doi.org/10.1016/S0921-5093(97)00689-8.
[580] Agnew SR, Vinogradov AY, Hashimoto S, Weertman JR. Overview of fatigue performance of Cu processed by severe plastic deformation. Journal of Elec Materi 1999;28:1038–44. https://doi.org/10.1007/s11664-999-0181-0.
[581] Hanlon T, Kwon Y-N, Suresh S. Grain size effects on the fatigue response of nanocrystalline metals. Scr Mater 2003;49:675–80. https://doi.org/10.1016/S1359-6462(03)00393-2.
[582] Hanlon T, Tabachnikova ED, Suresh S. Fatigue behavior of nanocrystalline metals and alloys. Int J Fatigue 2005;27:1147–58. https://doi.org/10.1016/j.ijfatigue.2005.06.035.
[583] Sangid MD, Pataky GJ, Sehitoglu H, Rateick RG, Niendorf T, Maier HJ. Superior fatigue crack growth resistance, irreversibility, and fatigue crack growth–microstructure relationship of nanocrystalline alloys. Acta Mater 2011;59:7340–55. https://doi.org/10.1016/j.actamat.2011.07.058.
[584] Lei YB, Wang ZB, Xu JL, Lu K. Simultaneous enhancement of stress- and strain-controlled fatigue properties in 316L stainless steel with gradient nanostructure. Acta Mater 2019;168:133–42. https://doi.org/10.1016/j.actamat.2019.02.008.
[585] Boyce BL, Ii HAP. Anomalous Fatigue Behavior and Fatigue-Induced Grain Growth in Nanocrystalline Nickel Alloys. Metall and Mat Trans A 2011;42:1793–804. https://doi.org/10.1007/s11661-011-0708-x.
[586] Anderson PM, Carpenter JS, Gram MD, Li L. Mechanical properties of nanostructured metals. Handbook of Nanomaterials Properties: Springer; 2014. p. 495–553.
[587] Long J, Pan Q, Tao N, Dao M, Suresh S, Lu L. Improved fatigue resistance of gradient nanograined Cu. Acta Mater 2019;166:56–66. https://doi.org/10.1016/j.actamat.2018.12.018.
[588] Pan QS, Long JZ, Jing LJ, Tao NR, Lu L. Cyclic strain amplitude-dependent fatigue mechanism of gradient nanograined Cu. Acta Mater 2020;196:252–60. https://doi.org/10.1016/j.actamat.2020.06.047.
[589] Li X, Lu L, Li J, Zhang X, Gao H. Mechanical properties and deformation mechanisms of gradient nanostructured metals and alloys. Nat Rev Mater 2020;5:706–23. https://doi.org/10.1038/s41578-020-0212-2.
[590] Cavaliere P. Fatigue properties and crack behavior of ultra-fine and nanocrystalline pure metals. Int J Fatigue 2009;31:1476–89. https://doi.org/10.1016/j.ijfatigue.2009.05.004.
[591] Fan GJ, Fu LF, Wang GY, Choo H, Liaw PK, Browning ND. Mechanical behavior of a bulk nanocrystalline Ni–Fe alloy. J Alloy Compd 2007;434–435:298–300. https://doi.org/10.1016/j.jallcom.2006.08.174.
[592] Yang Y, Imasogie B, Fan GJ, Liaw PK, Soboyejo WO. Fatigue and Fracture of a Bulk Nanocrystalline NiFe Alloy. Metall and Mat Trans A 2008;39:1145–56. https://doi.org/10.1007/s11661-008-9487-4.
[593] Rupert TJ, Gianola DS, Gan Y, Hemker KJ. Experimental Observations of Stress-Driven Grain Boundary Migration. Science 2009;326:1686–90. https://doi.org/10.1126/science.1178226.
[594] Mughrabi H, Höppel HW. Cyclic deformation and fatigue properties of very fine-grained metals and alloys. Int J Fatigue 2010;32:1413–27. https://doi.org/10.1016/j.ijfatigue.2009.10.007.
[595] Gutkin MY, Ovid'ko † IA. Nanocracks at grain boundaries in nanocrystalline materials. Philos Mag Lett 2004;84:655–63. https://doi.org/10.1080/09500830512331329123.
[596] McDowell DL, Gall K, Horstemeyer MF, Fan J. Microstructure-based fatigue modeling of cast A356-T6 alloy. Eng Fract Mech 2003;70:49–80. https://doi.org/10.1016/S0013-7944(02)00021-8.
[597] Xue Y, Wright AM, McDowell DL, Horstemeyer MF, Solanki K, Hammi Y. Micromechanics study of fatigue damage incubation following an initial overstrain. J Eng Mater Technol 2010;132:021010. https://doi.org/10.1115/1.4000227.
[598] Tanaka K, Mura T. A dislocation model for fatigue crack initiation 1981.
[599] Meyers MA. Dynamic Behavior of Materials. New York: John Wiley and Sons Inc.; 1994.
[600] Follansbee P, Armstrong P, Hockett J, Dudder G, Erlich D. High strain rate compression testing. ASM Handbook 1985;8:190–207.
[601] Nemat-Nasser S. Introduction to high strain rate testing. ASM Handbook 2000;8:427–8.
[602] Ramesh KT. High rates and impact experiments. Handbook of Experimental Solid Mechanics 2008;933.
[603] Jia D, Ramesh KT. A rigorous assessment of the benefits of miniaturization in the Kolsky bar system. Exp Mech 2004;44:445–54. https://doi.org/10.1007/BF02427955.
[604] Hornbuckle BC, Turnage SA, Williams CL, Giri AK, Casem D, Solanki K, et al. Critical assessment of the extreme mechanical behavior of a stable nanocrystalline alloy under shock loading. Acta Mater 2022;236:118105. https://doi.org/10.1016/j.actamat.2022.118105.
[605] Jordan JL, Siviour CR, Sunny G, Bramlette C, Spowart JE. Strain rate-dependant mechanical properties of OFHC copper. J Mater Sci 2013;48:7134–41. https://doi.org/10.1007/s10853-013-7529-9.
[606] House JW, Lewis JC, Gillis PP, Wilson LL. Estimation of flow stress under high rate plastic deformation. Int J Impact Eng 1995;16:189–200. https://doi.org/10.1016/0734-743X(94)00042-U.
[607] Kocks UF, Argon AS, Ashby MF. Thermodynamics and Kinetics of Slip. Progr Mater Sci 1975;19.

[608] Zerilli FJ, Armstrong RW. Dislocation-mechanics-based constitutive relations for material dynamics calculations. J Appl Phys 1987;61:1816–25. https://doi.org/10.1063/1.338024.
[609] Johnson GR, Cook WH. Fracture characteristics of three metals subjected to various strains, strain rates, temperatures and pressures. Eng Fract Mech 1985;21:31–48. https://doi.org/10.1016/0013-7944(85)90052-9.
[610] Follansbee PS, Regazzoni G, Kocks UF. Mechanical Properties at High Rates of Strain. In: Proceedings of the Third Conference on the Mechanical Properties of Materials at High Rates of Strain; 1984. p. 9–12.
[611] Follansbee PS, Kocks UF. A constitutive description of the deformation of copper based on the use of the mechanical threshold stress as an internal state variable. Acta Metall 1988;36:81–93. https://doi.org/10.1016/0001-6160(88)90030-2.
[612] Fan Y, Osetsky Y, Yip S, Yildiz B. Onset Mechanism of Strain-Rate-Induced Flow Stress Upturn. PhysRevLett 2012;109:135503. https://doi.org/10.1103/PhysRevLett.109.135503.
[613] Huang M, Rivera-Díaz-del-Castillo PEJ, Bouaziz O, van der Zwaag S. A constitutive model for high strain rate deformation in FCC metals based on irreversible thermodynamics. Mech Mater 2009;41:982–8. https://doi.org/10.1016/j.mechmat.2009.05.007.
[614] Nadgornyi E. Dislocation dynamics and mechanical properties of crystals. Prog Mater Sci 1988;31:1–530. https://doi.org/10.1016/0079-6425(88)90005-9.
[615] Xiong L, Rigelesaiyin J, Chen X, Xu S, McDowell DL, Chen Y. Coarse-grained elastodynamics of fast moving dislocations. Acta Mater 2016;104:143–55.
[616] Rittel D, Bhattacharyya A, Poon B, Zhao J, Ravichandran G. Thermomechanical characterization of pure polycrystalline tantalum. Mater Sci Eng A 2007;447:65–70. https://doi.org/10.1016/j.msea.2006.10.064.
[617] Yanilkin AV, Krasnikov VS, Kuksin AY, Mayer AE. Dynamics and kinetics of dislocations in Al and Al–Cu alloy under dynamic loading. Int J Plast 2014;55:94–107. https://doi.org/10.1016/j.ijplas.2013.09.008.
[618] Jia D, Wang YM, Ramesh KT, Ma E, Zhu YT, Valiev RZ. Deformation behavior and plastic instabilities of ultrafine-grained titanium. Appl Phys Lett 2001;79:611–3. https://doi.org/10.1063/1.1384000.
[619] Tucker MT, Horstemeyer MF, Gullett PM, El Kadiri H, Whittington WR. Anisotropic effects on the strain rate dependence of a wrought magnesium alloy. Scr Mater 2009;60:182–5. https://doi.org/10.1016/j.scriptamat.2008.10.011.
[620] Ulacia I, Dudamell NV, Gálvez F, Yi S, Pérez-Prado MT, Hurtado I. Mechanical behavior and microstructural evolution of a Mg AZ31 sheet at dynamic strain rates. Acta Mater 2010;58:2988–98. https://doi.org/10.1016/j.actamat.2010.01.029.
[621] Jia D, Ramesh KT, Ma E, Lu L, Lu K. Compressive behavior of an electrodeposited nanostructured copper at quasistatic and high strain rates. Scr Mater 2001;45:613–20. https://doi.org/10.1016/S1359-6462(01)01071-5.
[622] Khan AS, Meredith CS. Thermo-mechanical response of Al 6061 with and without equal channel angular pressing (ECAP). Int J Plast 2010;26:189–203. https://doi.org/10.1016/j.ijplas.2009.07.002.
[623] Duvall GE, Graham RA. Phase transitions under shock-wave loading. RevModPhys 1977;49:523–79. https://doi.org/10.1103/RevModPhys.49.523.
[624] Meyers MA, Murr LE. Defect Generation in Shock-Wave Deformation. In: Meyers MA, Murr LE, editors. Shock Waves and High-Strain-Rate Phenomena in Metals: Concepts and Applications, Boston, MA: Springer US; 1981, p. 487–530. Doi: 10.1007/978-1-4613-3219-0_30.
[625] Dodd B, Bai Y. Adiabatic Shear Localization: Frontiers and Advances. Elsevier; 2012.
[626] Dormeval R. Adiabatic shear phenomena. DGM Informationsgesellschaft mbH, Impact Loading and Dynamic Behavior of Materials 1988;1:43–56.
[627] Bourne NK. On Thresholds for Dynamic Strength in Solids. J Dynamic Behavior Mater 2021;7:325–37. https://doi.org/10.1007/s40870-021-00301-y.
[628] Jones DR, Fensin SJ, Trujillo CP, Martinez DT, Gray GT. Stress and Strain Rate Effects on Incipient Spall in Tantalum. EPJ Web Conf 2018;183:03021. https://doi.org/10.1051/epjconf/201818303021.
[629] Park H-S, Rudd RE, Cavallo RM, Barton NR, Arsenlis A, Belof JL, et al. Grain-Size-Independent Plastic Flow at Ultrahigh Pressures and Strain Rates. PhysRevLett 2015;114:065502. https://doi.org/10.1103/PhysRevLett.114.065502.
[630] Piriz AR, López Cela JJ, Tahir NA, Hoffmann DHH. Richtmyer-Meshkov instability in elastic-plastic media. PhysRevE 2008;78:056401. https://doi.org/10.1103/PhysRevE.78.056401.
[631] Tiamiyu AA, Pang EL, Chen X, LeBeau JM, Nelson KA, Schuh CA. Nanotwinning-assisted dynamic recrystallization at high strains and strain rates. Nat Mater 2022;21:786–94. https://doi.org/10.1038/s41563-022-01250-0.
[632] Walters WP, Zukas JA. Fundamentals of Shaped Charges. Wiley; 1989.
[633] Gurevitch AC, Murr LE, Shih HK, Niou C-S, Advani AH, Manuel D, et al. Characterization and comparison of microstructures in the shaped-charge regime: copper and tantalum. Mater Charact 1993;30:201–16. https://doi.org/10.1016/1044-5803(93)90022-N.
[634] Meyers MA, Andrade UR, Chokshi AH. The effect of grain size on the high-strain, high-strain-rate behavior of copper. Metall Mater Trans A 1995;26:2881–93. https://doi.org/10.1007/BF02669646.
[635] Kelly SC, Thadhani NN. Shock compression response of highly reactive Ni + Al multilayered thin foils. J Appl Phys 2016;119. https://doi.org/10.1063/1.4942931.
[636] Chen J, Mathaudhu SN, Thadhani N, Dongare AM. Unraveling the Role of Interfaces on the Spall Failure of Cu/Ta Multilayered Systems. Sci Rep 2020;10:1–15. https://doi.org/10.1038/s41598-019-57048-9.
[637] Bringa EM, Caro A, Victoria M, Park N. The atomistic modeling of wave propagation in nanocrystals. JOM 2005;57:67–70. https://doi.org/10.1007/s11837-005-0119-9.
[638] Dai CD, Eakins DE, Thadhani NN. Dynamic densification behavior of nanoiron powders under shock compression. J Appl Phys 2008;103. https://doi.org/10.1063/1.2908209.
[639] Xiong Y, Xiao S, Deng H, Zhu W, Hu W. Investigation of the shock-induced chemical reaction (SICR) in Ni + Al nanoparticle mixtures. PCCP 2017;19:17607–17. https://doi.org/10.1039/C7CP03176A.
[640] Cheng JL, Hng HH, Lee YW, Du SW, Thadhani NN. Kinetic study of thermal- and impact-initiated reactions in Al–Fe2O3 nanothermite. Combust Flame 2010;157:2241–9. https://doi.org/10.1016/j.combustflame.2010.07.012.
[641] Yang Y, Wang S, Sun Z, Dlott DD. Propagation of shock-induced chemistry in nanoenergetic materials: The first micrometer. J Appl Phys 2004;95:3667–76. https://doi.org/10.1063/1.1652250.
[642] Advani AH, Thadhani NN. Shock-induced reaction synthesis of isomorphous (Cu-Ni) and immiscible (Cu-Nb) compounds. Metall Mater Trans A 1999;30:1367–79. https://doi.org/10.1007/s11661-999-0285-4.
[643] Holian BL, Lomdahl PS. Plasticity Induced by Shock Waves in Nonequilibrium Molecular-Dynamics Simulations. Science 1998. https://doi.org/10.1126/science.280.5372.2085.
[644] Germann TC, Holian BL, Lomdahl PS, Ravelo R. Orientation Dependence in Molecular Dynamics Simulations of Shocked Single Crystals. PhysRevLett 2000;84:5351–4. https://doi.org/10.1103/PhysRevLett.84.5351.
[645] Murr LE. Effects of Peak Pressure, Pulse Duration, and Repeated Loading on the Residual Structure and Properties of Shock Deformed Metals and Alloys. In: Meyers MA, Murr LE, editors. Shock Waves and High-Strain-Rate Phenomena in Metals: Concepts and Applications, Boston, MA: Springer US; 1981, p. 753–77. Doi: 10.1007/978-1-4613-3219-0_42.
[646] Cao B, Bringa EM, Meyers MA. Shock Compression of Monocrystalline Copper: Atomistic Simulations. Metall Mater Trans A 2007;38:2681–8. https://doi.org/10.1007/s11661-007-9248-9.
[647] Jarmakani HN, Bringa EM, Erhart P, Remington BA, Wang YM, Vo NQ, et al. Molecular dynamics simulations of shock compression of nickel: From monocrystals to nanocrystals. Acta Mater 2008;56:5584–604. https://doi.org/10.1016/j.actamat.2008.07.052.
[648] Hsiung LM, Lassila DH. Shock-induced deformation twinning and omega transformation in tantalum and tantalum–tungsten alloys. Acta Mater 2000;48:4851–65. https://doi.org/10.1016/S1359-6454(00)00287-1.
[649] Lu CH, Remington BA, Maddox BR, Kad B, Park HS, Kawasaki M, et al. Laser compression of nanocrystalline tantalum. Acta Mater 2013;61:7767–80. https://doi.org/10.1016/j.actamat.2013.09.016.

[650] Comley AJ, Maddox BR, Rudd RE, Prisbrey ST, Hawreliak JA, Orlikowski DA, et al. Strength of Shock-Loaded Single-Crystal Tantalum [100] Determined using In Situ Broadband X-Ray Laue Diffraction. PhysRevLett 2013;110:115501. https://doi.org/10.1103/PhysRevLett.110.115501.
[651] Wehrenberg CE, Comley AJ, Barton NR, Coppari F, Fratanduono D, Huntington CM, et al. Lattice-level observation of the elastic-to-plastic relaxation process with subnanosecond resolution in shock-compressed Ta using time-resolved in situ Laue diffraction. PhysRevB 2015;92:104305. https://doi.org/10.1103/PhysRevB.92.104305.
[652] Wehrenberg CE, McGonegle D, Bolme C, Higginbotham A, Lazicki A, Lee HJ, et al. In situ X-ray diffraction measurement of shock-wave-driven twinning and lattice dynamics. Nature 2017;550:496–9. https://doi.org/10.1038/nature24061.
[653] Wu D, Chen K, Zhu Y, Zhao L, Huang M, Li Z. Unveiling grain size effect on shock-induced plasticity and its underlying mechanisms in nano-polycrystalline Ta. Mech Mater 2021;160:103952. https://doi.org/10.1016/j.mechmat.2021.103952.
[654] Stiegler JO, Mansur LK. Radiation Effects in Structural Materials. Annu Rev Mater Sci 1979;9:405–54. https://doi.org/10.1146/annurev.ms.09.080179.002201.
[655] Stoller RE. Primary Radiation Damage Formation. Comprehensive Nuclear Materials, Elsevier 2012:293–332. https://doi.org/10.1016/B978-0-08-056033-5.00027-6.
[656] Zinkle SJ, Busby JT. Structural materials for fission & fusion energy. Mater Today 2009;12:12–9. https://doi.org/10.1016/S1369-7021(09)70294-9.
[657] Was GS. Fundamentals of Radiation Materials Science. New York, NY: Springer New York; 2017. Doi: 10.1007/978-1-4939-3438-6.
[658] Zinkle SJ, Was GS. Materials challenges in nuclear energy. Acta Mater 2013;61:735–58. https://doi.org/10.1016/j.actamat.2012.11.004.
[659] Knaster J, Moeslang A, Muroga T. Materials research for fusion. Nat Phys 2016;12:424–34. https://doi.org/10.1038/nphys3735.
[660] Sagaradze VV, Shalaev VI, Arbuzov VL, Goshchitskii BN, Tian Y, Qun W, et al. Radiation resistance and thermal creep of ODS ferritic steels. J Nucl Mater 2001;295:265–72. https://doi.org/10.1016/S0022-3115(01)00511-6.
[661] Alamo A, Bertin JL, Shamardin VK, Widент P. Mechanical properties of 9Cr martensitic steels and ODS-FeCr alloys after neutron irradiation at 325°C up to 42dpa. J Nucl Mater 2007;367–370:54–9. https://doi.org/10.1016/j.jnucmat.2007.03.166.
[662] Alamo A, Horsten M, Averty X, Materna-Morris EI, Rieth M, Brachet JC. Mechanical behavior of reduced-activation and conventional martensitic steels after neutron irradiation in the range 250–450°C. J Nucl Mater 2000;283–287:353–7. https://doi.org/10.1016/S0022-3115(00)00076-3.
[663] Wharry JP, Swenson MJ, Yano KH. A review of the irradiation evolution of dispersed oxide nanoparticles in the b.c.c. Fe-Cr system: Current understanding and future directions. J Nucl Mater 2017;486:11–20. https://doi.org/10.1016/j.jnucmat.2017.01.009.
[664] Han W, Demkowicz MJ, Mara NA, Fu E, Sinha S, Rollett AD, et al. Design of Radiation Tolerant Materials Via Interface Engineering. Adv Mater 2013;25:6975–9. https://doi.org/10.1002/adma.201303400.
[665] Demkowicz MJ, Hoagland RG, Hirth JP. Interface Structure and Radiation Damage Resistance in Cu-Nb Multilayer Nanocomposites. PhysRevLett 2008;100:136102. https://doi.org/10.1103/PhysRevLett.100.136102.
[666] Misra A, Demkowicz MJ, Zhang X, Hoagland RG. The radiation damage tolerance of ultra-high strength nanolayered composites. JOM 2007;59:62–5. https://doi.org/10.1007/s11837-007-0120-6.
[667] Zhang X, Hattar K, Chen Y, Shao L, Li J, Sun C, et al. Radiation damage in nanostructured materials. Prog Mater Sci 2018;96:217–321. https://doi.org/10.1016/j.pmatsci.2018.03.002.
[668] Cheng GM, Xu WZ, Wang YQ, Misra A, Zhu YT. Grain size effect on radiation tolerance of nanocrystalline Mo. Scr Mater 2016;123:90–4. https://doi.org/10.1016/j.scriptamat.2016.06.007.
[669] Beyerlein IJ, Caro A, Demkowicz MJ, Mara NA, Misra A, Uberuaga BP. Radiation damage tolerant nanomaterials. Mater Today 2013;16:443–9. https://doi.org/10.1016/j.mattod.2013.10.019.
[670] Nita N, Schaeublin R, Victoria M. Impact of irradiation on the microstructure of nanocrystalline materials. J Nucl Mater 2004;329–333:953–7. https://doi.org/10.1016/j.jnucmat.2004.04.058.
[671] Andrievskii RA. Effect of irradiation on the properties of nanomaterials. Phys Metals Metallogr 2010;110:229–40. https://doi.org/10.1134/S0031918X10090061.
[672] Chang Y-Q, Guo Q, Zhang J, Chen L, Long Y, Wan F-R. Irradiation effects on nanocrystalline materials. Front Mater Sci 2013;7:143–55. https://doi.org/10.1007/s11706-013-0199-3.
[673] Barr CM, Li N, Boyce BL, Hattar K. Examining the influence of grain size on radiation tolerance in the nanocrystalline regime. Appl Phys Lett 2018;112. https://doi.org/10.1063/1.5016822.
[674] Sharma G, Mukherjee P, Chatterjee A, Gayathri N, Sarkar A, Chakravartty JK. Study of the effect of α irradiation on the microstructure and mechanical properties of nanocrystalline Ni. Acta Mater 2013;61:3257–66. https://doi.org/10.1016/j.actamat.2013.02.014.
[675] Du C, Jin S, Fang Y, Li J, Hu S, Yang T, et al. Ultrastrong nanocrystalline steel with exceptional thermal stability and radiation tolerance. Nat Commun 2018;9:1–9. https://doi.org/10.1038/s41467-018-07712-x.
[676] Wurster S, Pippan R. Nanostructured metals under irradiation. Scr Mater 2009;60:1083–7. https://doi.org/10.1016/j.scriptamat.2009.01.011.
[677] Mohamed W, Miller B, Porter D, Murty K. The Role of Grain Size on Neutron Irradiation Response of Nanocrystalline Copper. Materials 2016;9:144. https://doi.org/10.3390/ma9030144.
[678] Fu EG, Wang H, Carter J, Shao L, Wang YQ, Zhang X. Fluence-dependent radiation damage in helium (He) ion-irradiated Cu/V multilayers. Phil Mag 2013;93:883–98. https://doi.org/10.1080/14786435.2012.735773.
[679] Jiao Z, Was GS. The role of irradiated microstructure in the localized deformation of austenitic stainless steels. J Nucl Mater 2010;407:34–43. https://doi.org/10.1016/j.jnucmat.2010.07.006.
[680] Zhang T, Vieh C, Wang K, Dai Y. Irradiation-induced evolution of mechanical properties and microstructure of Eurofer 97. J Nucl Mater 2014;450:48–53. https://doi.org/10.1016/j.jnucmat.2013.12.007.
[681] Lupinacci A, Chen K, Li Y, Kunz M, Jiao Z, Was GS, et al. Characterization of ion beam irradiated 304 stainless steel utilizing nanoindentation and Laue microdiffraction. J Nucl Mater 2015;458:70–6. https://doi.org/10.1016/j.jnucmat.2014.11.050.
[682] Fave L, Pouchon MA, Döbeli M, Schulte-Borchers M, Kimura A. Helium ion irradiation induced swelling and hardening in commercial and experimental ODS steels. J Nucl Mater 2014;445:235–40. https://doi.org/10.1016/j.jnucmat.2013.11.004.
[683] Krumwiede DL, Yamamoto T, Saleh TA, Maloy SA, Odette GR, Hosemann P. Direct comparison of nanoindentation and tensile test results on reactor-irradiated materials. J Nucl Mater 2018;504:135–43. https://doi.org/10.1016/j.jnucmat.2018.03.021.
[684] Aydogan E, Weaver JS, Maloy SA, El-Atwani O, Wang YQ, Mara NA. Microstructure and mechanical properties of FeCrAl alloys under heavy ion irradiations. J Nucl Mater 2018;503:250–62. https://doi.org/10.1016/j.jnucmat.2018.03.002.
[685] Duan B, Heintze C, Bergner F, Ulbricht A, Akhmadaliev S, Oñorbe E, et al. The effect of the initial microstructure in terms of sink strength on the ion-irradiation-induced hardening of ODS alloys studied by nanoindentation. J Nucl Mater 2017;495:118–27. https://doi.org/10.1016/j.jnucmat.2017.08.014.
[686] Liu C, Yu C, Hashimoto N, Ohnuki S, Ando M, Shiba K, et al. Micro-structure and micro-hardness of ODS steels after ion irradiation. J Nucl Mater 2011;417:270–3. https://doi.org/10.1016/j.jnucmat.2011.01.067.
[687] El-Atwani O, Nathaniel JE, Leff AC, Muntifering BR, Baldwin JK, Hattar K, et al. The role of grain size in He bubble formation: Implications for swelling resistance. J Nucl Mater 2017;484:236–44. https://doi.org/10.1016/j.jnucmat.2016.12.003.
[688] Demkowicz MJ, Misra A, Caro A. The role of interface structure in controlling high helium concentrations. Curr Opin Solid State Mater Sci 2012;16:101–8. https://doi.org/10.1016/j.cossms.2011.10.003.
[689] Yu KY, Liu Y, Fu EG, Wang YQ, Myers MT, Wang H, et al. Comparisons of radiation damage in He ion and proton irradiated immiscible Ag/Ni nanolayers. J Nucl Mater 2013;440:310–8. https://doi.org/10.1016/j.jnucmat.2013.04.069.
[690] Zhang X, Fu EG, Misra A, Demkowicz MJ. Interface-enabled defect reduction in He ion irradiated metallic multilayers. JOM 2010;62:75–8. https://doi.org/10.1007/s11837-010-0185-5.

[691] Li N, Martin MS, Anderoglu O, Misra A, Shao L, Wang H, et al. He ion irradiation damage in Al/Nb multilayers. J Appl Phys 2009;105:123522. https://doi.org/10.1063/1.3138804.
[692] Li N, Fu EG, Wang H, Carter JJ, Shao L, Maloy SA, et al. He ion irradiation damage in Fe/W nanolayer films. J Nucl Mater 2009;389:233–8. https://doi.org/10.1016/j.jnucmat.2009.02.007.
[693] Ma E. Alloys created between immiscible elements. Prog Mater Sci 2005;50:413–509. https://doi.org/10.1016/j.pmatsci.2004.07.001.
[694] Wei LC, Averback RS. Phase evolution during ion-beam mixing of Ag–Cu. J Appl Phys 1997;81:613–23. https://doi.org/10.1063/1.364202.
[695] Allen TR, Gan J, Cole JI, Miller MK, Busby JT, Shutthanandan S, et al. Radiation response of a 9 chromium oxide dispersion strengthened steel to heavy ion irradiation. J Nucl Mater 2008;375:26–37. https://doi.org/10.1016/j.jnucmat.2007.11.001.
[696] Russell KC. PHASE STABILITY UNDER IRRADIATION. PROGRESS IN MATERIALS SCIENCE n.d.:206.
[697] Swenson MJ, Wharry JP. Nanocluster irradiation evolution in Fe-9%Cr ODS and ferritic-martensitic alloys. J Nucl Mater 2017;496:24–40. https://doi.org/10.1016/j.jnucmat.2017.08.045.
[698] Chen T, Aydogan E, Gigax JG, Chen D, Wang J, Wang X, et al. Microstructural changes and void swelling of a 12Cr ODS ferritic-martensitic alloy after high-dpa self-ion irradiation. J Nucl Mater 2015;467:42–9. https://doi.org/10.1016/j.jnucmat.2015.09.016.
[699] Lescoat M-L, Monnet I, Ribis J, Dubuisson P, de Carlan Y, Costantini J-M, et al. Amorphization of oxides in ODS materials under low and high energy ion irradiations. J Nucl Mater 2011;417:266–9. https://doi.org/10.1016/j.jnucmat.2011.01.065.
[700] Motta AT, Lemaignan C. A ballistic mixing model for the amorphization of precipitates in Zircaloy under neutron irradiation. J Nucl Mater 1992;195:277–85. https://doi.org/10.1016/0022-3115(92)90519-Q.
[701] Ashkenazy Y, Vo NQ, Schwen D, Averback RS, Bellon P. Shear induced chemical mixing in heterogeneous systems. Acta Mater 2012;60:984–93. https://doi.org/10.1016/j.actamat.2011.11.014.
[702] Sauvage X, Renaud L, Deconihout B, Blavette D, Ping DH, Hono K. Solid state amorphization in cold drawn Cu/Nb wires. Acta Mater 2001;49:389–94. https://doi.org/10.1016/S1359-6454(00)00338-4.
[703] Russell KC. Phase instability under cascade damage irradiation. J Nucl Mater 1993;206:129–38. https://doi.org/10.1016/0022-3115(93)90120-N.
[704] Lu C, Lu Z, Wang X, Xie R, Li Z, Higgins M, et al. Enhanced Radiation-tolerant Oxide Dispersion Strengthened Steel and its Microstructure Evolution under Helium-implantation and Heavy-ion Irradiation. Sci Rep 2017;7:40343. https://doi.org/10.1038/srep40343.
[705] Certain A, Kuchibhatla S, Shutthanandan V, Hoelzer DT, Allen TR. Radiation stability of nanoclusters in nano-structured oxide dispersion strengthened (ODS) steels. J Nucl Mater 2013;434:311–21. https://doi.org/10.1016/j.jnucmat.2012.11.021.
[706] Enrique RA, Bellon P. Compositional Patterning in Systems Driven by Competing Dynamics Of Different Length Scale. PhysRevLett 2000;84:2885–8. https://doi.org/10.1103/PhysRevLett.84.2885.
[707] Pochet P, Bellon P, Chaffron L, Martin G. Phase Transformations under Ball Milling: Theory versus Experiment. MSF 1996;225–227:207–16. https://doi.org/10.4028/www.scientific.net/MSF.225-227.207.
[708] Enrique RA, Bellon P. Compositional patterning in immiscible alloys driven by irradiation. PhysRevB 2001;63:134111. https://doi.org/10.1103/PhysRevB.63.134111.
[709] Chee SW, Stumphy B, Vo NQ, Averback RS, Bellon P. Dynamic self-organization in Cu alloys under ion irradiation. Acta Mater 2010;58:4088–99. https://doi.org/10.1016/j.actamat.2010.03.039.
[710] Shu S, Bellon P, Averback RS. Role of point-defect sinks on irradiation-induced compositional patterning in model binary alloys. PhysRevB 2015;91:214107. https://doi.org/10.1103/PhysRevB.91.214107.
[711] Liu JC, Li J, Mayer JW. Temperature effect on ion-irradiation-induced grain growth in Cu thin films. J Appl Phys 1990;67:2354–8. https://doi.org/10.1063/1.345530.
[712] Atwater HA, Thompson CV, Smith HI. Ion-bombardment-enhanced grain growth in germanium, silicon, and gold thin films. J Appl Phys 1988;64:2337–53. https://doi.org/10.1063/1.341665.
[713] Tai K, Averback RS, Bellon P, Ashkenazy Y, Stumphy B. Temperature dependence of irradiation-induced creep in dilute nanostructured Cu–W alloys. J Nucl Mater 2012;422:8–13. https://doi.org/10.1016/j.jnucmat.2011.11.068.
[714] Tai K, Averback RS, Bellon P, Ashkenazy Y. Irradiation-induced creep in nanostructured Cu alloys. Scr Mater 2011;65:163–6. https://doi.org/10.1016/j.scriptamat.2011.04.001.
[715] Brimbal D, Décamps B, Henry J, Meslin E, Barbu A. Single- and dual-beam in situ irradiations of high-purity iron in a transmission electron microscope: Effects of heavy ion irradiation and helium injection. Acta Mater 2014;64:391–401. https://doi.org/10.1016/j.actamat.2013.10.052.
[716] Brimhall JL, Simonen EP. Effect of helium on void formation in nickel. J Nucl Mater 1977;68:235–43. https://doi.org/10.1016/0022-3115(77)90242-2.
[717] McGruer JN, Choyke WJ, Townsend JR, Chang JH, Yesso JD, Spitznagel JA, et al. The effects of sequential and simultaneous helium implantation on void formation in a 304 stainless steel. J Nucl Mater 1978;74:174–7. https://doi.org/10.1016/0022-3115(78)90548-2.
[718] Würschum R, Herth S, Brossmann U. Diffusion in Nanocrystalline Metals and Alloys—A Status Report. Adv Eng Mater 2003;5:365–72. https://doi.org/10.1002/adem.200310079.
[719] Divinski SV, Lee JS, Herzig C. Grain Boundary Diffusion and Segregation in Compacted and Sintered Nanocrystalline Alloys. J Metastable Nanocryst Mater 2004;19:55–68. https://doi.org/10.4028/www.scientific.net/JMNM.19.55.
[720] Chattopadhyay PP, Pabi SK, Manna I. On the enhancement of diffusion kinetics in nanocrystalline materials. Mater Chem Phys 2001;68:80–4. https://doi.org/10.1016/S0254-0584(00)00282-0.
[721] Kaszkur Z, Juszczyk W, Łomot D. Self-diffusion in nanocrystalline alloys. PCCP 2015;17:28250–5. https://doi.org/10.1039/C5CP00312A.
[722] Darling KA, Mathaudhu S, Kecskes L. Demonstration of ultrahigh-strength nanocrystalline copper alloys for military applications. US Army Research Lab Rep Project Number 2012. WP-2139-2012.
[723] Sevillano JG, Aldazabal J. Ductilization of nanocrystalline materials for structural applications. Scr Mater 2004;51:795–800.
[724] Weston DP, Harris SJ, Capel H, Ahmed N, Shipway PH, Yellup JM. Nanostructured Co–W coatings produced by electrodeposition to replace hard Cr on aerospace components. Trans IMF 2010;88:47–56.
[725] Karanth Y, Sharma S, Darling K, El Kadiri H, Solanki K. Oxidation Behavior of Nanocrystalline Alloys Materials 2024;17:5842. https://doi.org/10.3390/ma17235842.
[726] Sharma S, Karanth Y, Srinivasan S, Hornbuckle BC, Darling KA, Solanki K. Oxidation behavior of nanocrystalline Copper-Tantalum alloys. J Alloy Compd 2025;1011:178386. https://doi.org/10.1016/j.jallcom.2024.178386.
[727] Myung J-S, Lim H-J, Kang S-G. Oxidation behavior of nanocrystalline Al alloys containing 5 and 10 at.% Ti. Oxid Met 1999;51:79–95. https://doi.org/10.1023/A:1018802218912.
[728] Köster U, Triwikantoro. Oxidation of amorphous and nanocrystalline Zr-Cu-Ni-Al Alloys. J Metastable Nanocryst Mater 2001;10:29–36. https://doi.org/10.4028/www.scientific.net/JMNM.10.29.
[729] Raman RKS, Gupta RK, Koch CC. Resistance of nanocrystalline vis-à-vis microcrystalline Fe–Cr alloys to environmental degradation and challenges to their synthesis. Phil Mag 2010;90:3233–60. https://doi.org/10.1080/14786435.2010.484402.
[730] Kumar R, Singh Raman RK, Bakshi SR, Raja VS, Parida S. Effect of Nanocrystalline Structure on the Oxidation Behavior of Fe–20Cr–3Al Alloy at High Temperatures. Oxid Met 2022;97:307–21. https://doi.org/10.1007/s11085-021-10090-3.
[731] Liu Z, Gao W, Dahm KL, Wang F. Oxidation behaviour of sputter-depositedNi–Cr–Al micro-crystalline coatings. Acta Mater 1998;46:1691–700. https://doi.org/10.1016/S1359-6454(97)00346-7.
[732] Xie Y, Su C, Huang Z, Shu X, You L, Peng X. Improvement of oxidation resistance and alumina regrowth ability of Ni-30Cr-5Al alloy without and with Y: Nanocrystallization effect. Corros Sci 2023;223:111472. https://doi.org/10.1016/j.corsci.2023.111472.
[733] Yang X, Peng X, Xu C, Wang F. Electrochemical Assembly of Ni – xCr – yAl Nanocomposites with Excellent High-Temperature Oxidation Resistance. J Electrochem Soc 2009;156:C167. https://doi.org/10.1149/1.3082378.

[734] Comparison of the Oxidation Behavior of Nanocrystalline and Coarse-Grain Copper | High Temperature Corrosion of Materials n.d. https://link.springer.com/article/10.1007/s11085-005-4381-6 (accessed November 6, 2023).
[735] Fu GY, Niu Y, Gesmundo F. Microstructural effects on the high temperature oxidation of two-phase Cu–Cr alloys in 1 atm O2. Corros Sci 2003;45:559–74. https://doi.org/10.1016/S0010-938X(02)00141-5.
[736] Zhao Z, Wang J, Chen M, Zhang J, Wang F, Young DJ. Comparative study on the initial oxidation behavior of conventional and nanocrystalline MCrAlY coatings - effect of microstructure evolution and dynamic mechanisms. Acta Mater 2022;239:118264. https://doi.org/10.1016/j.actamat.2022.118264.
[737] Effect of Nanocrystalline Structure on the Oxidation Behavior of Fe–20Cr–3Al Alloy at High Temperatures | High Temperature Corrosion of Materials n.d. https://link.springer.com/article/10.1007/s11085-021-10090-3 (accessed November 6, 2023).
[738] Metals | Free Full-Text | Mechanical Alloying of Elemental Powders into Nanocrystalline (NC) Fe-Cr Alloys: Remarkable Oxidation Resistance of NC Alloys n.d. https://www.mdpi.com/2075-4701/11/5/695 (accessed November 6, 2023).
[739] Nano- and Microcrystal Coatings and Their High-Temperature Applications - Gao - 2001 - Advanced Materials - Wiley Online Library n.d. https://onlinelibrary.wiley.com/doi/abs/10.1002/1521-4095(200107)13:12/13%3C1001::AID-ADMA1001%3E3.0.CO;2-V?casa_token=0O-MuqUQQ-kAAAAA:je40UlvNKuJyPdZ5qKQz0Z0a7kaCqCpCOiPsIOIdvS7DBKJkguqlPgewlP3iDv6OXShacvJc6f5UFL0 (accessed November 6, 2023).
[740] Young DJ. High temperature oxidation and corrosion of metals, vol. 1. Elsevier; 2008.
[741] Pilling NB. The oxidation of metals at high temperature. J Inst Met 1923;29:529–82.
[742] Wagner C. Theoretical analysis of the diffusion processes determining the oxidation rate of alloys. J Electrochem Soc 1952;99:369.
[743] Zhang Z, Zhou F, Lavernia EJ. On the analysis of grain size in bulk nanocrystalline materials via x-ray diffraction. Metall Mater Trans A 2003;34:1349–55. https://doi.org/10.1007/s11661-003-0246-2.
[744] Trimby PW, Cao Y, Chen Z, Han S, Hemker KJ, Lian J, et al. Characterizing deformed ultrafine-grained and nanocrystalline materials using transmission Kikuchi diffraction in a scanning electron microscope. Acta Mater 2014;62:69–80. https://doi.org/10.1016/j.actamat.2013.09.026.
[745] Sneddon GC, Trimby PW, Cairney JM. Transmission Kikuchi diffraction in a scanning electron microscope: A review. Mater Sci Eng R Rep 2016;110:1–12. https://doi.org/10.1016/j.mser.2016.10.001.
[746] Trimby PW. Orientation mapping of nanostructured materials using transmission Kikuchi diffraction in the scanning electron microscope. Ultramicroscopy 2012;120:16–24. https://doi.org/10.1016/j.ultramic.2012.06.004.
[747] Dingley DJ, Nowell MM. The Use of Electron Backscatter Diffraction for the Investigation of Nano Crystalline Materials and the Move Towards Orientation Imaging in the TEM. Microchim Acta 2004;147:157–65. https://doi.org/10.1007/s00604-004-0186-6.
[748] Rebuffi L, Sánchez del Río M, Busetto E, Scardi P. Understanding the instrumental profile of synchrotron radiation X-ray powder diffraction beamlines. J Synchrotron Radiat 2017;24:622–35.
[749] Hornbuckle BC, Koju RK, Kennedy G, Jannotti P, Lorenzo N, Lloyd JT, et al. Direct observation of deformation and resistance to damage accumulation during shock loading of stabilized nanocrystalline Cu-Ta alloys. Nat Commun 2024;15:1–11. https://doi.org/10.1038/s41467-024-53142-3.
[750] Guduru RK, Scattergood RO, Koch CC, Murty KL, Guruswamy S, McCarter MK. Mechanical properties of nanocrystalline Fe–Pb and Fe–Al2O3. Scr Mater 2006;54:1879–83. https://doi.org/10.1016/j.scriptamat.2006.02.014.
[751] Shen TD, Koch CC. Formation, solid solution hardening and softening of nanocrystalline solid solutions prepared by mechanical attrition. Acta Mater 1996;44:753–61. https://doi.org/10.1016/1359-6454(95)00178-6.
[752] Guduru RK, Darling KA, Scattergood RO, Koch CC, Murty KL. Mechanical properties of electrodeposited nanocrystalline copper using tensile and shear punch tests. J Mater Sci 2007;42:5581–8.
[753] Darling KA, Hornbuckle BC, Marvel CJ, Hammond VH, Solanki K. Effect of constrained inter-granular regions on the inverse Hall-petch phenomena. Mater Sci Eng A 2023;875:145125. https://doi.org/10.1016/j.msea.2023.145125.
[754] Zhang X, Aifantis KE. Interpreting the softening of nanomaterials through gradient plasticity. J Mater Res 2011;26:1399–405. https://doi.org/10.1557/jmr.2011.123.
[755] Konstantinidis DA, Aifantis EC. On the "Anomalous" hardness of nanocrystalline materials. Nanostruct Mater 1998;10:1111–8. https://doi.org/10.1016/S0965-9773(98)00145-7.
[756] Adlakha I, Bhatia MA, Tschopp MA, Solanki KN. Atomic scale investigation of grain boundary structure role on intergranular deformation in aluminium. Phil Mag 2014;94:3445–66. https://doi.org/10.1080/14786435.2014.961585.
[757] Solanki KN, Ward DK, Bammann DJ. A Nanoscale Study of Dislocation Nucleation at the Crack Tip in the Nickel-Hydrogen System. Metall and Mat Trans A 2011;42:340–7. https://doi.org/10.1007/s11661-010-0451-8.
[758] Hu Y-J, Wang Y, Wang WY, Darling KA, Kecskes LJ, Liu Z-K. Solute effects on the Σ3 111 [11-0] tilt grain boundary in BCC Fe: Grain boundary segregation, stability, and embrittlement. Comput Mater Sci 2020;171:109271.
[759] Hu Y-J, Fellinger MR, Butler BG, Wang Y, Darling KA, Kecskes LJ, et al. Solute-induced solid-solution softening and hardening in bcc tungsten. Acta Mater 2017;141:304–16.
[760] Wang Y, Huang C, Ma X, Zhao J, Guo F, Fang X, et al. The optimum grain size for strength-ductility combination in metals. Int J Plast 2023;164:103574. https://doi.org/10.1016/j.ijplas.2023.103574.
[761] Lu L, Wang LB, Ding BZ, Lu K. High-tensile ductility in nanocrystalline copper. J Mater Res 2000;15:270–3. https://doi.org/10.1557/JMR.2000.0043.
[762] Wang YM, Wang K, Pan D, Lu K, Hemker KJ, Ma E. Microsample tensile testing of nanocrystalline copper. Scr Mater 2003;48:1581–6. https://doi.org/10.1016/S1359-6462(03)00159-3.
[763] Dao M, Lu L, Shen YF, Suresh S. Strength, strain-rate sensitivity and ductility of copper with nanoscale twins. Acta Mater 2006;54:5421–32. https://doi.org/10.1016/j.actamat.2006.06.062.
[764] Sharma S, Hornbuckle BC, Karanth Y, Darling K, Beura V, Sharma S, et al. Investigation of microstructural and thermal stability of Ni-Y-Zr ternary nanocrystalline alloy. Mater Charact 2024;217:114378. https://doi.org/10.1016/j.matchar.2024.114378.
[765] Cai XC, Liang JJ, Xu LD, Sun BR, Chen Z, Wen KK, et al. Ultrastrong nanocrystalline oxide-dispersion-strengthened ferritic alloy with exceptional thermal stability. Mater Sci Eng A 2021;821:141616. https://doi.org/10.1016/j.msea.2021.141616.
[766] Li L, Xu W, Saber M, Zhu Y, Koch CC, Scattergood RO. Long-term stability of 14YT–4Sc alloy at high temperature. Mater Sci Eng A 2015;647:222–8. https://doi.org/10.1016/j.msea.2015.09.012.
[767] Li YJ, Savan A, Ludwig A. Atomic scale understanding of phase stability and decomposition of a nanocrystalline CrMnFeCoNi Cantor alloy. Appl Phys Lett 2021;119. https://doi.org/10.1063/5.0069107.
[768] Lu P, Abdeljawad F, Rodriguez M, Chandross M, Adams DP, Boyce BL, et al. On the thermal stability and grain boundary segregation in nanocrystalline PtAu alloys. Materialia 2019;6:100298. https://doi.org/10.1016/j.mtla.2019.100298.
[769] Chookajorn T, Schuh CA. Nanoscale segregation behavior and high-temperature stability of nanocrystalline W–20at.% Ti. Acta Mater 2014;73:128–38. https://doi.org/10.1016/j.actamat.2014.03.039.
[770] Khalajhedayati A, Rupert TJ. High-temperature stability and grain boundary complexion formation in a nanocrystalline Cu-Zr alloy. JOM 2015;67:2788–801. https://doi.org/10.1007/s11837-015-1644-9.
[771] Lei T, Shin J, Gianola DS, Rupert TJ. Bulk nanocrystalline Al alloys with hierarchical reinforcement structures via grain boundary segregation and complexion formation. Acta Mater 2021;221:117394. https://doi.org/10.1016/j.actamat.2021.117394.
[772] Huang T-Y, Kalidindi AR, Schuh CA. Grain growth and second-phase precipitation in nanocrystalline aluminum–manganese electrodeposits. J Mater Sci 2018;53:3709–19. https://doi.org/10.1007/s10853-017-1764-4.
[773] Hornbuckle BC, Smeltzer JA, Sharma S, Nagar S, Marvel CJ, Cantwell PR, et al. A high-temperature nanostructured Cu-Ta-Li alloy with complexion-stabilized precipitates. Science 2025;387:1413–7. https://doi.org/10.1126/science.adr0299.
[774] Gale WF, Totemeier TC, editors. Front Matter. Smithells Metals Reference Book (Eighth Edition), Oxford: Butterworth-Heinemann; 2004, p. iii. Doi: 10.1016/B978-0-7506-7509-3.50046-4.

[775] Caron P, Khan T. Improvement of creep strength in a nickel-base single-crystal superalloy by heat treatment. Mater Sci Eng 1983;61:173–84.
[776] Reed R, Cox D, Rae C. Damage accumulation during creep deformation of a single crystal superalloy at 1150 C. Mater Sci Eng A 2007;448:88–96.
[777] Tian S, Zhu X, Wu J, Yu H, Shu D, Qian B. Influence of temperature on stacking fault energy and creep mechanism of a single crystal nickel-based superalloy. J Mater Sci Technol 2016;32:790–8. https://doi.org/10.1016/j.jmst.2016.01.020.
[778] Okamoto NL, Kashioka D, Hirato T, Inui H. Specimen- and grain-size dependence of compression deformation behavior in nanocrystalline copper. Int J Plast 2014;56:173–83. https://doi.org/10.1016/j.ijplas.2013.12.003.
[779] Wang L, Teng J, Liu P, Hirata A, Ma E, Zhang Z, et al. Grain rotation mediated by grain boundary dislocations in nanocrystalline platinum. Nat Commun 2014;5:1–7. https://doi.org/10.1038/ncomms5402.
[780] Zhang BB, Tang YG, Mei QS, Li XY, Lu K. Inhibiting creep in nanograined alloys with stable grain boundary networks. Science 2022. https://doi.org/10.1126/science.abq7739.
[781] Huang R, Kou Z, Tang S, Wu S, Lai Q, Zhang W, et al. Improved creep resistance of a nanograined Fe-Ni alloy through a diffusional phase transformation mechanism. Scr Mater 2024;253:116311. https://doi.org/10.1016/j.scriptamat.2024.116311.
[782] Cottrell AH, Aytekin V. Andrade's Creep Law and the Flow of Zinc Crystals. Nature 1947;160:328–9. https://doi.org/10.1038/160328a0.
[783] Shan GB, Chen YZ, Li YJ, Zhang CY, Dong H, Cong YB, et al. High temperature creep resistance of a thermally stable nanocrystalline Fe-5 at.% Zr steel. Scr Mater 2020;179:1–5. https://doi.org/10.1016/j.scriptamat.2019.12.036.
[784] Xu L, Cai X, Wen K, Wu Y, Zhu H, Xin S, et al. Superior creep resistance of a microstructurally stable nanocrystalline oxide-dispersion-strengthened ferritic alloy. Scr Mater 2024;252:116283. https://doi.org/10.1016/j.scriptamat.2024.116283.
[785] Qian L, Wu B, Fu H, Yang W, Sun W, Zhou X-Y, et al. Atomistic simulations of the enhanced creep resistance and underlying mechanisms of nanograined-nanotwinned copper. Mater Sci Eng A 2022;855:143912. https://doi.org/10.1016/j.msea.2022.143912.
[786] Sun S, Gao P, Sun G, Cai Z, Hu J, Han S, et al. Nanostructuring as a route to achieve ultra-strong high- and medium-entropy alloys with high creep resistance. J Alloy Compd 2020;830:154656. https://doi.org/10.1016/j.jallcom.2020.154656.
[787] Wani I, Rai N, Murty KL, Gollapudi S. Understanding the effect of grain boundary solute segregation on the creep behaviour of thermally stable nanocrystalline materials: a theoretical approach. Phil Mag 2024;104:1191–206. https://doi.org/10.1080/14786435.2024.2383252.
[788] Mohamed FA. Interpretation of superplastic flow in terms of a threshold stress. J Mater Sci 1983;18:582–92. https://doi.org/10.1007/BF00560647.
[789] Hondros ED, Henderson PJ. Role of grain boundary segregation in diffusional creep. Metall Trans A 1983;14:521–30. https://doi.org/10.1007/BF02643770.
[790] Chichili DR, Ramesh KT, Hemker KJ. The high-strain-rate response of alpha-titanium: experiments, deformation mechanisms and modeling. Acta Mater 1998;46:1025–43. https://doi.org/10.1016/S1359-6454(97)00287-5.
[791] Kuksin AY, Yanilkin AV. Atomistic simulation of the motion of dislocations in metals under phonon drag conditions. Phys Solid State 2013;55:1010–9. https://doi.org/10.1134/S1063783413050193.
[792] Chen X, Xiong L, McDowell DL, Chen Y. Effects of phonons on mobility of dislocations and dislocation arrays. Scr Mater 2017;137:22–6. https://doi.org/10.1016/j.scriptamat.2017.04.033.
[793] Lea L, Brown L, Jardine A. Time limited self-organised criticality in the high rate deformation of face centred cubic metals. Commun Mater 2020;1:93. https://doi.org/10.1038/s43246-020-00090-2.
[794] Williams DB, Carter CB. The Transmission Electron Microscope. In: Williams DB, Carter CB, editors. Transmission Electron Microscopy: A Textbook for Materials Science, Boston, MA: Springer US; 1996, p. 3–17. Doi: 10.1007/978-1-4757-2519-3_1.
[795] Xu GQ, Demkowicz MJ. Healing of nanocracks by disclinations. PhysRevLett 2013;111. https://doi.org/10.1103/PhysRevLett.111.145501.
[796] Meraj Md, Pal S. Healing mechanism of nanocrack in nanocrystalline metals during creep process. Appl Phys A 2017;123:138. https://doi.org/10.1007/s00339-017-0760-5.
[797] Barr CM, Duong T, Bufford DC, Milne Z, Molkeri A, Heckman NM, et al. Autonomous healing of fatigue cracks via cold welding. Nature 2023;620:552–6. https://doi.org/10.1038/s41586-023-06223-0.
[798] Kaoumi D, Motta AT, Birtcher RC. A thermal spike model of grain growth under irradiation. J Appl Phys 2008;104:073525. https://doi.org/10.1063/1.2988142.
[799] Han WZ, Demkowicz MJ, Fu EG, Wang YQ, Misra A. Effect of grain boundary character on sink efficiency. Acta Mater 2012;60:6341–51. https://doi.org/10.1016/j.actamat.2012.08.009.
[800] Nelson RS, Hudson JA, Mazey DJ. The stability of precipitates in an irradiation environment. J Nucl Mater 1972;44:318–30. https://doi.org/10.1016/0022-3115(72)90043-8.
[801] Wilkes P. Phase stability under irradiation — a review of theory and experiment. J Nucl Mater 1979;83:166–75. https://doi.org/10.1016/0022-3115(79)90602-0.
[802] Marwick AD. Segregation in irradiated alloys: The inverse Kirkendall effect and the effect of constitution on void swelling. J Phys F 1978;8:1849–61. https://doi.org/10.1088/0305-4608/8/9/008.
[803] Pollock TM, Tin S. Nickel-based superalloys for advanced turbine engines: chemistry, microstructure and properties. J Propul Power 2006;22:361–74. https://doi.org/10.2514/1.18239.
[804] Brenner SS. Tensile strength of whiskers. J Appl Phys 1956;27:1484–91. https://doi.org/10.1063/1.1722294.
[805] Šob M, Wang LG, Vitek V. Theoretical tensile stress in tungsten single crystals by full-potential first-principles calculations. Mater Sci Eng A 1997;234–236:1075–8. https://doi.org/10.1016/S0921-5093(97)00329-8.
[806] Sudharshan Phani P, Johanns KE, George EP, Pharr GM. A simple stochastic model for yielding in specimens with limited number of dislocations. Acta Mater 2013;61:2489–99. https://doi.org/10.1016/j.actamat.2013.01.023.
[807] Callister W, Rethwisch D. Materials Science and Engineering: An Introduction. 10th ed. Wiley; 2018.
[808] Shan Z, Stach EA, Wiezorek JMK, Knapp JA, Follstaedt DM, Mao SX. Grain Boundary-Mediated Plasticity in Nanocrystalline Nickel. Science 2004;305:654–7. https://doi.org/10.1126/science.1098741.
[809] Guo D, Song S, Luo R, Goddard WA, Chen M, Reddy KM, et al. Grain boundary sliding and amorphization are responsible for the reverse hall-petch relation in superhard nanocrystalline boron carbide. PhysRevLett 2018;121:145504. https://doi.org/10.1103/PhysRevLett.121.145504.
[810] Dao M, Lu L, Asaro RJ, De Hosson JTM, Ma E. Toward a quantitative understanding of mechanical behavior of nanocrystalline metals. Acta Mater 2007;55:4041–65. https://doi.org/10.1016/j.actamat.2007.01.038.
[811] Irifune T, Kurio A, Sakamoto S, Inoue T, Sumiya H. Ultrahard polycrystalline diamond from graphite. Nature 2003;421:599–600. https://doi.org/10.1038/421599b.
[812] Huang Q, Yu D, Xu B, Hu W, Ma Y, Wang Y, et al. Nanotwinned diamond with unprecedented hardness and stability. Nature 2014;510:250–3. https://doi.org/10.1038/nature13381.
[813] Sumiya H, Irifune T. Hardness and deformation microstructures of nano-polycrystalline diamonds synthesized from various carbons under high pressure and high temperature. J Mater Res 2007;22:2345–51. https://doi.org/10.1557/jmr.2007.0295.
[814] Solozhenko VL, Kurakevych OO, Le Godec Y. Creation of Nanostuctures by Extreme Conditions: High-Pressure Synthesis of Ultrahard Nanocrystalline Cubic Boron Nitride. Adv Mater 2012;24:1540–4. https://doi.org/10.1002/adma.201104361.
[815] Dubrovinskaia N, Solozhenko VL, Miyajima N, Dmitriev V, Kurakevych OO, Dubrovinsky L. Superhard nanocomposite of dense polymorphs of boron nitride: Noncarbon material has reached diamond hardness. Appl Phys Lett 2007;90:101912. https://doi.org/10.1063/1.2711277.
[816] Tian Y, Xu B, Yu D, Ma Y, Wang Y, Jiang Y, et al. Ultrahard nanotwinned cubic boron nitride. Nature 2013;493:385–8. https://doi.org/10.1038/nature11728.
[817] Dubrovinskaia N, Dubrovinsky L. Controversy about ultrahard nanotwinned cBN. Nature 2013;502:E1–2. https://doi.org/10.1038/nature12620.
[818] Tian Y, Xu B, Yu D, Ma Y, Wang Y, Jiang Y, et al. Tian et al. reply. Nature 2013;502:E2–3. Doi: 10.1038/nature12621.
[819] Wen B, Xu B, Wang Y, Gao G, Zhou X-F, Zhao Z, et al. Continuous strengthening in nanotwinned diamond. Npj Comput Mater 2019;5:1–6. https://doi.org/10.1038/s41524-019-0256-2.

[820] Taheri Mousavi SM, Zou G, Zhou H, Gao H. Anisotropy governs strain stiffening in nanotwinned-materials. Nat Commun 2018;9:1586. https://doi.org/10.1038/s41467-018-03972-9.
[821] Li B, Sun H, Chen C. Reply to 'Anisotropy governs strain stiffening in nanotwinned-materials.'. Nat Commun 2018;9:1585. https://doi.org/10.1038/s41467-018-03967-6.
[822] Xiao J, Wen B, Xu B, Zhang X, Wang Y, Tian Y. Intersectional nanotwinned diamond-the hardest polycrystalline diamond by design. Npj Comput Mater 2020;6:1–7. https://doi.org/10.1038/s41524-020-00387-3.
[823] Li XY, Jin ZH, Zhou X, Lu K. Constrained minimal-interface structures in polycrystalline copper with extremely fine grains. Science 2020;370:831–6. https://doi.org/10.1126/science.abe1267.
[824] Lu K. A novel metastable structure in polycrystalline metals with extremely fine grains: schwarz crystal. Metall Mater Trans A 2024;55:1–19. https://doi.org/10.1007/s11661-023-07232-4.
[825] Thomson W. LXIII. On the division of space with minimum partitional area. The London, Edinburgh, and Dublin Philosophical Magazine and Journal of Science 1887;24:503–14. Doi: 10.1080/14786448708628135.
[826] Aste DW Tomaso. The Pursuit of Perfect Packing. 2nd ed. Boca Raton: CRC Press; 2008. Doi: 10.1201/9781420068184.
[827] Mackay AL. Periodic minimal surfaces. Nature 1985;314:604–6. https://doi.org/10.1038/314604a0.
[828] Scriven LE. Equilibrium bicontinuous structure. Nature 1976;263:123–5. https://doi.org/10.1038/263123a0.
[829] Jin Z, Li X, Lu K. Formation of stable schwarz crystals in polycrystalline copper at the grain size limit. PhysRevLett 2021;127:136101. https://doi.org/10.1103/PhysRevLett.127.136101.
[830] Ogata S, Li J, Yip S. Ideal pure shear strength of aluminum and copper. Science 2002;298:807–11.
[831] Smith WF. Structure and Properties of Engineering Alloys. McGraw-Hill; 1993.
[832] Huang L, Lin W, Wang K, Song S, Guo C, Chen Y, et al. Grain boundary-constrained reverse austenite transformation in nanostructured Fe alloy: model and application. Acta Mater 2018;154:56–70. https://doi.org/10.1016/j.actamat.2018.05.021.
[833] Xu W, Zhang B, Li XY, Lu K. Suppressing atomic diffusion with the Schwarz crystal structure in supersaturated Al–Mg alloys. Science 2021;373:683–7. https://doi.org/10.1126/science.abh0700.
[834] Rong Y. Phase transformations and phase stability in nanocrystalline materials. Curr Opin Solid State Mater Sci 2005;9:287–95. https://doi.org/10.1016/j.cossms.2006.07.003.
[835] Cech RE, Turnbull D. Heterogeneous nucleation of the martensite transformation. JOM 1956;8:124–32. https://doi.org/10.1007/BF03377656.
[836] Waitz T, Tsuchiya K, Antretter T, Fischer FD. Phase Transformations of Nanocrystalline Martensitic Materials. MRS Bull 2009;34:814–21. https://doi.org/10.1557/mrs2009.231.
[837] Xu X, Thadhani N. Shock synthesis and characterization of nanostructured NITINOL alloy. Mater Sci Eng A 2004;384:194–201. https://doi.org/10.1016/j.msea.2004.06.014.
[838] Zhang XY, Wu XL, Liu Q, Zuo RL, Zhu AW, Jiang P, et al. Phase transformation accommodated plasticity in nanocrystalline nickel. Appl Phys Lett 2008;93:031901. https://doi.org/10.1063/1.2953545.
[839] Narayan J, Chen Y, Moon RM, Carpenter RW. Characterization of metal precipitates in magnesium oxide. Philos Mag A 1984;49:287–300. https://doi.org/10.1080/01418618408234929.
[840] Tian CS, Qian D, Wu D, He RH, Wu YZ, Tang WX, et al. Body-centered-cubic ni and its magnetic properties. PhysRevLett 2005;94:137210. https://doi.org/10.1103/PhysRevLett.94.137210.
[841] Korneva A, Straumal B, Kilmametov A, Lityńska-Dobrzyńska L, Chulist R, Gondek Ł, et al. The phase transformations induced by high-pressure torsion in Ti–Nb-based alloys. Microsc Microanal 2022;28:946–52. https://doi.org/10.1017/S1431927621012277.
[842] Ivanisenko Y, Kilmametov A, Rösner H, Valiev RZ. Evidence of α → ω phase transition in titanium after high pressure torsion. Int J Mater Res 2008;99:36–41. https://doi.org/10.3139/146.101606.
[843] Edalati K, Horita Z, Yagi S, Matsubara E. Allotropic phase transformation of pure zirconium by high-pressure torsion. Mater Sci Eng A 2009;523:277–81. https://doi.org/10.1016/j.msea.2009.07.029.
[844] Edalati K, Toh S, Ikoma Y, Horita Z. Plastic deformation and allotropic phase transformations in zirconia ceramics during high-pressure torsion. Scr Mater 2011;65:974–7. https://doi.org/10.1016/j.scriptamat.2011.08.024.
[845] Straumal BB, Kilmametov AR, Korneva A, Mazilkin AA, Straumal PB, Zięba P, et al. Phase transitions in Cu-based alloys under high pressure torsion. J Alloy Compd 2017;707:20–6. https://doi.org/10.1016/j.jallcom.2016.12.057.
[846] Jang J, Lance MJ, Wen S, Tsui TY, Pharr GM. Indentation-induced phase transformations in silicon: influences of load, rate and indenter angle on the transformation behavior. Acta Mater 2005;53:1759–70. https://doi.org/10.1016/j.actamat.2004.12.025.
[847] Pharr GM, Oliver WC, Harding DS. New evidence for a pressure-induced phase transformation during the indentation of silicon. J Mater Res 1991;6:1129–30. https://doi.org/10.1557/JMR.1991.1129.
[848] Daibin GVD, Ge Y. Indentation-induced phase transformations in semiconductors. CRC Press; 2003.
[849] Morris JC, Callahan DL, Kulik J, Patten JA, Scattergood RO. Origins of the ductile regime in single-point diamond turning of semiconductors. J Am Ceram Soc 1995;78:2015–20. https://doi.org/10.1111/j.1151-2916.1995.tb08612.x.
[850] Blackley WS, Scattergood RO. Ductile-regime machining model for diamond turning of brittle materials. Precis Eng 1991;13:95–103. https://doi.org/10.1016/0141-6359(91)90500-I.
[851] Bifano TG, Dow TA, Scattergood RO. Ductile-regime grinding: a new technology for machining brittle materials. Journal of Engineering for Industry 1991;113:184–9. https://doi.org/10.1115/1.2899676.
[852] De Cooman BC. Structure–properties relationship in TRIP steels containing carbide-free bainite. Curr Opin Solid State Mater Sci 2004;8:285–303. https://doi.org/10.1016/j.cossms.2004.10.002.
[853] Machon D, Pischedda V, Le Floch S, San-Miguel A. Perspective: High pressure transformations in nanomaterials and opportunities in material design. J Appl Phys 2018;124:160902. https://doi.org/10.1063/1.5045563.
[854] Zhang L, Wang Y, Lv J, Ma Y. Materials discovery at high pressures. Nat Rev Mater 2017;2:1–16. https://doi.org/10.1038/natrevmats.2017.5.
[855] McMillan PF. New materials from high-pressure experiments. Nature Mater 2002;1:19–25. https://doi.org/10.1038/nmat716.
[856] McMillan PF. Chemistry of materials under extreme high pressure-high-temperature conditions. Chem Commun 2003:919–23. https://doi.org/10.1039/B300963G.
[857] Christian J. The Theory of Transformations in Metals and Alloys. Newnes; 2002.
[858] Kaur I, Mishin Y, Gust W. Fundamentals of Grain and Interphase Boundary Diffusion. 3rd ed. Wiley; 1995.
[859] Fang QF. Atomistic simulation of the atomic structure and diffusion within the core region of an edge dislocation in aluminum. PhysRevB 2000;62:9317–24. https://doi.org/10.1103/PhysRevB.62.9317.
[860] Purja Pun GP, Mishin Y. A molecular dynamics study of self-diffusion in the cores of screw and edge dislocations in aluminum. Acta Mater 2009;57:5531–42. https://doi.org/10.1016/j.actamat.2009.07.048.
[861] Chesser I, Koju RK, Mishin Y. Atomic-level mechanisms of short-circuit diffusion in materials. Int J Mater Res 2024;115:85–105. https://doi.org/10.1515/ijmr-2023-0202.
[862] Cottrell AH, Dexter DL. Dislocations and plastic flow in crystals. Am J Phys 1954;22:242–3. https://doi.org/10.1119/1.1933704.
[863] Cahn JW. Thermodynamic aspects of Cottrell atmospheres. Phil Mag 2013;93:3741–6. https://doi.org/10.1080/14786435.2013.793853.
[864] Mishin Y, Cahn JW. Thermodynamics of Cottrell atmospheres tested by atomistic simulations. Acta Mater 2016;117:197–206. https://doi.org/10.1016/j.actamat.2016.07.013.
[865] Bhatia MA, Groh S, Solanki KN. Atomic-scale investigation of point defects and hydrogen-solute atmospheres on the edge dislocation mobility in alpha iron. J Appl Phys 2014;116:064302. https://doi.org/10.1063/1.4892630.

[866] Lehtinen A, Laurson L, Granberg F, Nordlund K, Alava MJ. Effects of precipitates and dislocation loops on the yield stress of irradiated iron. Sci Rep 2018;8:1–12. https://doi.org/10.1038/s41598-018-25285-z.
[867] Gurrutxaga-Lerma B, Balint DS, Dini D, Eakins DE, Sutton AP. A dynamic discrete dislocation plasticity method for the simulation of plastic relaxation under shock loading. Proceedings of the Royal Society A: Mathematical, Physical and Engineering Sciences 2013;469:20130141. https://doi.org/10.1098/rspa.2013.0141.
[868] Oh SH, Legros M, Kiener D, Dehm G. In situ observation of dislocation nucleation and escape in a submicrometre aluminium single crystal. Nat Mater 2009;8:95–100. https://doi.org/10.1038/nmat2370.
[869] Lloyd JT. High-rate dislocation motion in stable nanocrystalline metals. J Mater Res 2019;34:2252–62. https://doi.org/10.1557/jmr.2019.59.
[870] Huang K, Logé RE. A review of dynamic recrystallization phenomena in metallic materials. Mater Des 2016;111:548–74. https://doi.org/10.1016/j.matdes.2016.09.012.
[871] Kassner ME, Barrabes SR. New developments in geometric dynamic recrystallization. Mater Sci Eng A 2005;410–411:152–5. https://doi.org/10.1016/j.msea.2005.08.052.
[872] McQueen HJ. Development of dynamic recrystallization theory. Mater Sci Eng A 2004;387–389:203–8. https://doi.org/10.1016/j.msea.2004.01.064.
[873] Gourdet S, Montheillet F. An experimental study of the recrystallization mechanism during hot deformation of aluminium. Mater Sci Eng A 2000;283:274–88. https://doi.org/10.1016/S0921-5093(00)00733-4.
[874] Pari LD, Misiolek WZ. Theoretical predictions and experimental verification of surface grain structure evolution for AA6061 during hot rolling. Acta Mater 2008;56:6174–85. https://doi.org/10.1016/j.actamat.2008.08.050.
[875] Hornbuckle BC, Luckenbaugh TL, Fudger SJ, Roberts AJ, Jannotti P, Byun TS, et al. Role of geometric dynamic recrystallization in nanocrystalline alloys. Materialia 2023;30:101807. https://doi.org/10.1016/j.mtla.2023.101807.
[876] Williams CL. Structure-property relationships under extreme dynamic environments: shock recovery experiments. Synthesis SEM Lectures on Experimental Mechanics 2019;2:1–155. https://doi.org/10.2200/S00880ED1V01Y201810SEM004.
[877] Brown AD, Wayne L, Pham Q, Krishnan K, Peralta P, Luo S-N, et al. Microstructural effects on damage nucleation in shock-loaded polycrystalline copper. Metall and Mat Trans A 2015;46:4539–47. https://doi.org/10.1007/s11661-014-2482-z.
[878] Wayne L, Krishnan K, DiGiacomo S, Kovvali N, Peralta P, Luo SN, et al. Statistics of weak grain boundaries for spall damage in polycrystalline copper. Scr Mater 2010;63:1065–8. https://doi.org/10.1016/j.scriptamat.2010.08.003.
[879] Escobedo JP, Dennis-Koller D, Cerreta EK, Patterson BM, Bronkhorst CA, Hansen BL, et al. Effects of grain size and boundary structure on the dynamic tensile response of copper. J Appl Phys 2011;110:033513. https://doi.org/10.1063/1.3607294.
[880] Bhatia MA, Mathaudhu SN, Solanki KN. Atomic-scale investigation of creep behavior in nanocrystalline Mg and Mg–Y alloys. Acta Mater 2015;99:382–91. https://doi.org/10.1016/j.actamat.2015.07.068.
[881] Hu Y-J, Li J, Darling KA, Wang WY, VanLeeuwen BK, Liu XL, et al. Nano-sized superlattice clusters created by oxygen ordering in mechanically alloyed Fe alloys. Sci Rep 2015;5:11772. https://doi.org/10.1038/srep11772.
[882] Hirata A, Fujita T, Wen YR, Schneibel JH, Liu CT, Chen MW. Atomic structure of nanoclusters in oxide-dispersion-strengthened steels. Nat Mater 2011;10:922–6. https://doi.org/10.1038/nmat3150.
[883] Darling KA, Hornbuckle BC, Fullenwider BP, Ostlind AM, Roberts AJ, Giri AK. Nano-structured alloy material and method of synthesizing. US20230302531A1, 2023.
[884] Subramanian PR, Laughlin DE. The Cu-Ta (Copper-Tantalum) system. Bull Alloy Phase Diagr 1989;10:652–5. https://doi.org/10.1007/BF02877637.
[885] Okamoto H, Okamoto H. Phase diagrams for binary alloys, vol. 44. OH: ASM international Materials Park; 2000.
[886] Hasegawa M. Chapter 3.3 - Ellingham Diagram. In: Seetharaman S, editor. Treatise on Process Metallurgy, Boston: Elsevier; 2014, p. 507–16. Doi: 10.1016/B978-0-08-096986-2.00032-1.
[887] Sundahl RC, Sivertsen JM. Stacking faults in silver-lithium alloys. J Appl Phys 1963;34:994–5. https://doi.org/10.1063/1.1729581.
[888] Tisone TC, Sundahl RC, Chin GY. The stacking fault energy in noble metal alloys. Metall Trans 1970;1:1561–7. https://doi.org/10.1007/BF02642001.
[889] Park M, Schuh CA. Accelerated sintering in phase-separating nanostructured alloys. Nat Commun 2015;6:1–6. https://doi.org/10.1038/ncomms7858.
[890] Park M, Chookajorn T, Schuh CA. Nano-phase separation sintering in nanostructure-stable vs. bulk-stable alloys. Acta Mater 2018;145:123–33. https://doi.org/10.1016/j.actamat.2017.11.030.
[891] Naunheim Y, Schuh CA. A challenge to the sintering of nanocrystalline metals: Organic burnout and oxide reduction compete with powder consolidation. Acta Mater 2023;247:118743. https://doi.org/10.1016/j.actamat.2023.118743.
[892] Oliver C, Schuh CA. Optimization of the Mo-Cr binary system for nanophase separation sintering. Materialia 2022;22:101410. https://doi.org/10.1016/j.mtla.2022.101410.
[893] Oliver C, Schuh CA. Design of a rapidly sintering Mo-W-Cr alloy. J Alloy Compd 2023;938:168492. https://doi.org/10.1016/j.jallcom.2022.168492.
[894] Oliver C, Schuh CA. The structural evolution and densification mechanisms of nanophase separation sintering. Metall Mater Trans A 2021;52:4946–56. https://doi.org/10.1007/s11661-021-06437-9.
[895] Naunheim Y, Perrin A, Oliver CE, Stone K, Schuh CA. A limit to accelerated free-sintering: nano-phase separation interferes with organic debinding. Metall Mater Trans A 2023;54:4041–52. https://doi.org/10.1007/s11661-023-07152-3.
[896] Bose A, Lund AC, Reidy JP, Craven CA, Gibson MA, Barbati AC, et al. Additive manufacturing of a novel Cr-Ni alloy using the bound metal deposition technique. Int J Powder Metall 2021;57:17–30.
[897] Bose A, Schuh CA, Tobia JC, Tuncer N, Mykulowycz NM, Preston A, et al. Traditional and additive manufacturing of a new Tungsten heavy alloy alternative. Int J Refract Metal Hard Mater 2018;73:22–8. https://doi.org/10.1016/j.ijrmhm.2018.01.019.
[898] HITEMMP | arpa-e.energy.gov n.d. http://arpa-e.energy.gov/technologies/programs/hitemmp.
[899] Martínez V de P, Aguilar C, Marín J, Ordoñez S, Castro F. Mechanical alloying of Cu–Mo powder mixtures and thermodynamic study of solubility. Materials Letters 2007;61:929–33. https://doi.org/10.1016/j.matlet.2006.11.070.
[900] Solanki K, Williams CL, Darling KA. A Review of the Anomalous Dynamic Behavior in Magnesium Alloys. JOM 2024;76:1594–608. https://doi.org/10.1007/s11837-024-06376-x.
[901] Rajulapati KV, Scattergood RO, Murty KL, Horita Z, Langdon TG, Koch CC. Mechanical Properties of Bulk Nanocrystalline Aluminum-Tungsten Alloys. Metall Mater Trans A 2008;39:2528–34. https://doi.org/10.1007/s11661-008-9593-3.
[902] Koch CC. Ductility in Nanostructured and Ultra Fine-Grained Materials: Recent Evidence for Optimism. J Metastable Nanocrystalline Mater 2003;18:9–20. https://doi.org/10.4028/www.scientific.net/JMNM.18.9.
[903] Richter G, Hillerich K, Gianola DS, Mönig R, Kraft O, Volkert CA. Ultrahigh Strength Single Crystalline Nanowhiskers Grown by Physical Vapor Deposition. Nano Lett 2009;9:3048–52. https://doi.org/10.1021/nl9015107.
[904] https://web.mit.edu/2.813/www/readings/Ellingham_diagrams.pdf.
[905] Heat Treating of Copper and Copper Alloys. 2016. https://doi.org/10.31399/asm.hb.v04e.a0006276.